

MODELLING THE EFFECTS OF TREES ON A CONTAMINATED GROUNDWATER PLUME FROM A GOLD TAILINGS STORAGE FACILITY IN THE ORKNEY DISTRICT



Suzanne Grindley

0718517w

Supervisors: Dr. Peter Dye and Dr. Christopher Curtis

Declaration

I declare that this Dissertation is my own, unaided work unless where specific acknowledgment has been made. It is being submitted for the Master of Science within the School of Geography, Archaeology and Environmental Science at the University of the Witwatersrand, Johannesburg under the supervision of Dr. P.J. Dye and Dr. C. Curtis. This work contributes towards an externally funded contract research project which was undertaken by a larger project team within the Department of Animal, Plant and Environmental Sciences at the University of the Witwatersrand, Johannesburg under the supervision of I. Weiersbye.



23 October 2014

Signed by Suzanne Grindley

Date

0718517W

Abstract

The aim of this dissertation was to determine the likely impacts that planting woodlands would have on the storage, transport and discharge of mine water and contaminants, over a plume originating from the West Complex tailings storage facility within the Vaal River mine lease. The hydrological model MIKE SHE was run on a grid comprising of 120m square cells, for a pre-woodland period from 2001 to 2010. Sulphate was used as an indicator of the contaminant plume concentrations and transport across the study area. Six future woodland planting scenarios (2025 to 2034) were then simulated to determine the effects of mature *Searsia lancea*, *Eucalyptus dunnii* and *Tamarix usneoides*, and different planting scenarios on the contaminant plume. Results indicated that planting these deep-rooted species will be effective in decreasing the groundwater levels, groundwater flux and the quantity of contaminants reaching the river. Before tree water and contaminant uptake can be further modelled with improved accuracy within MIKE SHE, the limitations of the use of only one contaminant uptake value for the vegetation needs to be overcome, so that different uptake rates among different tree species can be shown.

Acknowledgements

I would like to acknowledge and thank the following organizations, institutions and individuals for their technical assistance and support in and out of the field:

- Dr. Peter Dye and Dr. Christopher Curtis for their constant support and guidance throughout this dissertation.
- Isabel Weiersbye for the help and data on contaminant uptake by woodland species, and reviewing the dissertation.
- Jason Hallows, Silvia Leiriao and Bruce Eady at DHI South Africa for their constant support and help in setting up the MIKE SHE hydrological model.
- AngloGold Ashanti for arranging security provided for the pre-dawn field work. Also their assistance with other arrangements, and providing data and reports.
- Koos Vivier and Ferdinand Mostert at AGES Gauteng, for the time and advice with regard to the set-up of the MIKE SHE Model.
- Bruce McLeorth at Red Earth CC for assistance in the measurements of soil infiltration rates, as well as the use of his equipment for these measurements.
- Jacob Mahlangu and Ben Oageng for their constant help throughout the numerous fieldtrips.
- Professor Sally Archibald and the CSIR for the use of their Scholander Pressure Chamber System, for the measurements of water stress of the plants.
- Wayne Costopoulos from Civil Engineering at the University of the Witwatersrand for the use of their hydraulic auger. Even though we could only get to 0.5m depth, the use of the drill was appreciated.
- The Geography Department at the University of the Witwatersrand for the use of their equipment and laboratory.
- The School of Animal, Plants and Environmental Sciences at the University of the Witwatersrand for the use of their equipment.
- South African Weather Service for the meteorological data provided for the study site.
- Department of Water and Forestry for the flow data provided for the Schoonspruit River.
- Council of Geosciences for the use of their hydraulic auger rig.

Table of Contents

Declaration.....	1
Abstract.....	2
Acknowledgements	3
List of Figures.....	8
List of Tables	16
Abbreviations	19
1 Introduction	20
1.1 Phytoremediation	22
1.2 Mine Woodlands Project.....	22
1.3 Mine Woodlands Project West Complex TSF Trial	23
1.4 Aims	25
1.5 Objectives	26
2 Study Site.....	27
2.1 West Complex Tailings Dam Area	27
3 Literature Review	29
3.1 Acid Mine Drainage.....	29
3.2 Potential solutions for AMD	30
3.3 Phytoremediation	31
3.4 Types of Phytoremediation	31
3.5 Case Studies of Phytoremediation Technology	33
3.6 Advantages of Phytoremediation	35
3.7 Disadvantages of Phytoremediation.....	35
3.8 Hydrological Modelling.....	36
3.9 MIKE SHE.....	36

3.10	<i>Case Studies of MIKE SHE</i>	40
3.10.1	Case Study in the Gyeongacheon Watershed, South Korea.....	40
3.10.2	Case Study in New South Wales, Australia	40
4	Methodology	42
4.1	MIKE SHE Simulation Scenarios	42
4.2	Current Scenario	44
4.2.1	Display Module.....	44
4.2.2	Simulation Specification Module.....	45
4.2.3	Water Quality Simulation Specification	46
4.2.4	Model and Domain Module	47
4.2.5	Topography Module.....	49
4.2.6	Climate Module.....	50
4.2.7	Land Use Module.....	53
4.2.8	Overland Flow Module	57
4.2.9	Unsaturated Flow Module.....	58
4.2.10	Saturated Zone Module.....	65
4.2.11	Water Quality Sources Module.....	74
4.2.12	River and Lakes Module	76
4.3	Future Woodlands Scenario	84
4.3.1	Display Module.....	84
4.3.2	Simulation Specification Module.....	84
4.3.3	Model and Domain Module	84
4.3.4	Species Module	84
4.3.5	Topography Module.....	86
4.3.6	Climate Module.....	87
4.3.7	Land Use Module.....	87

4.3.8	Overland Flow Module	95
4.3.9	Unsaturated Flow Module.....	95
4.3.10	Saturated Zone Module.....	95
4.3.11	Water Quality Module	95
4.3.12	River and Lakes Module	96
5	Results.....	97
5.1	Infiltration Results	97
5.2	Rhodamine Results	100
5.3	Plant Water Stress Test Results	101
5.4	Calibration Results.....	103
5.4.1	General Calibration.....	103
5.4.2	Model Domain	106
5.4.3	Topography	106
5.4.4	Overland Flow Module	106
5.4.5	Unsaturated Flow and Saturated Zone Module.....	108
5.5	Evapotranspiration Rates	109
5.6	Groundwater Levels.....	113
5.6.1	Simulation Line One	113
5.6.2	Simulation Line Two	125
5.6.3	Simulation Line Three	135
5.6.4	Overview of Scenario Impacts.....	143
5.7	Sulphate Concentrations	150
5.7.1	Transect One	152
5.7.2	Transect Two	171
5.8	Groundwater Flow Rates	186
5.8.1	Simulation Point 3.1.....	186

5.8.2	Simulation Point 3.5.....	187
5.9	Sulphate Mass Flux.....	189
6	Discussions and Conclusions.....	196
6.1	Tree Root Access to Groundwater.....	196
6.2	Overland Flow and Soil Infiltration.....	197
6.3	Hydraulic Conductivity Calibration.....	197
6.4	Evapotranspiration and Groundwater Uptake by Trees.....	198
6.5	Changes in Water Table Levels.....	199
6.6	Changes in Sulphate Concentrations in the UZ and SZ.....	199
6.7	Sulphate Uptake by Trees.....	200
6.8	Groundwater Flow Rate and Sulphate Mass Flux.....	200
6.9	Run Times and Grid Cell Sizes.....	200
6.10	Future Simulation Improvements.....	201
6.11	Recommendation for further research.....	201
6.12	Conclusion.....	202
7	References.....	204
8	Appendices.....	A1
8.1	Appendix A (Mike She Input Values).....	A1
8.2	Appendix B (Maps showing the Future Planting Scenarios).....	B1
8.3	Appendix C (Graphs showing the change per year observed for Scenarios 3 to 6).....	C1

List of Figures

Figure 1: The potential locations of MWP planting blocks to the west of the West Complex TSF	24
Figure 2: The location of the study site within the Vaal River mine lease area.....	27
Figure 3: Schematic of the MIKE SHE hydrological modules interactions	37
Figure 4: The <i>display module</i> set-up.....	44
Figure 5: The default settings used for the time step control.....	45
Figure 6: The default settings used for the WQ time step control	46
Figure 7: The extent of the study site and the core focus area.....	48
Figure 8: The 5m DEM of the study site, with an overlay identifying the TSFs and the Schoonspruit River	49
Figure 9: The hourly rainfall (mm) over nine years for the study area.....	52
Figure 10: The daily reference evapotranspiration rate (mm/day) for the study area.....	53
Figure 11: The difference in cover density on the West Complex TSF.....	54
Figure 12: The yearly LAI and RD estimated for the grasslands on top of the TSF	56
Figure 13: The yearly LAI and RD estimated for the <i>Phragmites</i> on top of the TSF.....	56
Figure 14: The yearly LAI and RD estimated for the surrounding grasslands	56
Figure 15: The available options for the <i>Unsaturated Flow module</i>	59
Figure 16: The double ring infiltrometer filled with water, at the start of a test.....	61
Figure 17: The geology underlying the major soil types of the study site.....	63
Figure 18: Schematic showing the geological, water quality, and water table layers.....	66
Figure 19: The geological units found in the study site (30 – 50m)	67
Figure 20: The water table depth for January 2001 for the study site.....	69
Figure 21: The zero-flux boundary (Red) and the flux boundary (Green).....	70
Figure 22: Conceptual diagram of the water table within the West Complex TSF	72
Figure 23: The location of boreholes used for SO ₄ concentration measurements	73
Figure 24: The initial concentrations of the SO ₄ for 2001	74
Figure 25: The water level and the discharge for the upstream open boundary of the Schoonspruit River (www.dwaf.gov.co.za)	81
Figure 26: The water level and the discharge for the downstream open boundary of the Schoonspruit River (www.dwaf.gov.co.za)	81
Figure 27: The upstream SO ₄ concentration for the Schoonspruit River (AngloGold Ashanti).....	82
Figure 28: The downstream SO ₄ concentration for the Schoonspruit River (AngloGold Ashanti)	83

Figure 29: The sensitivity of the MIKE SHE model to the ET uptake factor.....	85
Figure 30: The method for releasing of Rhodamine B down boreholes. a.) showing the hose pipe with funnel, b.) the release of Rhodamine B down funnel and c.) the capping of the casing to ensure sediment doesn't block the casing.....	90
Figure 31: The lid of the Scholander pressure chamber with a leaf petiole protruding through the bung..	92
Figure 32: The <i>E. camaldulensis</i> (Site 1) (left) and <i>S. lancea</i> (Site 5) (right) used for the water stress test	93
Figure 33: The <i>T. usneoides</i> (Site 6) used for the water stress test	94
Figure 34: The sealing of the leaf in the pressure chamber system lid by means of Prestik.....	94
Figure 35: The infiltration rate of the Alluvium soil.....	97
Figure 36: The infiltration rates for the Black Reef soil	98
Figure 37: The near steady state infiltration rate for the Alluvium soil	99
Figure 38: The near steady state infiltration rate for the Black Reef soil	99
Figure 39: Baseline solution under the UV torch	100
Figure 40: Fluorescence of the solution derived from the leaves taken two weeks after tracer release ...	100
Figure 41: The mean and range of readings based on five leaves at each site from the Scholander pressure chamber tests for <i>E. camaldulensis</i> (red) <i>S. lancea</i> (green) and <i>T. usneoides</i> (blue).....	102
Figure 42: The location of the water stress test sites with <i>E. camaldulensis</i> found at sites 1 to 3, <i>S. lancea</i> at sites 4 and 5, and <i>T. usneoides</i> at sites 6 and 7	103
Figure 43: The water balance of the current scenario's initial simulation run.....	104
Figure 44: The water balance of the calibrated simulation	105
Figure 45: The location of the simulation points	107
Figure 46: The maximum overland water depths for the current scenario	107
Figure 47: The simulated vs. observed data for the groundwater table at borehole VR04	108
Figure 48: The observed (dotted) and simulated (line) groundwater levels at borehole VR04, using revised conductivity values	109
Figure 49: The simulated evapotranspiration rates, for the grassland observed at point 2.1	110
Figure 50: The simulated evapotranspiration rates for <i>S. lancea</i> , observed at simulation point 2.1 for the planting scenario 1	111
Figure 51: The simulated evapotranspiration rates for <i>E. dunnii</i> , observed at simulation point 2.1 for the planting scenario 2	112
Figure 52: The simulated evapotranspiration rates for <i>T. usneoides</i> , observed at simulation point 3.5 for the planting scenario 1	112
Figure 53: The change in depth (m) of the groundwater level at simulation point 1.1	114

Figure 54: The change in depth (m) of the groundwater level at simulation point 1.2.....	114
Figure 55: The change in depth (m) of the groundwater level at simulation point 1.3.....	115
Figure 56: The effectiveness of the mature trees over the simulation period, for simulation point 1.1....	115
Figure 57: The effectiveness of the mature trees over the simulation period, for simulation point 1.2....	116
Figure 58: The effectiveness of the mature trees over the simulation period, for simulation point 1.3....	116
Figure 59: The performance (%) of scenarios, at points 1.1 to 1.3, compared with scenario 1 & 2.....	118
Figure 60: The change in depth (m) of the groundwater level at simulation point 1.4.....	118
Figure 61: The change in depth (m) of the groundwater level at simulation point 1.5.....	118
Figure 62: The effectiveness of the mature trees over the simulation period, for simulation point 1.4....	119
Figure 63: The effectiveness of the mature trees over the simulation period, for simulation point 1.5....	119
Figure 64: The performance (%) of scenarios compared with 1 & 2 at simulation points 1.4 and 1.5....	120
Figure 65: The change in depth (m) of the groundwater level at simulation point 1.6.....	121
Figure 66: The effectiveness of the mature trees over the simulation period, for simulation point 1.6....	122
Figure 67: The performance (%) of scenarios compared with scenarios 1 & 2, at simulation point 1.6..	123
Figure 68: The change in depth (m) of the groundwater level at simulation point 1.7.....	123
Figure 69: The effectiveness of the mature trees over the simulation period, for simulation point 1.7....	124
Figure 70: The performance (%) of scenarios compared with scenarios 1 & 2, at simulation point 1.7..	125
Figure 71: The change in depth (m) of the groundwater level at simulation point 2.1	126
Figure 72: The change in depth (m) of the groundwater level at simulation point 2.2.....	126
Figure 73: The change in depth (m) of the groundwater level at simulation point 2.3.....	126
Figure 74: The effectiveness of the mature trees over the simulation period, for simulation point 2.1....	127
Figure 75: The effectiveness of the mature trees over the simulation period, for simulation point 2.2....	127
Figure 76: The effectiveness of the mature trees over the simulation period, for simulation point 2.3....	128
Figure 77: The performance of scenarios, at simulation point 2.1 to 2.3, compared with scenarios 1 & 2	129
Figure 78: The change in depth (m) of the groundwater level at simulation point 2.4.....	129
Figure 79: The change in depth (m) of the groundwater level at simulation point 2.5.....	130
Figure 80: The effectiveness of the matured trees over the simulation period, for simulation point 2.4..	130
Figure 81: The effectiveness of the mature trees over the simulation period, for simulation point 2.5....	131
Figure 82: The mean performance of scenarios 3/4 and 5/6 as a percentage of the mean performance in scenarios 1/2, at simulation point 2.4 and 2.5	132
Figure 83: The change in depth (m) of the groundwater level at simulation point 2.6.....	132
Figure 84: The change in depth (m) of the groundwater level at simulation point 2.7.....	133
Figure 85: The effectiveness of the mature trees over the simulation period, for simulation point 2.6....	133

Figure 86: The effectiveness of the mature trees over the simulation period, for simulation point 2.7....	134
Figure 87: The performance (%) of scenarios, at simulation point 2.6 and 2.7, when compared with scenarios 1 & 2.....	135
Figure 88: The change in depth (m) of the groundwater level at simulation point 3.1	136
Figure 89: The change in depth (m) of the groundwater level at simulation point 3.3.....	136
Figure 90: The change in depth (m) of the groundwater level at simulation point 3.5.....	137
Figure 91: The effectiveness of the mature trees over the simulation period, for simulation point 3.1....	138
Figure 92: The effectiveness of the mature trees over the simulation period, for simulation point 3.3....	138
Figure 93: The effectiveness of the mature trees over the simulation period, for simulation point 3.5....	138
Figure 94: The performance of scenarios, at simulation point 3.1, 3.3 and 3.5, when compared with scenarios 1 & 2.....	140
Figure 95: The change in depth (m) of the groundwater level at simulation point 3.2.....	140
Figure 96: The change in depth (m) of the groundwater level at simulation point 3.4.....	141
Figure 97: The effectiveness of the mature trees over the simulation period, for simulation point 3.2....	142
Figure 98: The effectiveness of the mature trees over the simulation period, for simulation point 3.4....	142
Figure 99: The effectiveness of the mature trees over the simulation period, for simulation point 3.4....	142
Figure 100: The performance of scenarios, at simulation point 3.2 and 3.4, compared with scenarios 1 & 2	143
Figure 101: The overall average change in groundwater level observed for the planting scenarios across all simulation points.....	143
Figure 102: The impacts planting scenario 1 had on the groundwater level within the core focus area of the study site	144
Figure 103: The impacts planting scenario 2 had on the groundwater level within the core focus area of the study site	146
Figure 104: The impacts planting scenario 3 had on the groundwater level within the core focus area of the study site	147
Figure 105: The impacts planting scenario 4 had on the groundwater level within the core focus area of the study site	148
Figure 106: The impacts planting scenario 5 had on the groundwater level within the core focus area of the study site	149
Figure 107: The impacts planting scenario 6 had on the groundwater level within the core focus area of the study site	150
Figure 108: The location of the two transects used for the SO ₄ concentration analysis	151
Figure 109: The SO ₄ concentrations, below ground (mbgl), for the current scenario at point 1.1	152

Figure 110: The SO ₄ concentrations, below ground (mbgl), for the future scenario 1 at point 1.1	153
Figure 111: The SO ₄ concentrations, below ground (mbgl), for the scenario 2 at point 1.1	154
Figure 112: The SO ₄ concentrations, below ground (mbgl), for the scenario 3 at point 1.1	155
Figure 113: The SO ₄ concentrations, below ground (mbgl), for the scenario 4 at point 1.1	156
Figure 114: The SO ₄ concentrations, below ground (mbgl), for the scenario 5 at point 1.1	157
Figure 115: The SO ₄ concentrations, below ground (mbgl), for the scenario 6 at point 1.1	158
Figure 116: The correlation between the SO ₄ concentrations and the water content for scenario 4 at point 1.3	159
Figure 117: The SO ₄ concentrations, below ground (mbgl), for the current scenario at point 1.2	160
Figure 118: The SO ₄ concentrations, below ground (mbgl), for the scenario 1 at point 1.2	161
Figure 119: The SO ₄ concentrations, below ground (mbgl), for the scenario 2 at point 1.2	162
Figure 120: The SO ₄ concentrations, below ground (mbgl), for the scenario 3 at point 1.2	163
Figure 121: The SO ₄ concentrations, below ground (mbgl), for the scenario 4 at point 1.2	163
Figure 122: The SO ₄ concentrations, below ground (mbgl), for the scenario 5 at point 1.2	164
Figure 123: The SO ₄ concentrations, below ground (mbgl), for the scenario 6 at point 1.2	165
Figure 124: The SO ₄ concentrations, below ground (mbgl), for the current scenario at point 1.3	166
Figure 125: The SO ₄ concentrations, below ground (mbgl), for the scenario 1 at point 1.3	167
Figure 126: The SO ₄ concentrations, below ground (mbgl), for the scenario 2 at point 1.3	168
Figure 127: The SO ₄ concentrations, below ground (mbgl), for the scenario 3 at point 1.3	169
Figure 128: The SO ₄ concentrations, below ground (mbgl), for the scenario 4 at point 1.3	170
Figure 129: The SO ₄ concentrations, below ground (mbgl), for the scenario 5 at point 1.3	171
Figure 130: The SO ₄ concentrations, below ground (mbgl), for the scenario 6 at point 1.3	171
Figure 131: The SO ₄ concentrations, below ground (mbgl), for the current scenario at point 2.1	172
Figure 132: The SO ₄ concentrations, below ground (mbgl), for the scenario 1 at point 2.1	173
Figure 133: The SO ₄ concentrations, below ground (mbgl), for the scenario 2 at point 2.1	173
Figure 134: The SO ₄ concentrations, below ground (mbgl), for the scenario 3 at point 2.1	174
Figure 135: The SO ₄ concentrations, below ground (mbgl), for the scenario 4 at point 2.1	175
Figure 136: The SO ₄ concentrations, below ground (mbgl), for the scenario 5 at point 2.1	175
Figure 137: The SO ₄ concentrations, below ground (mbgl), for the scenario 6 at point 2.1	176
Figure 138: The SO ₄ concentrations, below ground (mbgl), for the current scenario at point 2.2	177
Figure 139: The SO ₄ concentrations, below ground (mbgl), for the scenario 1 at point 2.2	177
Figure 140: The SO ₄ concentrations, below ground (mbgl), for the scenario 2 at point 2.2	178
Figure 141: The SO ₄ concentrations, below ground (mbgl), for the scenario 3 at point 2.2	179
Figure 142: The SO ₄ concentrations, below ground (mbgl), for the scenario 4 at point 2.2	179

Figure 143: The SO ₄ concentrations, below ground (mbgl), for the scenario 5 at point 2.2	180
Figure 144: The SO ₄ concentrations, below ground (mbgl), for the scenario 6 at point 2.2	180
Figure 145: The SO ₄ concentrations, below ground (mbgl), for the current scenario at point 2.3	181
Figure 146: The SO ₄ concentrations, below ground (mbgl), for the scenario 1 at point 2.3	182
Figure 147: The SO ₄ concentrations, below ground (mbgl), for the scenario 2 at point 2.3	182
Figure 148: The SO ₄ concentrations, below ground (mbgl), for the scenario 3 at point 2.3	183
Figure 149: The SO ₄ concentrations, below ground (mbgl), for the scenario 4 at point 2.3	184
Figure 150: The SO ₄ concentrations, below ground (mbgl), for the scenario 5 at point 2.3	185
Figure 151: The SO ₄ concentrations, below ground (mbgl), for the scenario 6 at point 2.3	185
Figure 152: The change in groundwater flow rate (m ³ /sec) observed for each scenario across the simulation period for simulation point 3.1	187
Figure 153: The change in groundwater flow rate (m ³ /sec) observed for each scenario across the simulation period for simulation point 3.5	188
Figure 154: Direction of groundwater flow within the core study site	189
Figure 155: Sulphate mass flux (g/m ² /s), for simulation point 3.2, for the current scenario and scenario 1	190
Figure 156: Sulphate mass flux (g/m ² /s), for simulation point 3.2, for the current scenario and scenario 2	190
Figure 157: Sulphate mass flux (g/m ² /s), for simulation point 3.2, for the current scenario and scenario 3	191
Figure 158: Sulphate mass flux (g/m ² /s), for simulation point 3.2, for the current scenario and scenario 4	191
Figure 159: Sulphate mass flux (g/m ² /s), for simulation point 3.2, for the current scenario and scenario 5	192
Figure 160: Sulphate mass flux (g/m ² /s), for simulation point 3.2, for the current scenario and scenario 6	192
Figure 161: Sulphate mass flux (g/m ² /s), for simulation point 3.4, for the current scenario and scenario 1	193
Figure 162: Sulphate mass flux (g/m ² /s), for simulation point 3.4, for the current scenario and scenario 2	193
Figure 163: Sulphate mass flux (g/m ² /s), for simulation point 3.4, for the current scenario and scenario 3	194
Figure 164: Sulphate mass flux (g/m ² /s), for simulation point 3.4, for the current scenario and scenario 4	194

Figure 165: Sulphate mass flux ($\text{g/m}^2/\text{s}$), for simulation point 3.4, for the current scenario and scenario 5	195
Figure 166: Sulphate mass flux ($\text{g/m}^2/\text{s}$), for simulation point 3.4, for the current scenario and scenario 6	195
Figure 167: Diagram of the true nature of deep rooted trees (<i>E. marginata</i>) rooting system.....	199
Figure 168: The future planting scenario one (left) and scenario two (right)	B2
Figure 169: The future planting scenario three (left) and scenario four (right)	B2
Figure 170: The future planting scenario five (left) and scenario six (right).....	B2
Figure 171: The decreasing trend of Scenarios 3 and 4 for simulation point 1.1	C2
Figure 172: The decreasing trend of Scenarios 5 and 6 for simulation point 1.1	C2
Figure 173: The decreasing trend of Scenarios 3 and 4 for simulation point 1.2	C3
Figure 174: The decreasing trend of Scenarios 5 and 6 for simulation point 1.2	C3
Figure 175: The decreasing trend of Scenarios 3 and 4 for simulation point 1.3	C4
Figure 176: The decreasing trend of Scenarios 5 and 6 for simulation point 1.3	C4
Figure 177: The decreasing trend of Scenarios 3 and 4 for simulation point 1.4	C5
Figure 178: The decreasing trend of Scenarios 5 and 6 for simulation point 1.4	C5
Figure 179: The decreasing trend of Scenarios 3 and 4 for simulation point 1.5	C6
Figure 180: The decreasing trend of Scenarios 5 and 6 for simulation point 1.5	C6
Figure 181: The decreasing trend of Scenarios 3 and 4 for simulation point 1.6	C7
Figure 182: The decreasing trend of Scenarios 5 and 6 for simulation point 1.6	C7
Figure 183: The decreasing trend of Scenarios 3 and 4 for simulation point 1.7	C8
Figure 184: The decreasing trend of Scenarios 5 and 6 for simulation point 1.7	C8
Figure 185: The decreasing trend of Scenarios 3 and 4 for simulation point 2.1	C9
Figure 186: The decreasing trend of Scenarios 5 and 6 for simulation point 2.1	C9
Figure 187: The decreasing trend of Scenarios 3 and 4 for simulation point 2.2	C10
Figure 188: The decreasing trend of Scenarios 5 and 6 for simulation point 2.2	C10
Figure 189: The decreasing trend of Scenarios 3 and 4 for simulation point 2.3	C11
Figure 190: The decreasing trend of Scenarios 5 and 6 for simulation point 2.3	C11
Figure 191: The decreasing trend of Scenarios 3 and 4 for simulation point 2.4	C12
Figure 192: The decreasing trend of Scenarios 5 and 6 for simulation point 2.4	C12
Figure 193: The decreasing trend of Scenarios 3 and 4 for simulation point 2.5	C13
Figure 194: The decreasing trend of Scenarios 5 and 6 for simulation point 2.5	C13
Figure 195: The decreasing trend of Scenarios 3 and 4 for simulation point 2.6	C14
Figure 196: The decreasing trend of Scenarios 5 and 6 for simulation point 2.6	C14

Figure 197: The decreasing trend of Scenarios 3 and 4 for simulation point 2.7	C15
Figure 198: The decreasing trend of Scenarios 5 and 6 for simulation point 2.7	C15
Figure 199: The decreasing trend of Scenarios 3 and 4 for simulation point 3.1	C16
Figure 200: The decreasing trend of Scenarios 5 and 6 for simulation point 3.1	C16
Figure 201: The decreasing trend of Scenarios 3 and 4 for simulation point 3.2	C17
Figure 202: The decreasing trend of Scenarios 5 and 6 for simulation point 3.2	C17
Figure 203: The decreasing trend of Scenarios 3 and 4 for simulation point 3.3	C18
Figure 204: The decreasing trend of Scenarios 5 and 6 for simulation point 3.3	C18
Figure 205: The decreasing trend of Scenarios 3 and 4 for simulation point 3.4	C19
Figure 206: The decreasing trend of Scenarios 5 and 6 for simulation point 3.4	C19
Figure 207: The decreasing trend of Scenarios 3 and 4 for simulation point 3.5	C20
Figure 208: The decreasing trend of Scenarios 5 and 6 for simulation point 3.5	C20

List of Tables

Table 1: The Manning's n and m values for the various ground covers (Morgan, 1995)	39
Table 2: The various management scenarios being modelled	43
Table 3: The sources of all data used for the MIKE SHE simulations	43
Table 4: The options chosen for the precipitation rate sub-module	50
Table 5: The missing data gaps in the hourly rainfall data	51
Table 6: The LAI and root depth for the current land use types found in the study site (Canadell <i>et al.</i> , 1996; Dye <i>et al.</i> , 2006; Dye <i>et al.</i> , 2008).....	55
Table 7: The settings selected for the Richards Equation Unsaturated Flow module.....	59
Table 8: The dominant soil profiles found within the study site (Potgieter and Calitz, 2005)	63
Table 9: The soil profiles for Profile C and D on the west side of the TSF.....	64
Table 10: The hydraulic conductivities for each geological units found at the study site (AngloGold Ashanti, 2011a).....	66
Table 11: The geological properties for all the geological units of the study site (AngloGold Ashanti, 2011a)	66
Table 12: The descriptions of the available outer boundary conditions (DHI Software, 2007)	69
Table 13: The descriptions of the available internal boundary conditions (DHI Software, 2007)	71
Table 14: The properties of the Schoonspruit River (DHI Software, 2007)	77
Table 15: The available boundary conditions available (DHI Software, 2007).....	80
Table 16: The available boundary types for open boundary conditions	80
Table 17: The components set for the advection dispersion module	83
Table 18: The maximum and minimum ET uptake factor for the plant species	86
Table 19 : The future scenarios ET uptake factor (Mntungwa et al., 2014)	86
Table 20: The planting scenarios for the future woodlands	87
Table 21: The LAI for the future scenario simulations.....	88
Table 22: The calculated hydraulic conductivities for the soils.....	98

Table 23: The soil profiles observed from the test pits	99
Table 24: The results of the Scholander pressure chamber system tests	101
Table 25: The original vs. calibrated input values for the hydraulic conductivity.....	108
Table 26: The highest final change that occurred at simulation points 1.1 to 1.3.....	117
Table 27: The highest final change observed at simulation points 1.4 and 1.5	120
Table 28: The highest final change that occurred at simulation points 1.6.....	122
Table 29: The highest final change that occurred at simulation points 1.7.....	124
Table 30: The highest final change observed at simulation points 2.1 to 2.3	128
Table 31: The highest final change observed at simulation points 2.4 and 2.5	131
Table 32: The highest final change that occurred at simulation points 2.4 and 2.5	134
Table 33: The highest final change observed at simulation points 3.1, 3.3 and 3.5	139
Table 34: The highest final change observed at simulation points 3.2 and 3.4	141
Table 35: The MIKE SHE input data for the Simulation Specification Module	A1
Table 36: The MIKE SHE input data for the <i>Water Quality Simulation Specification Module</i>	A4
Table 37: The MIKE SHE input data for the <i>Species Module</i>	A5
Table 38: The MIKE SHE input data for the <i>Model Domain and Grid Module</i>	A5
Table 39: The MIKE SHE input data for the <i>Topography Module</i>	A6
Table 40: The MIKE SHE input data for the <i>Climate Module</i>	A6
Table 41: The MIKE SHE input data for the <i>Land Use Module</i>	A7
Table 42: The MIKE SHE input data for the <i>River and Lakes Module</i>	A7
Table 43: The MIKE SHE input data for the <i>Overland Flow Module</i>	A10
Table 44: The MIKE SHE input data for the <i>Unsaturated Flow Module</i>	A10
Table 45: The MIKE SHE input data for the soil profiles definitions	A11
Table 46: The MIKE SHE input data for the <i>Saturated Zone Module</i>	A12
Table 47: The MIKE SHE input data for the original geological units	A13
Table 48: The MIKE SHE input data for the calibrated geological units	A13

Table 49: The MIKE SHE input data for the <i>Water Quality Sources Module</i>	A13
Table 50: The MIKE SHE input data for the <i>Storing of Results Module</i>	A14

Abbreviations

AGA	-	AngloGold Ashanti
AMD	-	Acid Mine Drainage
DEAT	-	Department of Environmental Affairs and Tourism
DEM	-	Digital Elevation Model
DRIT	-	Double Ring Infiltrometer Test
DMR	-	Department of Mineral Resources
DWAF	-	Department of Water Affairs and Forestry
EIA	-	Environmental Impact Assessment
EMP	-	Environmental Management Plan
ET	-	Evapotranspiration
IDW	-	Inverse Distance Weighting
LAI	-	Leaf Area Index
MWP	-	Mine Woodlands Project
RT	-	Reference evapotranspiration
RD	-	Rooting Depth
SAWS	-	South African Weather Service
SZ	-	Saturated Zone
TSF	-	Tailing Storage Facilities
UV	-	Ultraviolet
UZ	-	Unsaturated Zone
WQ	-	Water Quality

1 Introduction

South Africa has one of the most sophisticated mining industries in the world, and was the largest producer of gold in the world up until 2007 (Kruger, 2008). The Witwatersrand Basin Goldfields (WBG), which is situated in the north-central part of South Africa, has been mined for gold since 1886 (Robb and Meyer, 1995; Rosner and van Schalkwyk, 2000). In 1886, gold was extracted from the coarsely-crushed ore using mercury amalgam but, since 1915 when mining reached more extreme depths, pyritic ore was encountered and mercury amalgam was deemed inefficient. Since 1915, gold has been extracted with cyanide (Tutu *et al.*, 2008). Due to the extensive and long-term mining within the WBG, a large volume of gold mine waste has been produced. In South Africa, roughly 450 million tonnes of waste are produced annually, with 70% of this waste being generated by the mining industry. Of this waste the WBG is responsible for 23% (AngloGold Ashanti, 2004; AngloGold Ashanti, 2011a). Gold mining waste is considered to be the single largest source of pollution and waste in South Africa (Oelofse *et al.*, 2007). The waste produced from gold mining is stored in rock dumps, sand dumps and tailings dams. The waste found in the tailings dams is the most common form of waste produced during gold mining. The use of hydraulic transportation of waste by pipelines to disposal sites is the most commonly used method of transport as it is the most cost effective means of solids transportation (Rosner and van Schalkwyk, 2000; Oelofse *et al.*, 2007).

The WBG covers an area of approximately 25 000 km² and is roughly 350 km in length, running from north-east to south-west, and approximately 150 km wide (AngloGold Ashanti, 2004; Tutu *et al.*, 2008; Dye and Weiersbye, 2010). There are seven major gold fields within the WBG, which have produced approximately 45 000 tonnes of gold and 150 000 tonnes of uranium (Robb and Meyer, 1995). The former accounts for 35% of all the gold mined across the globe (Robb and Meyer, 1995). Since the beginning of mining within the WBG, there have been approximately 6 billion tonnes of waste produced, which have mostly been stored in tailing storage facilities (TSF) and their footprints cover between 400 – 500 km² of the WBG and have resulted in an artificially raised groundwater table and contamination of streams, soil, sediments

and groundwater (Rosner and van Schalkwyk, 2000; Dye *et al.*, 2008; Dye and Weiersbye, 2010).

The TSFs within the WBG are major sources of pollution, and have been acknowledged as the most costly environmental problem being faced by the mining industry (Sheoran and Sheoran, 2006; Oelofse *et al.*, 2007). As mining in South Africa plays a central role in the economic, political and social environment, the regulation of the dumping of mine waste in the past was not strictly monitored, nor was it environmentally sound (Sheoran and Sheoran, 2006). Relatively low pH water has been recorded close to the TSFs, indicating the escape of Acid Mine Drainage (AMD) from the tailings dams and into the groundwater system of the region (Rosner and van Schalkwyk, 2000; Tutu *et al.*, 2008). AMD is produced when sulphide-bearing material is exposed to oxygen and water (Akcil and Koldas, 2006). The adverse effects of AMD include contamination of groundwater and surface water with elevated levels of cyanide and trace elements such as Cu, Co, Cd, Cl, Fe, Im, Mn, Pb, Ra, S, U and Zn (Rosner and van Schalkwyk, 2000; Tutu *et al.*, 2008). AMD is also responsible for degradation of soil quality, introducing harmful heavy metals and large quantities of salts that harm aquatic flora and fauna, and allowing these metals to seep into the surrounding environment (Winde and Sandham, 2004; Akcil and Koldas, 2006; Oelofse *et al.*, 2007; Adler *et al.*, 2007).

In Section 24(a) of the South African Constitution, it states that everyone has the right to an environment that is not harmful to his or her health or well-being (Swart, 2003). However, the long-term exposure of humans to AMD does not meet the section 24(a) stipulations, as long-term exposure to water contaminated with AMD has been linked with an increased rate of cancer, decreased cognitive function and the appearance of skin lesions (Oelofse *et al.*, 2007). The Minerals Act of 1991 (Act 50 of 1991) stipulates the legal requirements enforcing the environmental protection, the management of the environmental impacts and the rehabilitation of environments affected by prospecting and mining in South Africa (Swart, 2003). Before the closure of mines, the main requirement of the Department of Minerals Resources (DMR) and the Department of Environmental Affairs & Tourism (DEAT) is that there is an Environmental Management Plan (EMP) in place. The EMP, based on the more commonly known Environmental Impact Assessment (EIA), must be submitted and officially approved before a mine can be granted a closure certificate (Oelofse *et al.*, 2007). A further requirement of DEAT and DMR is that rehabilitation of surface land affected by prospecting or mining, is carried out

by the holder of the prospecting permit and/or the mining authority concerned (Swart, 2003; Adler *et al.*, 2007). The WBG falls mostly within the Highveld Grassland Biome but includes some Savanna vegetation types (Mucina and Rutherford, 2006). With an estimated value of R29 000 per square kilometre of grassland at risk and the other threats to human health from AMD it is understandable why AMD has become such a visible and highly political issue within South Africa of late (AngloGold Ashanti, 2004; Weiersbye and Witkowski, 2007; Oelofse *et al.*, 2007; Dye and Weiersbye, 2010).

Conventional clean up techniques are considered to be extremely expensive, the solutions short-term, and have led to a search for a more creative, cost-effective and environmentally-sound way in which to treat the problem of AMD with regards to TSFs and their surrounding areas (Sheoran and Sheoran, 2006). As AMD follows the pathway of surface and groundwater flow the best way in which the contamination from AMD can be controlled is in the control of the water entry and exit from the gold mine TSF sites (Oelofse *et al.*, 2007). One of the new techniques that has emerged in combating soil and water contamination by AMD is the process of phytoremediation (Cunningham and Ow, 1996).

1.1 Phytoremediation

Phytotechnology and more specifically phytoremediation is the use of plants to immobilize and take up contaminants, essentially to clean up the environment (Pilon-Smits, 2005). Phytoremediation is considered a viable AMD clean-up technique - as the roots of many plants are able to absorb heavy metals and other contaminants from within the soil (phytoabstraction), as well as have the ability to immobilize contaminants in the root zone (phytostabilization), thus reducing the amount of AMD reaching nearby groundwater and river systems (Cunningham and Ow, 1996; Dye *et al.*, 2008; ITRC, 2009; Dye and Weiersbye, 2010).

1.2 Mine Woodlands Project

In the WBG, within the AngloGold Ashanti gold fields properties, the Mine Woodlands Project (MWP) is currently implementing phytoremediation to remediate contaminated soils surrounding the TSF sites, as well as control the seepage of water in and around the TSFs (AngloGold Ashanti, 2004; Dye *et al.*, 2008). The MWP was started in 1996 as a partnership between AngloGold Ashanti (AGA) and the University of the Witwatersrand, with support from the

National Research Foundation (NRF) and the Department of Trade and Industry (DTI), South Africa. The MWP was initiated to meet three primary objectives, namely; to limit the amount the pollution by planting vegetation on tops of the TSFs, to decontaminate and rehabilitate the polluted groundwater and soil around the TSFs and to provide a sustainable solution to the remediation of TSF and surrounding areas (AngloGold Ashanti, 2004; Dye *et al.*, 2008).

The aim of the MWP is to replace the naturally-occurring grasslands and open woodlands with densely planted blocks of deep-rooted trees, with higher leaf areas, a shorter or no dormancy period, and in some species a greater capacity for taking up and sequestering contaminants. The MWP also investigates a wide range of plants for different purposes, for example, the use of indigenous forbs on the TSFs (AngloGold Ashanti, 2004). The MWP team has chosen mainly trees as a remediation tool, as even though they may take over 10 years to reach optimum height, they could be effective for decades, providing a long-term cost-effective remediation of the AMD contamination plume within the area of interest. By establishing woodlands in appropriate areas the evapotranspiration rate of the area can be greatly increased, thereby reducing the flow of water and contaminants into adjacent lands and surface drainage channels, and lowering the groundwater levels.

1.3 Mine Woodlands Project West Complex TSF Trial

Several trials and block plantings of trees within the West Wits, Vaal River and Welkom districts have already been established. Between 2003 and 2008 an estimated 320 hectares of trees were planted (Dye and Weiersbye, 2010). Within the Vaal Reef site, the West Complex tailings dam, which needs urgent remediation, provides a good case study site for determining the effectiveness of phytoremediation as a solution for AMD as there are clear plumes emitting from the western, northern, eastern, and southern sides. This dissertation will focus only on the plume emitting from the western side of the West Complex TSF, which drains towards the Schoonspruit River (Figure 1). To the north-west of the West Complex TSF there are a number of agricultural small holdings, and directly across the river there is a large residential area (Kanana) (Figure 2).

The MWP trial is currently being extended into the western side with the planting of woodlands between the Schoonspruit River and the West Complex TSF (Figure 1). The first blocks of trees that have been established comprise *Searsia lancea*, planted in the 2011/2012 and 2012/2013

planting seasons and the rest of the area will be planted in later phases, possibly comprising additional tree species. The *S. lancea* trees will take eight to ten years before they form a closed canopy and begin to effectively lower the water table of the area and to absorb the contaminants leaching from the TSFs. The development of a mature root system and near-maximum leaf area are critical requirements for optimizing water and contaminant uptake.

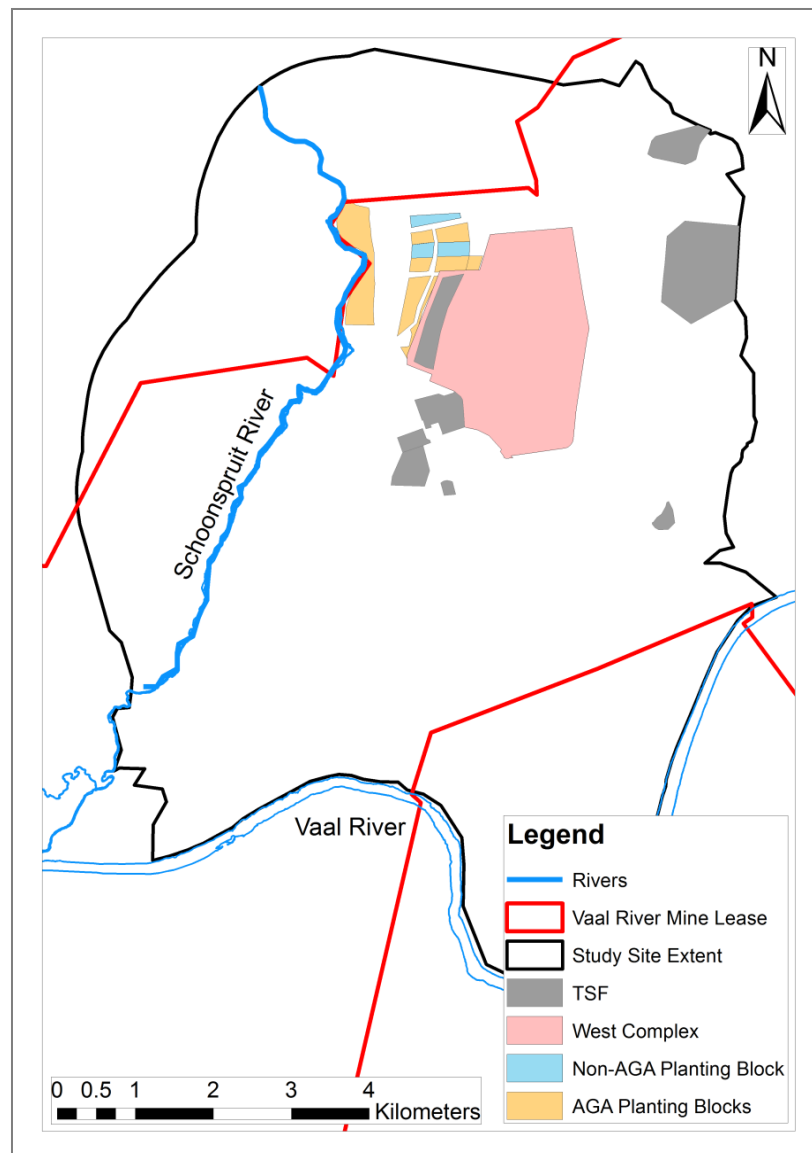


Figure 1: The potential locations of MWP planting blocks to the west of the West Complex TSF

1.4 Aims

This dissertation aims to assess the likely future impacts of phytoremediation woodlands on the storage, transport and discharge of contaminants within a typical contamination plume originating on the western side of the West Complex TSF within the Vaal River mine lease area. Previous studies in the area have mainly considered the groundwater only. By only incorporating the plant uptake of water and contaminants in a very superficial way, these studies did not take into account the rooting depth, leaf area index, evapotranspiration and other characteristics of plants. This dissertation aims to bridge the gap, by considering the entire hydrological cycle (including the unsaturated zone and surface processes), as well as the impacts any trees will have on the groundwater flow to the Schoonspruit River. To achieve this, all the available information was used to create a general hydrological simulation. A hydrological model (MIKE SHE) was used to model two scenarios:

- A current pre-woodland scenario, just existing natural grasslands and old lands.
- A future post-planting scenario simulating the effects of matured woodlands planted in the area.

To model how the various planting options will affect the contamination plume, the model needs to accurately depict the contamination plume moving laterally from the West Complex TSF. Typically AMD is characterized by low pH values, high concentrations of heavy metals such as lead, zinc, manganese, iron, aluminium, copper as well as high concentrations of sulphates (Naicker *et al.*, 2003; Sheoran and Sheoran, 2006; Mendez and Maier, 2008). As in an earlier groundwater study conducted in the region (AngloGold Ashanti, 2011a), this dissertation will model only sulphate (SO_4) and use this as an indicator of plume extent and contaminant concentration. This was previously considered to be a reliable method as (1) SO_4 is a major species in the West Complex TSF plume. The TSFs found in the Vaal Reef mine lease area typically have greater than 0.7% pyrite, (2) SO_4 do not decay over time, and (3) SO_4 are soluble and therefore are readily available for plant uptake. Therefore, by limiting the monitoring of the impacts of phytoremediation to only SO_4 concentrations within the soil, subsoil and groundwater, the general effects of phytoremediation on the plume as a whole will be shown.

1.5 Objectives

The objectives of this dissertation were as follows:

- Gather relevant datasets from various sources to set up MIKE SHE for the study area. There was a large amount of data available from AngloGold Ashanti and consultant reports. These described topography, geology, soil profiles, water table depths, vegetation cover, evapotranspiration, trenches and berms, climate data and groundwater chemical composition.
- Estimate the rate of groundwater flow across the study area.
- Estimate the depth at which tree roots can take up groundwater.
- Simulate water and contaminant (SO_4) movement in a current pre-woodland scenario. Other possible changes brought about by the vegetation, such as changes in carbon, nutrient and redox conditions, were not included within this project, but are recommended for further research.
- Simulate water and contaminant (SO_4) movement in a future mature woodland scenario. This included simulating different planting and management options. Again, the scope was necessarily limited to exclude the many other potential soil changes brought about by the trees.
- Draw conclusions on the eventual impacts the woodlands have on the contamination plume.

2 Study Site

The specific site (Figure 1) investigated for this dissertation lies in the western section of the AGA Vaal River mine lease in the Orkney District and is centred on the West Complex TSF dam (Figure 2).

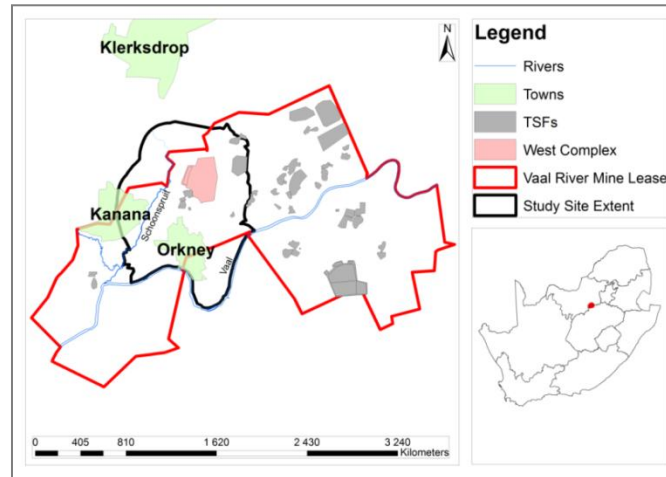


Figure 2: The location of the study site within the Vaal River mine lease area

2.1 West Complex Tailings Dam Area

The areas surrounding the West Complex TSF have mainly seasonally-dormant shallow-rooted grasslands with some trees, reed-beds and shrubs found within run-off and seepage zones (Dye *et al.*, 2008; Dye and Weiersbye, 2010). Tree distribution is also determined by the location of sinkholes, as well as where they have been manually planted. Natural woodland development is inhibited by veld fires and low rainfall (Dye *et al.*, 2008; Dye and Weiersbye, 2010).

The contamination plume originating from the West Complex TSF is characterized by elevated levels of sulphates, chlorides, nitrates, and metals (Dye *et al.*, 2008; AngloGold Ashanti, 2011a; Dye and Weiersbye, 2010). Radionuclides have also been found in the contamination plume (Rosner and van Schalkwyk, 2000).

The West Complex TSF has been extensively researched, and much of the data required to run the MIKE SHE hydrological model was readily available. The main geological units found within the study area are the Ventersdorp Super group, the Black Reef Quartzite Formation and

the overlying Malmani sub-group, which consists of chert-rich and chert-poor dolomites (AngloGold Ashanti, 2005). These geologies act as a hydraulic control, with varying degrees of permeability and porosity, and therefore determine the levels and movements of groundwater in the area. The Black Reef Quartzite is the least permeable, and acts as a barrier to the groundwater. This barrier causes the groundwater to move westwards and eastwards from within the TSF. The Dolomite found at the site is significantly more permeable than the Black Reef Quartzite, however is still less permeable than the Ventersdorp Lava and Alluvium found alongside the Schoonspruit River. Above the Malmani dolomites there are younger geological units which form part of the Transvaal sequence, specifically the Pretoria Group Shale, the Ventersdorp Lavas as well as the Hekpoort Andesites (AngloGold Ashanti, 2003). The geological profile of the West Complex TSF area consists of soil to depths of 2m, weathered dolomite from depths of 2m to 8m, a zone of cavities, which is filled with a soft black earth mass of hydrated manganese oxides as well as iron oxides and occasionally barium or cobalt (AngloGold Ashanti, 2003). The soils of the region are made up of clayey silty sand with residual dolomite, shale or Ventersdorp lavas depending on the area. Borehole data show that water tables in the West Complex TSF area range in depth from 0.2 to 11m below the surface (AngloGold Ashanti, 2005).

The climate of the region is temperate, with short cold winters (May to September) and warm to hot wet summers (October to March). The region predominantly receives its rainfall within the summer months, consisting of more than 60% of the annual rainfall (Rosner and van Schalkwyk, 2000; Herbert, 2008 and Tutu *et al.*, 2008). The annual rainfall range for the area is between 404 – 988mm, the average rainfall is 657mm, the average potential evaporation rate is 1780mm, and the annual evapotranspiration rate is approximately 566mm (Rosner and van Schalkwyk, 2000; Tutu *et al.*, 2008; Dye *et al.*, 2008). For this region the mean number of frost days is 34 (Herbert, 2008). The West Complex TSF was first deposited in the 1950s and is currently at a height of approximately 30m above ground level. A trench along the western side of the West Complex TSF has been acknowledged as slowing the amount of contaminants that are leaking into the neighbouring land (AngloGold Ashanti, 2011b). Using the MIKE SHE model, the plume that is currently emerging west of the TSFs was recreated showing the pathway through the Ventersdorp Lava and some dolomite, and onwards to the Schoonspruit River as well as the Ariston plots area to the north (AngloGold Ashanti, 2011b).

3 Literature Review

The global population is rapidly increasing, putting a significant strain on the water resources of the world (Graham and Butt, 2005). The shortage being experienced around the world is aggravated by the lack of coordinated governance (Adler *et al.*, 2007), with most countries having several different departments responsible for the governance of the water within the country's borders. However, water cannot be treated in such an isolated manner (Graham and Butt, 2005). Mining industries are one of the biggest water polluters around the world, with Acid Mine Drainage (AMD) being recognized as the most difficult pollution to manage within the surrounding regions of the mining mine waste deposits (Sheoran and Sheoran, 2006; Oelofse *et al.*, 2007). AMD is one of the major forms of pollution from mine waste deposits across the globe. With an expected loss of 80% of useable property in the regions surrounding tailings storage facilities (TSFs) due to mining activities, pressure from politicians, environmentalists and the public, has been put on the mining industry to curb AMD pollution and to remediate contaminated soils (Weiersbye and Witkowski, 2007). AMD does not only affect the land of an area, AMD is also responsible for the pollution of surface and groundwater, as well as human health issues (Oelofse *et al.*, 2007; Dennis *et al.*, 2008).

3.1 Acid Mine Drainage

The creation of AMD occurs when sulphides within the deposited material, or other waste products, are exposed to oxygen or water. Once the sulphide has been exposed to oxidizing conditions, an acidic sulfate-rich drainage is created. Sources of AMD vary from seepage out of waste deposits, surface and underground mine works to ponds (Oelofse *et al.*, 2007). The type of heavy metal contamination of AMD depends on the type and amount of sulphides, as well as the type of rock or soil in the waste (Akcil and Koldas, 2006; Oelofse *et al.*, 2007). AMD within South Africa is characterised by elevated concentrations of sulphates, chlorides, nitrates, metals and naturally occurring radionuclides, and cyanide in some cases (Winde and Sandham, 2004; Dye *et al.*, 2008; Tutu *et al.*, 2008). AMD is also characterised by low pH readings, high electrical conductivity and has a reddish brown colour (Oelofse *et al.*, 2007).

The effects of AMD on the surrounding regions are vast. Not only does it contaminate the soil and water but AMD also affects the fauna, flora and humans in these regions (Truong, 2000; Oelofse *et al.*, 2007). These effects are not necessarily localized to the immediate surrounding areas as the contaminants that enter the water system will affect areas downstream from the TSFs (Weiersbye and Witkowski, 2007). Contamination of groundwater within the region has a variety of implications, firstly, the effects on the organisms living within the rivers and streams of the region. Secondly, AMD contaminates the drinking water of animals and humans. Continued exposure of humans to water contaminated by AMD has been proved to lead to serious health issues, including increased rates of cancer, decreased cognitive function and skin lesions (Sheoran and Sheoran, 2006; Oelofse *et al.*, 2007). AMD is not the only source of pollution from TSF, wind pollution and surface water pollution also occurs. Wind pollution, or dust pollution, is caused by the wind blowing the loose sand from the tops and sides of the TSF, and spreading these particulates into the surrounding areas. Surface water pollution is caused by the surface run-off from rainfall events washing the loose sand, and contaminates, from the TSFs away into the surrounding areas and down into the groundwater (Truong, 2000).

3.2 Potential solutions for AMD

Due to government criteria which must be met before any closure of mines is allowed, the need to neutralize AMD and the remediation of the contaminated groundwater and soil of the region surrounding the TSFs is of great importance to the mining industry (Dye and Weiersbye, 2010). AMD can be easily neutralized by using chemicals such as lime, calcium, carbonates or caustic soda (Sheoran and Sheoran, 2006). However, such neutralizing of AMD can lead to more environmental problems than originally experienced. This may happen because adding a base to AMD can produce a sludge that will need to be removed and more than likely, require additional costs (Sheoran and Sheoran, 2006; Weiersbye and Witkowski, 2007). Therefore, purely neutralizing the AMD is not only a more expensive and impractical solution but is also considered impossible due to the vast amounts of wastes that are produced from mining activities globally (Truong, 2000). Several other techniques for remediation of contaminated soil and groundwater include; (1) Leaching of the pollutants by flushing a contaminated area with water, and then recovering the leachate and treating it on-site - this is again considered to be an expensive solution (Truong, 2000; Barcelo and Poschenrieder, 2003). (2) Excavation or storage

of wastes at more appropriate sites. (3) Electro-kinetical treatment, where heavy metals in the soil migrate towards the electrodes that have been placed in the soil. (4) Vitrification, the use of thermal energy for soil fusion which allows for physical or chemical stabilization (Barcelo and Poschenrieder, 2003). These are in theory all viable methods but, due to the vast amount of waste generated annually by mining companies, most of these methods are deemed non-viable due to the high volume and cost of the remediation (Barcelo and Poschenrieder, 2003). These methods are all considered to be short-term solutions and it has been accepted that the problem being faced with AMD, within South Africa, will still be a problem for years after the mines have been closed (Oelofse *et al.*, 2007). Therefore, there is a need for a longer-term and more cost-effective solution.

3.3 Phytoremediation

Phytoremediation is considered to be one of the possible long-term solutions to controlling AMD seepage from TSFs and the remediation of contaminated soil and groundwater (Cunningham and Ow, 1996). In the early 1990s, the idea of using plants to clean or decrease the toxicity of solids, surfaces and waste waters contaminated by metals, organics, xenobiotics, explosives and radionuclides was first introduced (Barcelo and Poschenrieder, 2003). The first field studies researching the use of plants to remediate contaminated soil was conducted in Woburn, Britain, where researchers used hyperaccumulators (both herbaceous and woody plant species) that accumulate and tolerate high levels of metals in their roots (McGrath *et al.*, 1993; Baker *et al.*, 1994). Phytoremediation technologies are based on the use of hyperaccumulator, as well as accumulator species, as their roots can absorb higher levels of metal contaminants and immobilize greater variety of pollutants such as sulphur and heavy metals, than most other non-accumulator plants.

3.4 Types of Phytoremediation

There are numerous ways in which these plants are used within the phytoremediation process. For example, some plants are just used to absorb the metal contaminants from the soil, while other forms of phytoremediation use plants to control the flow of water in and out of the contaminated sites (Brooks *et al.*, 2001). The different processes include: (1) phytoextraction, (2) phytostabilisation, (3) phytoresaturation, (4) phytovolatilization, (5) phytodegradation, (6) phytodesalination and (7) phytohydraulics. Of these techniques the technique that has been

found to be the most useful and commonly used to combat AMD is phytoextraction (Ali *et al.*, 2013).

(1) Phytoextraction is the removal of elements, such as salts and heavy metals, from the soil by plants (Garbisu and Alkorta, 2000; Brooks *et al.*, 2001; Barcelo and Poschenrieder, 2003; Hooda, 2007; ITRC, 2009; Ali *et al.*, 2013). The removal of these elements involves the use of metal accumulating plants, whereby the elements are removed from the soil through by the plant's roots and then transported to the shoots of the plants, where the metals accumulate (Barcelo and Poschenrieder, 2003; Hooda, 2007; ITRC, 2009; Ali *et al.*, 2013). In some instances the plants are harvested (known as phytomining) for the valuable heavy metals when the soil in the area has met regulatory levels (Flathman and Lanza, 1998; Barcelo and Poschenrieder, 2003; Hooda, 2007). Research has shown that plants most suitable for phytoextraction tend to have higher than average growth rates, produce more above-ground biomass and a higher shoot-root ratio. They also tend to have highly branched root systems, a high tolerance to heavy metals, and are unappetizing to herbivores (Flathman and Lanza, 1998; Hooda, 2007; Ali *et al.*, 2013).

(2) Phytostabilisation is another commonly used technique, using plants to immobilize contaminants in the soil, preventing their entry into groundwater, as well as reducing their bioavailability and movement (Flathman and Lanza, 1998; Barcelo and Poschenrieder, 2003; Batista *et al.*, 2007; Mendez and Maier, 2008; Ali *et al.*, 2013). The focus of phytostabilisation is not the removal of the metal contaminants by the roots of the plants but rather a reduction of the risks to the environment (Batista *et al.*, 2007; Mendez and Maier, 2008; Ali *et al.*, 2013). The common use of the phytostabilisation technique provides an area with a vegetative cap for containment and stabilization of an area. The plant roots provide a water erosion solution as well as immobilization of the metals (Rosselli *et al.*, 2003; Mendez and Maier, 2008; Hooda, 2007). The types of plants required for phytostabilisation are those that are able to withstand drought and high levels of salt and heavy metals. Some studies show that a combination of grasses and trees works best (Hooda, 2007; Mendez and Maier, 2008).

(3) Phytosaturation provides a solution to water and wind erosion, essentially using a fast-growing plant species that provides a contaminated area with high ground coverage, which therefore prevents migration of soil particles by wind and surface water run-off (Barcelo and Poschenrieder, 2003). This technique reduces the overall spread of the contaminant. However for

phytoresaturation to be successful, the soil of the area first needs to be reconditioned (Barcelo and Poschenrieder, 2003).

(4) Phytovolatilization is the use of plants to absorb the pollutants from the soil of the contaminated area. The pollutants are then converted to a volatile form and released into the atmosphere through transpiration from the plant leaves (Barcelo and Poschenrieder, 2003; Hooda, 2007; ITRC, 2009; Ali *et al.*, 2013). Phytovolatilization has been found to be successful for some organic contaminants but only for a few inorganic contaminants (Hooda, 2007; Ali *et al.*, 2013). A disadvantage of phytovolatilization is that it does not remove the contaminants from the system, but merely transfers them from soil to atmosphere, where it can be deposited elsewhere (Ali *et al.*, 2013).

(5) Phytodegradation is another technique that is successful for organic pollutants. Phytodegradation occurs when organic compounds are decomposed within the plant by plant enzymes (Flathman and Lanza, 1998; Barcelo and Poschenrieder, 2003; ITRC, 2009; Ali *et al.*, 2013).

(6) Phytodesalination, perhaps the newest and most recently reported technique of phytoremediation, refers to the use of halophytic plants species that remove salts from soils with high salt contamination. This enables the soil to support normal plant growth (Ali *et al.*, 2013).

(7) Phytohydraulics, also referred to as phytoabstraction, is where plant species with high water usage are planted. These species are normally deep-rooted, evergreen with a high leaf area and are able to absorb large amounts of water, thus lowering the water table and reducing the further lateral spread of pollutants (Barcelo and Poschenrieder, 2003; ITRC, 2009). The possible advantageous effects of phytohydraulics are that it reduces the flow of water and contaminants through shallow aquifers and within the soil horizons into neighbouring lands and surface channels (Dye and Weiersbye, 2010) and significantly increases the rate of evapotranspiration which could, in turn, effectively balance out the rate of seepage from the contaminant source (Dye *et al.*, 2008).

3.5 Case Studies of Phytoremediation Technology

Phytoremediation technologies have been used in a variety of circumstances to control petroleum spillage, pesticide contamination, and acid mine drainage. Previous studies into petroleum

spillage have shown that with the use of phytoextraction, specifically hybrid Poplar trees, there have been an uptake of contaminants into the plant tissues, specifically roots, shoots and leaves (Burken and Schnoor, 1997; Newman *et al.*, 1999). A similar study using Alfalfa showed a decrease in contaminants in the groundwater (Zhang *et al.*, 1998). Similar results are seen in pesticide remediation, with Paterson and Schnoor (1992) recording uptake of Alachlor pesticide into Maize plant tissues with the use of phytoextraction. While a trial study conducted by Schnoor *et al.* (1997) shows a total decrease in Dioxane with the use of Poplar trees.

Studies have also been conducted into the uptake of high concentrations of essential plant elements, such as Copper (Cu), Iron (Fe), Magnesium (Mg), and Zinc (Zn) which are all commonly found heavy metals found in AMD. There are various studies that show the effect of phytoextraction and phytostabilization with regards to Cu. In some of the studies, as much as 1000 mg/kg of Cu can be accumulated in plant tissue and as much as a 70% decrease in solution concentration (Speir *et al.*, 1992; Kumar *et al.*, 1995; Blaylock *et al.*, 1997; Phytotech, Inc., 1997). With regards to Fe uptake in plants through the use of phytoextraction and phytostabilization, there have been recorded uptakes of Fe into plant tissue, ranging from 45 mg/kg to as high as 3709 mg/kg (Kadlec and Knight, 1996; Keiffer and Ungar, 1996). There has been a bigger success in the study of uptake of Mg through phytoextraction and phytostabilization. In some studies there have been recordings of as much as 8260 mg/kg of Mg accumulated in the plant tissues, with the use of Barley and various grasses (Cipollini and Pickering, 1986; Keiffer and Ungar, 1996; Keiffer, 1996). Other successful studies have been conducted showing the ability of Indian mustard plants and Alpine Pennycress plants as well as Hybrid Poplar trees as effective phytoextraction and phytostabilization species for Zn contaminated sites. Studies have recorded Zn accumulation in plant tissues as highly concentrated as 25 000 mg/kg (Kumar *et al.*, 1995; Salt *et al.*, 1995; Blaylock *et al.*, 1997; Hinchman *et al.*, 1997).

The ideal vegetation for phytoremediation would be plants that can grow easily in soils with high concentrations of contaminants and have high rates of soil-to-shoot transfer (Barcelo and Poschenrieder, 2003). For the WBG deep-rooted woody species are the most-effective absorbers of heavy metals and maintain the highest levels of regeneration occurring within the contaminated soils (Weiersbye and Witkowski, 2007). Planting deep-rooted perennials would extract water from their root-zones and then transpire the water to the atmosphere. A result of

this process is that the vegetation will lower the water table and absorb any freshwater that could possibly seep from the TSFs (Demetriou and Punthakey, 1999).

3.6 Advantages of Phytoremediation

Since the first field studies were conducted, the advantages of phytoremediation over other techniques in the remediation of contaminated areas have become much more evident. The major advantages are that the technique is a cost-effective, green technology which uses solar energy and that the remediation occurs in-situ (therefore there are no added costs of having to remove the wastes) (Flathman and Lanza, 1998; ITRC, 2009; Weiersbye, 2010). A demonstration of the cost-effectiveness of phytoremediation over other more conventional techniques has established that phytoremediation costs approximately 10% to 50% less (Cunningham and Ow, 1996; Flathman and Lanza, 1998; Weiersbye, 2010). Another advantage of phytoremediation is that in some instances (phytoextraction and phytomining) the trees used to remediate the soils can generate some income (Hooda, 2007; ITRC, 2009; Ali *et al.*, 2013).

The use of plants has a high acceptance amongst the general public which is due to the fact that plants provide a more aesthetically pleasing alternative to chemical or mechanical treatments (Truong, 2000; Sheoran and Sheoran, 2006; ITRC, 2009). Phytoremediation techniques are one of only a few remediation techniques that can be applied to both organic and inorganic pollutants, as well as being able to remediate a wide variety of combinations of contaminants in a variety of media, i.e. soil, water and atmosphere (ITRC, 2009). A beneficial by-product of phytoremediation is that the plants are effective in erosion and sediment control within the surroundings of the TSFs (Truong, 2000; ITRC, 2009). Another benefit of phytoremediation is that the treatment is non-disruptive to the landscape and to those living in the surrounding areas, and can be extremely effective for large volumes of wastes (Batista *et al.*, 2007). Using natural processes minimizes on-going maintenance and may provide a long-term solution to the problem of AMD (Sheoran, 2005; ITRC, 2009).

3.7 Disadvantages of Phytoremediation

Even though there are many advantages of phytoremediation, there are also some disadvantages. The success of the process relies heavily on the root density and depth of the roots, the salt tolerance of the plant as well as environmental factors such as frost and flooding. The use of

woodlands holds considerable promise but takes many years for the trees to reach maturity to remediate the soil (Cunningham and Ow, 1996; Demetriou and Punthakey, 1999; Truong, 2000; Barcelo and Poschenrieder, 2003). Another disadvantage of phytoremediation is that plants are highly susceptible to damage by fires and attacks by pathogens, especially during periods of drought (Dye and Weiersbye, 2010). An ironic disadvantage is that phytoremediation often calls for the destruction of pre-existing vegetation in the area (Cunningham and Ow, 1996). Due to these limitations, there is a need for caution in the use of phytoremediation. Yet, the benefits may far outweigh these limitations and phytoremediation can be a highly useful, green, cost-effective treatment for the remediation of contaminated soils and groundwater.

3.8 Hydrological Modelling

The demand for water has generated a growing need for a better understanding of the hydrological cycle. With this demand, there has been an increase in the creation and use of hydrological models (Singh *et al.*, 1999; Graham and Butt, 2005). The use of hydrological models is important as it provides the necessary information for decision making concerning the management and use of water and land resources in a watershed, province, country or continent (Singh *et al.*, 1999). Numerical models allow the integration of diverse and complex information pertaining to the hydrological processes. The use of these numerical models allows for scope to analyse a variety of management options that may include a variety of hydrological processes (Demetriou and Punthakey, 1999). Many hydrological models do not include all hydrological processes, but focus on groundwater or surface water, which limits their usefulness in certain applications.

3.9 MIKE SHE

MIKE SHE is one of the leading hydrological models that include all hydrological processes that are affected by land-use change. MIKE SHE can cover all the major processes of the hydrological cycle, including processes for evapotranspiration, overland flow, unsaturated flow, groundwater flow, channel flow and all their possible interactions (Figure 3) (Demetriou and Punthakey, 1999; Singh *et al.*, 1999). MIKE SHE is an advanced hydrological model, and with the use of the MIKE SHE Advection-Dispersion Module describes the flow of water and solutes within a catchment (Refsgaard *et al.*, 1999). A major advantage of MIKE SHE is the way in which it can treat a variety of water management issues with a wide range of temporal and

spatial scales. In other hydrological models, all the hydrological processes are solved using a uniform time step, which could possibly lead to high computational times for large study areas (Demetriou and Punthakey, 1999; Singh *et al.*, 1999; Graham and Butt, 2005; DHI Software, 2007).

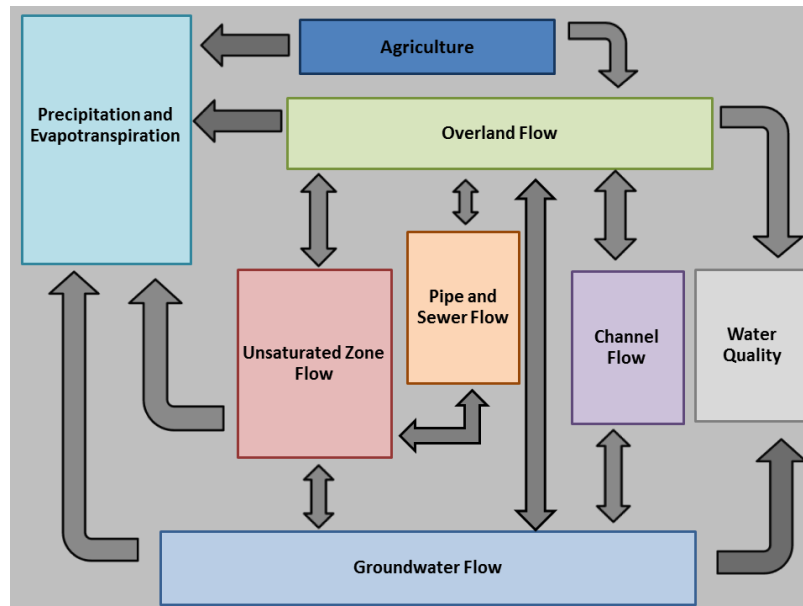


Figure 3: Schematic of the MIKE SHE hydrological modules interactions

MIKE SHE has a variety of different modules that allow users to model the whole hydrological cycle as closely to the user's study site as possible. Some of these modules, which are described below, include; (1) climate, (2) unsaturated flow, (3) overland flow, (4) channel flow, (5) saturated flow and (6) water quality. These are not all the modules offered by MIKE SHE, but generally represent the most important processes within the hydrological cycle.

(1) The climate module simulates the precipitation entering and exiting the area of interest, as well as the evapotranspiration (ET) (Graham and Butt, 2005). Evaporation of water within the study site may be from direct water surfaces, but may also include the evaporation of rainfall that is on leaves, as well as evaporation from the soil (Demetriou and Punthakey, 1999; Graham and Butt, 2005; Cui and Zornberg, 2008). Evaporation within a study region, within the MIKE SHE model, specifically refers to the change of water state from a liquid state to a gas state, or more specifically, water vapour (Allen *et al.*, 1998; Graham and Butt, 2005). When evaporation occurs from the soil surface, the amount of evaporation that occurs depends on the canopy density of the plants in the area, and the amount of water available within the soil (Allen *et al.*, 1998).

Transpiration within the MIKE SHE model refers to the evaporation of water from plant tissue, more specifically the stomata, which are small openings found on the leaf of the plant (Allen *et al.*, 1998). The amount of transpiration that can occur is strongly related to the plant physiology, most notably the depth of the roots, the characteristics of the leaves, and the ability of the plant to absorb water (Graham and Butt, 2005; Cui and Zornberg, 2008; Allen *et al.*, 1998). Therefore, different plants may have different transpiration rates. Evaporation and transpiration are processes that occur at the same time, with little to distinguish between the two, and are measured as one, ET, within the MIKE SHE model (Allen *et al.*, 1998).

(2) The unsaturated flow module within MIKE SHE refers to the soil and sub-soil moisture of the study site. This is of importance within the hydrological cycle, as soil moisture will contribute to the amount of ET that occurs, as well as how much rainfall will be absorbed and how much will become surface run-off. In the MIKE SHE model, unsaturated flow is considered to only occur vertically, due to gravity, and no horizontal movement of water is considered (Demetriou and Punthakey, 1999; DHI Software, 2007). For a user to consider horizontal flow of water, there are a variety of equations within MIKE SHE that will allow the user to implement horizontal flow. However, horizontal flow generally has a very low flow rate.

(3) The overland flow module simulates the movement of surface water that fails to infiltrate into the soil if the soil is fully saturated, or pooling of water that occurs due to lack of infiltration (DHI Software, 2007). MIKE SHE determines the overland flow using information on the topography of the region, as well as the flow resistance. Flow resistance is an important factor when considering the velocity of overland flow. Plants and plant debris can decrease the energy of the overland flow by imparting a degree of roughness to the flow. This roughness in turn decreases the velocity of the overland flow (Morgan, 1995). Most overland flow simulations use the Manning's n to represent roughness. Manning's n allows for the total roughness, that being the roughness of the soil particles, surface microtopography and vegetation combined, to be expressed in one variable. The amount of roughness depends heavily on the plant cover of an area, relying on the density and height of the plants (Chorley, 1971; Morgan, 1995).

Typical values for Manning's n can be seen in Table 1. The overland flow module within MIKE SHE uses Manning's m . Manning's m is the inverse of the Manning's n value and is related to

Sticklers roughness coefficient (Tegelhoffova, 2010). The lower the Manning's m value is, the higher the turbulence and the greater the decrease in the velocity of the overland flow.

Table 1: The Manning's n and m values for the various ground covers (Morgan, 1995)

LAND USE OF COVER	MANNING'S N	MANNING'S M
Bare Soil	0.010 – 0.049	100 – 20.42
Bermuda Grass – sparse to good cover	0.015 – 0.480	66.67 – 2.08
Natural Rangeland	0.100 – 0.320	10 – 3.13
Concrete or asphalt	0.010 – 0.013	100 – 76.92
Gravelled surface	0.012 – 0.030	83.33 – 33.33

Detention storage is another factor taken into account within the overland flow module. Overland flow in a region can only occur once the detention storage, or sometimes known as depression storage, is exceeded (Morgan, 1995). The term detention storage refers to the amount of water that is needed to “fill” the depressions in the microtopography in the area of interest (Chorley, 1971). In normal situations, detention storage can absorb up to 5mm of rainfall in a storm event, and this value does not change with the amount of rainfall received, but rather by the characteristics of the soil and surface of the area (Chorley, 1971). Clay soils have less infiltration that occurs within the soil, meaning less rain needs to fall to fill up the depressions. While sandy soils allow for more infiltration and therefore need more rain than clay soils do to fill up the depressions of the same region. The MIKE SHE overland flow module also takes into account the loss of water in overland flow due to evaporation and infiltration within the study area (Demetriou and Punthakey, 1999; Graham and Butt, 2005).

(4) The channel flow in MIKE SHE uses another model that the DHI Company has produced, MIKE 11. MIKE 11 allows users to give an accurate depiction of a 1D model of the river or stream that may lie within the study site (Graham and Butt, 2005).

(5) Finally, the saturated groundwater flow module calculates the subsurface flow of water within the catchment (Demetriou and Punthakey, 1999). The groundwater flow of a region plays an important role within the regions hydrological cycle, as during times of drought, groundwater flow can sustain streams (Graham and Butt, 2005).

Even though MIKE SHE is a powerful and highly useful model, there are some disadvantages that normally cause difficulties/deterrents for users. The first disadvantage is that MIKE SHE

requires a large amount of data, which for some regions are unavailable, or are of extremely high cost (Graham and Butt, 2005). The second disadvantage is the complexity of MIKE SHE which could cause there to be a high execution time, and finally, MIKE SHE could cause a possible over-parameterized description of simple applications (Graham and Butt, 2005). Even with all these disadvantages, the case study conducted by Demetriou and Punthakey (1999) as well as others show the potential strengths of using MIKE SHE with regard to the management of water.

3.10 Case Studies of MIKE SHE

3.10.1 Case Study in the Gyeongacheon Watershed, South Korea

A case study was conducted using MIKE SHE to determine the effects changes in land use would have on the Gyeongacheon watershed hydrology, which is situated near Seoul in current day South Korea (Im *et al.*, 2009). The model was used to assess the changes in land use from 1980 to 2000 (Im *et al.*, 2009). Satellite imagery was used to model the changes that occurred specifically between February 1980, April 1990 and May 2000. This was to show the changes from non-urban areas to urbanized areas resulting from urban sprawl (Im *et al.*, 2009). The 1980 model was set up with the mainly forest land use, the 1990 model was set up with a decreased forest area and finally the 2000 model was set up with mainly urban areas as land use, with little to no forests (Im *et al.*, 2009). The models were set up using the relevant land uses while the remaining parameters were kept constant, and a repeated rainfall period was used to ensure that the effects of climate variability would not introduce errors (Im *et al.*, 2009). The results from the model showed that there was an increase in run off of 10% between 1980 and 1990, and a further 15% increase between 1990 and 2000 (Im *et al.*, 2009). Further results showed a decline in the evapotranspiration in area from 521mm in 1980 to 503mm in 2000 (Im *et al.*, 2009). This showing case study supports previous perceptions that urbanization increases surface run off, decreases groundwater recharge and reduces evapotranspiration (Im *et al.*, 2009).

3.10.2 Case Study in New South Wales, Australia

The case study by Demetriou and Punthakey (1999) was conducted in Australia, to look at possible groundwater management options available to combat the rising water table and subsequent land salinization that is occurring within the New South Wales territory. The MIKE

SHE integrated model was used to determine if the current pumping of groundwater into an evaporation basin was an effective management option (Demetriou and Punthakey, 1999). The MIKE SHE model was used to compare historical conditions (1987 to 1995) as well as predictive conditions (1995 to 2020) to determine the environmental impact the current management option was having (Demetriou and Punthakey, 1999). A variety of scenarios were set up to test the various management options, specifically; the implementation of an on-farm recycling pond, use of deep rooted perennials, tree planting, and the use of pumps. For the various management options, various needs were trying to be met. By implementing an on-farm recycling pond the hope is that any excess surface run-off from precipitation and any excess water from irrigation would collect in these ponds. To simulate this management option the pond was set up as a leakage point into the water table.

The hope was that by using deep-rooted perennials the groundwater of the area would be extracted into the root zone (phytoextraction) and then this excess water would be released into the atmosphere through transpiration from the tree leaves (Demetriou and Punthakey, 1999). To model this management option, the rooting depth of the summer crops was increased from 0.5m in depth to 2m. The management option of tree planting was chosen as an option to capture possible excess water from the irrigation of the area. To simulate this option a simple implementation of using pumps to represent the extraction of water by plants was used (Demetriou and Punthakey, 1999). The final management option for the case study was to use pumping within the area to extra the salty groundwater and deposit it in evaporation basins, in the hopes of slowing or possible reversing the rising groundwater. This option was set up using an additional 48 pumps in the area, and extracting water (Demetriou and Punthakey, 1999).

With the use of MIKE SHE for these various management options, it was shown that on-farm recycling and additional pumping into evaporation basins were the best performers in slowing the rising water table (Demetriou and Punthakey, 1999). This case study and previous case study (Im *et al.*, 2009; Zhang *et al.*, 2009) show the power of using MIKE SHE to predict impacts of current land use options, as well as the possible future predictions on the impacts of other management options might have an area. Not only is MIKE SHE a powerful predictive model, but it can also be used to measure change that has occurred historically, such as in the case study of Im *et al.* (2009).

4 Methodology

4.1 MIKE SHE Simulation Scenarios

The MIKE SHE hydrological model describes a full range of hydrological processes which include rainfall, runoff, ponding, infiltration, evapotranspiration, storage in the unsaturated zone (UZ), recharge of the saturated zone (SZ), water table levels, root growth, root water uptake, lateral movement of groundwater, contaminant concentrations and transport. To determine the effects that woodlands under various management regimes have on the contamination plume originating from the West Complex TSF, a number of model scenarios were run. Firstly, the current scenario, from 2001 to 2010, was run using all available past data and data gained from fieldwork in this study.

Once the current scenario had been set-up, the model was then calibrated against known groundwater level data to ensure the most accurate depiction of the current situation. Once calibration was complete, the current scenario model was run to get final results for the current scenario for comparisons against the future scenario simulations. The next step was to run the various planting options in six separate tree-planting scenarios (Table 2). These future simulations were based on a mixture of current scenario parameter values and inputs (climate, soil, topography, etc.) and future scenario values of mature woodland parameters such as leaf area index, rooting depth and land use change within the MIKE SHE set up. The future scenarios were run for a nine-year period, showing the effects the fully matured trees will have on the contamination plume. The 2001 – 2010 climatic data were merely repeated for these years, as the period to mature woodland establishment is too short to reflect climate changes (Im *et al.*, 2009). The woodland set-up specifications, rooting depth, leaf area index and land use, were all modelled using data from previous research in the MWP (AngloGold Ashanti, 2003; AngloGold Ashanti, 2005; Potgieter and Calitz, 2005; Weiersbye and Witkowski, 2007; AngloGold Ashanti, 2009; AngloGold Ashanti, 2011a). For the remaining model inputs, a variety of sources provided appropriate values and these are shown in Table 3. The scenarios and associated model inputs will be discussed in greater depth in the following sections.

Table 2: The various management scenarios being modelled

SCENARIOS	MANAGEMENT OPTIONS	EFFECTS TO SIMULATE
Current Scenario	Modelling of the study site as it currently is.	To compare with the future scenarios.
Future Scenario 1	<i>Tamarix usneoides</i> planted up to 5m groundwater contour, <i>S. lancea</i> planted in the potential planting blocks shown in Figure 168, in AGA land and Private property.	The effects of the hyperaccumulators trees on the contamination plume.
Future Scenario 2	<i>T. usneoides</i> planted up to 5m groundwater contour, <i>Eucalyptus dunnii</i> planted in the potential planting blocks shown in Figure 168, in AGA land and private property.	The effects of the deep rooted trees on the contamination plume.
Future Scenario 3	<i>S. lancea</i> planted in the potential planting blocks shown in Figure 169, in AGA land and Private property. No <i>T. usneoides</i> planted.	The effects of <i>T. usneoides</i> on the contamination plume entering the Schoonspruit River.
Future Scenario 4	<i>Eucalyptus dunnii</i> planted in the potential planting blocks shown in Figure 169, in AngloGold Ashanti land only. No <i>T. usneoides</i> planted.	The effects of <i>T. usneoides</i> on the contamination plume entering the Schoonspruit River.
Future Scenario 5	<i>T. usneoides</i> planted up to 5m groundwater contour. <i>S. lancea</i> planted in the potential planting blocks shown in Figure 170, in AngloGold Ashanti land only.	Determine the effect of not establishing woodlands on privately owned blocks of land on the contamination plume.
Future Scenario 6	<i>T. usneoides</i> planted up to 5m groundwater contour. <i>E. dunnii</i> planted in the potential planting blocks shown in Figure 170, in AngloGold Ashanti land only	Determine the effect of not establishing woodlands on privately owned blocks of land on the contamination plume.

Table 3: The sources of all data used for the MIKE SHE simulations

SIMULATION MODULES	DATA REQUIRED	SOURCE OF DATA
Climate	Precipitation Reference evapotranspiration	South African Weather Service (SAWS)
Overland flow	Topography Land use Infiltration rate	AngloGold Ashanti AngloGold Ashanti Mine Woodlands Project/Fieldwork
Vegetation	Tree rooting depth and leaf area index Tree uptake rates of SO ₄ Vegetation water use	Previous research by the Mine Woodlands Project
Unsaturated flow	Soil profiles Soil characteristics	Previous geotechnical reports Fieldwork

Groundwater quality	SO ₄ concentrations Water depth (above sea level)	Borehole Data from AngloGold Ashanti
River System	Water levels Water flow Cross sections	Department of Water Affairs

4.2 Current Scenario

4.2.1 Display Module

There are some general set-up properties that need to be defined. The first set-up option in MIKE SHE models is the *Display module*. In this sub-module the user chooses how many objects to show, and then for each object, which kind of object the user wants i.e. image, shapefile, river, well or grid. For this study, there are three objects added, the three being shapefiles using a LO27 coordinate system. The shapefiles include the Schoonspruit River, the TSF and the Vaal River mine lease area. These are all overlain, and then displayed, as seen in Figure 4.

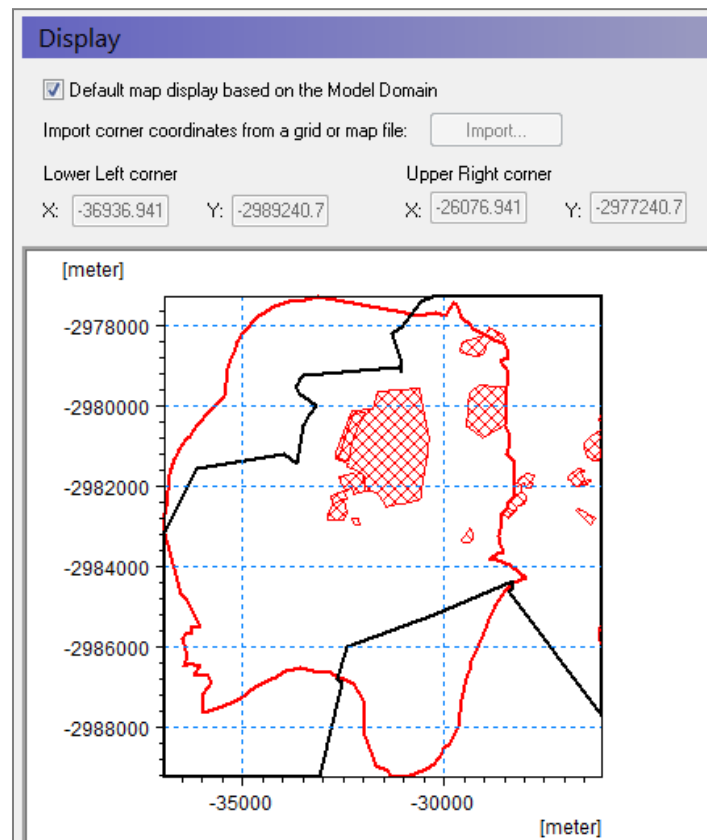


Figure 4: The *display module* set-up

4.2.2 Simulation Specification Module

In this module the user sets the parameters for the following settings: which modules to include in the simulation, the simulation title, the simulation period, the time step control and the various computational control parameters for the necessary modules. For the current scenario, the following modules were used: *Overland Flow*, *Unsaturated Flow*, *Evapotranspiration*, *River and Lakes*, *Saturated Flow* and *Water Quality modules*. The set-up parameters for each of these modules are discussed fully in the discussed below. The title for this simulation was “Current Scenario”. The simulation period was set with a start date of 1st January 2001 and an end date of 31st January 2010.

Once the simulation period and the simulation title were defined, the next parameter to set was the *time step control* options. Here the user sets the necessary *time steps* for each of the modules used within the model. For the current scenario the *time step controls* were all left as the default values, as seen in Figure 5. The defaults were deemed sufficient time steps for the model. The computational control parameters for each of the modules were also left as default values.

The image shows a software interface titled "Time step control". It contains three main sections with expandable/collapsible headers. The first section, "Time Steps", is expanded and shows four parameters: "Initial time step" (0.5 hrs), "Max allowed OL time step" (2 hrs), "Max allowed UZ time step" (12 hrs), and "Max allowed SZ time step" (24 hrs). The second section, "Increment of reduced time step length", is collapsed. The third section, "Parameters for Precipitation-dependent time step control", is also collapsed. The interface uses a light blue header bar and grey collapsible headers.

Time step control		
Time Steps		
Initial time step	0.5	[hrs]
Max allowed OL time step	2	[hrs]
Max allowed UZ time step	12	[hrs]
Max allowed SZ time step	24	[hrs]
Increment of reduced time step length		
Increment rate (0-1)	0.05	
Parameters for Precipitation-dependent time step control		
Max precipitation depth per time step	10	[mm]
Max infiltration amount per time step	10	[mm]
Input precipitation rate requiring its own time step	0.1	[mm/hr]

Figure 5: The default settings used for the time step control

4.2.3 Water Quality Simulation Specification

Before starting the set-up of the *Water Quality (WQ) module*, the user needs to define the *WQ simulation specifications*, which include similar options to the model simulation specifications. These options include: the *WQ simulation title*, *WQ simulation period* and the *WQ time step control*. The *WQ simulation title* was simply set as “Sulphate Water Quality Simulation for the Current Scenario”. The *WQ simulation period* was set to the same period used for the model, specifically from the 1st January 2001 until the 29th January 2010. The *WQ time step control* options were all left as default values (Figure 6). The user can select which processes of the hydrological cycle will affect the water quality. For this dissertation the focus was the subsurface movement of the SO₄ plume from the TSF. WQ would therefore be affected by the *Unsaturated Flow*, the *Evapotranspiration*, *River and Lakes* and the *SZ*. The *include water quality processes* option allows the model to specify decay in the hydrological processes such as *Overland Flow* and the sorption and decay of chemical species in the *SZ* and *Unsaturated Flow*. For this dissertation the *include water processes option* was not selected as SO₄ does not decay with time and was deemed to be outside the scope of this dissertation (AngloGold Ashanti, 2011a).

Water Quality Time Step Control			
	Saturated Zone (SZ)	Unsaturated Zone (UZ)	Overland (OL)
Max. Simulation time step:	1000000000	1000000000	1000000000 [hrs]
Max. Advective Courant Number:	0.8	0.8	0.8 [-]
Max. Dispersive Courant Number:	0.5	0.5	0.5 [-]
Max. Transport Limit:	0.95	0.95	0.95 [-]
Max. Macropore Courant Number :		0.8	[-]

Figure 6: The default settings used for the WQ time step control

4.2.3.1 Species (Chemical) Module

Within the *Species Module* a database was created containing all the chemical species being included within the model, together with their physical properties. For this dissertation, the only chemical species considered was SO₄. The type of species needed to be specified, which either can be set as *dissolved* or *sorbed*. *Dissolved* type species are chemical species that are mobile in the groundwater, while the *sorbed* type species are chemical species that are fixed to the soil matrix (DHI Software, 2007). For this dissertation the focus was the SO₄ found in the groundwater and therefore the *dissolved* type was selected. The next setting to be specified was the *ET uptake factor*. The *ET uptake factor* is defined as a chemical species factor and refers to the uptake of SO₄ by plants (DHI Software, 2007). Within MIKE SHE this factor cannot be defined for each plant species or even different spatial areas, a single value was given for all the plants across the whole study site. The *ET uptake factor* used for this dissertation had to be an average of the minimum and maximum values over all the plant types used in the individual scenarios. The *ET uptake factor* was calculated using the concentration factor equation which can be seen in Equation 1. For the current scenario the *ET uptake factor* was set as zero, as the current plants have little to no effect on the SO₄ concentrations within the study site.

$$\text{Concentration Factor} = \frac{\text{Concentration of Sulphate in foliage}}{\text{Concentration of sulphate in ground water}} \quad (\text{Eq. 1})$$

4.2.4 Model and Domain Module

In this sub-module the domain for the model was defined. This was to set the boundaries of the study area to be used within the MIKE SHE model. For the current scenario, the extent of the study site was defined by a shapefile (see Figure 7). This extent was chosen to allow the software to accurately model the hydrological cycle within the core area. The actual area of interest for the dissertation was the small section of land found between the West Complex TSF and the Schoonspruit River. However, the extent of the study site was selected along hydrological boundaries to ensure the model would accurately model the water movement within the area of interest. MIKE SHE required a buffer zone around the study site to ensure edge effects won't affect the output results within the core area. To create the polygon of the study site, there were a number of steps that had to be undertaken. The catchments of the Vaal River mine lease area, provided by AGA, were introduced into ARCGIS. These catchments however ended right along the Schoonspruit River, and so there was no buffer zone. Therefore, to simulate a realistic

boundary, which would provide a large enough buffer zone, on the north western side a simple polyline was drawn along the upper edge of the catchments along the Schoonspruit River. This can be seen in Figure 4.2-4 in red. Within ARCGIS, a buffer was created from the polyline using a distance of 1800m. This buffer was only created to the north west of the line. The 1800m distance was chosen to ensure that the study site extent boundary would be equidistance, from the centre of the West Complex TSF, throughout the study site. Therefore it provided the necessary buffer zone. Once the buffer was created, a polygon was created around the buffer along the western and northern sides.

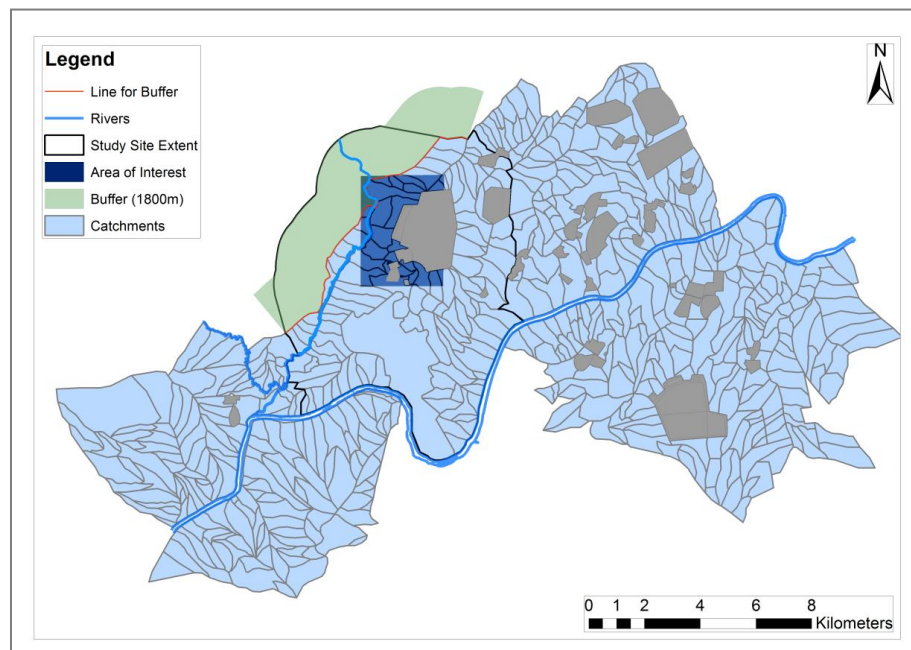


Figure 7: The extent of the study site and the core focus area

For the eastern side of the study site the polygon was drawn along the catchment boundaries which define a natural watershed. For the southern side the Vaal River was selected as the extent, as the Vaal River is a “no outflow” river at this stage. The Vaal River at this section has a high flow volume and little to no seepage out of the Vaal River and into the surrounding soils and/or geologies. The use of the Vaal River provided a realistic and simplistic outflow boundary to be modelled for the study site (Figure 7). The model domain was superimposed by a grid containing 300 cells horizontally and 399 cells vertically, with a cell size of 30m by 30m.

4.2.5 Topography Module

The topography of the area was introduced into MIKE SHE in the form of a 5m Digital Elevation Model (DEM). The elevation data were provided by AGA, in the form of spot heights and contour lines. The DEM first needed to be created within ARCGIS. This was performed using the TOPO to RASTER tool within ARCGIS. Contours (0.25m) as well as spot heights were used as input for the DEM. The DEM was created using a 5m resolution. Once the projection (LO27 Cape) had been given to the DEM it was then converted into an ASCII file and then brought into the MIKE ZERO Toolbox. With the use of the grid to MIKE tool, the ASCII file was converted into a .dfs2 file. This was then imported into the MIKE SHE model. The final image of the DEM within MIKE SHE can be seen in Figure 8. The red in the image shows the areas of higher elevation, while the darker green shows area with lower elevations. Given that the study site was on such a small scale, the use of a 5m DEM provided enough detail to ensure overland processes were accurately depicted.

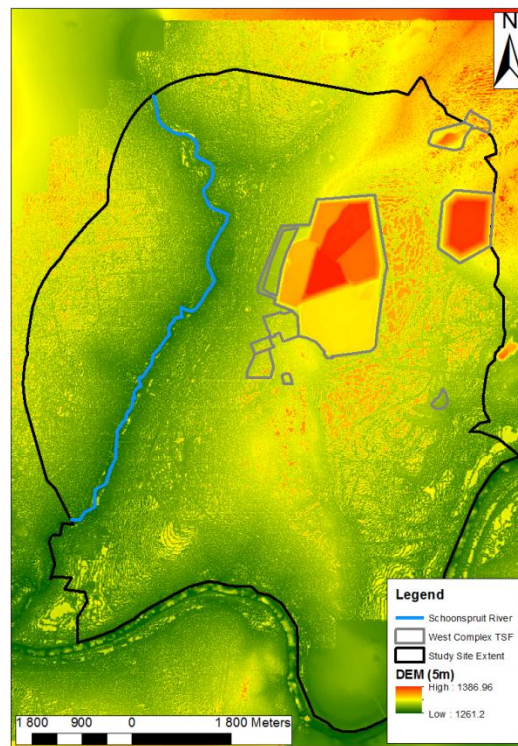


Figure 8: The 5m DEM of the study site, with an overlay identifying the TSFs and the Schoonspruit River

4.2.6 Climate Module

Within MIKE SHE the *Climate Module* was used to input precipitation rate and reference evapotranspiration for the study site for the allocated time frame. The set-up used for the current scenario is given below.

4.2.6.1 Precipitation Rate Sub-Module

For the precipitation data required by MIKE SHE, there were different selection options available. These were: *spatial distribution*, *temporal distribution* and *time series* file. The relevant options used for the current scenario are provided in Table 4 below.

Table 4: The options chosen for the precipitation rate sub-module

BOXES	OPTIONS AVAILABLE	OPTION USED
Spatial Distribution	<ul style="list-style-type: none">• Uniform• Station• Fully Distributed	Uniform
Temporal Distribution	<ul style="list-style-type: none">• Constant• Time Varying (.dfs0)	Time Varying (.dfs0)
Time Series File	<ul style="list-style-type: none">• Create a new file• Use already existing file	Create a new file

For the precipitation data, a new time series file (i.e. dfs0 file) was created to show the rainfall that fell from 1st January 2001 to 29th January 2010. This was accomplished within MIKE SHE, using hourly rainfall data obtained from the SAWS for Klerksdorp (climate Station number: 0436041, coordinates -26.9000, 26.6170). Klerksdorp weather station was chosen as this was the closest (8.21km) SAWS weather station to the study site. The rainfall data were inputted into a new empty .dfs0 file. When creating this file there were two options for type of precipitation data used. Firstly, *precipitation rate* which refers to the rainfall in mm/hr. and secondly, *rainfall* which refers to the rainfall in units of mm/day. The new .dfs0 file used for the current scenario used the *precipitation rate* option. The *precipitation rate* was chosen over the *rainfall* option as the SAWS rainfall data were available as hourly rates. Additionally there was concern in using *the rainfall* option as the method in which MIKE SHE converts the daily readings to hourly readings would not realistically depict the natural rainfall patterns of the area, as rainfall in the area is more sporadic in this region than other regions in the world.

Missing data was evident on some days. To fill in these blanks, rainfall data from a neighbouring station, Potchefstroom (climate Station number: 0437104A4, coordinates: - 26.7330, 27.0670),

was used. Such filling in of gaps in data does introduce a level of error. However there were only 7518 hours of missing data within the nine years (78894 hours), equivalent to 9.53% of the total data record from the Klerksdorp weather station. Of the 7518 hours of missing data, rain was only recorded on 3.33% of those hours at Potchefstroom. Therefore, even though 9.53% is high, the amount of rainfall missed was marginal, which lowers the level of error. However, 0.54% of the missing data was not able to be “filled” as the Potchefstroom weather station also had missing data for these hours. The “filling in” of these dates was done by averaging the rainfall from one day before and after the missing date.

Table 5: The missing data gaps in the hourly rainfall data

YEAR	Number Of Hours Missing From The Klerksdorp Rainfall Data	Amount Rain (Mm) At Potchefstroom In Gap Periods	Missing Hours Missing From The Potchefstroom Rainfall Data
2001	85	4	17
2002	321	18	3
2003	370	0	222
2004	1161	21	22
2005	334	13	1
2006	26	3	0
2007	116	4	0
2008	500	13	27
2009	2373	40	115
2010 (Jan)	2232	134	0
TOTAL	7518	25	407

Table 5 indicates the number of hours of data missing for each year for the Klerksdorp weather station, the amount of rain the Potchefstroom weather station received in those hours, and the number of missing hours of data that were not available from the Potchefstroom or Klerksdorp weather stations. Once the data had been formatted, corrected and inputted, MIKE SHE then produced a graph showing the rainfall pattern across the entire nine year time frame. This graph can be seen in Figure 9. The graph clearly illustrates the seasonal nature of rainfall in the study area.

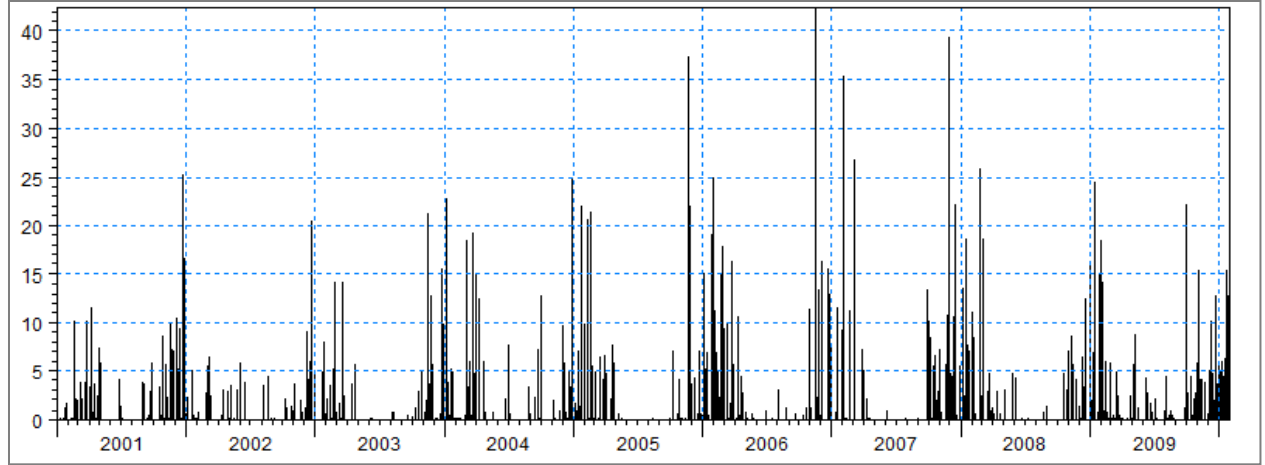


Figure 9: The hourly rainfall (mm) over nine years for the study area

4.2.6.2 Reference Evapotranspiration Sub-Module

MIKE SHE uses meteorological and vegetation data to predict the total amount of evapotranspiration and net rainfall, taking into account interception of rainfall by the canopy, drainage from the canopy to the soil, canopy surface evaporation, soil surface evaporation and the uptake of water by plant roots and plant transpiration (DHI Software, 2007).

The reference evapotranspiration (RT) is the rate of ET from a reference surface (a short, green grass) which has an unlimited availability of water. This is then multiplied by the crop coefficient taken from within the vegetation database (DHI Software, 2007). The *reference evapotranspiration sub-module* has a similar set-up to the *precipitation sub-module*. The same setting choices were made as for the *precipitation sub-module* (Table 4). This set-up resulted in a new time-series file being created for RT for the time frame of the current scenario. The dates used for this file were from January 2001 until January 2010. The RT daily rate was calculated using the FAO Penman-Monteith equation. This equation is widely accepted and used all regions and climates across the globe (Equation 2) (Allen *et al.*, 1998). It allows for the direct calculation of RT (Allen *et al.*, 1998). The equation describes a hypothetical short, green grass reference crop, assuming a height of 0.12m, and a fixed surface resistance of 70 m/sec, and an albedo of 0.23 (Allen *et al.*, 1998). Grass is a well-researched crop and is accepted worldwide as a reference surface even for taller non-grass crops (Allen *et al.*, 1998).

$$ET_o = \frac{0.408\Delta(R_n - G) + \gamma \frac{900}{T + 273} u_2 (e_s - e_a)}{\Delta + \gamma(1 + 0.34u_2)} \quad (\text{Eq. 2})$$

where ET_o is the reference evapotranspiration (mm/day), R_n is the net radiation at the crop surface (W/m^2), G is the soil heat flux density (unitless); T is the mean daily air temperature at 2m height ($^{\circ}C$), U_2 is the wind speed at 2m height (m/sec), e_s the saturation vapour pressure (kPa), e_a the actual vapour pressure (kPa), Δ the slope vapour pressure curve (kPa) and γ is the psychrometric constant ($kPa\ ^{\circ}C^{-1}$) (Allen *et al.*, 1998).

The FAO Penman-Monteith equation requires the following weather data; solar radiation, air temperature, air humidity and wind speed data for the area of interest. All the other parameters were derived from these inputs. Once the RT data were formatted, corrected and inputted into MIKE SHE, a graph was created to show the RT for the simulation period (Figure 10). The graph shows what one would expect, that in the rainy months the RT increases, while in the drier months it decreases. This seasonal pattern was due to lower temperatures, lower solar radiation and shorter days in winter. In some days the daily RT exceeds 10 mm/day, which occurs in the summer months. The zero values show days that there was no evapotranspiration due to cloud and/or rain.

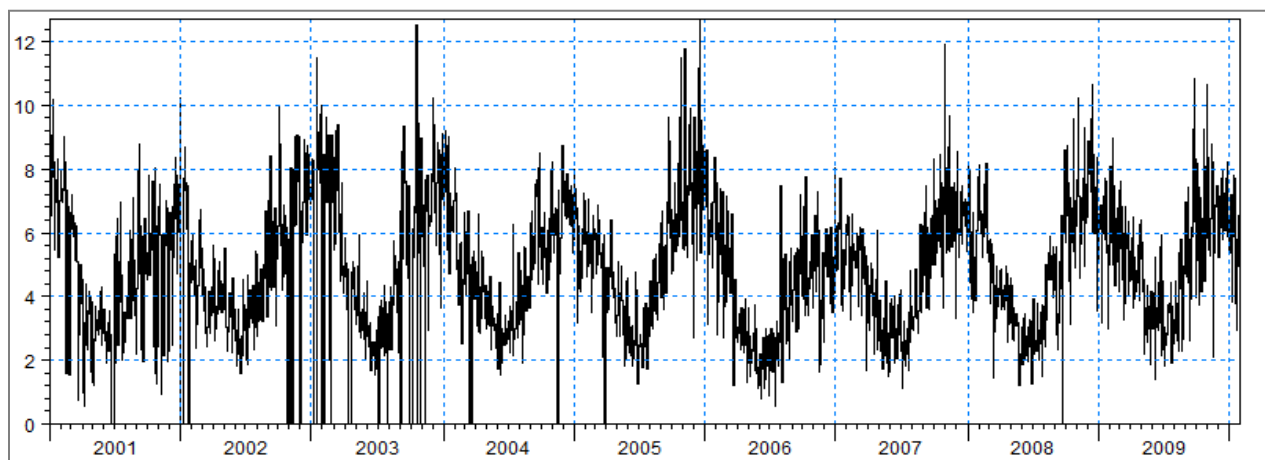


Figure 10: The daily reference evapotranspiration rate (mm/day) for the study area

4.2.7 Land Use Module

MIKE SHE requires that land use be defined for the area of interest. This is important, as it affects the hydrological balance at any given point. If the ground is mainly concrete, or built-up, then there will be little to no infiltration (the majority of the rain that reaches the ground will become run-off). However, if there is mainly vegetation, then infiltration can occur and run-off will decrease. In the study site the vegetation was mostly grassland. The TSF dominant plant

cover on the upper level is *Phragmites*. Therefore, the study site was split into two groups; the grasslands and the plant cover on top of the TSF. The plant cover of the TSF top had three different plants, firstly there were *Phragmites* found in the green polygons (Figure 11). Secondly, there are trees and grasses found in the yellow polygons, and finally the red polygons are considered to be bare ground. The MIKE SHE *Land Use module* requires the *leaf area index* and the *root depth* of the every category of vegetation.

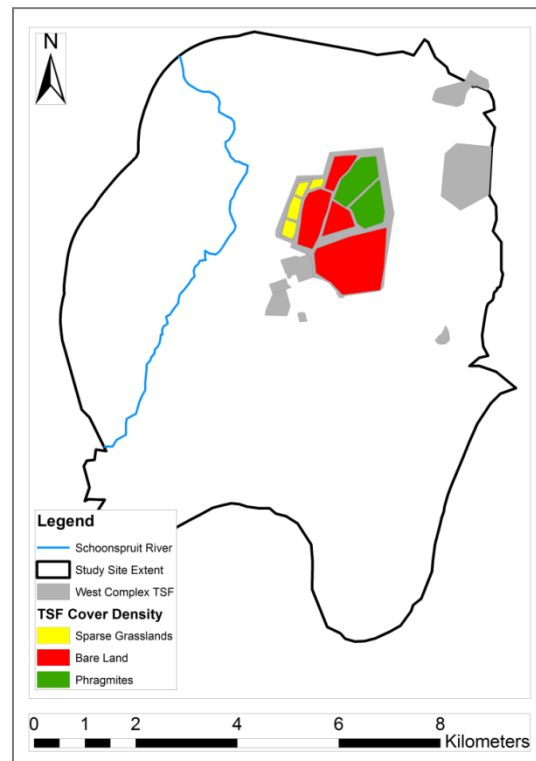


Figure 11: The difference in cover density on the West Complex TSF

4.2.7.1 Leaf Area Index

Leaf Area Index (LAI) is defined as the area of leaves per unit of ground area (DHI Software, 2007). The value of LAI is determined by the plant type, the season, the size/maturity of the plant, and the amount of stress on the plant (DHI Software, 2007). The LAI of a vegetation type is important as it plays a role in the amount of rainfall that reaches the ground, as well as the amount of ET that takes place (Chen *et al.*, 1997). In MIKE SHE simulations, LAI is a lumped value for any grid cell that defines the average leaf area coverage in that cell. In an open space, the LAI is given as an average of all vegetation in that area (DHI Software, 2007). In a forest the LAI includes both the forest canopy LAI and the understory canopy. LAI may be zero for bare

ground, where there is no interception and no water removal from the UZ (DHI Software, 2007). An LAI of between four and six is generally indicative of a 100% plant cover (Chen *et al.*, 2007). The grasslands that cover most of the study site have an LAI that increases to a maximum of approximately 1.2 in the late summer months, and a minimum of zero in the winter months (Dye *et al.*, 2006). The estimated LAI for the land use coverage for this study site can be seen in Table 6 (Canadell *et al.*, 1996; Dye *et al.*, 2006; Dye *et al.*, 2008). These values are used repetitively for all the years in the current scenario. This was implemented due to the fact that the grasslands and reeds show a similar seasonal pattern of development of LAI each year (Canadell *et al.*, 1996; Dye *et al.*, 2006; Dye *et al.*, 2008). Once the seasonal pattern of LAI over the year had been estimated the data was introduced into MIKE SHE, by creating a new .dfs0 file which had two columns; date and LAI.

Table 6: The LAI and root depth for the current land use types found in the study site (Canadell *et al.*, 1996; Dye *et al.*, 2006; Dye *et al.*, 2008)

MONTH	LAI (unitless)				ROOT DEPTH (mm)			
	Surrounding Grassland	TSF Grassland	Phragmites	Bare ground	Surrounding Grassland	TSF Grassland	Phragmites	Bare ground
January	0.75	0.375	6	0	1500	1500	1000	0
February	1.2	0.6	6	0	1500	1500	1000	0
March	1	0.5	4	0	1500	1500	1000	0
April	0.4	0.2	2	0	1500	1500	1000	0
May	0	0	0	0	1500	1500	1000	0
June	0	0	0	0	1500	1500	1000	0
July	0	0	0	0	1500	1500	1000	0
August	0	0	0	0	1500	1500	1000	0
September	0	0	0	0	1500	1500	1000	0
October	0.2	0.1	0.5	0	1500	1500	1000	0
November	0.3	0.15	2	0	1500	1500	1000	0
December	0.5	0.25	4	0	1500	1500	1000	0

4.2.7.2 Root Depth

Within MIKE SHE the rooting depth (RD) refers to the depth below ground (in mm) to which the roots extend. The RD defines the depth at which water can be extracted from within the UZ. The vegetation in the *land use module* needed the RD as well as the LAI. The introduction of the RD of the grasslands was completed in a similar manner as the LAI. A .dfs0 file was created, which included two columns; the date and the maximum RD. As grasslands mostly comprise perennial species, it was assumed that there was no change in their RD from year to year. The main functional difference between surrounding grasslands and TSF grasslands is reduced basal area and biomass in the latter. The graphs for the TSF coverage and the surrounding grasslands

can be seen in Figure 12, Figure 13 and Figure 14 respectively. These graphs show the LAI and the RD on the same set of axis.

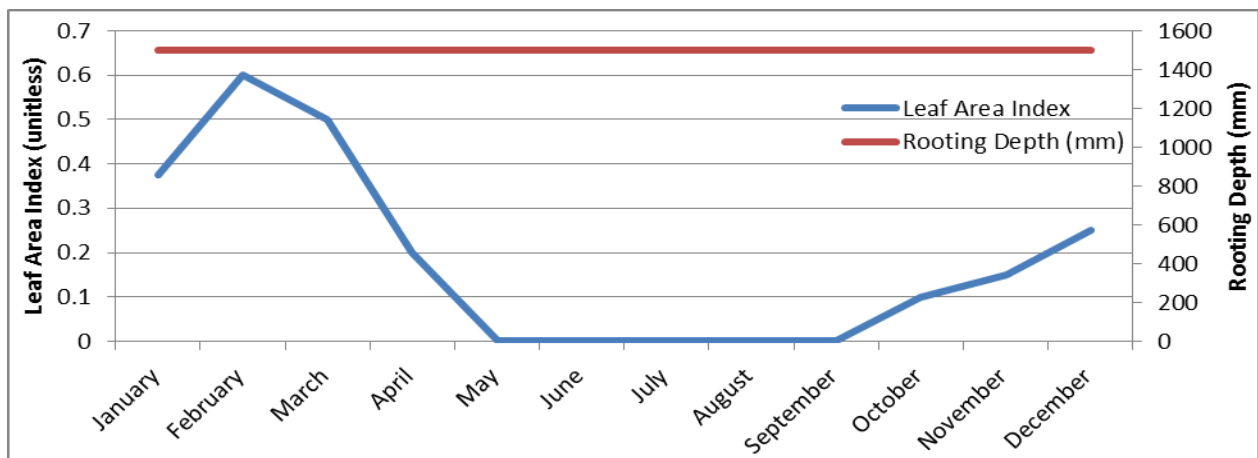


Figure 12: The yearly LAI and RD estimated for the grasslands on top of the TSF

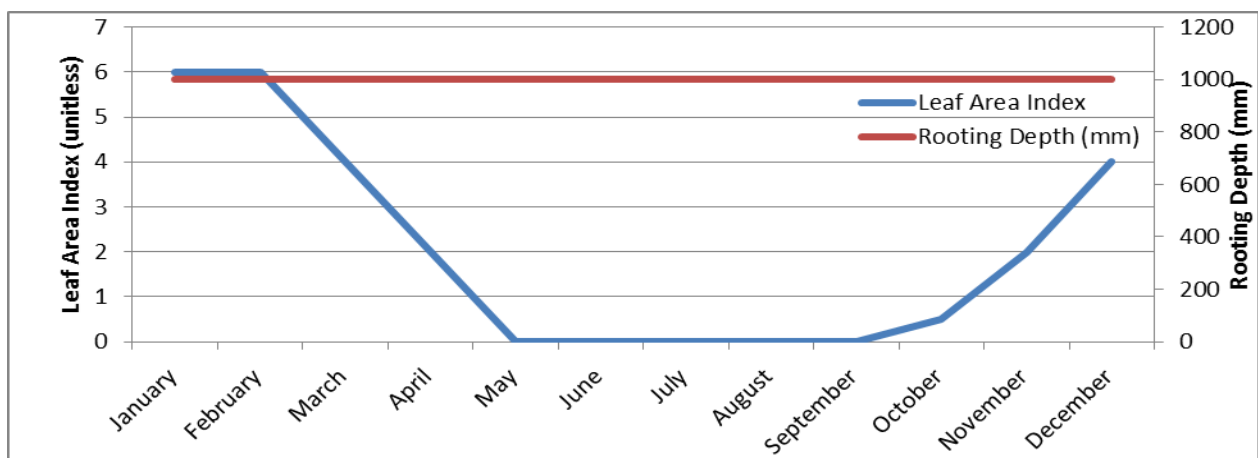


Figure 13: The yearly LAI and RD estimated for the *Phragmites* on top of the TSF

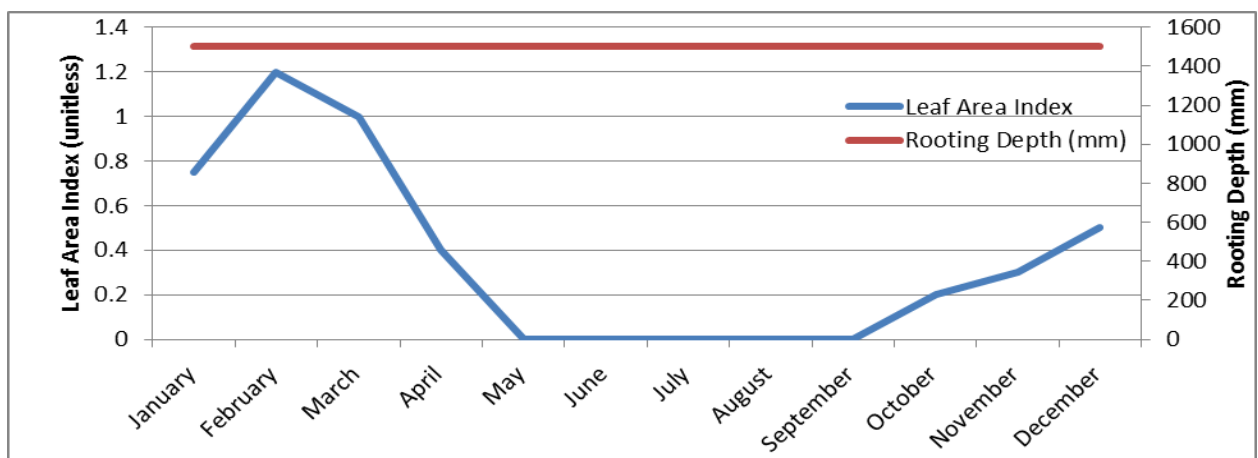


Figure 14: The yearly LAI and RD estimated for the surrounding grasslands

4.2.8 Overland Flow Module

The *Overland Flow module* was where the specifications for the lateral surface runoff to rivers was modelled and is the module that links MIKE SHE with MIKE 11. It models the interactions between the river flow and overland flow. Within this module there were two main options to choose from, namely: the *semi-distributed method* or the *finite difference method*. The *semi-distributed method* is used when modelling larger regional scenarios. The *finite difference method* is used for detailed overland flow for smaller-scale scenarios. For this study site, with an area of 75.45 km², the *finite difference method* was chosen.

Within the *finite difference method* there were a further two options available: *separated overland flow areas* or *overland-groundwater exchange*. *Separated overland flow* allows users to divide the study site into different zones. This is useful if there is an embankment or obstruction in the overland flow. By dividing the overland flow areas into zones, one zone will not be able to flow into another. The *overland-groundwater exchange* allows the user to specify when the unsaturated flow component is inactive. In this option the unsaturated flow component will become inactive when the soil profile of the area is completely saturated. It then allows the *Overland Flow module* component to exchange water with the *SZ module* component directly. This option provides the ability to control the exchange coefficient. For this project the study site was relatively flat and the quality of the DEM ensured an accurate depiction of the topography. Therefore, the need to specify the separated overland flow area was deemed unnecessary and subsequently the *overland-groundwater exchange* option was selected.

Once the *overland-groundwater exchange* option was chosen, there were further options to specify: the *Manning's m number*, *initial water depth* and the *detention storage*. The *Manning's m number* is equivalent to the Stickler roughness coefficient for riverbeds and is the inverse of the more conventional Manning's *n* (Morgan, 1995). Where the Manning's *n* is 0.01 for smooth channels and 0.1 for thickly vegetated channels, the values of the *Manning's m number* is the inverse. For a smooth channel the *Manning's m number* is 100, while for a thickly vegetated channel the *Manning's m number* is 10 (Morgan, 1995). If the *Manning's m number* is set to 0, the overland flow will be effectively switched off. Within the current scenario, the resistance to overland flow in grasslands was judged to be low, so the *Manning's m* was assigned an estimated value of 25. This value was recommended by Morgan (1995) for sparse grassland. The *detention*

storage option is used to limit the amount of water that can flow over the ground surface and reflects the amount of water that is ponded in the area (DHI Software, 2007). The *detention storage* value must be met before any overland flow can occur, this value is set in millimeters. The water trapped in the *detention storage* can still infiltrate to the *UZ*, and can also be used for evapotranspiration. The majority of the topsoil found in the study site had a sandy texture. For sandy soils the detention storage values fall between 2.3mm for farmed land, and 0.02mm for bare land (Morgan, 1995). The *detention storage* of the study site was deemed to be closer to 2.3mm than 0.02mm and therefore was set to 2mm. The final specification to be set was the *initial water depth*. This refers to the initial depth of water on the ground surface. Usually this value is set to 0mm (i.e. there is no water on the ground at the start of the simulation or at the start of a rainfall event). The *initial water depth* is normally set to a higher value if there has been a flood or there is a natural “film” of water constantly on the surface.

4.2.8.1 Initial Sulphate Concentration for the Overland Flow Module

The *initial SO₄ concentration* for the *Overland flow module* was set as zero, as there was little to no surface concentration data available. This was not deemed as a significant factor on the accuracy of the model, as the overland flow is the rainwater that drains over the surface during a rainfall event, and should be little to no SO₄ found within the rain.

4.2.8.2 Dispersion Coefficient along Columns and Rows

For the *Overland Flow module* there was the need to provide the dispersion coefficient for both columns and rows of the simulation grid. This coefficient is used to show how the chemical species being looked at, in this case SO₄, disperses with time (DHI Software, 2007). For these two values, both were set as default which was 0m²/sec. The default value was deemed sufficient as SO₄ have a long decay time that would not be affected within the nine year simulation period (AngloGold Ashanti, 2005).

4.2.9 Unsaturated Flow Module

Within the MIKE SHE *Unsaturated Flow module*, there are various equations which can be used to calculate vertical movement of soil water. For this study site, there was sufficient hydraulic characteristic data available, and therefore the Richards Equation option was chosen as it allows for the most accurate modelling of soil moisture content.

There were various further settings to choose from. These included; calculation column classification type, initial conditions, and macropore flow. Each of these had a variety of choices, and for the current scenario these selections can be seen in Figure 15. In Table 7 these settings are explained in more detail. The next step for the *UZ module* was the introduction of the different soil profiles of the study site. There were a variety of soils within the study site which were introduced through a .dfs2 file, refer to section Soil Profile Definitions 4.2.9.2.

Figure 15: The available options for the *Unsaturated Flow module*

Table 7: The settings selected for the Richards Equation Unsaturated Flow module

OPTION	DESCRIPTION	OPTIONS AVAILABLE	OPTION SELECTED	REASON FOR OPTION SELECTED
The Calculation Column Classification Type	Option to decrease computational time for larger study areas. This is done by changing the grid points used to do calculations in.	<ul style="list-style-type: none"> All grid points Specific grid points Combination of the above two options 	All grid points	The study site area is small, therefore calculations in all grid points were chosen.
Macropore Flow	In some soil types there is a level of flow through macropores. This can cause an impact on the infiltration rates and overland flow.	<ul style="list-style-type: none"> None Simple bypass Macropore flow Full macropore flow 	Simple bypass macropore flow	The level of detail available only allowed for the simple bypass macropore flow option to be selected.

Initial Conditions	This is where the initial soil pressure and water content conditions can be set for the start of the simulation	<ul style="list-style-type: none"> • Equilibrium pressure profile • Specified matrix potential • Specified water content 	Equilibrium pressure profile	The initial conditions were not known for the start of the simulations. The equilibrium pressure profile overcomes this limitation.
--------------------	---	---	------------------------------	---

4.2.9.1 Fieldwork

MIKE SHE required the *hydraulic conductivity* of the soil profiles found in the study area, to indicate the infiltration rates from the ground surface into the topsoil. Saturated hydraulic conductivity (Ksat) of a soil is one of the most important soil characteristics and is a key input requirement for physically-based models that simulate water movement in soil (Parr and Bertrand, 1960). MIKE SHE calculates the unsaturated hydraulic characteristics by using the relationship between the Ksat and the moisture-retention curve of the soils (DHI Software, 2007). There were five soil profiles identified for this site, Dolomite and Sand, Chert Rich Dolomite, soil forming on the Ventersdorp Lava, soil forming on the Black Reef Quartzite and finally the Alluvium profile found along the banks of the Schoonspruit River. The first three soil profiles had been previously studied for geotechnical reports of the area (AngloGold Ashanti, 2005; AngloGold Ashanti, 2011a), and therefore their soil properties such as, soil profile and hydraulic conductivity, were readily available. Descriptive data for the remaining two profiles (Black Reef Quartzite and Alluvial soils) were unavailable, and so infiltration tests were conducted for these soils at the following co-ordinates; Black Reef Quartzite: 26.690831°, -26.9321569° and Alluvial soils: 26.66211°, -26.930961°.

There are a variety of instruments available to measure the hydraulic conductivity of a soil. These include the Boutwell Permeameter, Constant Head Borehole Permeameter, Porous Probes, Guelph Permeameter, Single Ring infiltrometer and Double Ring infiltrometer. There is no single method that is satisfactory for all field conditions. Choice is governed by the availability of funds and equipment, and the precise problem that needs to be solved (Johnson, 1963). The use of ring infiltrometers for infiltration rate studies has been well established (Parr and Bertrand, 1960; Youngs, 1987; McKenzie *et al.*, 2002; Kohne *et al.*, 2011). Double Ring Infiltrometer Test (DRIT) is a simple test used to determine the infiltration of water within a soil, and is suitable for most soil types (Eijkelkamp, 2012). The use of the outer ring turns the single ring infiltrometer, a 3D single ring system, into a one dimensional model by allowing the water

in the inner ring to flow vertically, and reduces the complexity of the data analysis by not needing to account for the lateral flow (McKenzie *et al.*, 2002; Kohne *et al.*, 2011).

For the DRIT, the outer ring is placed on a relatively flat undisturbed surface; the surface is prepared by the removal of small stones and twigs and where necessary grass has been cut with scissors, to ensure minimal disturbance to the surface when the rings are inserted into the ground (Eijkelkamp, 2012). A plank of wood is then placed on the outer ring, which is then hammered into the ground to a depth of roughly 2cm. The inner ring is then placed on the ground and again a plank is used to force the ring into the ground. The rings are set at the same height, thereby ensuring the bottoms of the rings are at the same depth. A level is used to ensure that the rings are lying level with each other. Water is poured into the outer ring first. A plastic sheet is placed within the outer ring to break the flow of the water and ensuring that little or no disturbance of the ground surface occurs (McKenzie *et al.*, 2002; Kohne *et al.*, 2011). The use of the outer ring is so that the soil profile will be wet ensuring water from the inner ring will only infiltrate vertically when filled. Once the water in the outer ring is at the required mark, the sheet is removed, and the process is repeated for the inner ring (McKenzie *et al.*, 2002; Kohne *et al.*, 2011). See Figure 16.



Figure 16: The double ring infiltrometer filled with water, at the start of a test

The moment both rings are filled to the predetermined marker, the stopwatch is started and then the time taken for the water in the inner ring to drop by a predefined amount (0.5cm in this fieldwork) is recorded. The water in the inner ring is then brought back to the marker with a

measured amount of water (0.5cm in this fieldwork, which equates to 33.5ml). Throughout this process the inner ring water was maintained at the same head as the outer ring. Measuring of the infiltration rate is continued until a constant value is achieved, where a change of less than 10% is achieved during a measured time period. Depending on the type of soil, this constant is reached after one to two hours and in exceptional cases, after a day (Eijkelkamp, 2012). In this study, measurements were continued until a predefined time limit of two hours.

Once the test has been completed the points were then plotted on a graph of infiltration versus time. The near-saturated hydraulic conductivity of the soil is reached when the data points on the graph show linearity (when the infiltration rate line is parallel to the horizontal axis), and this is often seen towards the conclusion of measurements (McKenzie *et al.*, 2002; Kohne *et al.*, 2011; Eijkelkamp, 2012). Once the DRIT was complete, a pit was dug through the test area to provide the vertical soil profile. The Ksat was only determined for the surface, it is recommended for further research that the Ksat be calculated for all the soil profiles, as well as all soil types, to achieve a more accurate model output.

4.2.9.2 Soil Profile Definitions

On the east side of the West Complex TSF, two main geological formations give rise to two main soil profiles (Potgieter and Calitz, 2005). These can be seen in Figure 17 and are described as Profile A and Profile B in Table 8.

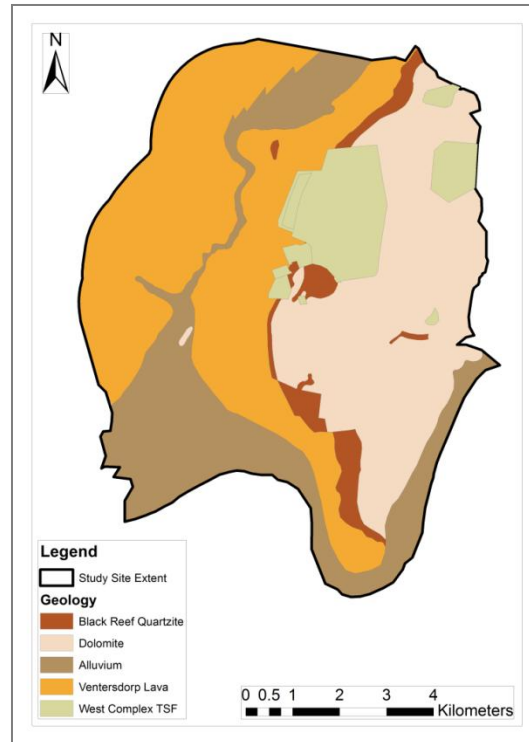


Figure 17: The geology underlying the major soil types of the study site

Table 8: The dominant soil profiles found within the study site (Potgieter and Calitz, 2005)

PROFILE A – Dolomite and Sand					
Depth	Soil Type	Hydraulic Conductivity	Classification of Soil	Database Selection	Source of Data
0 – 0.5m	Silty and/or Clayey Sand (Hillwash)	6×10^{-5} m/s	Silty Clay (SM) Silty Clayey Sands (SC-SM) Silty Clayey Sands with gravels (SC-SM)	Silty Clay (<i>Leij et al.</i> , 1996)	Potgieter and Calitz, 2005)
0.5 – 1m	Silty Sand with frequent Quartz and Chert Gravel (Residual Dolomite)	3×10^{-4} m/s	Well graded Sand Silt and gravel (SW-SM) Poorly graded Sand with Silty Clay and Gravel (SP-SC) Well graded Sand with Silty Clay and Gravel (SW-SC)	Sandy Gravel1 (Khaheel and Freeman, 1995)	Potgieter and Calitz, 2005)
1m -			Dolomite Bedrock		
PROFILE B – Chert Rich Dolomite					
Depth	Soil Type	Hydraulic Conductivity	Classification of Soil	Database Selection	Source of Data
0 – 0.6m	Silty Sand with scattered Dolomite	4×10^{-4} m/s	Well graded Sand with Silt and Gravel (SW-SM)	Sand Gravel Fines (Khaleel and Freemand,	Potgieter and Calitz, 2005)

	cobbles and boulders (Alluvium)			1995)	
0.6 – 1.25m	Clayey Silty Sand with Gravel (Residual Shale)	5×10^{-4} m/s	Well graded Sand with Silt and Gravel (SW-SM)	Sandy Gravel1 (Khaleel and Freeman, 1995)	Potgieter and Calitz, 2005)
1.25m -	Shale Bedrock				

For the western side of the West Complex TSF there was one geological formation, namely the Ventersdorp Lava, which produced one main soil profile. This soil profile (Profile C) is described in Table 9 below. The Data for these soil profiles was obtained from previous research on the TSF (Dressel, 2005). For this dissertation the assumption was made that Profile C characteristics were taken to be typical of all Ventersdorp Lava geology found in the area. The hydraulic conductivities for the soils in profile C were estimated by Dressel (2005) using particle size distribution data. Various calculations were used in these estimations, specifically the equations developed by Sherard *et al.* (1984) and Alyamani & Sen (1993) for the hydraulic conductivity of soils (Dressel, 2005). Once all the values had been calculated, Dressel (2005) then calculated the average hydraulic conductivity, and these were the values that were used for Profile C (Dressel, 2005). Profile D refers to the soil found on the Black Reef Quartzite geological formation, as seen in Table 9. The hydraulic conductivity values given for profile D and profile E were calculated with the use of the DRIT by Potgieter and Calitz (2005). These datasets were then used for the calculation of the hydraulic conductivity (Potgieter and Calitz, 2005).

Table 9: The soil profiles for Profile C and D on the west side of the TSF

PROFILE C – Ventersdorp					
Depth	Soil Type	Hydraulic Conductivity	Classification of Soil	Database Selection	Source of Data
0m – 0.5m	Red-Brown Silty Sand	5x10 ⁻⁶ m/s	Not Available	Sandy Clay (Leij <i>et al.</i> , 1996)	(Dressel, 2005)
0.5m – 1.5m	Ferruginised Hillwash	1x10 ⁻⁵ m/s	Not Available	Sandy Fines (Khaleel and Freeman, 1995)	(Dressel, 2005)
1.5m – 5m	Silt from Residual Andesite	1x10 ⁻⁷ m/s	Not Available	Silt (Leij <i>et al.</i> , 1996)	(Dressel, 2005)
5m -			Ventersdorp Lava Bedrock		
PROFILE D – Black Reef Quartzite					
Depth	Soil Type	Hydraulic Conductivity	Classification of Soil	Database Selection	Source of Data
0m – 0.25m	Sandy-Clay-	8.7x10 ⁻⁵ m/s	Sandy Clay Loam	Fieldwork	

	Loam		(Leij <i>et al.</i> , 1996)		
0.25m – 0.55m	Sandy-Clay-Loam	8.7x10 ⁻⁵ m/s	Sandy Clay Loam (Leij <i>et al.</i> , 1996)	Fieldwork	
0.55m -		Black Reef Quartzite			
PROFILE E - Alluvium					
Depth	Soil Type	Hydraulic Conductivity	Classification of Soil	Database Selection	Source of Data
0m – 0.3m		2.9x10 ⁻⁵ m/s	Clay Loam	ClayLoam (Leij <i>et al.</i> , 1996)	Fieldwork
0.3m – 0.65m		2.9x10 ⁻⁵ m/s	Clay Loam	ClayLoam (Leij <i>et al.</i> , 1996)	Fieldwork
0.65m -			Ventersdorp Lava		

Once the shapefile containing polygons of the soil types had been imported into MIKE SHE, the next step involved the specification of the soil properties, such as the soil depths, soil types, vertical discretization, hydraulic conductivity, and retention curve. Due to data limitations, the retention data were not readily available and thus a soil database was provided by DHI, which was created from the soil classifications created by Khaleel & Freeman (1995) and Leij *et al.* (1996). The retention curves were based on the texture of the particular soil at hand. Soils from the profiles were compared with the soil classification from the soil database to ensure the most appropriate soil was chosen, and then the relevant hydraulic conductivity was inputted.

4.2.9.3 Initial Sulphate Concentrations for the Unsaturated Zone Module

The initial SO_4 concentration for the *UZ module* was set as zero. This was due to the fact that there was a lack of data for the UZ SO_4 concentrations and these values were expected to be low. However, by using the *advection dispersion* option within MIKE SHE, the model is capable of calculating solute movement of sulphates (solute) based on the intercell flows calculated in the water movement simulation (DHI Software, 2007).

4.2.10 Saturated Zone Module

The *SZ module* is used to insert the geological data of the area. For this study site there were three geological types found in the area, namely; Ventersdorp Lavas, Black Reef Quartzite and Dolomite (Prinsloo *et al.*, 2006).

4.2.10.1 Geological Layers

There were a number of geological properties that were required for each geological unit found in the area. All the required data was taken from a previous hydrological study conducted at the site (de Sousa *et al.*, 2006). The Ventersdorp Lavas are predominantly found on the western side

of the TSF, with the Dolomite found on the eastern side of the West Complex TSF and the Black Reef Quartzite splitting the two, and running beneath the West Complex TSF, as seen in Figure 19. The TSF was also modelled using the calibrated values from the previous hydrological investigation. These values for the various geological units can be seen in Table 10 and Table 11. The depths to which the geological unit were set, was to 50m below the surface for all the geologies, but not the TSF (a schematic is shown in Figure 18).

Table 10: The hydraulic conductivities for each geological units found at the study site (AngloGold Ashanti, 2011a)

GEOLOGICAL UNIT	HORIZONTAL HYDRAULIC CONDUCTIVITY	VERTICAL HYDRAULIC CONDUCTIVITY
Ventersdorp Lava	4.93×10^{-6} m/s	0.00273 m/s
Black Reef Quartzite	4.12×10^{-7} m/s	2×10^{-4} m/s
Dolomite	6.72×10^{-6} m/s	2.53×10^{-4} m/s
Tailing Storage Facility	5.68×10^{-6} m/s	8×10^{-7} m/s

Table 11: The geological properties for all the geological units of the study site (AngloGold Ashanti, 2011a)

OTHER PROPERTIES	MEASUREMENTS
Specific Yield	0.2 (unitless)
Specific Storage	0.0001 (1/m)
Horizontal Dispersivity	0.2 (unitless)
Vertical Dispersivity	0.01 (unitless)
Porosity	0.02 (unitless)

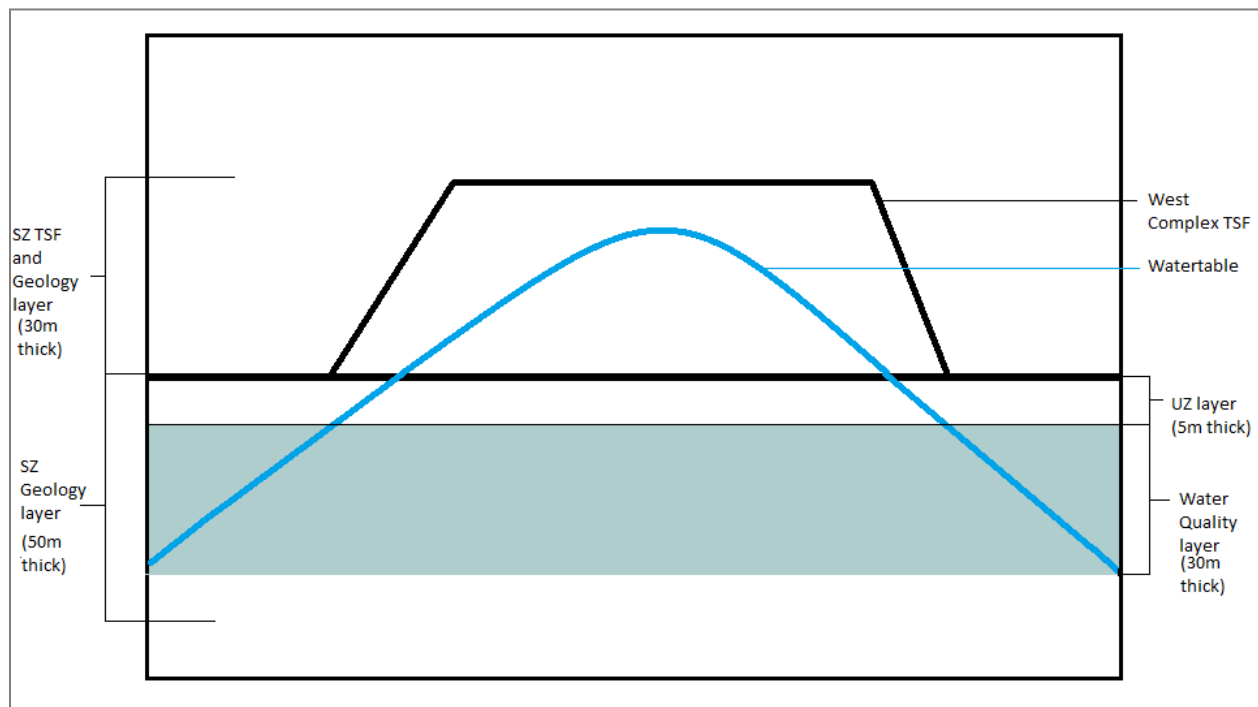


Figure 18: Schematic showing the geological, water quality, and water table layers

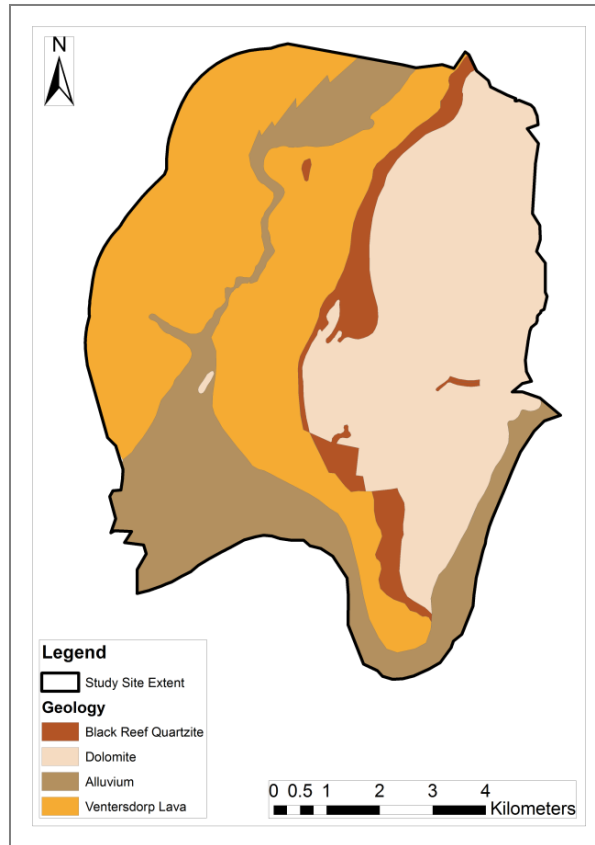


Figure 19: The geological units found in the study site (30 – 50m)

4.2.10.2 Water Quality Layers

The *WQ layers* allow the user to represent the conceptual layer system that applies to the chemical processes of the source. The *WQ layers* allow one to specify whether the *WQ layers* mimic the geological layers or not (DHI Software, 2007). For this model there was only one *WQ layers* included, to a depth of 50m. This then implies that there was only one water quality layer in the SZ.

4.2.10.3 Computational Layers

In the *Saturated Flow module* the following inputs were required: the *initial potential head*, *outer boundary conditions*, *internal boundary conditions* and the *initial concentration* of the geological layers of the model. In the *computational layers* one needs to specify where and how the calculations will be conducted. There were two options available firstly, *defined by geological layers* or secondly, *explicit definition of the lower levels*. The *defined by geological layers* option requires one calculation conducted in each geological layer. However, the *explicit*

definition of the lower levels option requires there will be a calculation conducted for each layer. For this simulation, the option to *define by geological layers* was selected as there was little to no data available to specify the layers within the SZ.

4.2.10.3.1 Initial Head

The *initial head* of a geological layer refers to the starting hydraulic head for the simulations and the initial estimate for the steady-state simulations (DHI Software, 2007). Therefore, the current water table of the area needed to be added to the simulation. The water table depths vary from 0 to 17mbgl. The water table levels for the area were available from borehole data for the month of January 2001. All the water table data came from the monitored boreholes found in the Vaal River mine lease area (Figure 20). The complete set of monitoring boreholes was used, however only three of these (January 2001) borehole sets fell within the study site. This data was then interpolated to cover the entire study site, and surrounding area, using the inverse distance weighting (IDW) interpolation method with ARCGIS. Once the water table had been interpolated it was then introduced into MIKE SHE. Once in MIKE SHE, the water table was subtracted from the topography to ensure that an elevation above sea level was provided. The water table for January 2001 can be seen in Figure 20. The red shows areas where the water table is deepest, while the green shows the shallower water table areas.

4.2.10.3.2 Outer Boundary Conditions

The *outer boundary conditions* allow the external boundaries of the study site to be defined. There were four available options of *outer boundary conditions*, namely *fixed head*, *zero flux*, *flux*, and *gradient*. The descriptions of each of these boundary conditions can be seen in Table 12.

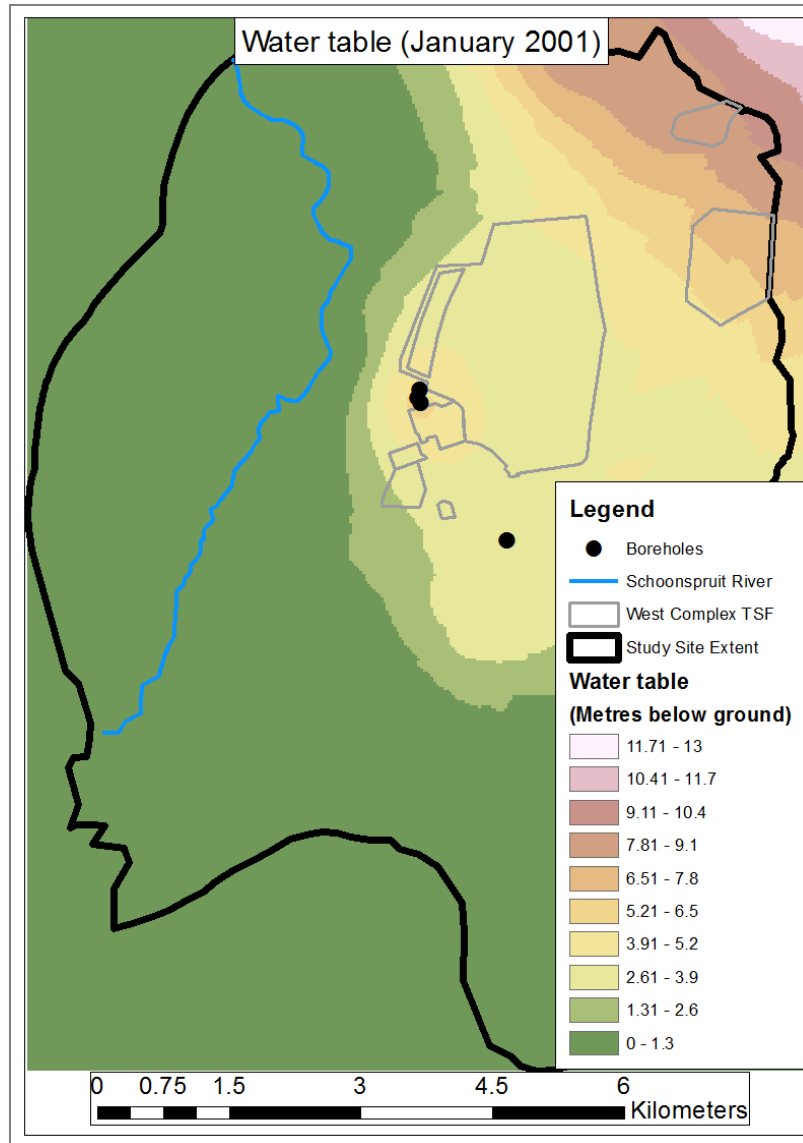


Figure 20: The water table depth for January 2001 for the study site

Table 12: The descriptions of the available outer boundary conditions (DHI Software, 2007)

TYPE	DESCRIPTION	UNIT
Fixed Head	This is when the user wants to introduce a head in the boundary. This will be a fixed value, fixed at the initial value from the initial conditions	Fixed head boundary can be specified as a fixed value (m) or as a .dfs0 or .dfs2 file
Zero Flux	A zero flux boundary is a boundary where there is a no-flow boundary, and is the default option within MIKE SHE	n/a
Flux	A flux boundary is a boundary where there is a time or constant varying flux across the boundary.	Flux boundary can be specified as a mean step-accumulated discharge (m^3/s) or step-accumulated volume (m^3)
Gradient	A Gradient Boundary is a constant or time varying gradient between the outer boundary and the internal cells.	A gradient boundary can be set as an instantaneous dimensionless or percent value. A positive gradient implies a flux into the study area

There were two outer boundary conditions for this simulation, seen in Figure 21. The southern boundary (green) was set to a flux boundary; this flux boundary was controlled by the groundwater hydraulic gradient with a fixed river level, allowing for water to leave the system. While the rest of the study site extent was set as zero-flux boundaries, seen in red, where no water is allowed to enter or exit the study site. This option, to set the southern boundary as flux and the northern boundary as zero-flux was allowed as the boundary of the study site had been set to hydrological boundaries, i.e. the Vaal River in the south and the catchment boundaries on the north, east and west boundaries. For the western boundary there were no catchment data beyond the Schoonspruit River, therefore the buffer of 1800m was created from the edge of the Vaal River lease area.

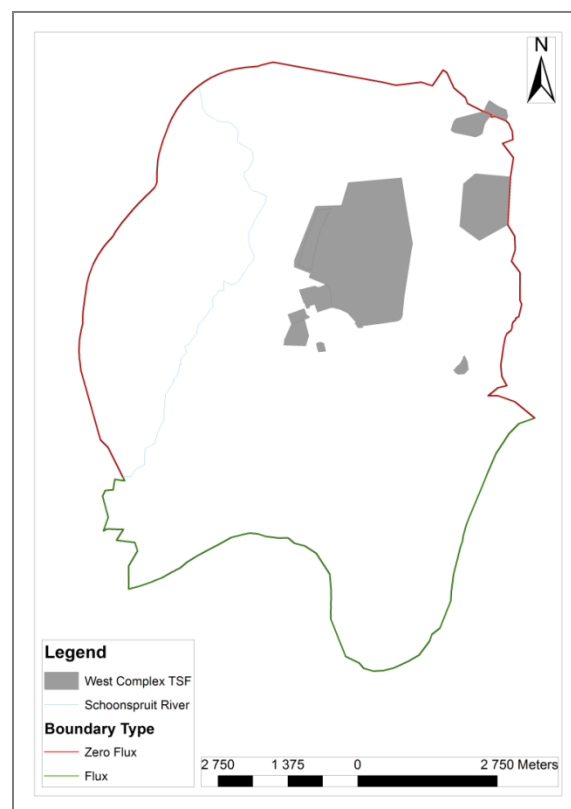


Figure 21: The zero-flux boundary (Red) and the flux boundary (Green)

The Vaal River, as the southern boundary, was deemed sufficient as within this stretch the river had little movement of water into the banks. This stretch of the river was therefore simulated assuming that only inflow into the Vaal River is allowed. For the flux boundary, found at the Vaal River, a value for the flux was required. To calculate this flux Darcy's Law was used.

Darcy's Law can be seen in Equation 3, where Q refers to discharge (m^3/day), T to transmissivity (m^2/day), i to gradient (dimensionless) and w to length of groundwater unit perpendicular to flow (m) (King and Hubbert, 1957).

$$Q = T \times i \times w \quad (\text{Eq. 3})$$

$$\begin{aligned} Q &= 7.25 \times 10^{-4} \times (0.006) \times (16680) \\ &= 0.0726 \, m^3 \, \text{per day} \\ &= 8.398 \times 10^{-7} \, m^3 \, \text{per second} \end{aligned}$$

4.2.10.3.3 Internal Boundary Conditions

The internal boundary conditions allow the user to define what kind of internal boundaries occur within the study site. There were four options namely the fixed head, fixed head drain, head controlled flux, and inactive cells. The descriptions of each of these internal boundary conditions can be seen in Table 13.

Table 13: The descriptions of the available internal boundary conditions (DHI Software, 2007)

TYPE	DESCRIPTION	UNIT
Fixed Head	A fixed head boundary is where the user specifies the head in the cell. If a Fixed Head is included it could become an infinite sink or source of water	Fixed head boundary can be specified as a fixed value (m) or as a .dfs0 or .dfs2 file
Fixed Head Drain	A fixed head drain boundary is one where the user sets the reference head, and when the cell water level is above the reference level then the boundary acts as a normal fixed head boundary condition. If the water falls below the reference level then the boundary condition is switched off. i.e. the flux is set as zero	Fixed head drain boundary can be specified as a fixed value (m) or as a .dfs0 or .dfs2 file
Head Controlled Flux	The head controlled flux is a similar internal boundary condition as the Fixed Head, however the Head Controlled Flux incorporated a flow resistance in the form of a specified leakage coefficient	Head controlled flux can be a prescribed value or a .dfs0 or .dfs2 file. The leakage coefficient can be specified either as a Simple Leakage Coefficient (1/time) or as a Total Conductance (length ² /time)
Inactive Cells	The inactive boundary conditions are the option used when an interior cell in the model needs to be inactive. This is done by assigning a hydraulic conductivity of zero to the cells if the model is in a transient state and a value of 10-15 if the model is in a steady-state.	

To accurately model the potential head of the West Complex TSF, an *internal boundary condition* was set along the borders of the TSF. For this the interior of the West Complex TSF was set to a *fixed head internal boundary* with a constant value of 1320m above sea level (red

arrow in Figure 22). This then created the realistic inverted bowl-shaped hydraulic head that naturally occurs in TSFs (DWAF, 2007). However, this constant value was determined by estimation as there was no piezometric data to confirm this. It is recommended for further research that tests are conducted to determine a more accurate *fixed head internal boundary* within the West Complex TSF.

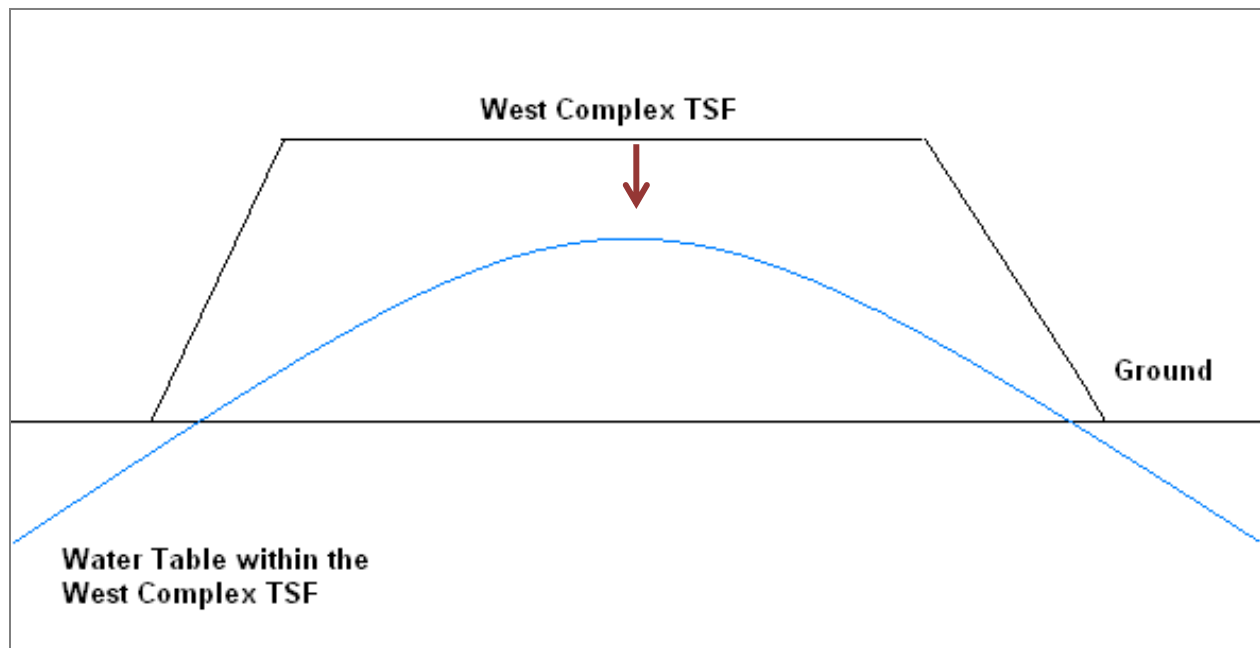


Figure 22: Conceptual diagram of the water table within the West Complex TSF

4.2.10.4 Initial Concentrations of Sulphate in the Saturated Zone

The *initial concentrations* option is where the initial conditions of each chemical species for each layer in the model are set. The *initial concentration* value is used by MIKE SHE as a starting concentration for the *WQ Simulations module*. This value can be set as a uniform value ($\mu\text{g}/\text{m}^3$) for the whole study site, or as a distributed value for the study site. As with the water table, there was sufficient data from the borehole data to provide distributed initial SO_4 concentrations for the study site. The location of the boreholes used for this dissertation can be seen in Figure 23. These SO_4 concentrations were then interpolated using the IDW interpolation method, using estimations from the AngloGold Ashanti (2011a) study of the SO_4 plume for the Vaal River mine lease area. The SO_4 concentrations for the study site can be seen in Figure 24. The complete set of monitoring boreholes data was used for the study site as for some months there was little to no boreholes located within the study site that were measured. For these months the

data from neighbouring boreholes were interpolated for the study site. This did introduce a level of error, but provides the model with the most accurate data available for this dissertation.

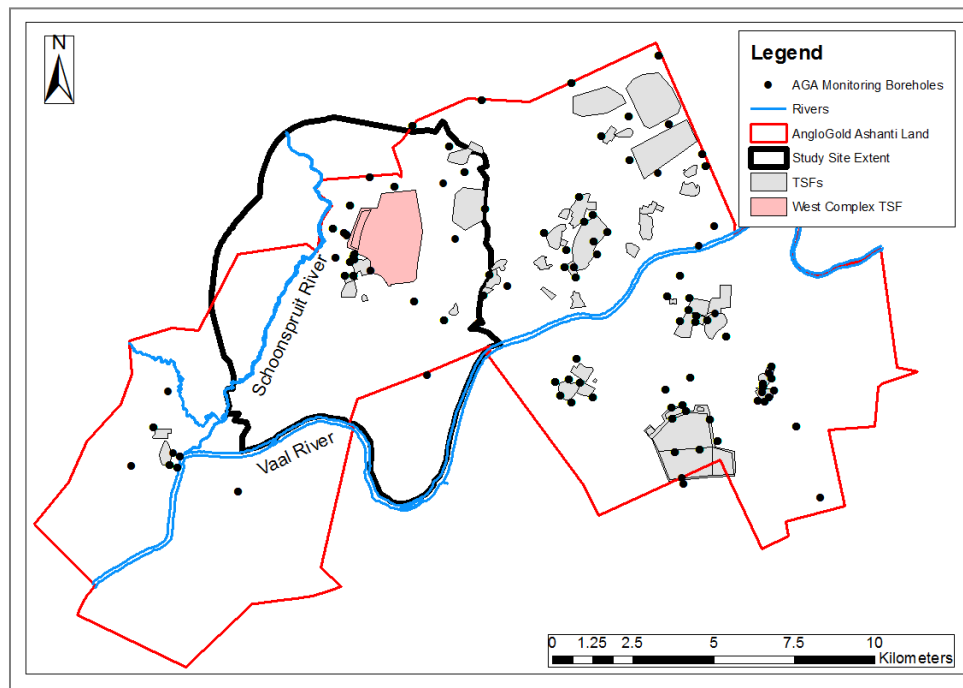


Figure 23: The location of boreholes used for SO₄ concentration measurements

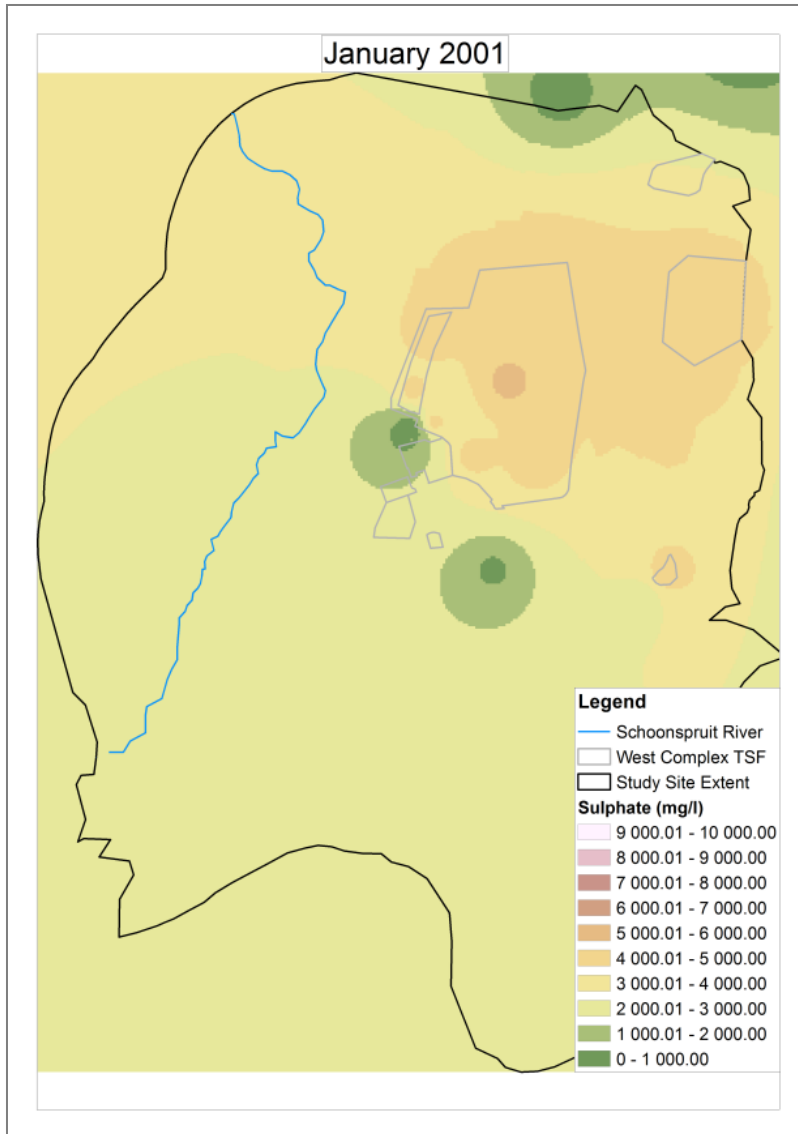


Figure 24: The initial concentrations of the SO₄ for 2001

4.2.11 Water Quality Sources Module

Within the *WQ Source module*, the specifications for where the solute transport occurs, which solute is found, and the extent of the solute are specified. The first option required was to define which chemical species to select for the solute of the study site. The relevant species from the species dialogue that had been previously created was selected. For this project, the chemical species observed was SO₄ in the seepage water originating from the West Complex TSF. The options for location of the solute are: *surface*, i.e. the solute is located on the ground surface, or *subsurface*, i.e. the solute is found in the saturated and/or UZ. As this dissertation's focus was the solute in the groundwater and the plume seeping from the TSF, the location of the solute in the

WQ module was set as *subsurface*. The next option that was set was the source type. Once again there were various options available depending on the location selection. As *subsurface* option was chosen, the following options were given for the source type: *UZ mass*, *SZ fixed concentration*, *SZ mass*. For this project, since the measurements of SO_4 were taken from the boreholes as fixed concentrations, the most logical selection was the *SZ fixed concentration* option. The final specification to set was the extent type. This was where the source was spatially described, either in the *entire domain* or in *part of the domain*. For this project the *full domain* was selected. Once the initial selections had been set, the following settings had to be specified: *the upper level*, *the lower level* and *the strength* of the SO_4 concentration.

4.2.11.1 Upper Level

The *upper level* refers to the upper elevation of the source of the WQ layer. This level was used by the interpolation algorithm to give the cells within the domain the water quality properties (DHI Software, 2007). For this dissertation the TSF was considered the source, and therefore the upper elevation of the water quality layer was set as 0m.

4.2.11.2 Lower Level

The *lower level* was the value used to set the bottom of the water quality sources. Once again this value was used by the interpolation algorithm to assign the water quality properties to the relevant cells in the model domain (DHI Software, 2007). This value was taken from the study conducted by AngloGold Ashanti (2011a). The value was set to include all the man-made structures, such as the actual TSF, trenches, water dams, the UZ, river and parts of the weathered zone of the underlying geological formations found in the area (AngloGold Ashanti, 2011a). Therefore, the value was set as 50m (see schematic in Figure 18).

4.2.11.3 Strength

In the *strength sub-module*, the user needs to introduce the concentration strength of the source; for this project, the strength of the SO_4 plume. The strength of the SO_4 can be set as a *uniform strength* (one concentration level for the whole site), *station based* (varying concentrations based on time) and finally *fully-distributed* (various concentration within the study site). For this project the option used was the *fully-distributed* option. This option was selected as the concentration of SO_4 from boreholes was readily available from a previous study conducted at

the study site (AngloGold Ashanti, 2003). The boreholes that were used for the *Unsaturated Flow module* strength data were all the monitoring boreholes. This data was imported into ARCGIS in the form of point data, in mg/l units. Once the data was in ARCGIS the point data was interpolated using the IDW interpolation method. Concentration levels of the SO₄ from the boreholes were introduced into MIKE SHE by means of a .dfs2 file. The varying concentration levels of the SO₄ can be seen in Figure 24. The use of the UZ strength data provided the best available option for the SZ strength data due to the lack of further saturated zone concentrations from the boreholes. It is recommended for further research that further borehole concentrations are measured to ensure a more accurate model and model output.

4.2.12 River and Lakes Module

For the *Rivers and Lakes Module*, the complementary river program, MIKE 11, was used to introduce the Schoonspruit River model within MIKE SHE. The MIKE SHE *River and Lakes Module* relies only on the user directing the software to the MIKE 11 simulation file. Therefore all the modelling required for the Schoonspruit River was conducted within MIKE 11 itself.

4.2.12.1 MIKE 11 Simulation Editor

The *Simulation Editor* in MIKE 11 is the location where the simulation and computational parameters are controlled. The *Network Editor* links with the other editors, namely; the *Cross Section Editor*, the *Boundary Editor* and the *Hydrodynamic Editor* (DHI Software, 2007). The *Simulation Editor* also allows the user to select which models to include. For this project, the models used were the hydrodynamic model and the advection dispersion model. The advection dispersion model was included as even though the WQ processes may be occurring within the Schoonspruit River, they were not the focus. The *WQ module* still needed to model the river to ensure an accurate depiction of current conditions at the study site. Therefore, only a simple Schoonspruit River model was required. The option to run the *steady state* simulation mode was selected over the *quasi steady state* so that the discharge and water levels at the boundaries correspond to the start time of the simulation of the MIKE SHE model (DHI Software, 2007).

For this dissertation the MIKE 11 model was run over the same time period as the MIKE SHE model. The *time step* selected for this model was set as every two minutes. Even though this was a relatively small time step for such a long period, it was necessary as instabilities arose within MIKE 11 and MIKE SHE during simulations where a larger time step was chosen. Another

setting specified in the *Simulation Editor* was the *result storing frequency* options. For this model the storing frequencies were set at once every day. Available discharge data for the Schoonspruit River were at a daily time step and therefore, a daily output of the MIKE 11 file was needed for the calibration step of the project.

4.2.12.2 MIKE 11 River Network Editor

The main function of the *River Network Editor* is to edit and view the dataset required for the network (DHI Software, 2007). Within the *Network Editor* the user digitizes the river network(s) and defines the hydraulic structures on the network(s). For this simulation there was only one network, the Schoonspruit River, and there were no hydraulic structures of importance that needed to be modelled. The Schoonspruit River polyline required for input was created from Google Earth. Once the river had been introduced, the next step was to provide some introductory properties for the Schoonspruit River branch that had been created. The following is required to be filled: *topo ID*, *upstream chainage*, *downstream chainage*, *flow direction*, *maximum dx* (distance) and *branch type*. These settings and their descriptions can be seen in Table 14.

Table 14: The properties of the Schoonspruit River (DHI Software, 2007)

BRANCH PROPERTY	DESCRIPTION	AVAILABLE OPTIONS	MODEL SETTINGS
Topo ID	The Topographical Identifier, which refers to the data defined in the Cross Section file.	User defined	Schoonspruit
Upstream Chainage	The chainage of the first point of the river.	Model default set to 0 m	0 m
Downstream Chainage	The chainage of the last point of the river.	Model default set to 9940.23222 m	9940.23222 m
Flow Direction	Indicator of how MIKE 11 will interpret the chainage direction of the river with respect to the natural flow direction.	Positive or Negative	Positive (flow is from upstream to downstream chainage)
Maximum dx	Maximum distance allowed between water level calculation points	10 000 m (Default)	Left as default – 10 000 m
Branch Type	Type of branch	Regular Link Channel Routing Kinematic Routing Stratified Mike 12	Regular Type – A normal branch composed of a number of calculation points defined from cross sections.

The final step in the *Network Editor* set up was to link the Schoonspruit River to the groundwater, i.e. linking MIKE 11 with MIKE SHE. This was a simple sub-module within the *Network Editor*, where one sets up the MIKE SHE Links. For this project, as there was only one network, the Schoonspruit River, there was only one MIKE SHE link. Here the upstream and downstream chainage were set to the same value as in Table 14. In the MIKE SHE link sub-module the following settings were required; conductance, leakage coefficient, flooding area. For the conductance this option was chosen to include conductance in the aquifer and the bed, rather than in the bed or the aquifer only. This was to ensure a realistic coupling of MIKE SHE and MIKE 11. The leakage coefficient refers to the amount of water that leaks from the river into the soil along the river. For this project the coefficient was set to 1×10^{-6} per second, to work in conjunction with the flux boundary within the *fixed head internal boundary* of the West Complex TSF. This was a value that was suggested by the Team at DHI – South Africa. As the Schoonspruit River rises and falls with change in rainfall, it has relatively high river banks, so was deemed that little to no flooding would occur over the banks, and therefore the flood area option was set to “no flooding”.

4.2.12.3 MIKE 11 Cross section Editor

The *Cross Section Editor* in MIKE 11 functions as a database, storing all the cross section data (DHI Software, 2007). It allows the user to provide the location and properties of the cross sections of the branch in question. The cross sections were created within ARCGIS and then brought into MIKE 11. Within ARCGIS, the 30m DEM was introduced and then using the cross section tool within the MIKE 11 plug-in, twenty cross sections were drawn across the river, as the DWAF provided cross sections of the river bed every 400m it was decided to use these intervals. Once these newly created cross sections were introduced into MIKE 11, they were altered to ensure they depicted realistic cross sections of the Schoonspruit River. This editing entailed the smoothing and deepening of the river bed as well as the river banks. The cross sections then provided a simplistic simulated river that was deemed sufficient for this project. The properties set for this project are further discussed in the following sections for the twenty cross sections used for this branch.

4.2.12.3.1 Resistance Numbers

This is the location where the user sets the bed resistance for each of the cross sections. There are two choices that need to be made for each cross section: *transversal distribution* and *resistance type*. Firstly, the *transversal distribution* defines the resistance across the cross sections (DHI Software, 2007). There are three options available to the user: *uniform*, *high/low flow zones* and *distributed*. *Uniform transversal distribution* is used when there is uniform resistance within the cross section, where a single value is applied for this type of distribution (DHI Software, 2007). *High/low flow zones* allow the specification of three resistance values; *the left high flow*, *the right high flow* and *low flow resistance*. Lastly, *distributed*, a resistance value is specified for every cross section (DHI Software, 2007). For this project, as the Schoonspruit River only needed to be a simple model the *uniform resistance* was selected for the *transversal distribution* option. The value of 1 was selected as this was the default setting for the MIKE 11 cross sections. The second choice required for the bed resistance was the *resistance type*; here the user can define the type of resistance method. The following methods are available to the user: *relative resistance*, *Manning's n*, *Manning's M*, *Chezy number* and *Darcy-Weisbach*. The *left high/low flow zones* and *relative resistance* values were set to the defaults values (Appendix C).

4.2.12.4 MIKE 11 Boundary Editor

The *Boundary Editor* within MIKE 11 is used to specify the various boundary conditions of the branch created in the *Network Editor* (DHI Software, 2007). For each of the boundary conditions in the branch the following properties need to be set: *boundary description*, *boundary type* and the *boundary location*. For the section of the Schoonspruit River being modelled there were only two boundaries, the upstream and downstream points, as there were no tributaries joining or splitting off this section. There was merely a start point (coordinates: 26.652372°, -26.915215°), i.e.: inflow, and an end point (coordinates: 26.619669°, -27.002534°), i.e.: outflow.

4.2.12.4.1 Boundary Description

The boundary description option refers to the nature of the boundary of the branch. There are six available options: *open*, *point source*, *distributed source*, *global*, *structures* and *closed*. A description of each boundary descriptions available is seen in Table 15. For this project, the two boundaries, namely the upstream and downstream boundaries were set as *open boundaries*.

Table 15: The available boundary conditions available (DHI Software, 2007)

TYPE	DESCRIPTION
Open Boundary	An open boundary can be specified at the free upstream and downstream ends of the model domain.
Point source Boundary	A point source boundary condition is used at locations where time-varying or constant lateral inflows or outflows occur.
Distributed Source Boundary	The distributed source boundary condition is used along river reaches within the model domain where time-varying or constant lateral distributed inflows or outflows are needed.
Global Boundary	The global boundary condition is applied when certain boundary conditions are valid over the entire model domain.
Structures Boundary	The structures boundary condition can be used in combination with three different types of structures, namely; dam, dam break and regulating structure.
Closed Boundary	The closed boundary description is used at free end points of the model domain where a zero flux condition across the boundary is acceptable.

4.2.12.4.2 Boundary Type

As the open boundary condition was selected for the two boundaries in this project, there were now six options available for the boundary type found at these open boundaries. These options and descriptions can be seen in Table 16. Water level and discharge data were readily available for the Schoonspruit River, for both upstream (Site number CH109, coordinates: 26.616530°, -26.819377°) and downstream (Site number C2H073, coordinates: 26.632254°, -26.984738°), from the Department of Water Affairs and Forestry (DWAF) (www.dwaf.gov.co.za). Therefore, the upstream boundary was set to the *inflow boundary type*, while the downstream boundary was set as a *Q-h boundary type*. The water level and discharge time series files for the upstream and downstream boundaries can be seen in Figure 25 and Figure 26 respectively.

Table 16: The available boundary types for open boundary conditions

TYPE OF BOUNDARY	DESCRIPTION
Inflow	The inflow boundary type is selected when there is a need for a time-varying hydrograph condition.
Water Level	The water level boundary type is selected when a time-varying water level condition is required.
Q-h	The Q-h boundary type is used when the relationship between the discharge and the water level is known
Bottom Level	The bottom level is specified when there is a variation in the bottom level. Used in sediment transport models.
Sediment Transport	Used to describe the variation of the inflow of the sediment. Used in sediment transport models.
Sediment Supply	Used when the bottom level or the sediment transport is not known in sediment transport models.

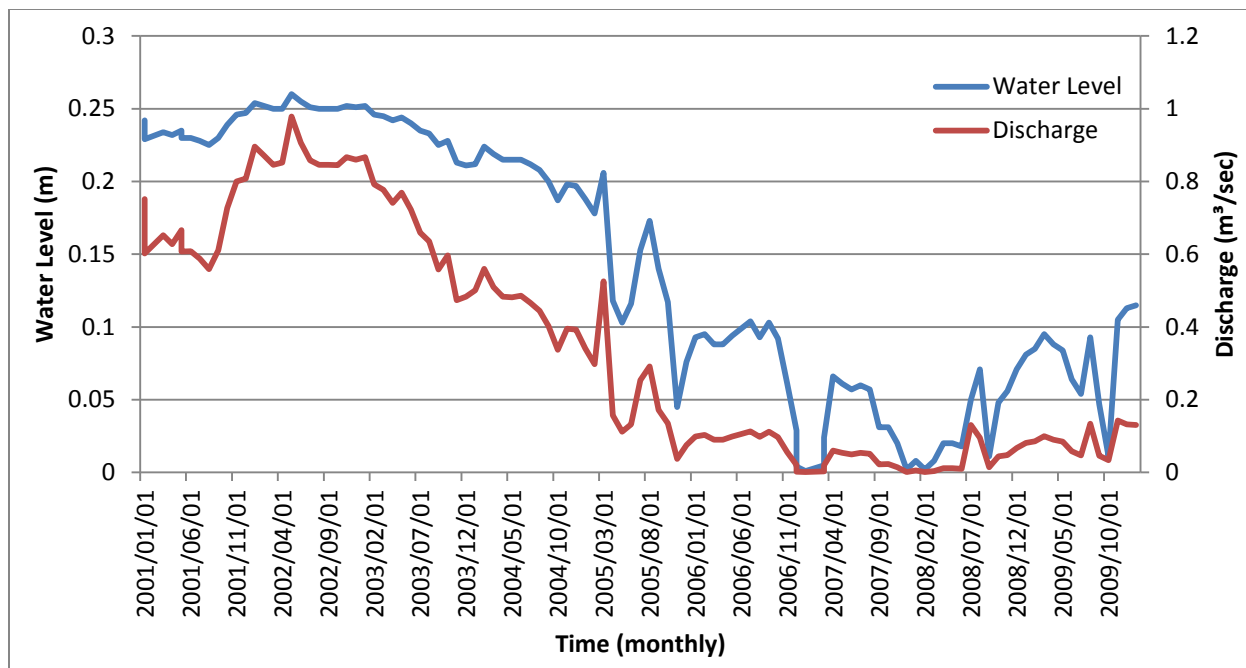


Figure 25: The water level and the discharge for the upstream open boundary of the Schoonspruit River
(www.dwaf.gov.co.za)

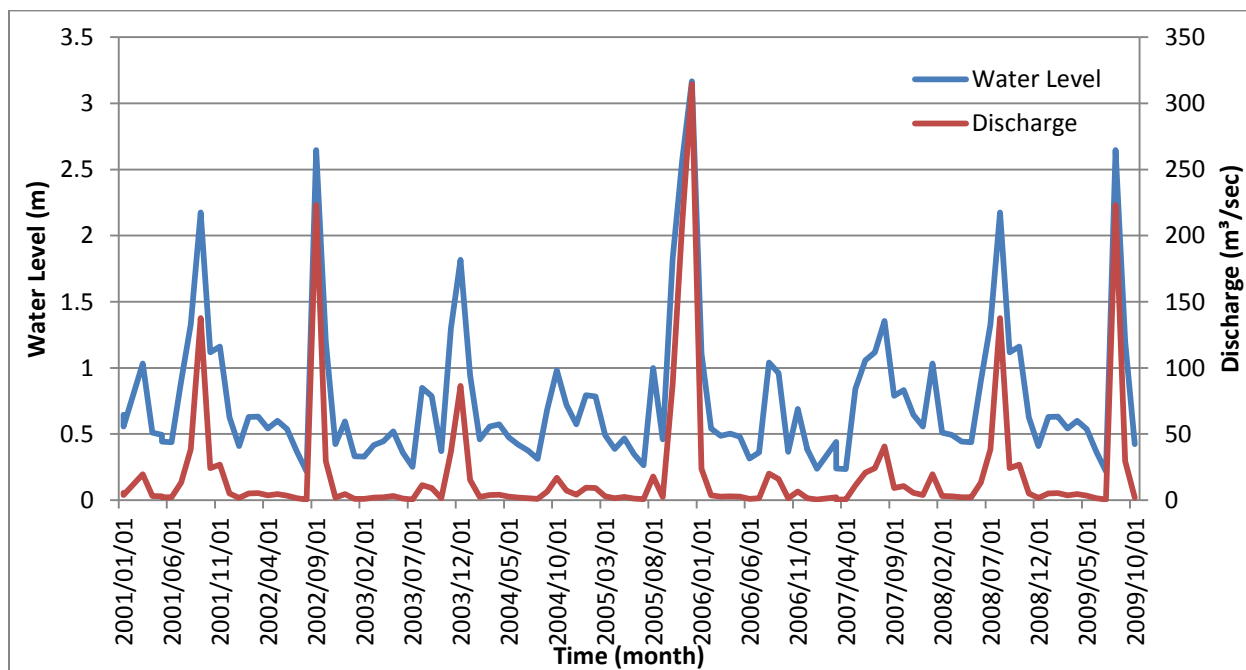


Figure 26: The water level and the discharge for the downstream open boundary of the Schoonspruit River
(www.dwaf.gov.co.za)

4.2.12.5 MIKE 11 Advection Dispersion

Even though the focus of this dissertation was on the contamination plume and not the change in concentration in the Schoonspruit River, there was still a need to model the WQ within the Schoonspruit River. Within MIKE 11 the Schoonspruit River was modelled as a sink for the SO_4 concentrations which was necessary to accurately depict the movement of the contamination plume. A very basic *Advection Dispersion* module was set up for the Schoonspruit River.

4.2.12.5.1 Boundary Concentrations

The first thing that needed to be specified was the SO_4 concentrations for the boundaries set up in the *Boundary Editor* module. The SO_4 concentrations for upstream and downstream within the Schoonspruit River were provided from the borehole data from AGA. Monthly concentrations were modelled for both upstream and downstream of the Schoonspruit River from January 2001 until January 2009. These time series files for the upstream and downstream concentrations can be seen in Figure 27 and Figure 28. The spikes in the SO_4 concentrations can be related to the lower water inflow level measured in Figure 25. The lower water level results in higher concentration as there is a less water to dissolve the SO_4 .

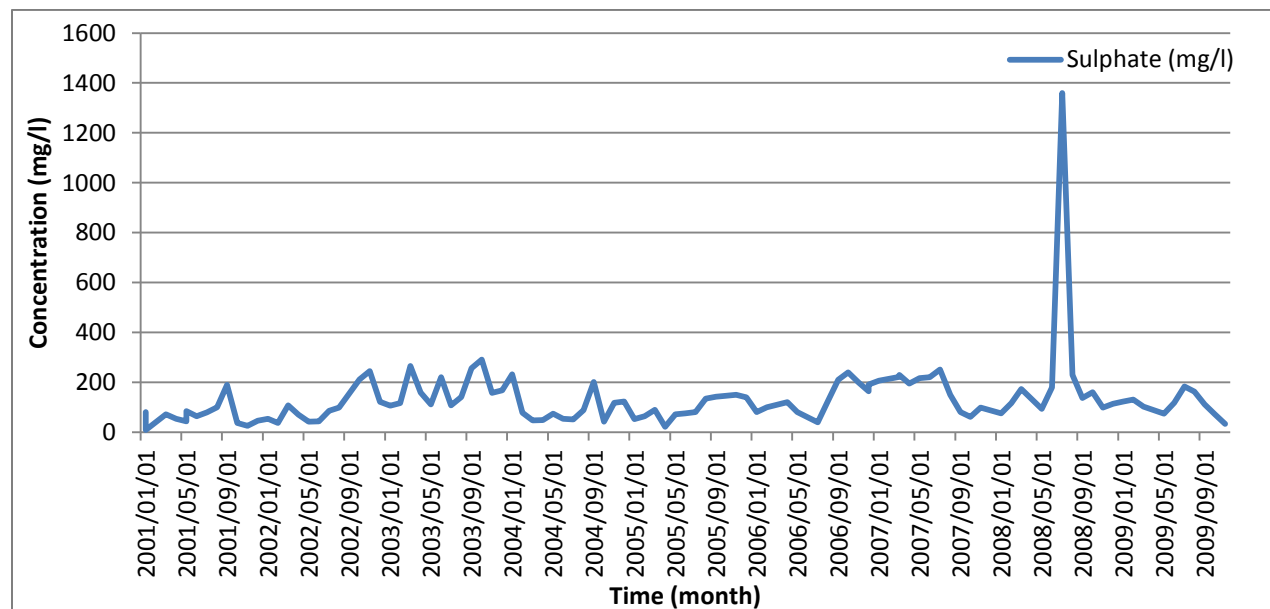


Figure 27: The upstream SO_4 concentration for the Schoonspruit River (AngloGold Ashanti)

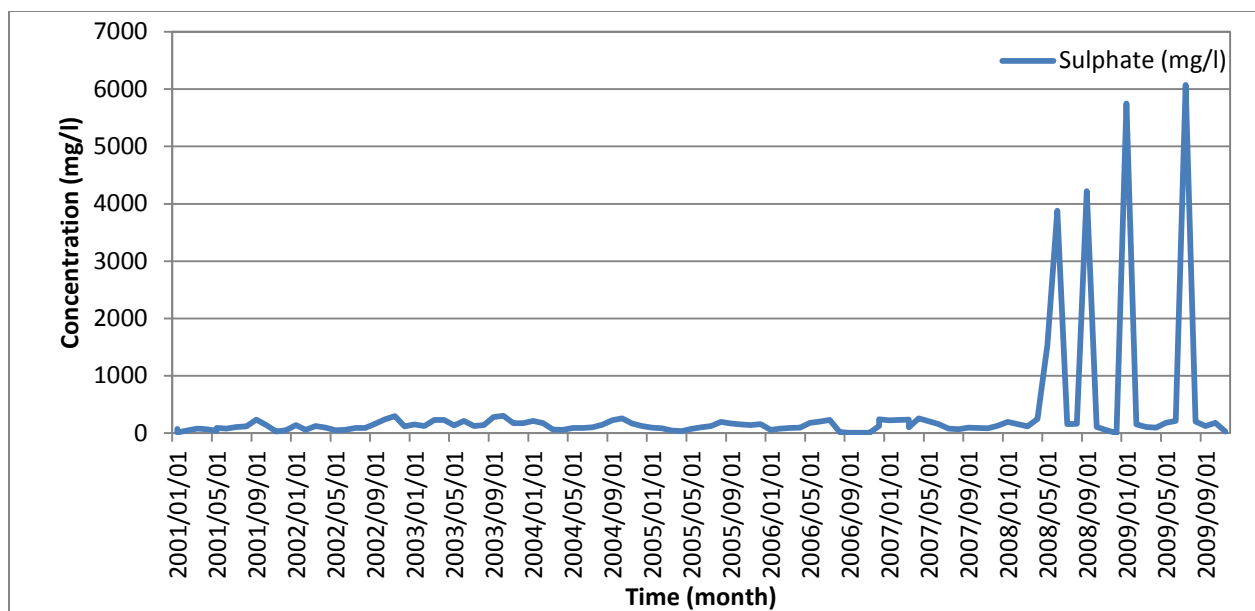


Figure 28: The downstream SO₄ concentration for the Schoonspruit River (AngloGold Ashanti)

4.2.12.5.2 Advection Dispersion Parameters

Within the advection dispersion parameters there were a variety of settings that needed to be defined. These include the *components, initial conditions, dispersion, decay, cohesive ST and additional outputs*. As the water quality of the Schoonspruit River was being modelled as simply as possible the majority of the settings were left as default (Appendix C), with only the component and the initial conditions being changed. For the components setting, the settings that were used can be seen in Table 17. The initial conditions for the upstream and downstream boundaries of the Schoonspruit River concentrations were set as follows. The upstream initial concentration was set to 80 mg/l and the downstream initial concentration was set to 75 mg/l. These values were chosen as they were the Schoonspruit River SO₄ concentrations at the start of the simulation.

Table 17: The components set for the advection dispersion module

SETTING	SET AS
Component	Sulphate
Units	mg/l
Type	Normal

4.3 Future Woodlands Scenario

In the future scenario, the majority of the modules remained the same. The only parameters that did change were in the *Land Use* and the *Water Quality modules*. These changes can be seen below.

4.3.1 Display Module

The *Display module* for the future scenarios was identical to the current scenario, and requires no further explanation.

4.3.2 Simulation Specification Module

Within the *Simulation Specification module*, the only section to change was the simulation period. For the future scenario the start date was arbitrarily defined as the 1st February 2025 with an end date of 28th February 2034. The simulation date was used as a future nine-year period, where mature trees (between 15 and 20 years old) are simulated.

4.3.3 Model and Domain Module

The *Model and Domain Module* remains the same as the current scenario, as the future scenario was run for the same study site area.

4.3.4 Species Module

The *ET uptake factor* was defined as chemical species factor and referred to the uptake of SO_4 by plants. The concentration of SO_4 found in the foliage of the *S. lancea*, *E. dunnii* and the *T. usneoides* was taken from previous research conducted by the MWP. These factors are representative of the ability of the plants to absorb SO_4 . On average *E. dunnii* had the ability to absorb roughly zero to one percent of SO_4 found in the soil water into the foliage, while *S. lancea* can take anywhere up to 14% (Mntungwa *et al.*, 2014). The *T. usneoides* are the best performers which can take up to 30% into the plants foliage, which accounts for the high *ET uptake factor*. Within MIKE SHE this factor cannot be defined for difference plant species, or even spatially, therefore the *ET uptake factor* used for this dissertation was an average of the values of all the plant types. This is an important limitation of the MIKE SHE model with regards to the purpose of this project.

To determine the effect of the *ET uptake factor* on the MIKE SHE model output, a sensitivity test was completed on the minimum and maximum *ET uptake factors* (Table 18). The minimum and maximum values were calculated with Equation 1 using the percentage of SO_4 found in the foliage of the trees as well as the concentration of SO_4 in the groundwater. For these calculations the concentration of SO_4 found in the groundwater was 1711mg/l (AngloGold Ashanti, 2011a). The minimum SO_4 concentrations found in the foliage for the *S. lancea* was 1% (of the mass of water uptake, comprises SO_4), the *E. dunnii* was 0.1% and the *T. usneoides* was 10%. While the maximum SO_4 concentrations found in the foliage for the *S. lancea* was 3%, the *E. dunnii* was 0.2% and the *T. usneoides* was 30% (Mntungwa *et al.*, 2014). To test the sensitivity of the MIKE SHE model to the *ET uptake factor* a sensitivity analysis was conducted using the average *ET uptake factor* provided in Table 18. For the sensitivity analysis the average *ET uptake factor* was used as a baseline and then the model was run using 80% and 120% of this average value. The results of the analysis are shown in Figure 29.

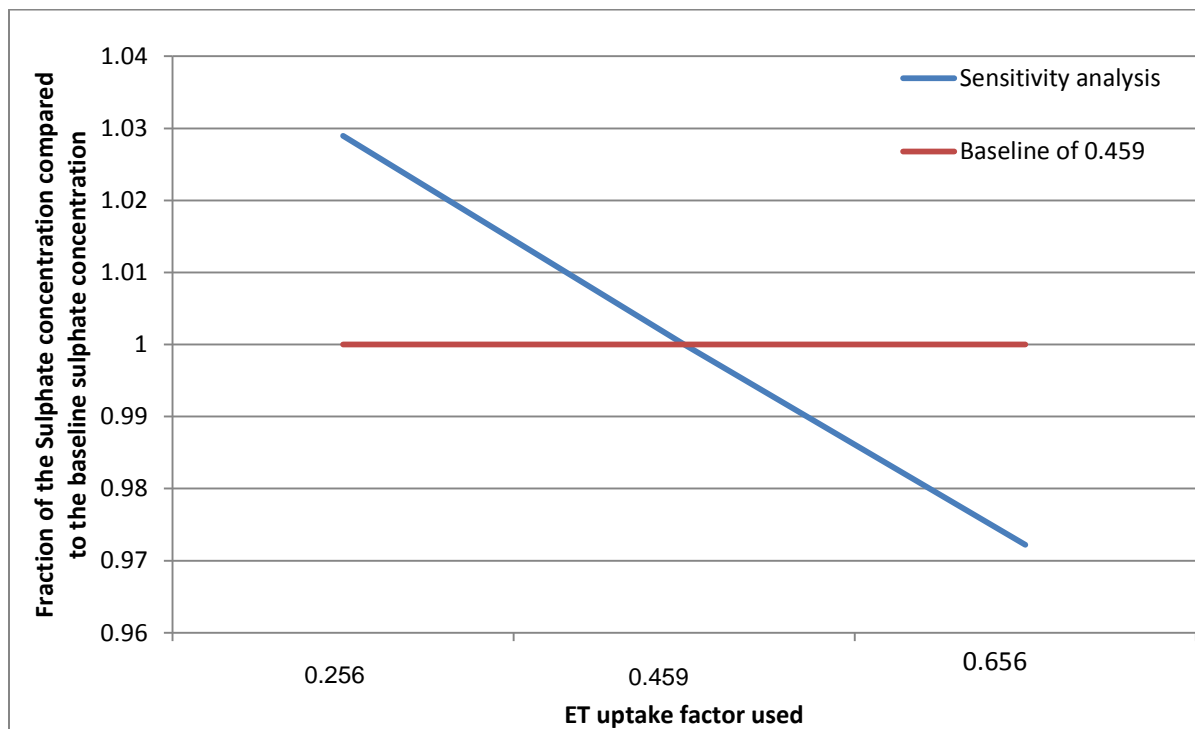


Figure 29: The sensitivity of the MIKE SHE model to the ET uptake factor

Table 18: The maximum and minimum ET uptake factor for the plant species

PLANT SPECIES	ET UPTAKE FACTOR (UNITLESS)	
	MINIMUM	MAXIMUM
<i>S. lancea</i>	0.082	0.158
<i>E. dunnii</i>	0.006	0.012
<i>T. usneoides</i>	0.701	1.753

The 80% and 120% simulations showed the effect of the *ET uptake factor* on the MIKE SHE model results. The results showed the effects that the *ET uptake factor* had on the SO₄ concentrations; a decrease in the average value by 20%, resulted in an increase from the baseline. While an increase of the average value by 20%, resulted in a decrease in the SO₄ concentrations. These results showed that the within the MIKE SHE model, the *ET uptake factor* was an important input that needs to be accurately defined for the future scenarios. However, this limitation cannot be overcome in this project due to deficiencies in the model structure. Therefore it was deemed sufficient to simulate the average *ET uptake factor* for the relevant future scenario simulations. These averages can be seen in Table 19.

Table 19 : The future scenarios ET uptake factor (Mntungwa et al., 2014)

PLANTING SCENARIO	PLANT SPECIES IN SCENARIO	AVERAGE ET UPTAKE FACTOR USED	
		Minimum	Maximum
Scenario 1	<ul style="list-style-type: none"> <i>S. lancea</i> <i>T. usneoides</i> 	0.082	0.158
		0.701	1.753
		Average = 0.674	
Scenario 2	<ul style="list-style-type: none"> <i>E. dunnii</i> <i>T. usneoides</i> 	0.006	0.012
		0.701	1.753
		Average = 0.618	
Scenario 3	<ul style="list-style-type: none"> <i>S. lancea</i> 	0.082	0.158
		Average = 0.12	
Scenario 4	<ul style="list-style-type: none"> <i>E. dunnii</i> 	0.006	0.012
		Average = 0.009	
Scenario 5	<ul style="list-style-type: none"> Grasslands <i>S. lancea</i> <i>T. usneoides</i> 	0.000	0.000
		0.082	0.158
		0.701	1.753
		Average = 0.449	
Scenario 6	<ul style="list-style-type: none"> Grasslands <i>E. dunnii</i> <i>T. usneoides</i> 	0.000	0.000
		0.006	0.012
		0.701	1.753
		Average = 0.412	

4.3.5 Topography Module

The *Topography Module* parameters remained the same as for the *model and domain module*.

4.3.6 Climate Module

The *Climate module* for the future scenarios had a change made in the module set-up, as the new run period required different precipitation and reference evapotranspiration .dfs0 files. The original climate file was modified to include new dates for a period in the future when all the woodlands could be fully established and mature. An arbitrary time period was chosen, from 1st Jan 2025 to 26th Feb 2034. Precipitation and RT data over this future period were identical to the current scenario climate file.

4.3.7 Land Use Module

The future scenario for the *Land Use module* was vastly different to that of the current scenario. This was due to the future scenario modelling the study site once the woodlands had been planted and were mature. Therefore the LAI between the woodland and grassland differed significantly. The RD was also vastly different, as the trees have varying root depths as they mature, and have much deeper rooting depth than grasslands. However, the rooting depth and the LAI of the grasslands on top of the TSF did not change. For the future scenarios, six woodland scenarios were modelled. These different scenarios can be seen in Table 20, and the maps showing the various woodlands scenarios can be seen in Appendix D.

Table 20: The planting scenarios for the future woodlands

SITUATION	SITUATION PLANTING PLAN
Scenario 1	<ul style="list-style-type: none">• <i>S. lancea</i> is planted throughout the planting blocks• <i>T. usneoides</i> planted near the Schoonspruit River
Scenario 2	<ul style="list-style-type: none">• <i>E. dunnii</i> planted throughout the planting blocks• <i>T. usneoides</i> planted near the Schoonspruit River
Scenario 3	<ul style="list-style-type: none">• <i>S. lancea</i> is planted throughout the planting blocks• No <i>T. usneoides</i>
Scenario 4	<ul style="list-style-type: none">• <i>E. dunnii</i> planted throughout the planting blocks• No <i>T. usneoides</i>
Scenario 5	<ul style="list-style-type: none">• Northern privately-owned blocks remain grasslands• <i>S. lancea</i> planted throughout the AGA-owned planting blocks• <i>T. usneoides</i> planted near the Schoonspruit River
Scenario 6	<ul style="list-style-type: none">• Northern privately-owned blocks remain grasslands• <i>E. dunnii</i> planted throughout the AGA-owned planting blocks• <i>T. usneoides</i> planted near the Schoonspruit River

4.3.7.1 Leaf Area Index

The LAI of the tree species being used for the future scenarios was estimated from previous research (Table 21) (Canadell *et al.*, 1996; Jackson *et al.*, 1996; Jarman *et al.*, 2004; Dye *et al.*, 2006) and field simulations.

Table 21: The LAI for the future scenario simulations

YEAR	Leaf Area Index (unitless)		
	<i>E. dunnii</i>	<i>S. lancea</i>	<i>T. usneoides</i>
Year 1	5	5.5	3
Year 2	5	5.5	3
Year 3	5	5.5	3
Year 4	5	5.5	3
Year 5	5	5.5	3
Year 6	5	5.5	3
Year 7	5	5.5	3
Year 8	5	5.5	3
Year 9	5	5.5	3

4.3.7.2 Maximum Rooting Depth

There was very little information that was available to determine the maximum depths of tree roots, especially within the Highveld mining environments. Therefore, there was a need to conduct fieldwork to determine if these plant species had access to the groundwater, with a groundwater level that varied from 0.2 to 11mbgl (AngloGold Ashanti, 2011a). This was an important attribute to define accurately, as the ability of the trees to reach the groundwater or not has a huge impact on their annual water use and effectiveness for phytoremediation.

4.3.7.2.1 Fieldwork

Tracer Release

The plan for the tracer release was to drill boreholes down to below the groundwater level, within close proximity to as many as 10 existing mature trees located in the study site. Boreholes were to be drilled close to small and large *S. lancea* and *E. camaldulensis* across the study site. A tracer dye would then be released into the SZ and two weeks later analysis would be conducted on leaf samples for the presence of the dye. Rhodamine B was selected, as this dye is readily taken up by plant roots, is known to accumulate within leaf tissues and does not cause any harm in the soils or geological materials (McLaughlin, 1982).

The preliminary drilling was done with the use of a hydraulic auger, loaned by the Department of Civil Engineering at the University of the Witwatersrand. However, this drill was not sufficient to drill through the compact soil due to the drill being too light and having too little hydraulic push. The next drilling attempt was with the use of truck-mounted hydraulic augers owned by the Council of Geosciences. This drilling attempt was successful in one location. Several sites were attempted however the auger was not able to penetrate through the rocks and at some points the resistance to the auger became too great.

To determine the depth of the roots for *S. lancea*, a borehole was drilled close to (within 3m) an existing mature *S. lancea* tree. This borehole reached a depth of 14m (coordinates: 26.67851°, -26.928966°). On attaining this depth, a PVC casing was inserted into the borehole. This casing was capped at the lower end to prevent sediment entering from below. The casing walls were slotted in the lower sections to allow inflow of groundwater while, excluding most sediment. A cap was placed on top of the casing to prevent entry of sediment from the top. A clean hosepipe was lowered inside the casing until it reached below the water table. A funnel was connected to the hosepipe upper end and an estimated 15mg of Rhodamine B dye, mixed in one litre of water, was released down the funnel (Figure 30). So as to ensure that the upper soil profile was not contaminated with dye, extreme care was taken to make sure no splashing occurred. Once the one litre solution was released, 10 litres of clean water was slowly poured over the hose pipe top to rinse both the inside and outside surfaces as it was withdrawn from the borehole. This rinsing ensured that no dye was accidentally released from the hosepipe surfaces onto the upper soil profiles surfaces.



Figure 30: The method for releasing of Rhodamine B down boreholes. a.) showing the hose pipe with funnel, b.) the release of Rhodamine B down funnel and c.) the capping of the casing to ensure sediment doesn't block the casing

Rhodamine Analyses

Leaf samples were taken before and after the Rhodamine B dye release. The top of the tree's leaves were picked to determine if the entire tree had access to the groundwater. Once the leaves had been picked and air dried, they were analysed in a laboratory. The analytical method from Donaldson and Robinson (1971) was used for this laboratory analysis. They outlined the steps to follow to determine if the Rhodamine B had been absorbed by the trees, and thus indicate if the trees had access to the groundwater. The following steps were followed in the laboratory as described in (Donaldson and Robinson, 1971), for both sets of leaves:

- The leaves were ground into slurry with the use of 95% ethyl alcohol.
- The slurry was heated to just below boiling point for five minutes.
- The slurry was then taken off the heat, and distilled water was added to the slurry to create 100ml of solution. This solution was then filtered through Whatman no. 50 filter paper. The filtrate was then washed with alcohol and finally the fluorescence was compared.

Due to time constraints the filtrate could not be measure in a professional laboratory with the use of a fluorometer. This constraint was overcome by using a UV torch in a blacked out container. The filtrates from before and after the tracer release were measured alongside each other, and the fluorometer intensity was then compared through a simple visibility test with the naked eye.

Pre-dawn xylem pressure potential measurements

After two failed time-consuming attempts, the drilling of boreholes was deemed impractical, a different approach was needed to gain more information on the plant root access to the groundwater. As there were too few opportunities to release tracer dye it was decided to measure the pre-dawn xylem pressure potential in the trees. There had been no rain in the study site for six months and the subsoil was very dry, therefore the low plant water stress found would suggest the trees were in contact with the water table. This alternative method to drilling used the Scholander pressure chamber system.

The pressure chamber system is a widely accepted technique used to measure the water stress of a plant (Boyers, 1995). The sample leaf is secured into a bung that fits in the centre of the

removable top of the chamber. The petiole is sealed from the inside with Prestik (Boyers 1995). After the lid is secured to the chamber, the leaf lies within the chamber and the petiole or stem protrudes through the lid (Figure 31). Pressurizing the leaf inside the chamber causes a difference between the inside and outside pressure which results in the leaf water being forced toward the outside (Boyers, 1995). The pressure inside the chamber that causes the water to be forced outside is a measure of the water stress of the tissue (Boyers, 1995). The more water stressed the plant is, the more dehydrated the leaf, and the higher the pressure required to force the xylem water to the outside (Boyers, 1995). This method has been successfully used for leaves, branches and roots of trees, and for this project was used on the leaves of the *S. lancea*, *E. camaldulensis* and *T. usneoides*.



Figure 31: The lid of the Scholander pressure chamber with a leaf petiole protruding through the bung

Measurements of plants range from 1.5 bars for unstressed plants with saturated soil to 20 or more bars for plants that are severely stressed (Scholander *et al.*, 1965; Cleary and Zaerr, 1984). Error can be introduced by following incorrect practices when using the pressure chamber system. Minimizing the time between cutting the sample and conducting the test is important (Ritchie and Hinckley, 1975). Any moisture lost from the leaf between cutting and measuring will affect the results, and therefore the measurements should be taken immediately after the cutting for accurate readings. The processing of the sample also plays a factor in the accuracy of the readings. If the leaf is damaged or re-cut then the tension in the xylem water columns is broken and accurate readings will not be obtained (Scholander *et al.*, 1965; Ritchie and Hinckley, 1975; Cleary and Zaerr, 1984). Another important factor in the accuracy of the

readings is the identification of the correct end-point. The pressure at which the xylem water first reaches the cut surface is essential to measure accurately. For plants with short petioles or stems this may be difficult to see, and the use of a magnifying glass is necessary, to ensure that an accurate end-point is recognized (Ritchie and Hinckley, 1975). An important factor to consider when interpreting the results from the Scholander pressure chamber system was the date of the last rainfall recorded in the area. This was the 27th March 2013. This indicates a very lengthy drying period of six months, and suggests that the trees are using groundwater to remain in a relatively unstressed state.

An advantage to using the Scholander pressure chamber system is that it is a portable machine that allows for the immediate testing of the leaves. It is also a low cost technique which is simple to use and has been found to be a reliable method for measuring plant water stress (Scholander *et al.*, 1965; Boyers, 1995). Pre-dawn measurements are preferred to midday measurements as the xylem water potential and the soil water potential have equilibrated through the night, thus giving a more precise water stress measurement (Cleary and Zaerr, 1984).

Only healthy, mature trees were chosen for this fieldwork. Trees used in the water stress tests included *E. camaldulensis* (Site 1: 26.673011°, -26.933389°), *S. lancea* (Site 5: 26.67851°, -26.928966°) found alongside the West Complex TSF, and *T. usneoides* (Site 6: 26.74238°, 26.949289°) found on the East Paydam TSF and are seen in Figure 32, Figure 33 respectively with the location of the trees used found in Figure 42.



Figure 32: The *E. camaldulensis* (Site 1) (left) and *S. lancea* (Site 5) (right) used for the water stress test



Figure 33: The *T. usneoides* (Site 6) used for the water stress test

The leaf sample measurements were taken before dawn, between 4am and 6am (on the 11th and 12th September 2013) to ensure that the sample trees had sufficient time to reach equilibrium between the xylem water and soil water. Once the chamber system was set up, the leaf sample was cut and within less than a minute the test was conducted. Once the leaf was secured, with the use of Prestik (Figure 34), to ensure the chamber would be air tight, the chamber was closed and pressurized air was slowly released into the chamber. The pressure at which water first appeared on the petiole cut surface was then recorded. Five sample leaves were sampled from each tree to obtain a mean reading.



Figure 34: The sealing of the leaf in the pressure chamber system lid by means of Prestik

To minimize errors that may arise from the pressure chamber test the following precautionary measures were taken. Firstly, each sample was cut and then measured before the next sample was cut. The maximum time between cutting and measuring was less than one minute. Secondly,

the leaves were all carefully chosen to select only fully grown leaves with minimal damage and a long enough petiole. At no point were samples re-cut. Lastly, the end-point was determined with the use of a magnifying glass and torch to illuminate the petiole. The end-point was determined by only one instrument operator to ensure a consistency in the readings.

4.3.7.2.2 MIKE SHE Inputs

For the future scenarios the trees were simulated to be stable mature woodland stands, with a rooting depth of 8.5mblg for *E. dunnii* and *S. lancea* and 5mblg for the *T. usneoides*.

4.3.8 Overland Flow Module

For the *Overland Flow module*, there were three options that could possibly be changed. These included the *Manning's m*, *detention storage* and the *initial water depth*. For the future scenario the only option changed was the *Manning's m*. The change from grassland to woodland was accompanied by ploughing/ripping and a greater litter layer on the soil surface. The roughness changed from a semi-smooth study site to a rough study site (Morgan, 1995). *Manning's m* was thus changed from 25 to 10. The detention storage remained at 2mm and the initial water depth remained at 0mm. The remaining options for the *Overland Flow module* for the future scenarios remain the same as those of the current scenario.

4.3.9 Unsaturated Flow Module

The only two changes within the *Unsaturated Flow module* that were available to change were the *initial concentration* and the *initial potential head*. These remain the same as those of the current scenario.

4.3.10 Saturated Zone Module

As before with the *Unsaturated Flow module*, the initial concentration and the initial potential head were merely repeated for the future time period.

4.3.11 Water Quality Module

For the *Water Quality module*, the concentrations of SO₄ in all the modules were merely repeated for the woodland simulation period.

4.3.12 River and Lakes Module

As with the *Climate module*, the river data were extended for the nine years. This was to ensure a realistic depiction of the Schoonspruit River, remembering that the Schoonspruit River flow was not the focus of the study.

5 Results

5.1 Infiltration Results

The MIKE SHE model requires a vast amount of data for use as input, however not all the data was available, such as the infiltration rate and soil profile for the alluvial soils and the soils above the Black Reef Quartzite. Therefore double ring infiltrometer tests were conducted for these soils to determine their infiltration rate. Once these tests were complete a pit was dug to determine the soil profiles. The infiltration rates recorded in the field with the double-ring infiltrometer were plotted in Excel, with the infiltration rate in red, and the cumulative infiltration in blue. The graphs for the Alluvium soils and Black Reef soils can be seen in Figure 35 and Figure 36 respectively. The orange boxes show the periods of near-constant infiltration rate which approximate near-saturated hydraulic conductivity. The datasets that fell in the orange box were then inputted into a separate graph, and a linear trend line was fitted.

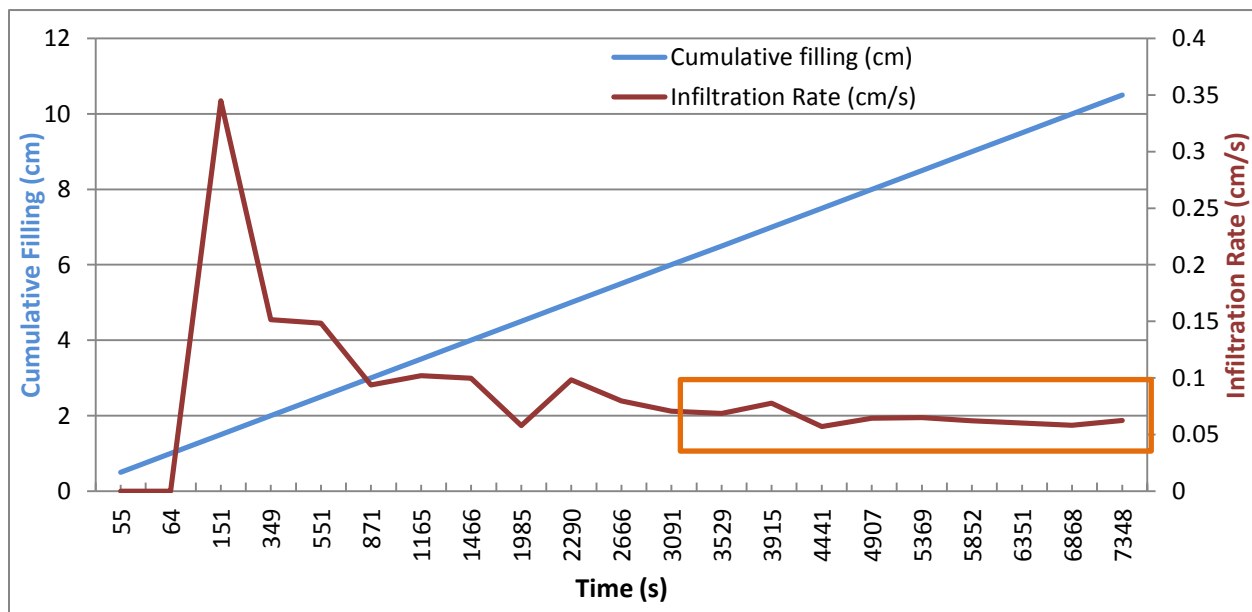


Figure 35: The infiltration rate of the Alluvium soil

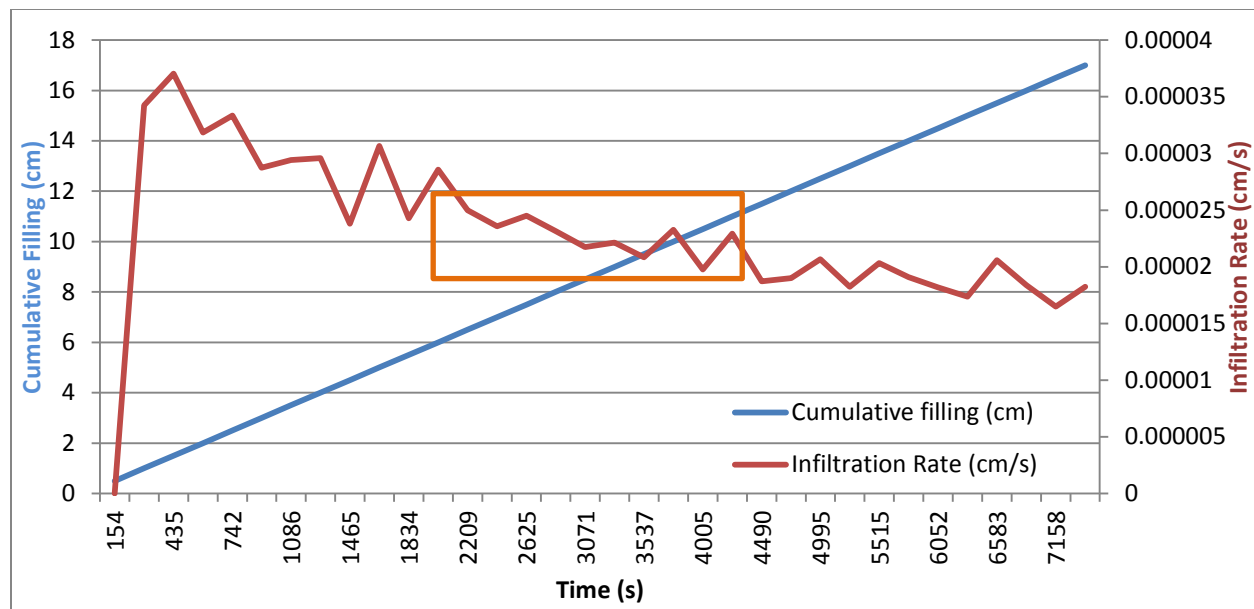


Figure 36: The infiltration rates for the Black Reef soil

The slope of the linear trend line gives the steady-state infiltration rate for the particular soil. This gradient was then multiplied by 1.45 to obtain the hydraulic conductivity (K_{sat}) of the soil (McKenzie *et al.*, 2002). The graphs showing the individual areas of linearity for the Alluvium and Black Reef soils can be seen in Figure 37 and Figure 38 respectively. The green line shows the linear trend line, and the calculated hydraulic conductivities of the soils can be seen in Table 22.

Table 22: The calculated hydraulic conductivities for the soils

Soil	Hydraulic Conductivity (m/sec)	
Alluvium	0.000725	7.25e-004
Black Reef	0.0000058	5.8e-006

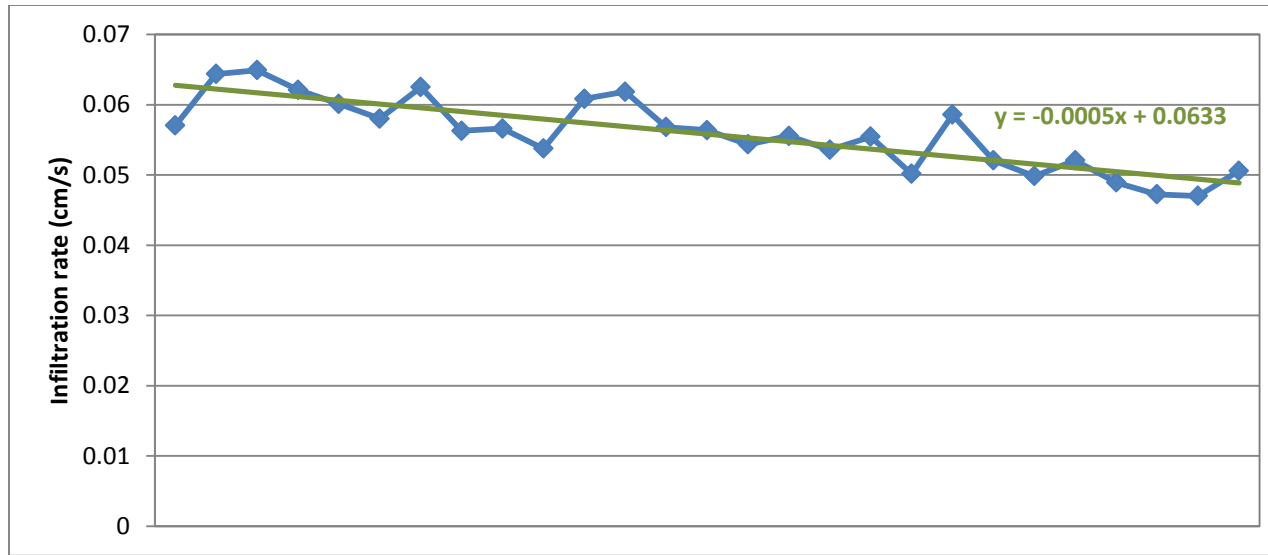


Figure 37: The near steady state infiltration rate for the Alluvium soil

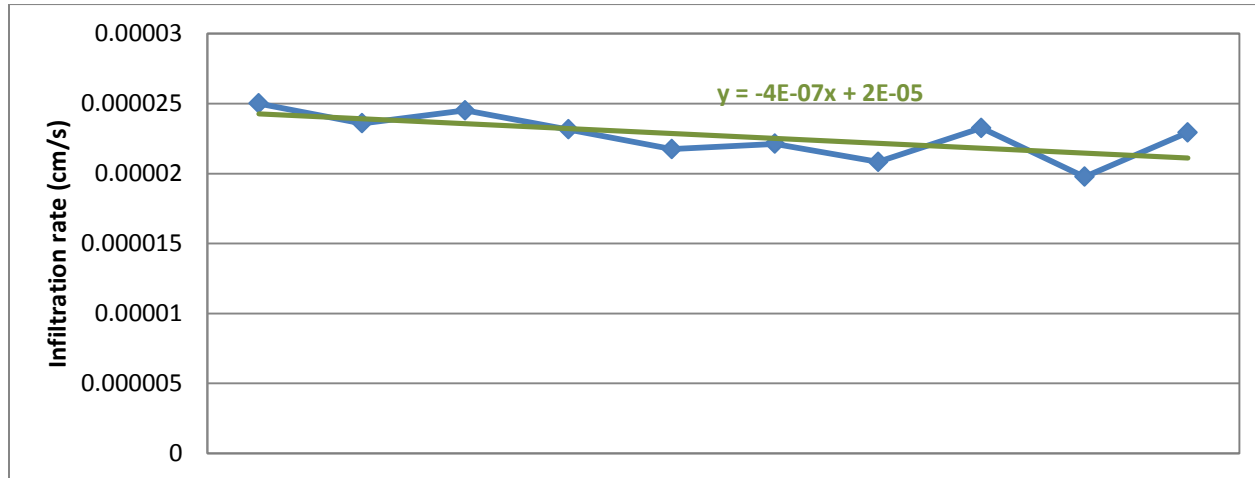


Figure 38: The near steady state infiltration rate for the Black Reef soil

Once the DRIT was complete, a pit was dug through the test area to show the spread of the water. From this pit the soil profile descriptions were obtained. This data can be seen in Table 23.

Table 23: The soil profiles observed from the test pits

Alluvium Test Pit Soil Profile Data				
Horizon	Depth (cm)	Clay (%)	Texture	Sand
A	30	45	Clay Loam	Medium
G1	65	60	Clay Loam	Medium
Black Reef Test Pit Soil Profile Data				
Horizon	Depth (cm)	Clay (%)	Texture	Sand
A	25	22	Sandy-Clay-Loam	Not known
B	55	25	Sandy-Clay-Loam	Not known

5.2 Rhodamine Results

The baseline leaves taken before the tracer release indicated no fluorescence present in the leaves (Figure 39).



Figure 39: Baseline solution under the UV torch

The leaf samples taken two weeks after tracer release were then analysed. New equipment (beakers and tubes) were used to ensure no contamination from earlier samples. The presence of fluorescence in the sample was checked by shining UV light through the samples. Fluorescence was clearly observed (Figure 40), indicating that there is water uptake from the saturated zone. The fluorescence visible under the UV light shone yellow in colour, whilst shining bright white closest to the torch.

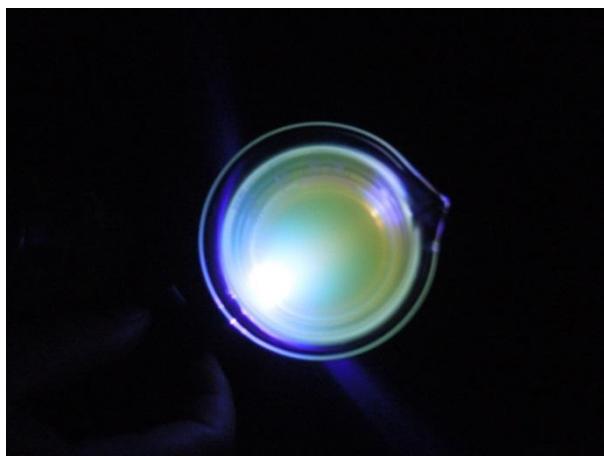


Figure 40: Fluorescence of the solution derived from the leaves taken two weeks after tracer release

5.3 Plant Water Stress Test Results

The results from the pressure chamber tests can be seen in Table 24 and in Figure 41. This graph shows the mean and range of values recorded at each site. These results show that the *S. lancea* (in green) with the deep water table (3.7mbgl) was the most stressed (de Villiers, 2014). The small difference seen between the upslope and downslope of the *T. usneoides* (in blue) was also expected, as the slope difference is relatively small. The water stress seen in the *E. camaldulensis* (in red) with the deep water table is still relatively low compared to the water stress of the *S. lancea* as this was due to the *E. camaldulensis* having a deeper root system, therefore being able to reach the deeper water table. Differences seen in between the two *E. camaldulensis* with shallow water table was not expected as these trees were located very close together. These results were then used for the rooting depth for the future scenarios.

Table 24: The results of the Scholander pressure chamber system tests

SITE	PLANT SPECIES	SAMPLE	PRESSURE (BARS)
Site 1	<i>E. camaldulensis</i> (Deep water table – 2.5mbgl)		
	NOTE: This tree was in a	Leaf 1	10.2
	fracture zone and therefore the	Leaf 2	10.1
	recorded water table depth could	Leaf 3	9.5
	be much deeper around the tree	Leaf 4	9.6
		Leaf 5	7.9
		Average	9.46
Site 2	<i>E. camaldulensis</i> (Shallow water table - 3.5mbgl)		
		Leaf 1	7
		Leaf 2	6.5
		Leaf 3	5.9
		Leaf 4	6.8
		Leaf 5	5.9
		Average	6.42
Site 3	<i>E. camaldulensis</i> (Shallow water table – 3.5 mbgl)		
		Leaf 1	5.6
		Leaf 2	6.5
		Leaf 3	5.8
		Leaf 4	5.8
		Leaf 5	5.5
		Average	5.84
Site 4	<i>S. lancea</i> (Shallow water table – 2mbgl)		
		Leaf 1	4.3
		Leaf 2	5.5
		Leaf 3	4.7
		Leaf 4	6
		Leaf 5	6
		Average	5.3
Site 5	<i>S. lancea</i> (Deep water table – 3.7mbgl)		

		Leaf 1	8
		Leaf 2	11
		Leaf 3	13.5
		Leaf 4	8.8
		Leaf 5	13.3
		Leaf 6	13.6
		Average	11.37
Site 6	<i>T. usneoides</i> (Downslope)		
		Leaf 1	6.9
		Leaf 2	8.1
		Leaf 3	7.8
		Leaf 4	7.6
		Leaf 5	7.4
		Leaf 6	8.1
		Leaf 7	7.2
		Leaf 8	6.7
		Average	7.48
Site 7	<i>T. usneoides</i> (Upslope)		
		Leaf 1	8.2
		Leaf 2	9.7
		Leaf 3	8.2
		Leaf 4	6.7
		Leaf 5	8.4
		Average	8.24

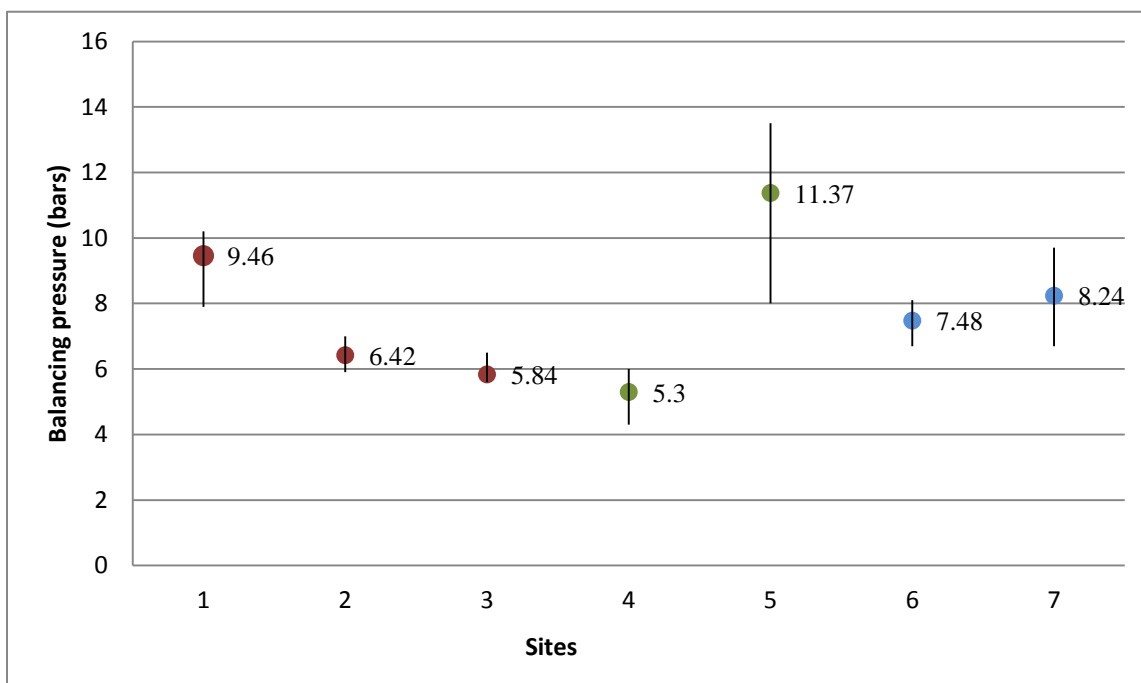


Figure 41: The mean and range of readings based on five leaves at each site from the Scholander pressure chamber tests for *E. camaldulensis* (red) *S. lancea* (green) and *T. usneoides* (blue)

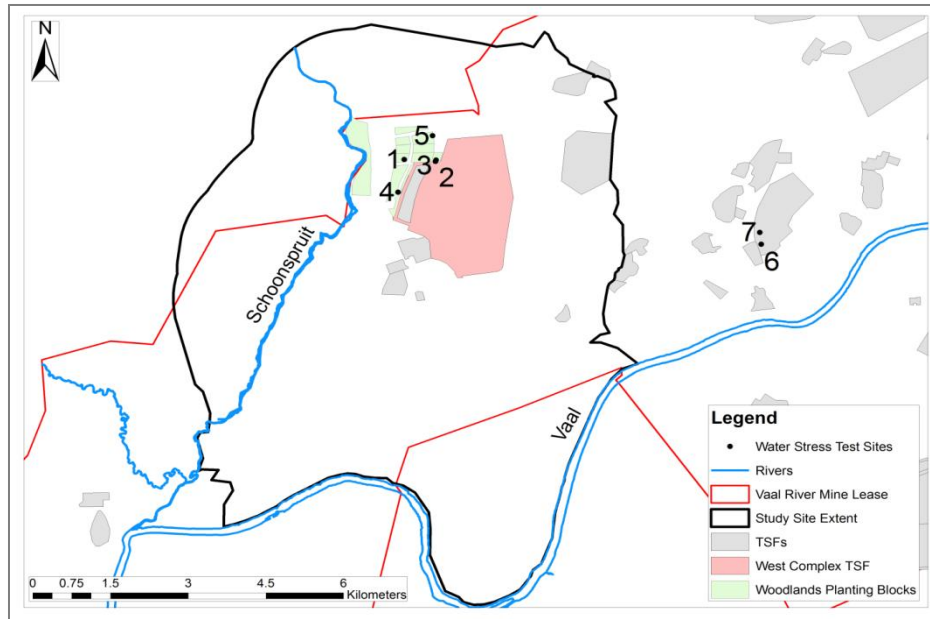


Figure 42: The location of the water stress test sites with *E. camaldulensis* found at sites 1 to 3, *S. lancea* at sites 4 and 5, and *T. usneoides* at sites 6 and 7

5.4 Calibration Results

5.4.1 General Calibration

Within MIKE SHE, determining the realism of the simulated water balance can be assessed from a water balance summary diagram of the simulation. The water balance diagram shows the sum of all inflows and outflows of the study area and the total error caused by calculation problems. As seen in Figure 43, the simulation using the initial parameter values generated a large error (55952mm). This was mainly associated with the boundary flow in the SZ (56425mm) flowing out of the study site. The cause of this error was likely due to the model using two geological layers in the *SZ module*. Too much lateral flow occurred within the SZ. The second geological layer was removed and this resulted in a drastic decrease in the boundary flow in the saturated flow, decreasing from an error value of 56425mm (Figure 43) to 28mm (Figure 44). This new boundary flow value was more realistic.

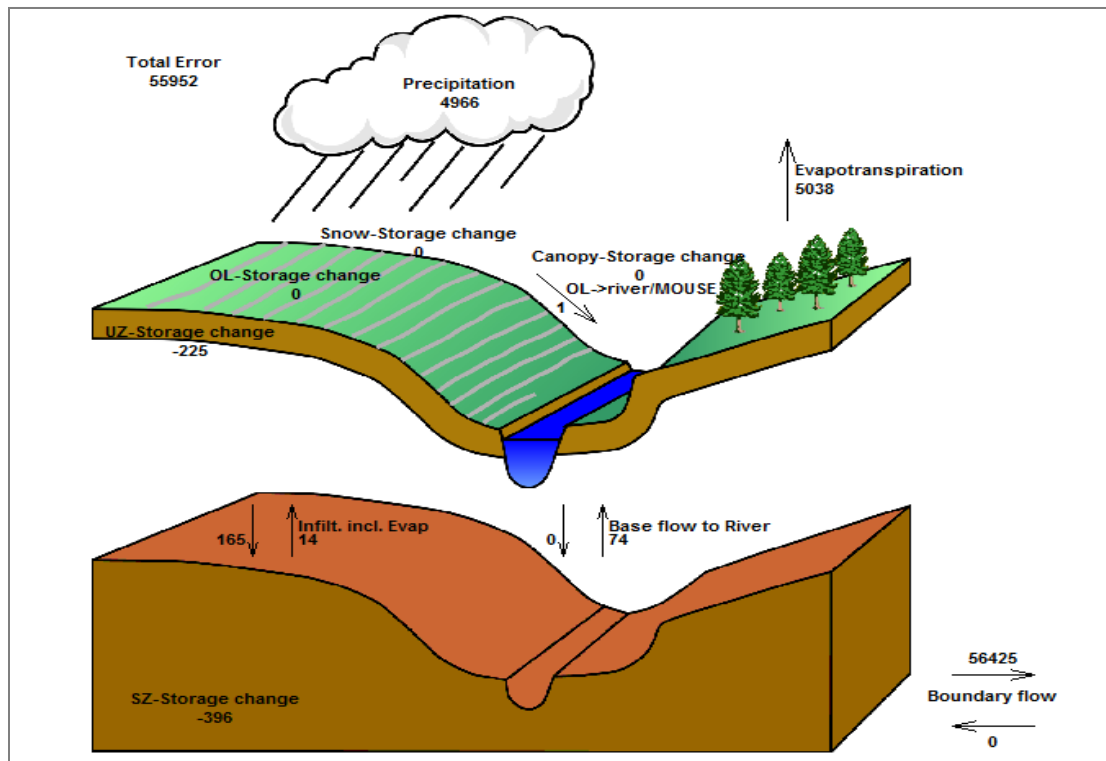


Figure 43: The water balance of the current scenario's initial simulation run

This new calibrated set-up (shown below in Figure 44) was considered acceptable for the study site as the model continued to model a depth of 50mbgl, which would result in an accurate depiction of the saturated and UZ. This decrease as well as all the changes that are mentioned below resulted in an improved water balance. These edits resulted in the total error decrease from 55952 to 0mm.

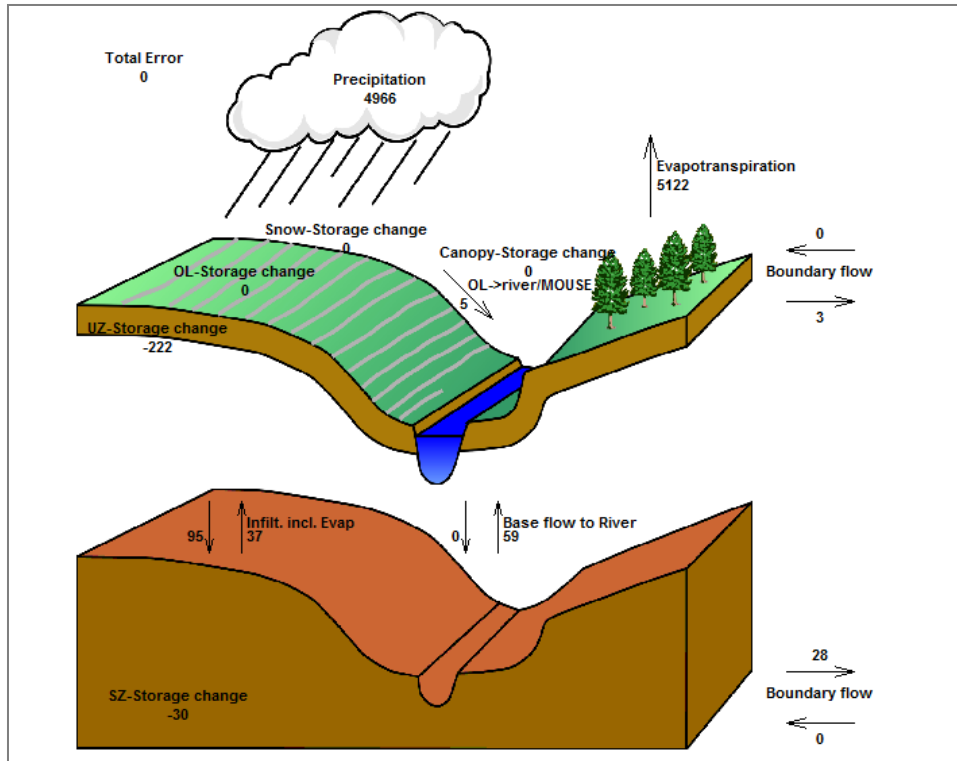


Figure 44: The water balance of the calibrated simulation

This change brought about a greater degree of realism. As seen in Figure 44 the ET (5122mm) was higher than the precipitation (4966mm). ET can exceed rainfall because there was additional water seeping from the TSF which does not originate from rainfall. All the tailings are pumped to the TSF as slurry and seepage of this water adds to the water balance. Movement of water from the SZ to the UZ is minor (37mm). The grassland occurring in the area was associated with a relatively low water uptake (ET). This value would be expected to increase once deep-rooted and evergreen trees are planted. The boundary flow in the *Unsaturated Flow module* (3mm) was insignificant, due to low unsaturated conductivities. The boundary flow in the *SZ module* (28mm) was higher due to higher conductivities. The low *Overland Flow module* to river number (5mm) was low as there was little overland flow that occurred in the area due to flat topography and a reasonable cover of grassland. The movement of water from the UZ to SZ (95mm) indicated an overall groundwater recharge of 2%. Base flow to the river amounts to 59mm. Return flow from the river to the SZ was zero, as expected from the topography and plume movement.

5.4.2 Model Domain

Originally the model was set up to have a grid cell size of 30 x 30m, with 300 by 399 cells in the model domain. However, the early run times were over 400 hours. This was due to the small size of the cells and the high number of cells in the domain. To overcome this problem, the grid cell size was changed from 30 x 30m to a larger size of 120 x 120m. This then altered the number of cells in the domain to 80 x 120 cells. This decreased the run time from 400 hours to less than an hour, which was more practical for repetitive simulations. This increase in cell size could cause a loss in detail of the results, but due to restrictions in time, as well as limitations in computational power, the loss was considered unavoidable. Previous research shows that MIKE SHE output is sensitive to grid cell size (Vazquez *et al.*, 2002) and therefore, for future research it is recommended that a more powerful computer is used.

5.4.3 Topography

The DEM initially used for the topography was of a 5m resolution. In view of the run time problem, the 5m DEM was re-sampled within ARCGIS to a 30m resolution, and then reintroduced into MIKE SHE.

5.4.4 Overland Flow Module

For the original current scenario created, the overland-groundwater exchange option was selected over the separated flow area option. Once calibration for the current scenario was complete, the depth of the overland water was analyzed to determine if the overland-groundwater exchange option was accurately depicting the overland flow. Overland water depths were taken for the simulation points situated throughout the core focus area (Figure 45) the choice of simulation sites is discussed in more detail in section 5.6. The overland water depths show that the maximum overland water depth was 0.158m (Figure 46). This value could be the result of pooling within a ditch and occurs within the beginning of the simulation period, falling in the period the model takes to stabilize. Therefore it was considered realistic from field observation and it was decided that the overland-groundwater exchange option selection for the overland flow module was sufficient for the scenarios.

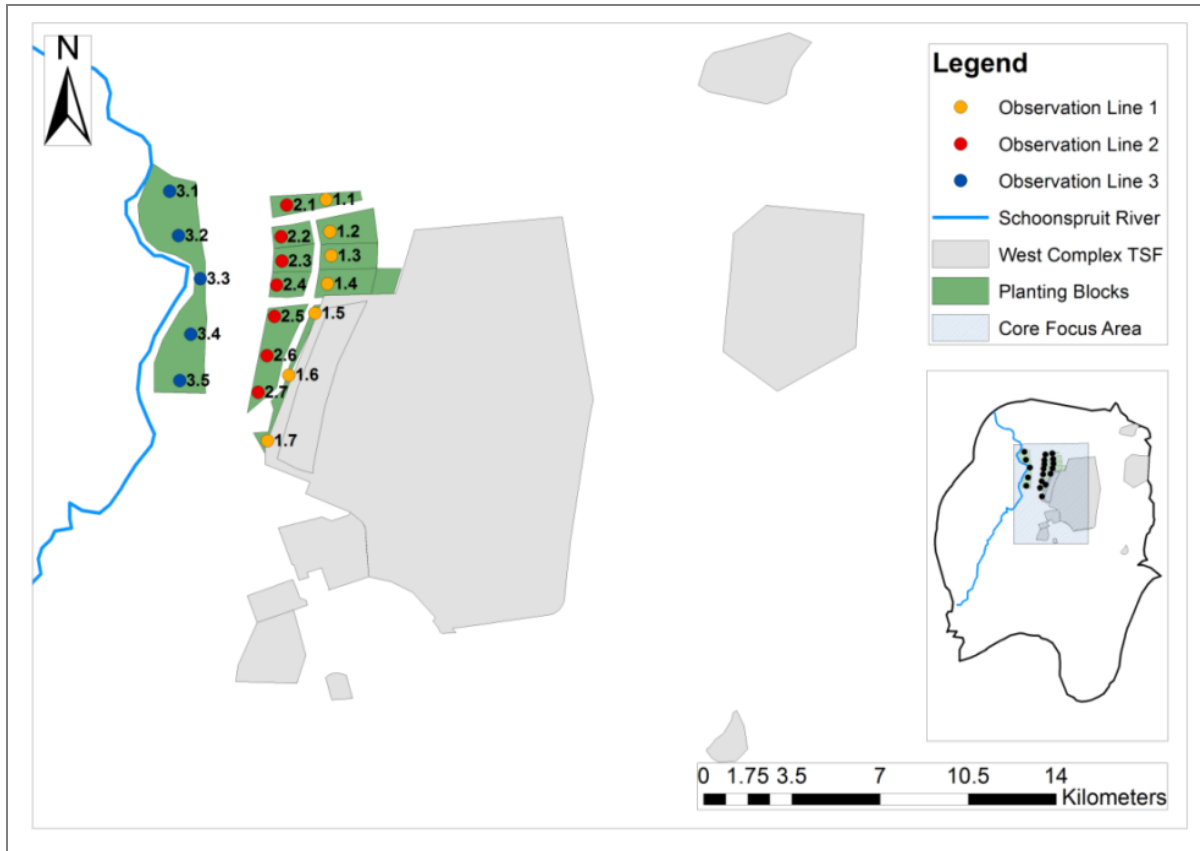


Figure 45: The location of the simulation points

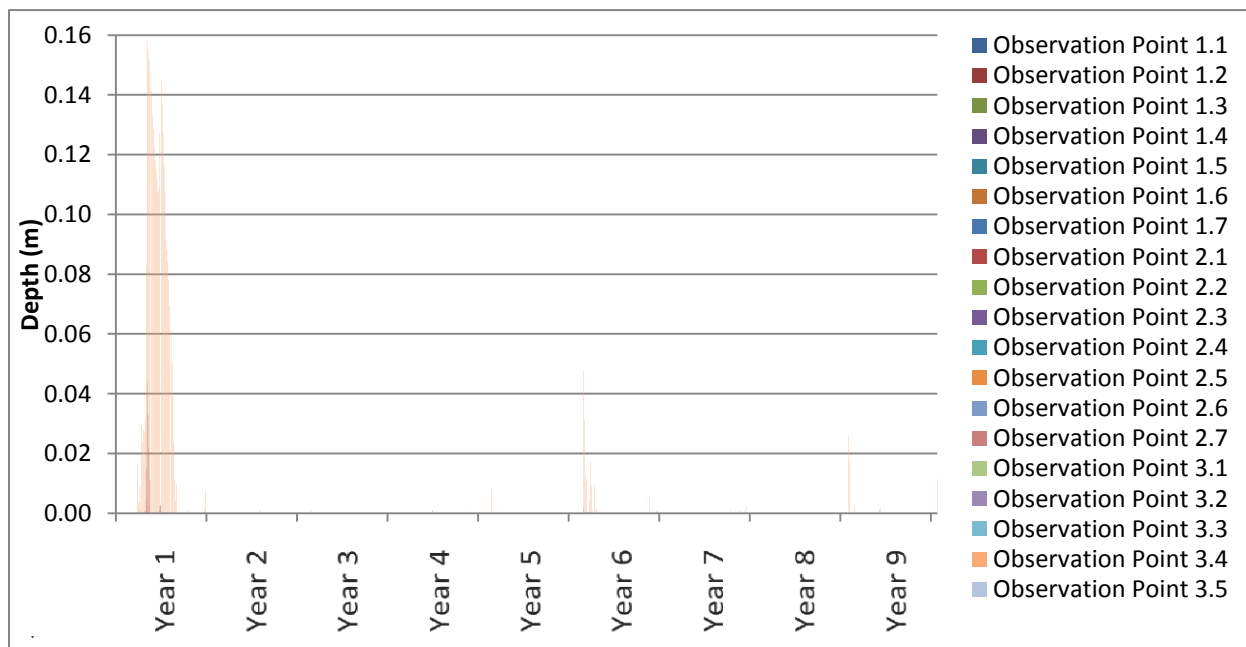


Figure 46: The maximum overland water depths for the current scenario

5.4.5 Unsaturated Flow and Saturated Zone Module

To calibrate the *Unsaturated Flow* and the *SZ modules*, the hydraulic head in the SZ was used. The groundwater table was calibrated by comparing observed borehole data to simulated data from the current scenario simulation.

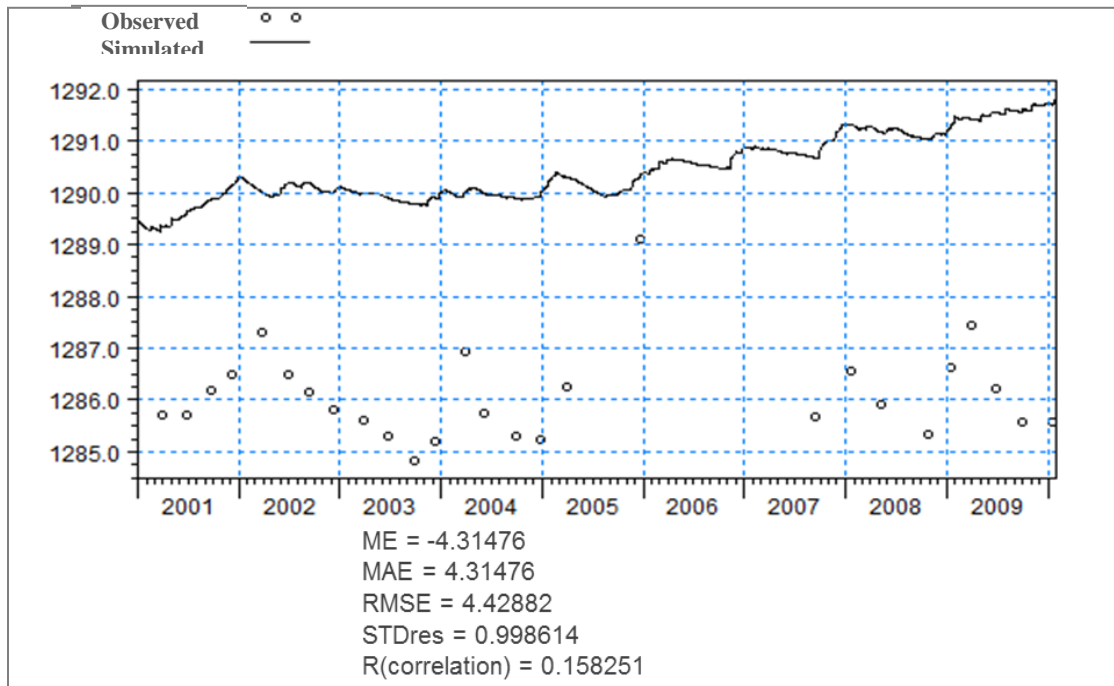


Figure 47: The simulated vs. observed data for the groundwater table at borehole VR04

The simulated water table levels were too low. Therefore calibration was needed to gain a better match between the observed and simulated water table depths. This was done by changing two important parameter values governing lateral flow of groundwater, namely the horizontal and vertical conductivities, under the advice by DHI – South Africa (Table 25). These were altered by trial and error until an improved match between observed and simulated depths were obtained in Figure 48. The RMSE in Figure 48 showed a decrease from 4.43 to 1.32 and supports the visual improvement in the match between simulated and measured depths.

Table 25: The original vs. calibrated input values for the hydraulic conductivity

GEOLOGICAL UNIT	VALUE	HORIZONTAL CONDUCTIVITY (m/s)	VERTICAL CONDUCTIVITY (m/s)
Ventersdorp	Original Value	4.93×10^{-7}	2.73×10^{-3}
	Calibrated Value	4.05×10^{-6}	2.73×10^{-3}
Dolomite	Original Value	4.12×10^{-8}	2×10^{-5}
	Calibrated Value	5.75×10^{-6}	2.53×10^{-3}

Alluvium	Original Value	4.93×10^{-7}	2.73×10^{-3}
	Calibrated Value	8.45×10^{-6}	2.45×10^{-4}
Black Reef	Original Value	6.72×10^{-7}	2.53×10^{-5}
	Calibrated Value	6.5×10^{-7}	2.73×10^{-3}
West Complex TSF	Original Value	5.68×10^{-7}	8×10^{-8}
	Calibrated Value	5.68×10^{-7}	8×10^{-4}

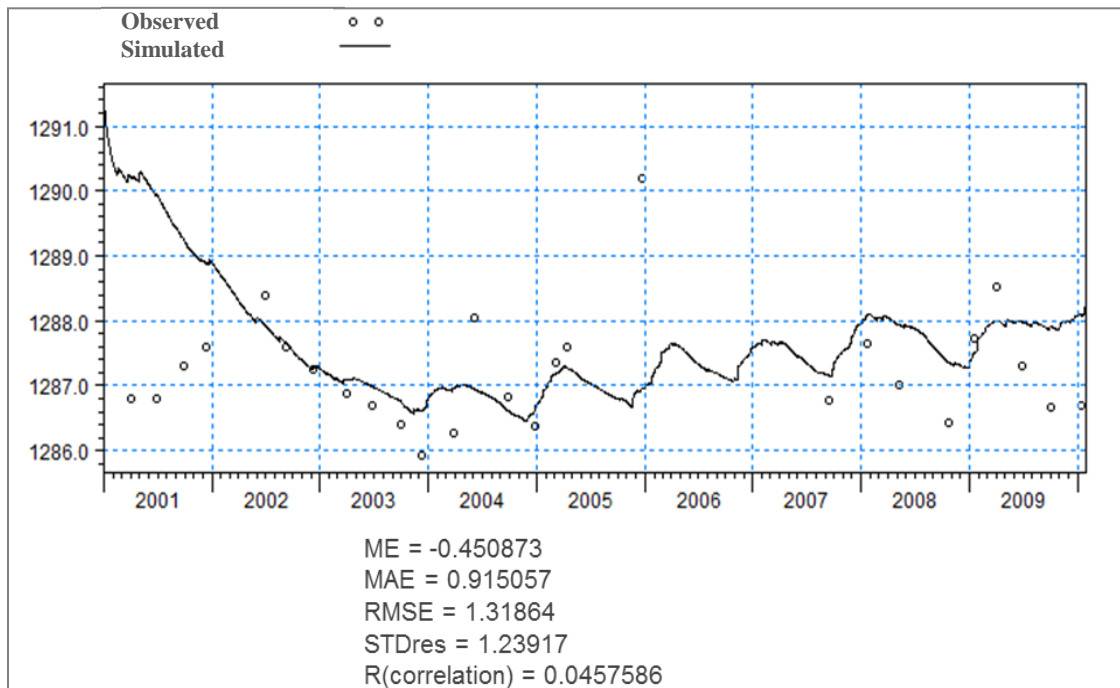


Figure 48: The observed (dotted) and simulated (line) groundwater levels at borehole VR04, using revised conductivity values

The other change to the *SZ module* was the outer boundary condition. This change was determined again through trial and error. Here the rate of outflow at the Vaal River outer boundary was changed from 8.793×10^{-7} m/sec to 0.00793 m/sec. This was done to decrease the outflow of the study site. As previously stated the *SZ module* was decreased from two geological layers to one layer. It should be noted that the first day of the simulation was not the first observed value, and that therefore the model needed to do interpolation between the first day of model and the first day of observations.

5.5 Evapotranspiration Rates

The current scenario and planting scenarios 1 and 2's simulated ET rates were analysed, to determine the impact that mature woodlands would have on the ET rates of the study area. The simulation points 2.1 for scenarios 1 and 2, and 3.3, for scenario 1 (Figure 45), were used to provide a brief overview of the impact that changing the land use of the area, from grasslands to

a woodland species (*S. lancea*, *E. dunnii* and *T. usneoides*), would have on the simulated ET rate. For simulation point 2.1, the current scenario was observed to follow a seasonal pattern where the maximum ET rate was observed between October and March (the wet summer) and the minimum ET rate was observed between April and September (the dry winter). As expected the ET rate of the grasslands was simulated to be zero over the dormant seasons in the winter months due to dry and cold conditions (Figure 49). Peak ET rates (between 1.5 and 2 mm/day) were simulated towards the beginning and end of each year when rainfall and long day lengths promote high ET rates. Across the entire nine year simulation period the grasslands showed a near constant trend in ET (red trend-line in Figure 49). This constant trend is the result of the same LAI and RD being used throughout the simulation period, to depict settled grass with little to no growth occurring.

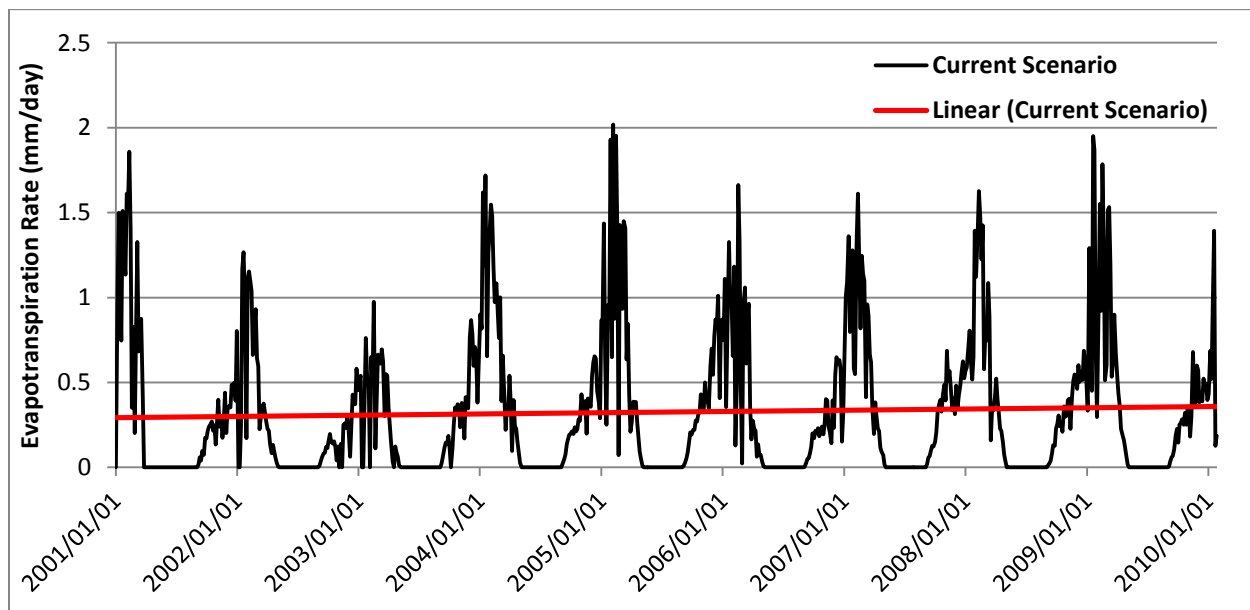


Figure 49: The simulated evapotranspiration rates, for the grassland observed at point 2.1

Planting scenario 1, (planted with *S. lancea* at point 2.1) shows a different ET pattern (Figure 50). This evergreen and deep-rooted tree shows no seasonal dormancy, although rates are reduced by the shorter days of winter. Both winter and summer ET rates were higher than for grassland. Annual ET was therefore increased by replacing grassland with woodland. The long-term trend in ET rate decreased (red trend-line in Figure 50) as the simulation period progressed, with annual peaks declining from 3.4 to 2.0 mm/day. This result is believed to be due to a deficiency in the model.

The pre-dawn plant water status readings showed a mature *S. lancea* tree to be experiencing a low level of water stress after a very long period of dryness (Figure 41), suggesting significant access to deep groundwater. MIKE SHE assumes an exponential decline in root mass with depth which is a useful assumption in many agricultural soils. However, where very deep subsoils and root systems are simulated, these water uptake models cannot account for root proliferation in the capillary zone which is a common phenomenon in trees (Kimber, 1974). Thus, as the water table drops, the uptake of water by the roots decreases.

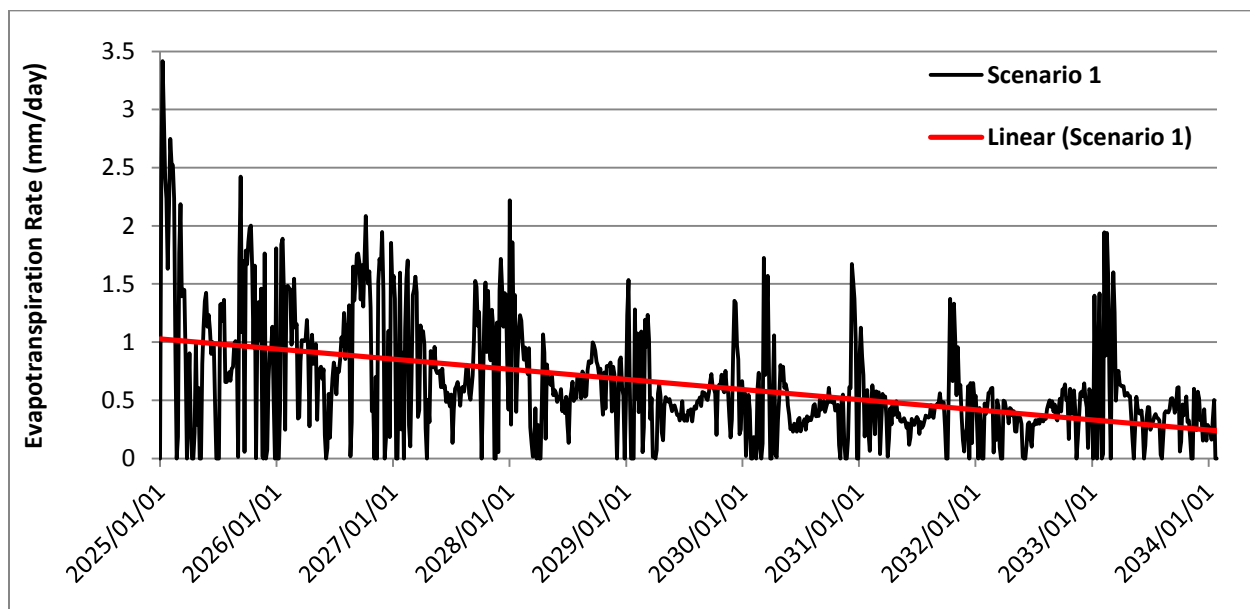


Figure 50: The simulated evapotranspiration rates for *S. lancea*, observed at simulation point 2.1 for the planting scenario 1

Planting scenario 2, at simulation point 2.1, depicts simulated ET for mature *E. dunnii* (Figure 51). As simulated for *S. lancea*, the simulated ET rate for *E. dunnii* showed no dormancy, but reduced ET in the winter months. The simulated *E. dunnii* ET rates were considerably lower than for *S. lancea*. This result is due to *S. lancea* being given a higher LAI index than *E. dunnii*. A higher LAI results in a higher evaporation and transpiration rate. As observed with the *S. lancea* ET rates, there was a noticeable decreasing trend over the entire simulation period, indicating that the roots appeared to be accessing less water each year as the groundwater table dropped.

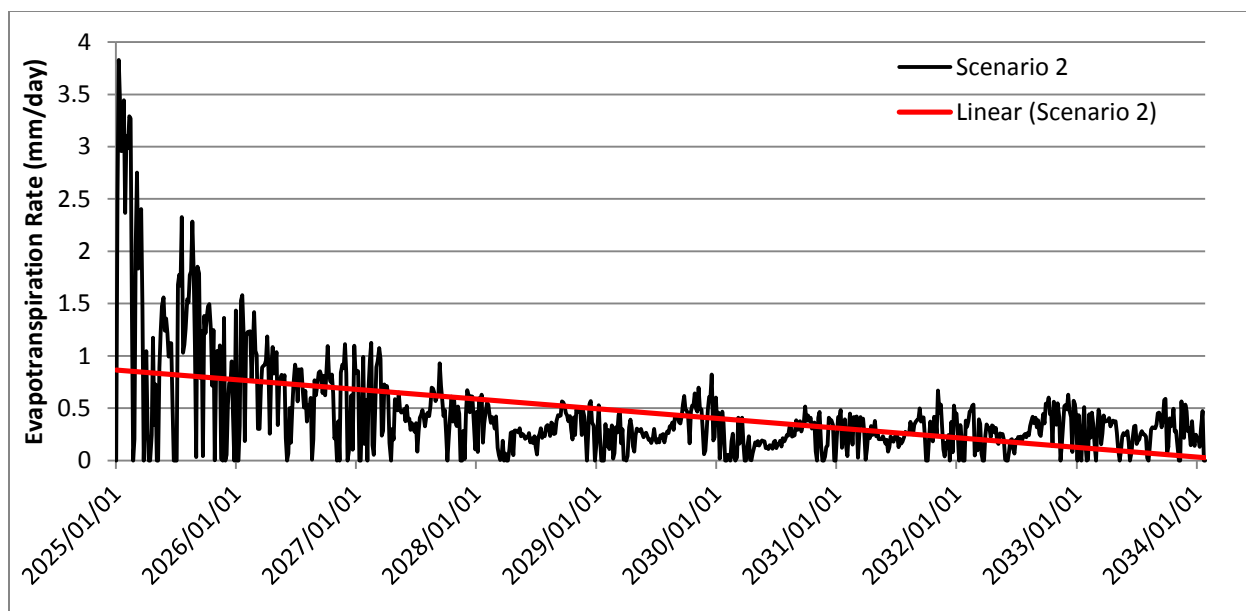


Figure 51: The simulated evapotranspiration rates for *E. dunnii*, observed at simulation point 2.1 for the planting scenario 2

Planting scenario 1 and simulation point 3.5 were used to provide an overview of the simulated ET for *T. usneoides* (Figure 52). The ET rates showed a higher maximum value when compared to the current scenario (grasslands) and *T. usneoides* exhibited few periods of dormancy. These ET rates were higher than those for *S. lancea*. This is attributed to *T. usneoides* shoots remaining largely green in favourable sites.

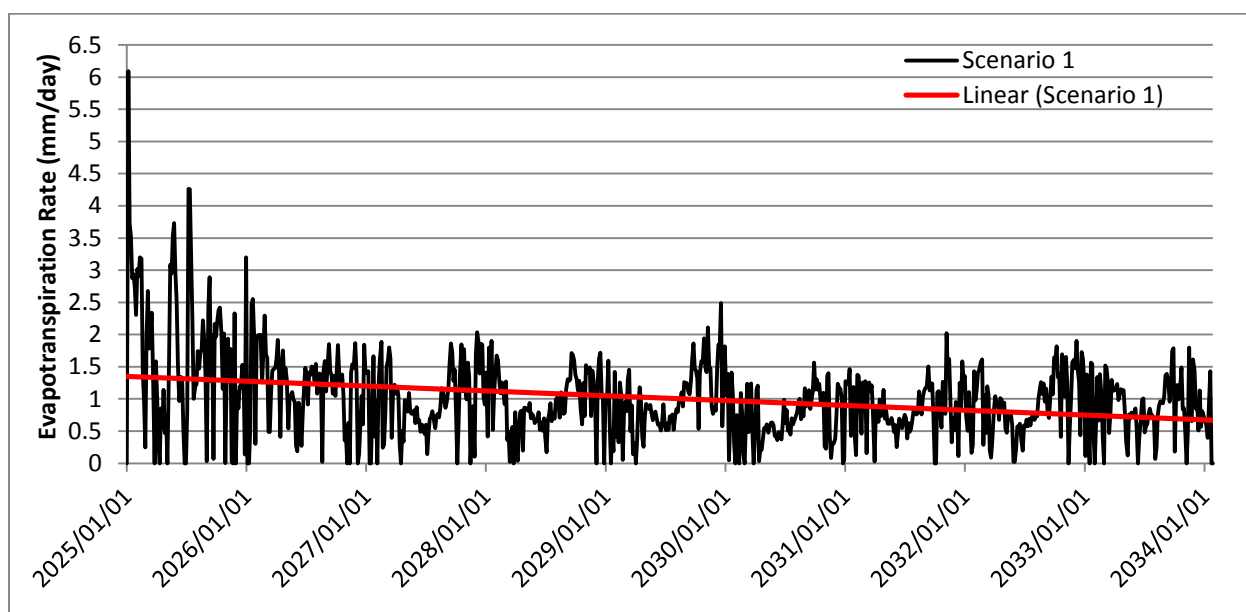


Figure 52: The simulated evapotranspiration rates for *T. usneoides*, observed at simulation point 3.5 for the planting scenario 1

5.6 Groundwater Levels

The change in groundwater level is a crucial aspect of the woodlands remediation and therefore was a focus of the results section. In order to determine the change in groundwater levels that occurred among different planting scenarios, points were chosen in the three main simulation lines as depicted in Figure 45. The purpose of these simulation lines was to show the change that was occurring throughout the core area of interest, between the West Complex TSF and the Schoonspruit River.

The first simulation line (shown as orange points in Figure 45) fell within the eastern planting blocks, stretching to the base of the West Complex TSF. This location was chosen to show the change that occurred directly on the plume seeping from the West Complex TSF. The second simulation line (shown as red points in Figure 45) occurred in between the West Complex TSF and the Schoonspruit River, providing insight into how the first line will affect the mid-slope seepage plume. The final simulation line (shown as blue points in Figure 45) was located in a proposed planting block along the Schoonspruit River. The purpose of this line was to show the influence of *T. usneoides* on the contamination plume just before it enters the Schoonspruit River. In the following graphs, a **positive** change shows a **decrease** in the groundwater depth, while a **negative** change shows an **increase** in the groundwater depth. The change was calculated as the future scenarios' groundwater depths subtracted from the current scenario groundwater depths. This change shows the effect of the mature trees on the equilibrium groundwater depths compared to the current grassland scenario.

5.6.1 Simulation Line One

For simulation line one, seven points were analyzed (Figure 45).

Simulation points 1.1, 1.2 and 1.3 (Figure 53, Figure 54, Figure 55) showed similar levels of change across the future simulation period. These results showed the formation of two distinct groupings of the woodlands planting scenarios. The first group comprised scenarios 1 to 4, while the second group contained scenario 5 and 6. The dips and rises visible in the graphs represented seasonal changes. A dip in the graphs showed the influence of the wet season, which resulted in a raised groundwater level that subsequently caused the change in the groundwater level to decrease. A rise showed the influence of the dry season, which resulted in a lowered groundwater level, which caused the change in groundwater level to increase. At all three of

these points there was a distinct increasing trend in the change of groundwater level experienced over the simulation period. This showed that the mature trees continued to decrease the groundwater level over the simulation period.

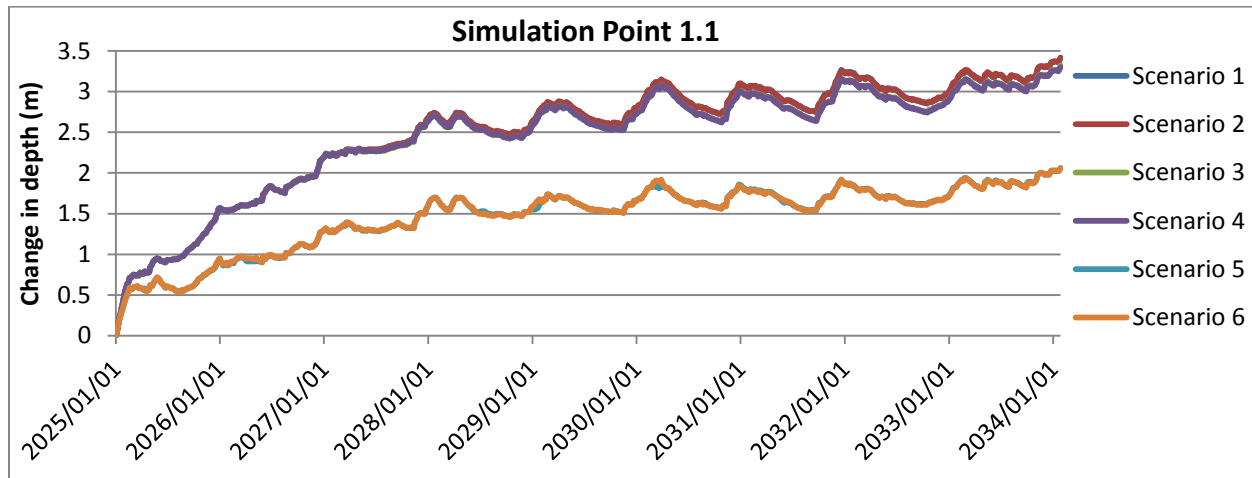


Figure 53: The change in depth (m) of the groundwater level at simulation point 1.1

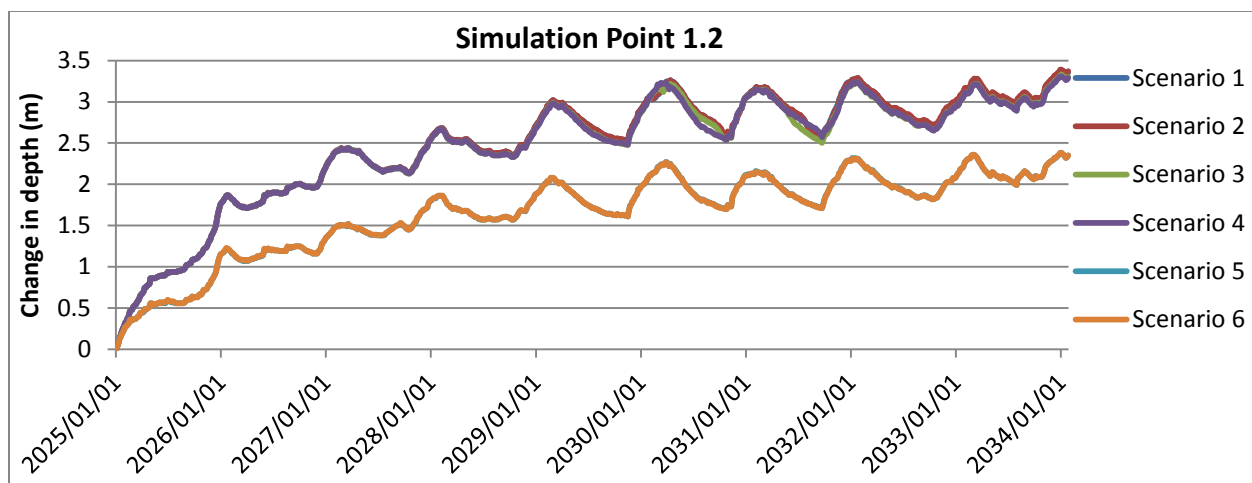


Figure 54: The change in depth (m) of the groundwater level at simulation point 1.2

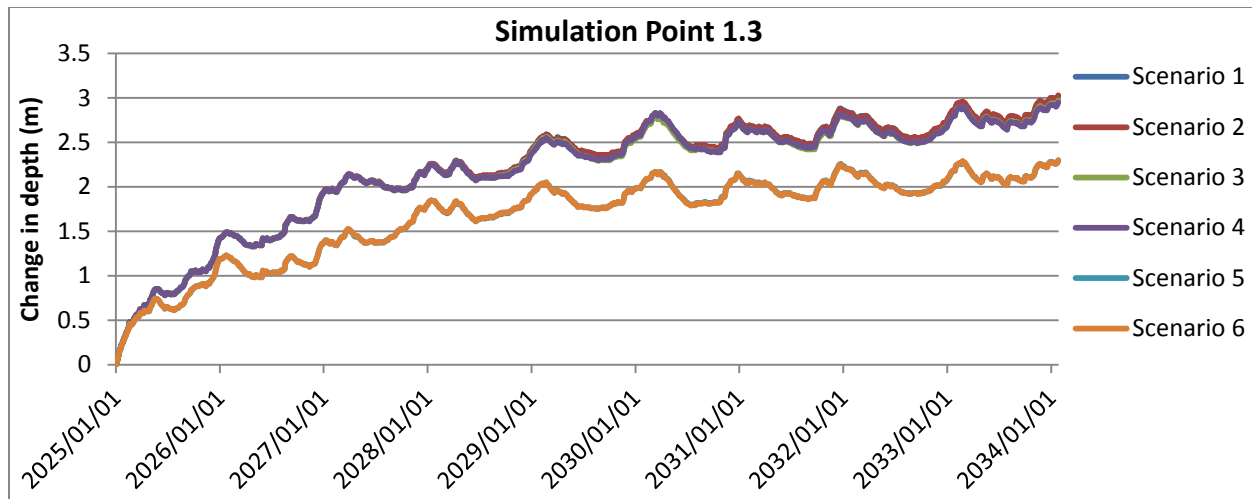


Figure 55: The change in depth (m) of the groundwater level at simulation point 1.3

The degree of change in level brought about by the mature trees decreased as the number of years increases for all the scenarios (Figure 56, Figure 57 and Figure 58). This was due to the first year showing a larger increase in depth (1.56m) than in subsequent years. This increase was due to the model having changed the land use from grassland to mature trees and needed this year to “settle”. An additional influence is the higher ET simulated in the first year, which trends downwards in subsequent years.

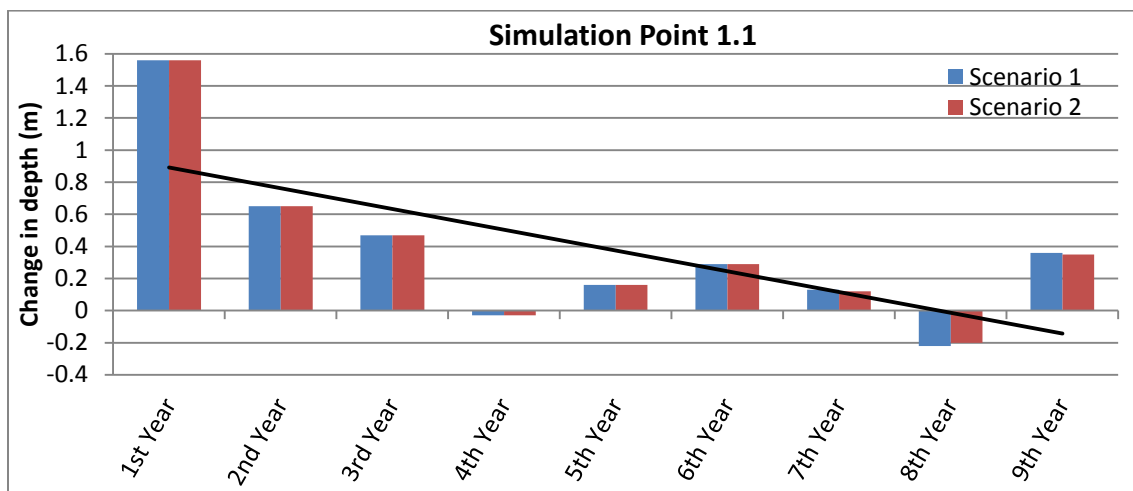


Figure 56: The effectiveness of the mature trees over the simulation period, for simulation point 1.1

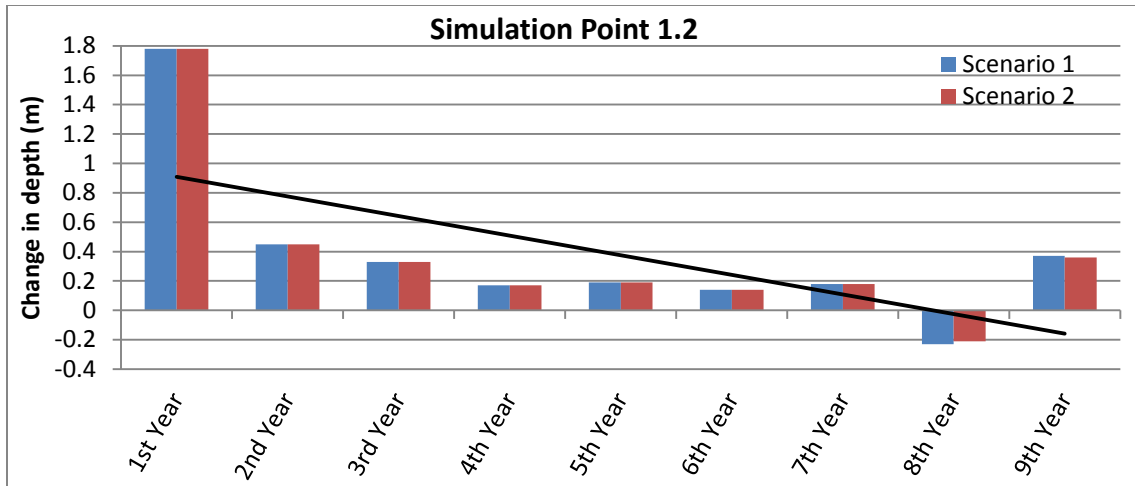


Figure 57: The effectiveness of the mature trees over the simulation period, for simulation point 1.2

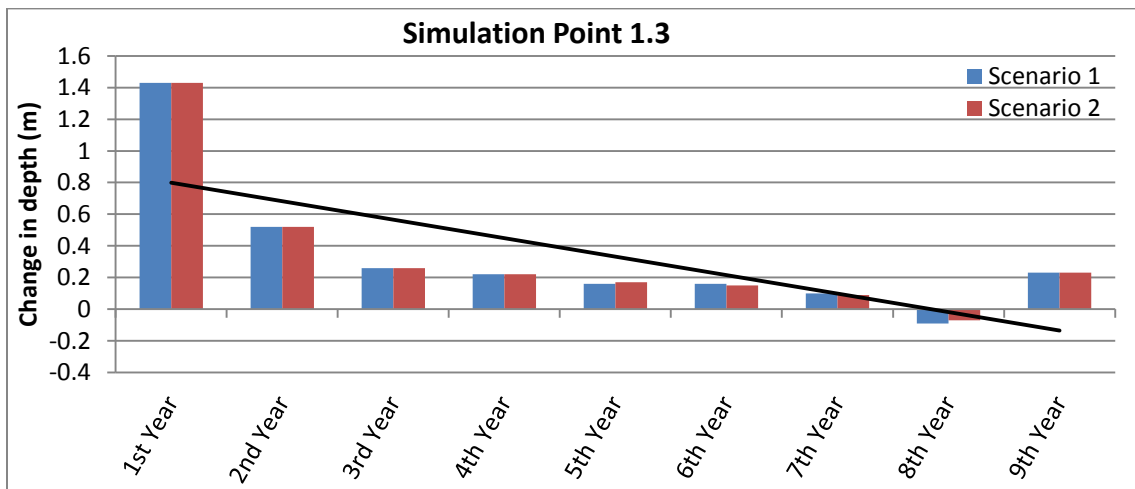


Figure 58: The effectiveness of the mature trees over the simulation period, for simulation point 1.3

The eighth year showed the only annual increase in groundwater level, which occurred directly after the highest rainfall year (Figure 9). This pattern was noticeable at points 1.1 to 1.3 (Figure 56, Figure 57 and Figure 58). The decreasing trend observed for scenarios 1 and 2 were the same as for scenarios 3 through 6 (See Appendix C).

The two scenario groupings that were noticeable at points 1.1 to 1.3 showed a higher degree of change in groundwater levels for the first group over the nine year simulation period than the second group. The highest final change that occurred across these three points was recorded at point 1.1 (3.42m). This degree of change was recorded for both scenario 1 and scenario 2 (Table 26). This result was due to point 1.1 lying the greatest distance from the West Complex TSF therefore it was less influenced by water seepage from the TSF than the other points.

Table 26: The highest final change that occurred at simulation points 1.1 to 1.3

SIMULATION POINT	FINAL CHANGE	
	Maximum final change experienced (m)	Scenario
Simulation Point 1.1	3.42	Scenario 1
		Scenario 2
Simulation Point 1.2	3.37	Scenario 2
Simulation Point 1.3	3.03	Scenario 2

Across all three points scenario 2 showed the greatest decrease in the groundwater level. Scenario 1 was only 0.01m less effective at points 1.2 and 1.3, the difference between the scenarios was 0.3%. Planting scenario 2 included *E. dunnii* and *T. usneoides*, whilst planting scenario 1 included *S. lancea* and *T. usneoides*. It was expected that scenario 2, with the simulated deeper *Eucalyptus* root system would extract groundwater more effectively than the shallower *S. lancea* root system. The difference in root system depths may be offset by the higher LAI simulated for *S. lancea*, which results in a higher evapotranspiration rate.

Scenarios 3 and 4, both with no *T. usneoides*, were not dissimilar from scenarios 1 and 2. On average scenarios 3 and 4 reduced the groundwater level by only 0.09m. Overall, scenarios 3 and 4 average performance was 98.62% of scenarios 1 and 2, while scenarios 5 and 6 performed at 61.4% (Figure 59). The marginal difference (1.38%) seen between scenarios 1 and 2 and scenarios 3 and 4 was a result of points 1.1 to 1.3 lying relatively far and upslope from the *T. usneoides* planting block situated along the Schoonspruit River. Therefore, the planting of *T. usneoides* had little effect on the results. Scenarios 5 and 6 (no trees in non-AGA blocks) resulted in a decrease in effectiveness of 38.6%. This is attributed to these points being further away from the non-AGA blocks, and very close to the TSF.

Simulation points 1.4 and 1.5 (Figure 60 and Figure 61 respectively) showed similar seasonal patterns to points 1.1 to 1.3, although these points showed a lower degree of change to the groundwater levels in previous points. The maximum final change observed between points 1.4 and 1.5 was 1.27m. This was a 50% smaller change than was observed at points 1.1 to 1.3. An explanation could be that points 1.4 and 1.5 were situated closer to the West Complex TSF than points 1.1 to 1.3, resulting in them having access to freer water from the seepage of water than from the West Complex TSF.

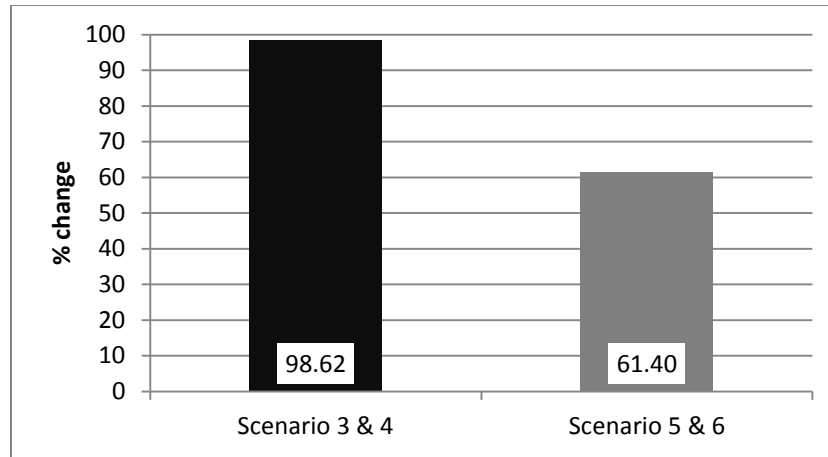


Figure 59: The performance (%) of scenarios, at points 1.1 to 1.3, compared with scenario 1 & 2

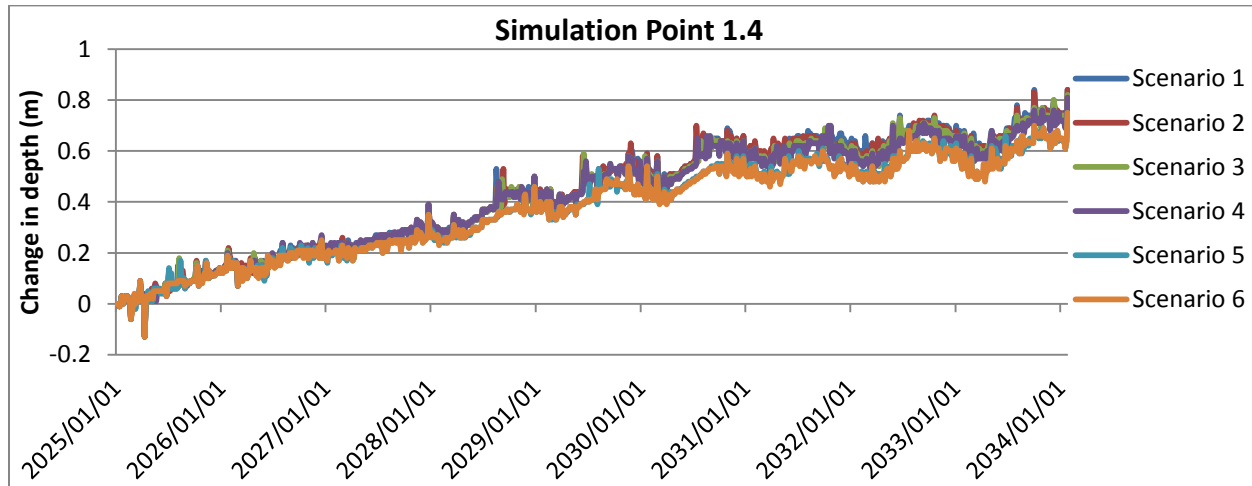


Figure 60: The change in depth (m) of the groundwater level at simulation point 1.4

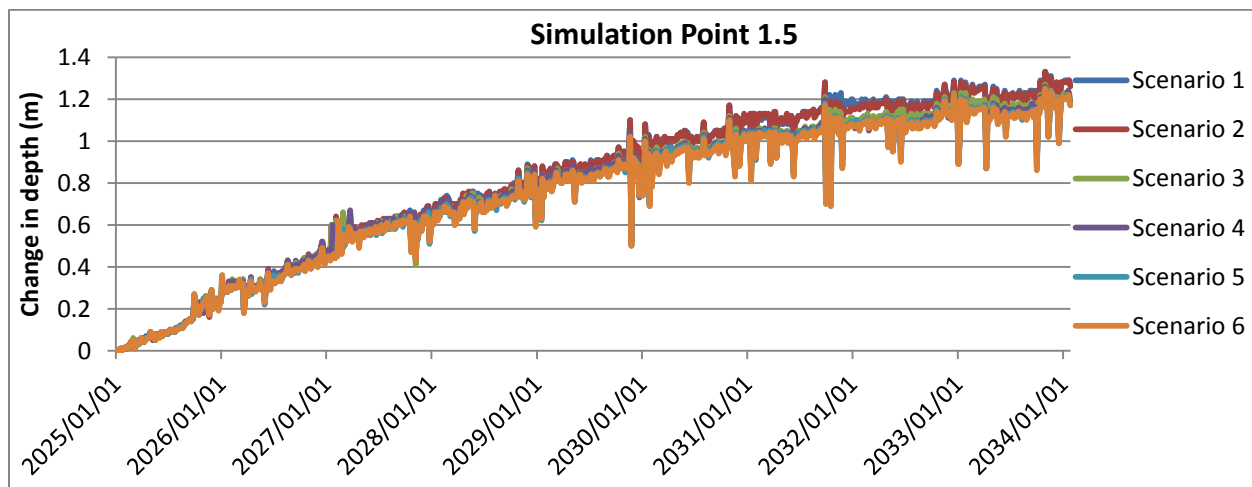


Figure 61: The change in depth (m) of the groundwater level at simulation point 1.5

At simulation points 1.4 and 1.5 the distinct groupings that were previously observed at points 1.1 to 1.3 were not as prominent. This was due to these points lying further away from the non-AGA owned blocks and closer to the TSF. There was also a decrease observed in the effectiveness of the mature woodlands over the years (Figure 62 and Figure 63). The higher first year value observed for points 1.1 to 1.3 was not as significant for point 1.4. This is again the result to these points being closer to the seepage source and having little upslope woodland.

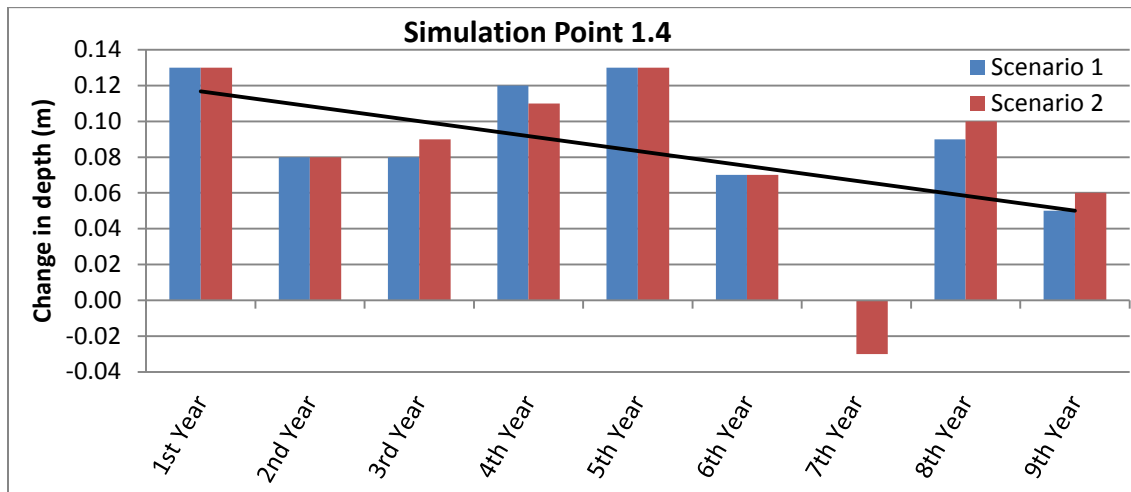


Figure 62: The effectiveness of the mature trees over the simulation period, for simulation point 1.4

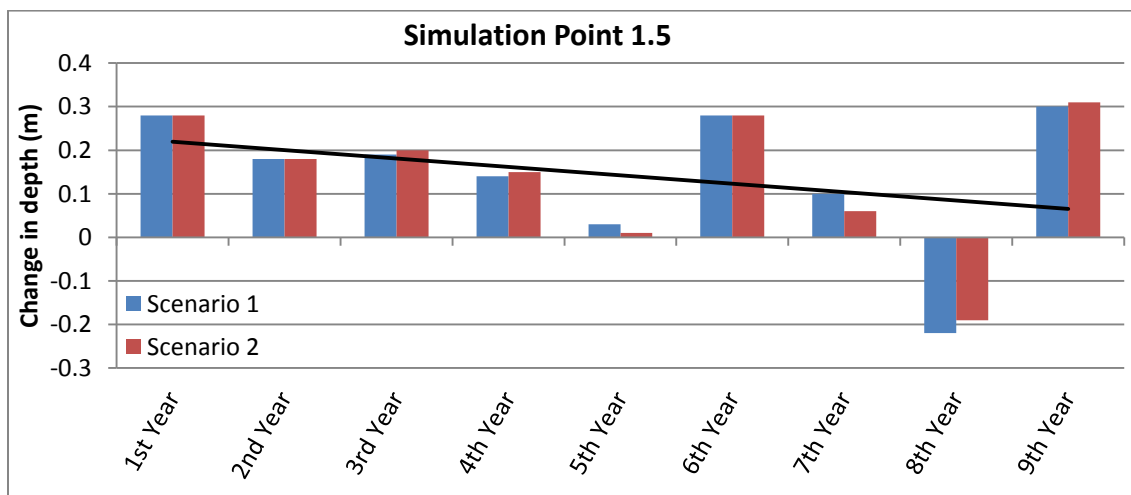


Figure 63: The effectiveness of the mature trees over the simulation period, for simulation point 1.5

For simulation points 1.4 and 1.5, the lack of noticeable grouping resulted in difficulty in determining which scenario was performing best. However, when the maximum final change was evaluated (Table 27) planting scenario 1 showed the greatest degree of change (1.27m) at

simulation point 1.5. At simulation point 1.4, both scenarios 1 and 2 performed equally well in reducing the groundwater level, similar to the result observed at points 1.1 to 1.3. The final degree of change experienced at points 1.4 and 1.5 however showed a lower degree of change than that at points 1.1 to 1.3. There was a 2.15m difference simulated in total change experienced at points 1.4 and 1.5. This is a result of the influence of strong seepage from the West Complex TSF being simulated by the model.

Table 27: The highest final change observed at simulation points 1.4 and 1.5

SIMULATION POINT	FINAL CHANGE	
	Maximum final change experienced (m)	Scenario
Simulation Point 1.4	0.84	Scenario 1
		Scenario 2
Simulation Point 1.5	1.27	Scenario 1

For simulation point 1.4, scenarios 3 and 4 showed a difference of 0.02m when compared with scenarios 1 and 2, whilst scenarios 4 and 5 showed a 0.09m difference. Simulation point 1.5 however, showed a 0.08m difference between scenarios 1 and 2 and scenarios 3 and 4, whilst scenarios 5 and 6 showed a further 0.01m difference from scenarios 3 and 4.

Scenarios 3 and 4 were observed to perform similarly to scenarios 1 and 2 (Figure 64). This was due to points 1.4 and 1.5 being largely free from the influence of the *T. usneoides* planting block. Meanwhile scenarios 5 and 6 continued to show the least change in groundwater levels (Figure 64).

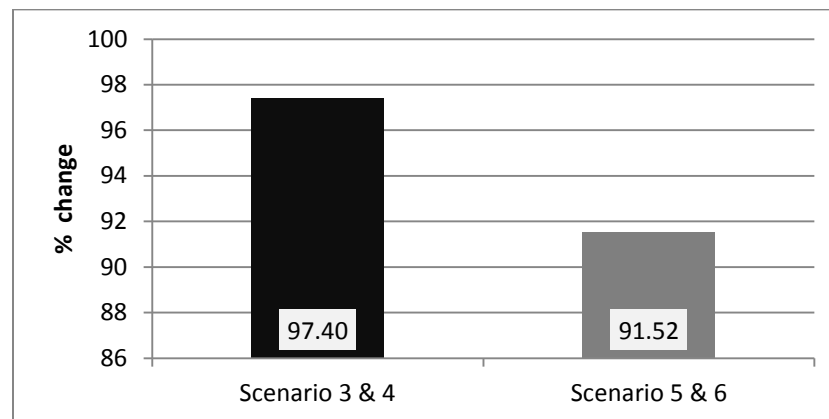


Figure 64: The performance (%) of scenarios compared with 1 & 2 at simulation points 1.4 and 1.5

Simulation point 1.6 (Figure 65) provided an anomaly whereby there was a steep increase in change experienced in 2027. This anomaly could be related to an extreme rainfall event in mid-2027 which was effective in raising the water table elevation. This simulation point also showed a less distinct seasonal pattern when compared to points 1.1 to 1.5. It also showed a degree of change in the groundwater level that was intermediate between points 1.1 to 1.3 and points 1.4 and 1.5. For point 1.6, the scenarios impacts were ranked differently to those observed at points 1.1 to 1.5. A first grouping at point 1.6 contained scenarios 1, 2, 5 and 6, whilst a second grouping contained scenarios 3 and 4. The choice of these groupings was decided when these groupings occurred naturally during analysis. This result was similar to that seen at point 1.7 (Figure 68). Both these points lie closest to the *T. usneoides* planting block, and are influenced by changes in *T. usneoides* evapotranspiration and groundwater levels. The small difference in change observed between scenarios 1 and 2 and scenarios 5 and 6 was due to the distance of points 1.6 from the non-AGA planting block. When considering the degree of change in the groundwater levels for each year, point 1.6 (Figure 66) followed a similar pattern to simulation points 1.1 to 1.3. There was the significantly higher first year value and the increase in the groundwater level in the eighth year. The decreasing trend of effectiveness through the years showed that at point 1.6 there was a slightly lower degree of change experienced than that experienced at points 1.1 to 1.3.

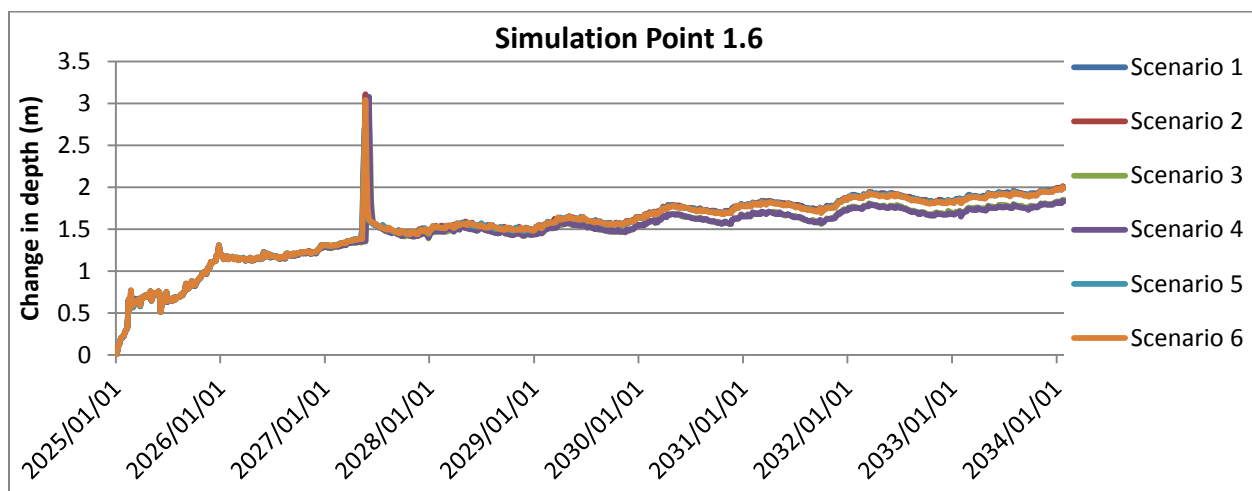


Figure 65: The change in depth (m) of the groundwater level at simulation point 1.6

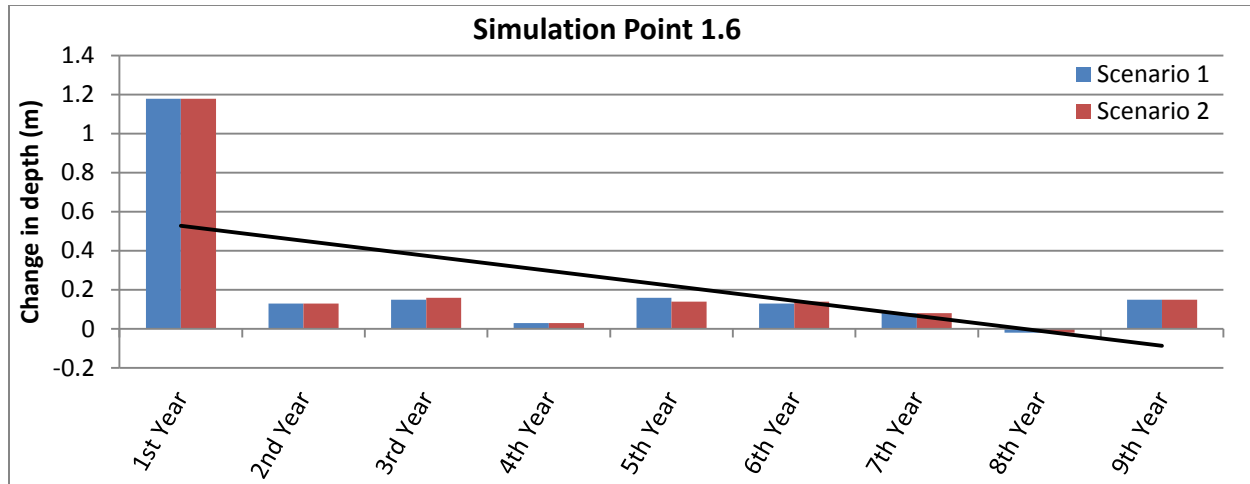


Figure 66: The effectiveness of the mature trees over the simulation period, for simulation point 1.6

The highest final change experienced at point 1.6 was recorded for scenario 1, with a 2m change in the groundwater levels (Table 28). Scenario 2 showed a similar degree of change as observed in scenario 1, with a difference of only 0.01m. Scenarios 5 and 6 were equally as effective in decreasing the groundwater as scenario 2, with a final change of 1.99m. As seen in Figure 65, scenarios 3 and 4 were the worst at decreasing the groundwater levels, with a change of only 1.85 and 1.83m being experienced respectively.

Table 28: The highest final change that occurred at simulation points 1.6

SIMULATION POINT	FINAL CHANGE	
	Maximum final change experienced (m)	Scenario
Simulation Point 1.6	2.00	Scenario 1

At points 1.1 through to 1.5 the most effective planting scenarios were scenarios 1 and 2 with scenarios 3 and 4 showing the next highest final change in groundwater level. However, with point 1.6, the most effective planting scenario was scenario 1 and 2 with scenario 5 and 6 observed to be the next best performer (Figure 67). Scenario 5 and 6 performing at 99.75% of scenarios 1 and 2 was the cause for the tight grouping of these scenarios observed in Figure 65. Point 1.6 showed the smallest difference in performance between the scenarios.

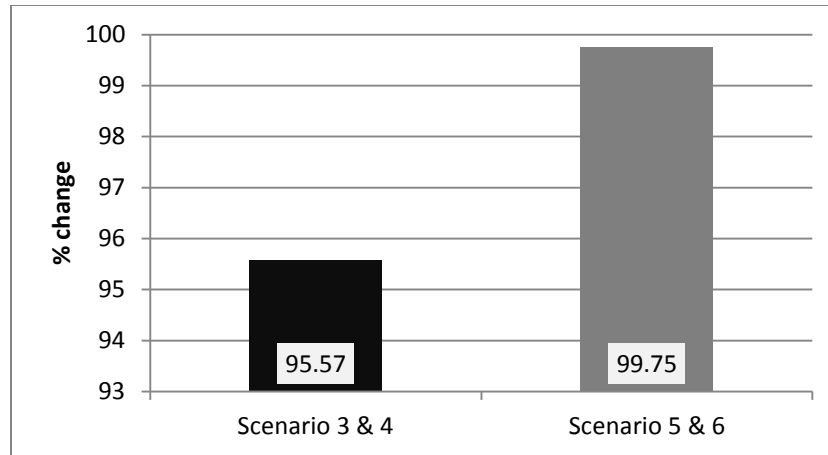


Figure 67: The performance (%) of scenarios compared with scenarios 1 & 2, at simulation point 1.6

Simulation point 1.7 was observed to be the point with the least change in groundwater level of all the points in simulation line one. The highest final change (scenario 5) was 0.25m, less than 10% of the change that was experienced at points 1.1 to 1.3. This change was observed between scenario 5 and 6, whilst scenarios 3 and 4 showed the lowest degree of change. The seasonal patterns were less pronounced at point 1.7 than at points 1.1 to 1.5, however they were more pronounced than at point 1.6.

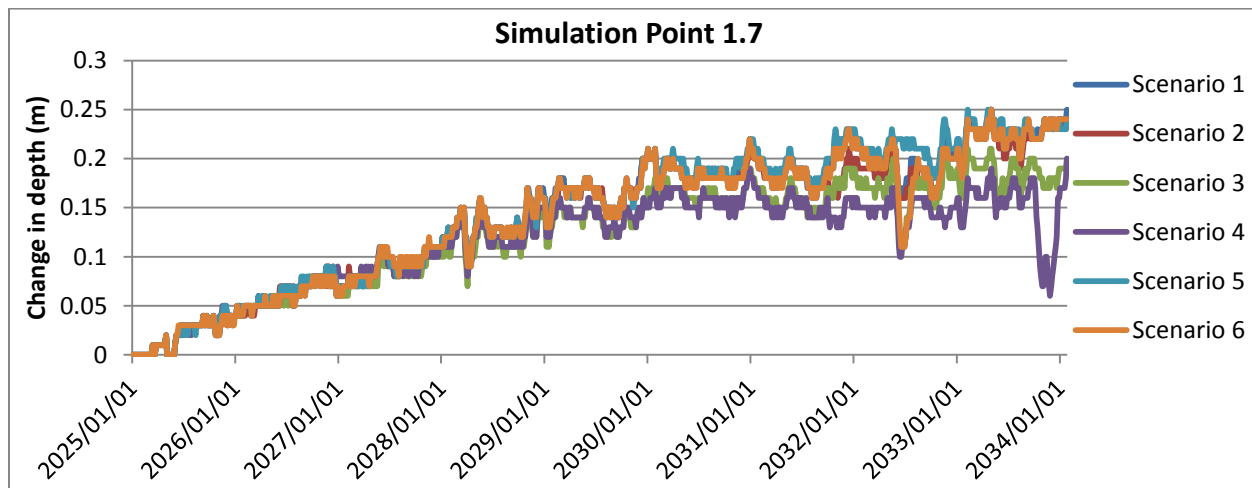


Figure 68: The change in depth (m) of the groundwater level at simulation point 1.7

At simulation point 1.7, there was the same decreasing trend in effectiveness of the mature woodlands. Due to the small degree of change that was seen in Figure 68, the effects of the mature woodlands at the end of the nine year simulation were significantly smaller than those experienced at points 1.1 through to point 1.6. Point 1.7 showed an anomaly in the seventh year

where scenario 2 showed an increase in the groundwater level whilst scenario 1 showed a decrease. Simulation point 1.4 showed a similar increase in the groundwater level experienced for the seventh year, however scenario 1 showed no decrease.

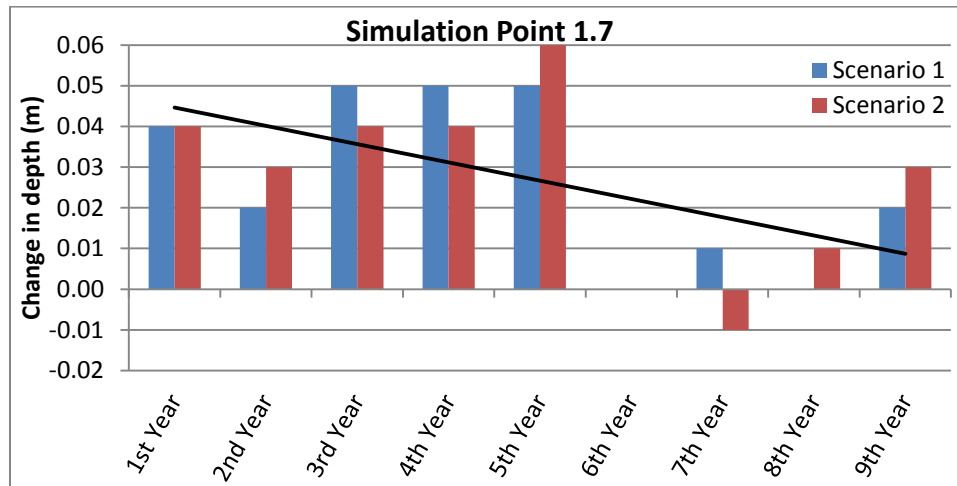


Figure 69: The effectiveness of the mature trees over the simulation period, for simulation point 1.7

A similar pattern to point 1.5 occurred at simulation point 1.7. Scenario 1 was the best performer, while scenarios 2, 5 and 6 were similar with a 0.01m difference observed. The final change in level at the end of the simulation period at point 1.7 proved to be the smallest at 0.25m (Table 29). This was 7.3% of the change found at 1.1.

Table 29: The highest final change that occurred at simulation points 1.7

SIMULATION POINT	FINAL CHANGE	
	Maximum final change experienced (m)	Scenario
Simulation Point 1.7	0.25	Scenario 1

At simulation point 1.7, scenarios 3 and 4 were observed as the scenarios with the smallest decrease in level, while scenarios 5 and 6 showed the highest degree of change. When considering the performance of the scenarios, scenarios 3 and 4 were observed to perform at 88.67% of scenarios 1 and 2, this means that scenarios 3 and 4 were 0.8867 times less effective than 1 and 2. For simulation line one, point 1.7 showed the only location where scenarios 5 and 6 showed the highest decrease of the groundwater table. Scenarios 5 and 6 showed a 1.17% increase in performance over scenarios 1 and 2 at point 1.7.

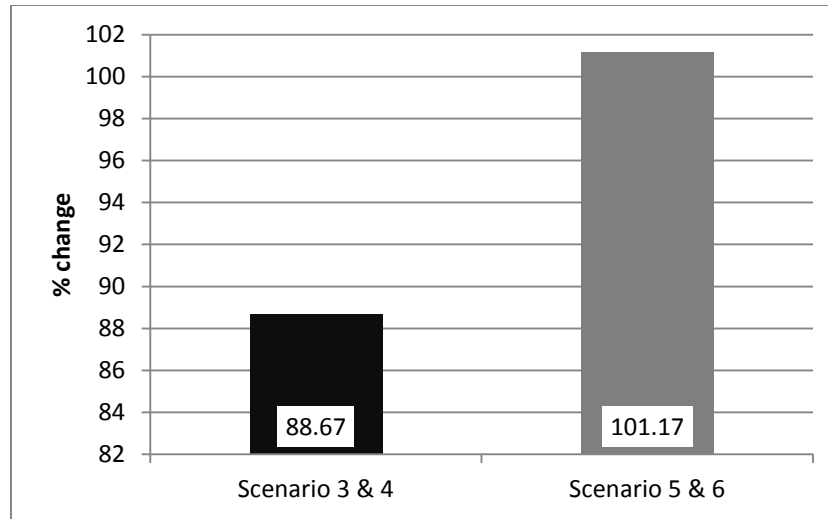


Figure 70: The performance (%) of scenarios compared with scenarios 1 & 2, at simulation point 1.7

5.6.2 Simulation Line Two

There were seven simulation points for simulation line two (Figure 45). These were located in between the West Complex TSF and the Schoonspruit River. This location was chosen to determine the mid-slope changes in water table depth.

For simulation points 2.1 through to 2.3 there were similar patterns observed in the change in the groundwater levels. Three scenario groups were observed. A first group containing scenarios 1 and 2, a second group containing scenarios 3 and 4 and finally a third group contained scenarios 5 and 6. Group one showed the highest degree of change across the simulation period. Group two showed similar patterns, but was observed to be less effective at decreasing the groundwater level. At simulation points 2.2 and 2.3 seasonal rises and dips were observed. This was less noticeable at point 2.1. This resulted from 2.1 falling in a deeper groundwater level area than found at points 2.2 and 2.3. The large difference seen between scenarios 1 and 2 and scenarios 5 and 6 were the results of points 2.1 to 2.3 falling in or around the non-AGA owned planting blocks. This highlighted the influence these blocks had on the groundwater level change. This was a similar pattern to that found at points 1.1 to 1.3. The equal performance of scenario 1 and 2 is again attributed to higher *S. lancea* LAI counterbalancing the effects of deeper roots in *E. dunnii* stands.

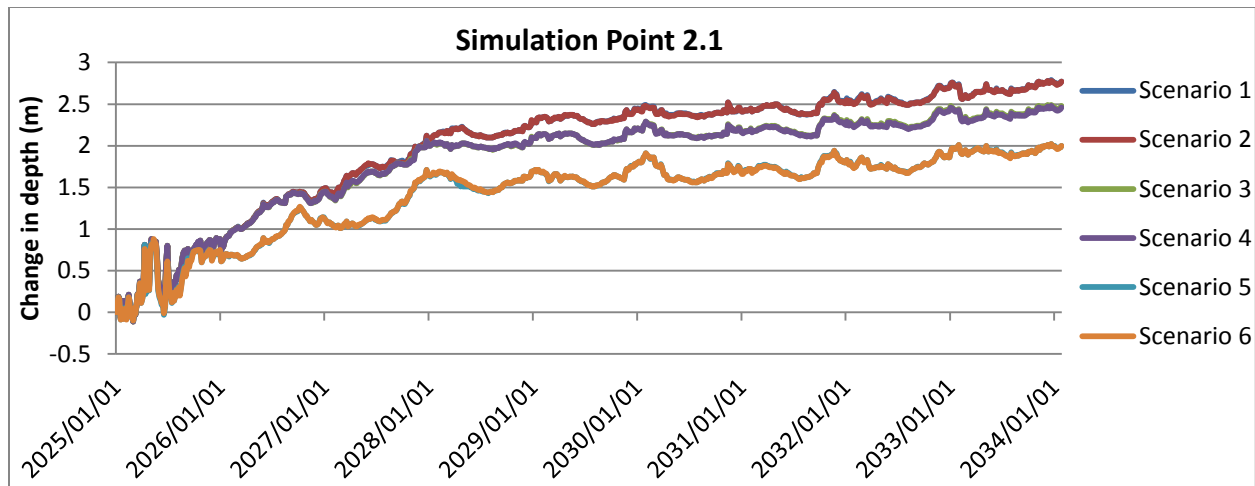


Figure 71: The change in depth (m) of the groundwater level at simulation point 2.1

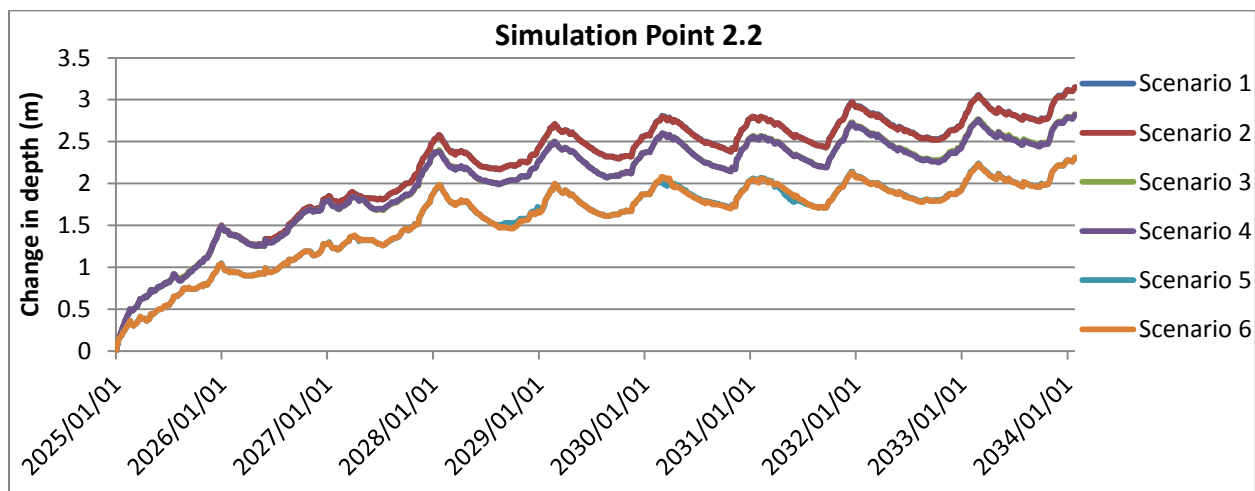


Figure 72: The change in depth (m) of the groundwater level at simulation point 2.2

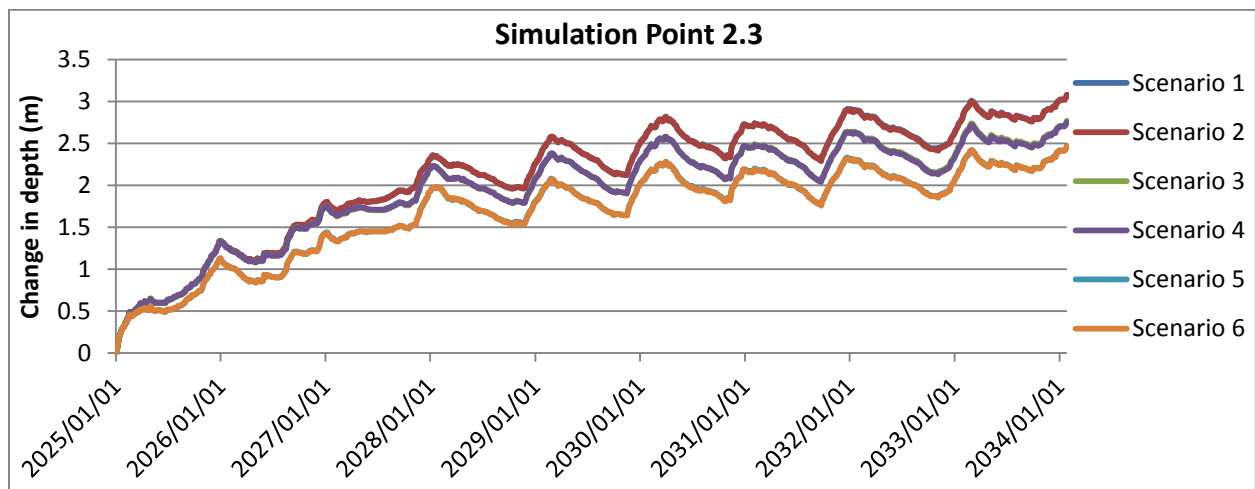


Figure 73: The change in depth (m) of the groundwater level at simulation point 2.3

Points 2.1 to 2.3 showed a similar decreasing trend in the change observed over the nine-year period (Figure 71, Figure 72 and Figure 74). Similar patterns were observed at these points to those seen at points 1.1 to 1.3. The first year value was noticeably higher at point 2.2 and 2.3 (Figure 75 and Figure 76), while at point 2.1 the first year was similar to the second year. Another similarity observed between points 1.1 and 1.3 and points 2.2 and 2.3 was the increase in groundwater level observed at 2028 (4th year) and 2032 (8th year). Once again, point 2.1 (Figure 74) broke the pattern and did not show the same level of increase in groundwater level.

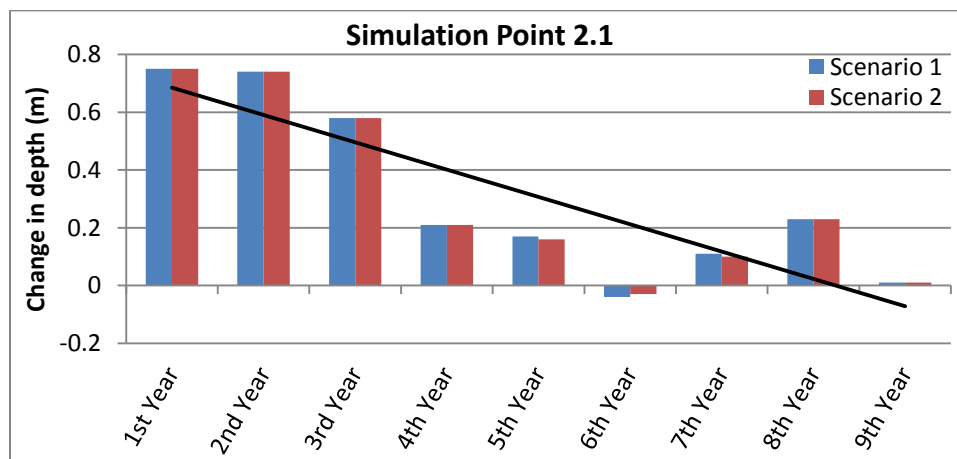


Figure 74: The effectiveness of the mature trees over the simulation period, for simulation point 2.1

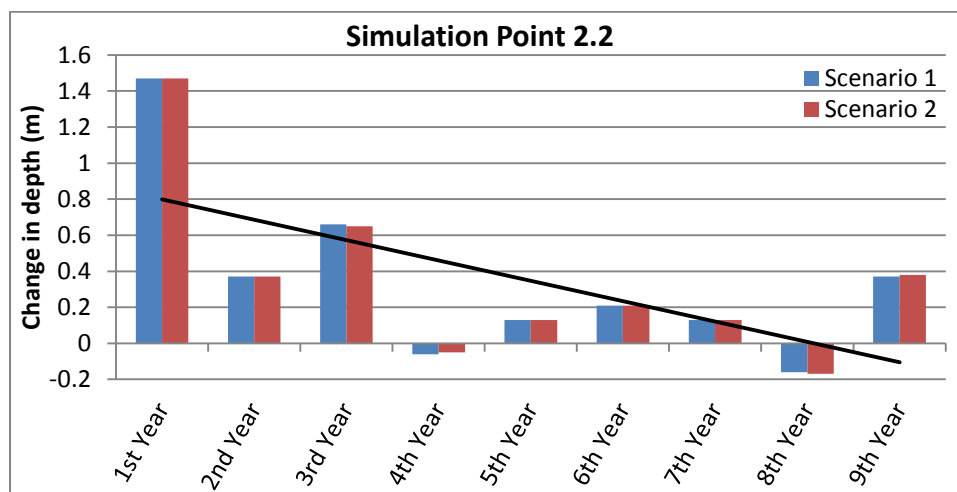


Figure 75: The effectiveness of the mature trees over the simulation period, for simulation point 2.2

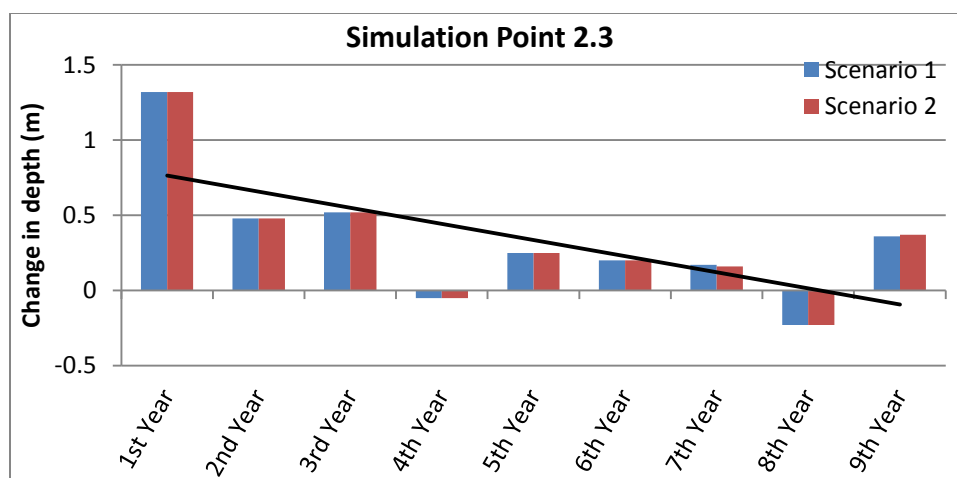


Figure 76: The effectiveness of the mature trees over the simulation period, for simulation point 2.3

Simulation point 2.1 showed a lower degree of change each year when compared with points 2.2 and 2.3. This could be the result of point 2.1 lying furthest away from the TSF and therefore having a deeper groundwater level. This means the plants had less opportunity to decrease the groundwater level. The decreasing trend observed for scenarios 1 and 2 were the same as for scenarios 3 through 6 (See Appendix C). The maximum final change observed for points 2.1 to 2.3 at the end of the simulation period was seen in scenarios 1 and 2, with a final change of 3.15m recorded.

Table 30: The highest final change observed at simulation points 2.1 to 2.3

SIMULATION POINT	FINAL CHANGE	
	Maximum final change experienced (m)	Scenario
Simulation Point 2.1	2.77	Scenario 1
		Scenario 2
Simulation Point 2.2	3.15	Scenario 1
		Scenario 2
Simulation Point 2.3	3.08	Scenario 1
		Scenario 2

To reiterate the importance of the planting scenario, Figure 77 showed that by not planting *T. usneoides* along the Schoonspruit River the degree of change observed decreased by over 7%. Not using the non-AGA owned planting blocks decreased the degree of change in groundwater level by over 25%. This highlighted the importance of the non-AGA owned planting blocks.

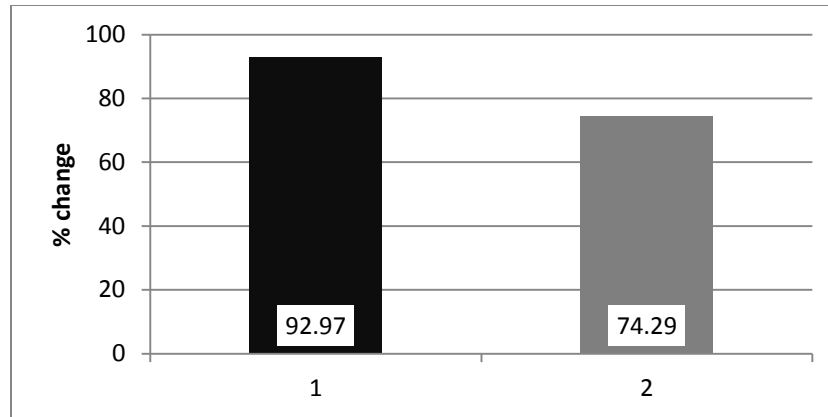


Figure 77: The performance of scenarios, at simulation point 2.1 to 2.3, compared with scenarios 1 & 2

At simulation points 2.4 and 2.5 there were only two scenario groupings visible in the results, similar to that seen at points 1.4 and 1.5 (Figure 78 and Figure 79). Group one contained scenarios 1, 2, 5 and 6 and group two contained scenarios 3 and 4. This grouping occurred at points 2.4 and 2.5 as they did not lie in or around the non-AGA owned planting blocks, so the effect of planting in these blocks was less noticeable.

Simulation point 2.4 (Figure 78) showed little to no seasonal variation, whilst point 2.5 (Figure 79) showed slight seasonal variation. Most noticeable was the flattening of the change in the groundwater at point 2.4, especially after 2028.

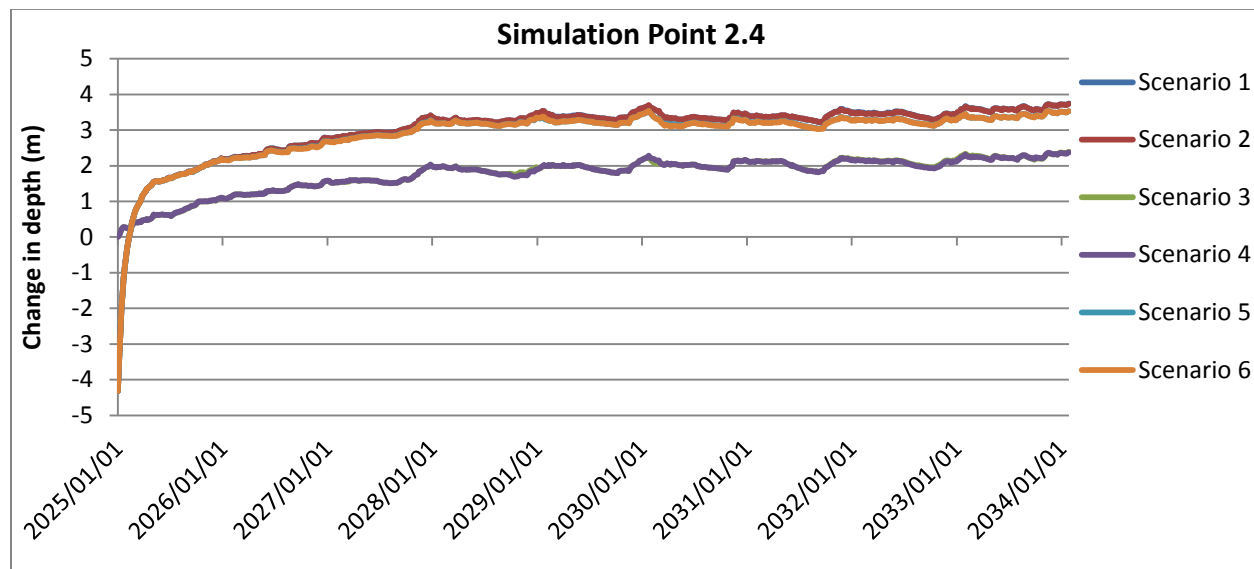


Figure 78: The change in depth (m) of the groundwater level at simulation point 2.4

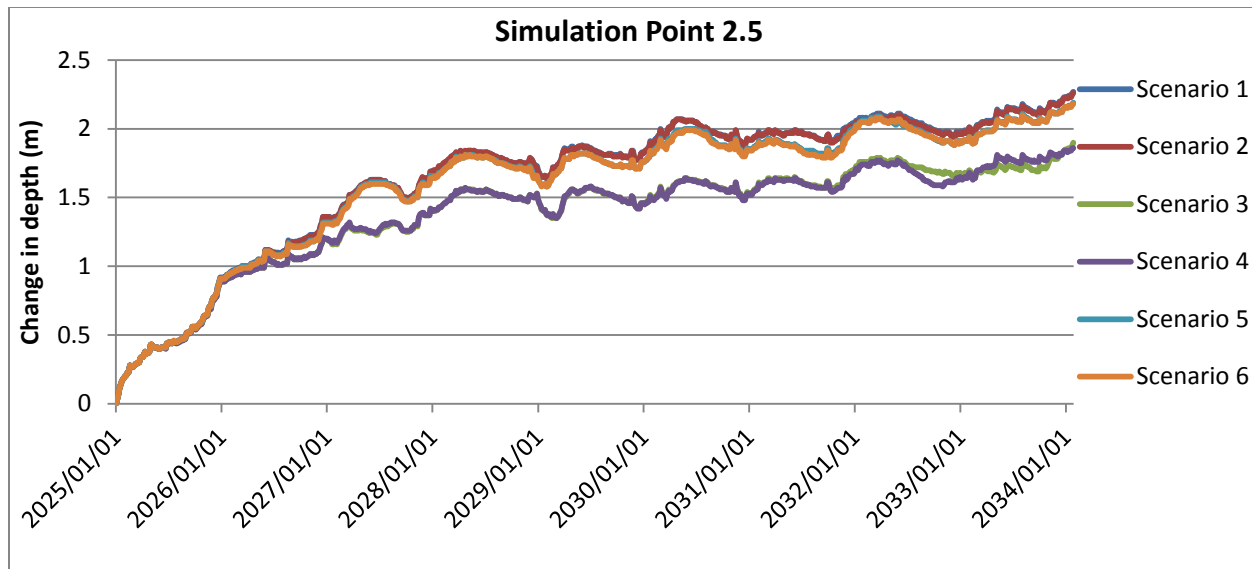


Figure 79: The change in depth (m) of the groundwater level at simulation point 2.5

The decrease in the trend in the change in groundwater level was steepest at simulation point 2.4 (Figure 80), with the first year change of 2.18m being the highest recorded for the points in simulation line one and two.

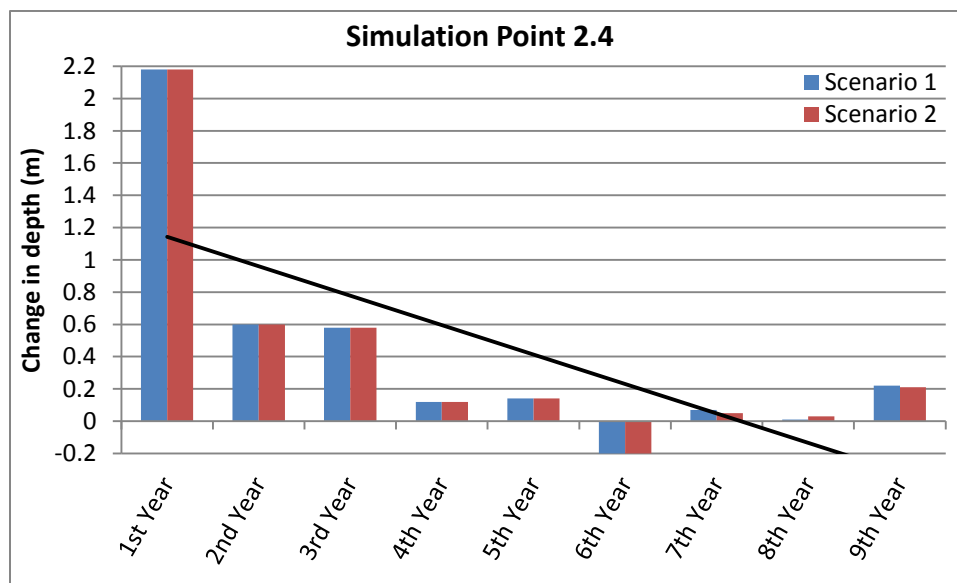


Figure 80: The effectiveness of the matured trees over the simulation period, for simulation point 2.4

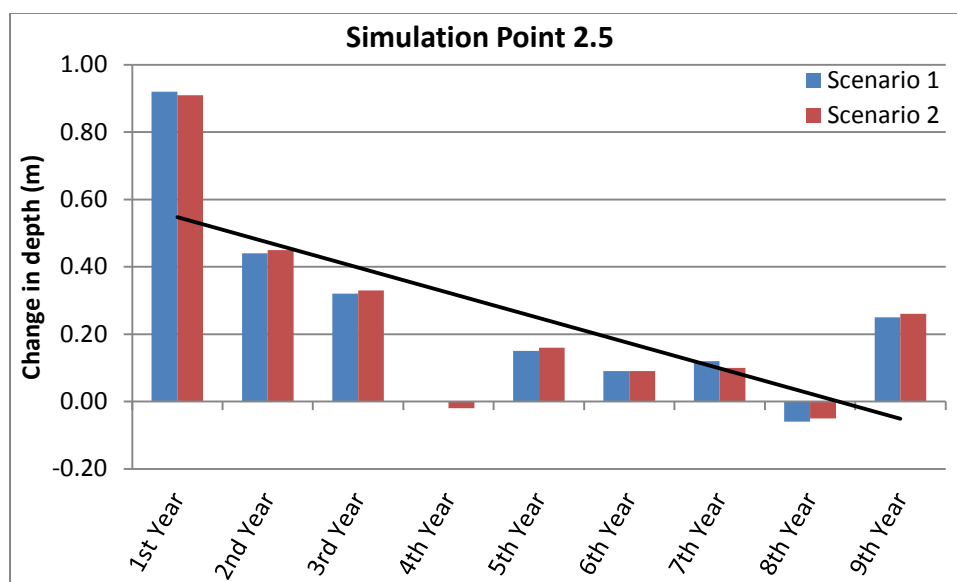


Figure 81: The effectiveness of the mature trees over the simulation period, for simulation point 2.5

Point 2.4 showed the highest final change of 3.75m (Table 31). The degree of decrease in groundwater level could have reached a point where the roots could no longer reach the groundwater. The performance of scenario 5 and 6 was dissimilar to the other scenarios. Scenarios 5 and 6 showed a difference of 0.22m at point 2.4 and 0.07m at point 2.5. Scenarios 3 and 4 showed a further difference of 1.14m at point 2.4 and 0.2m at point 2.5.

Table 31: The highest final change observed at simulation points 2.4 and 2.5

SIMULATION POINT	FINAL CHANGE	
	Maximum final change experienced (m)	Scenario
Simulation Point 2.4	3.75	Scenario 1
		Scenario 2
Simulation Point 2.5	2.27	Scenario 1
		Scenario 2

The performance of scenarios 5 and 6 against scenarios 1 and 2 (Figure 82), were considerably higher than observed for points 1.4 and 1.5. Scenarios 3 and 4 showed a significant decrease in performance. It was observed that at points 2.4 and 2.5 the effects of planting along the Schoonspruit River were more noticeable than at points 1.4 and 1.5.

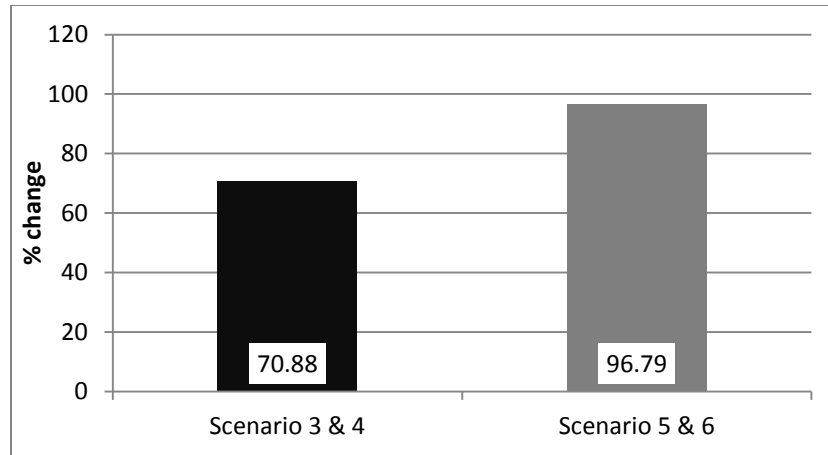


Figure 82: The mean performance of scenarios 3/4 and 5/6 as a percentage of the mean performance in scenarios 1/2, at simulation point 2.4 and 2.5

For simulation points 2.6 (Figure 83) and 2.7 (Figure 84), similar groupings were observed to points 2.4 and 2.5. However the difference between scenarios 1 and 2 and scenarios 5 and 6 was less. Points 2.6 and 2.7 showed similar groupings and seasonal patterns, but the degree of change experienced at these points differed significantly. There was a difference in the final change of 1.07m simulated between points 2.6 and 2.7.

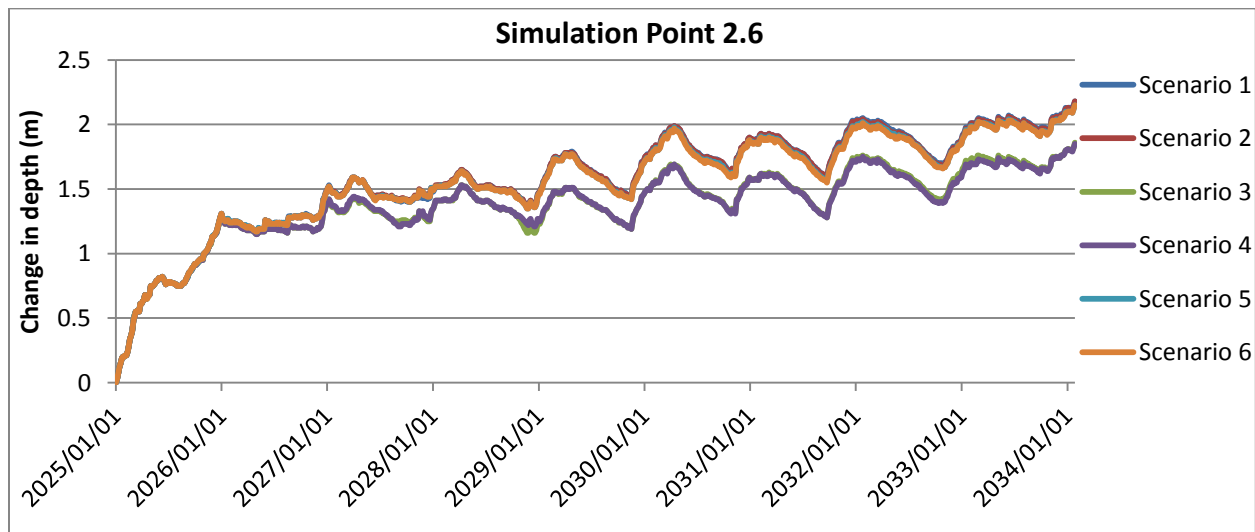


Figure 83: The change in depth (m) of the groundwater level at simulation point 2.6

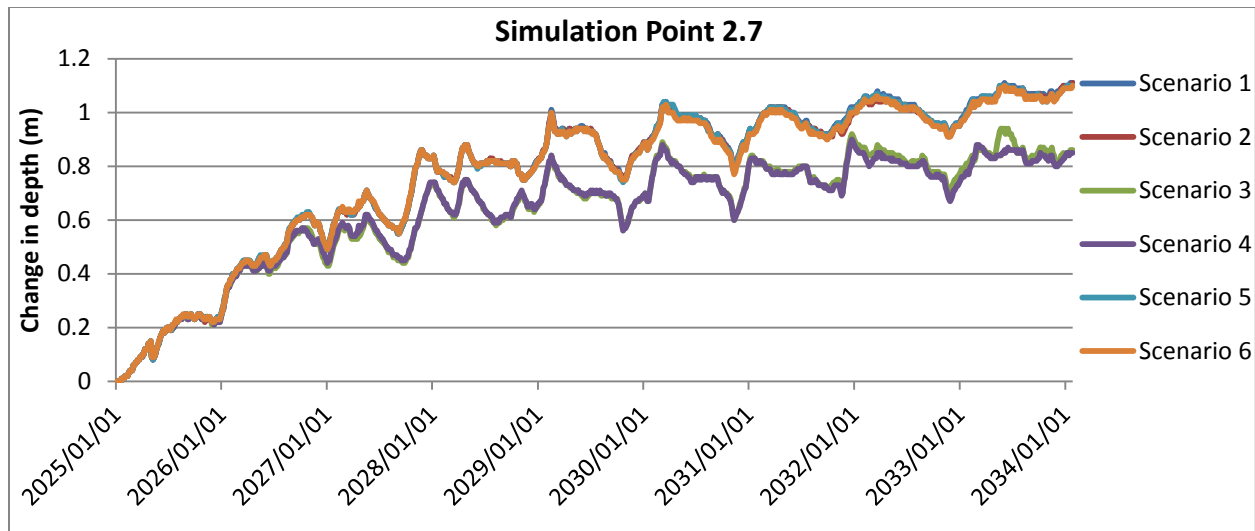


Figure 84: The change in depth (m) of the groundwater level at simulation point 2.7

Points 2.6 and 2.7 showed a trend of increasing depth change throughout the simulation period (Figure 85 and Figure 86, respectively). The rate of increase started to decrease as the simulation progressed, as previously observed for points 1.1 to 2.5. The eighth year continued to be a year of increase at all points. This was due to the previous year being the year with the highest rainfall. These first year values followed a similar pattern to those observed at points 1.6 and 1.7, with point 2.6 showing a higher value. The degree of change experienced at points 2.6 and 2.7 followed similar levels observed at 1.6 and 1.7. Simulation point 2.6 proved to be the only point where years 3 and 4 showed an increase in the groundwater.

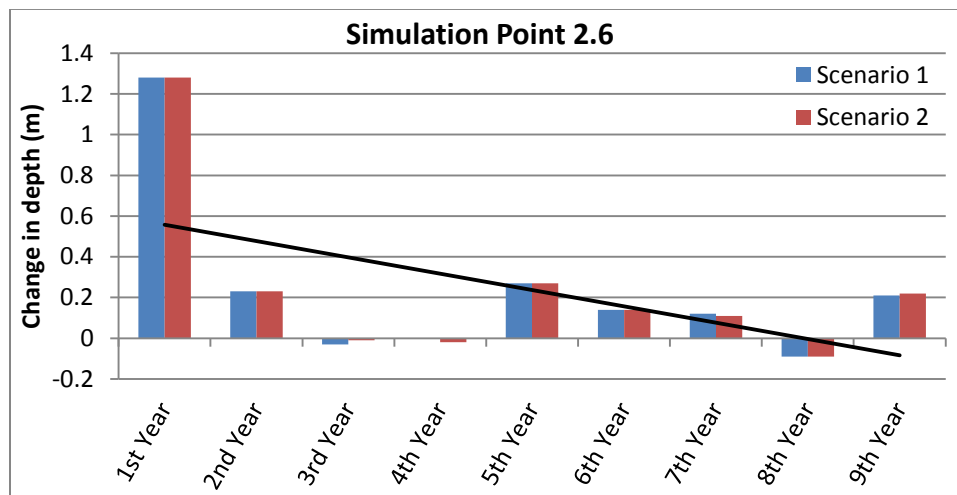


Figure 85: The effectiveness of the mature trees over the simulation period, for simulation point 2.6

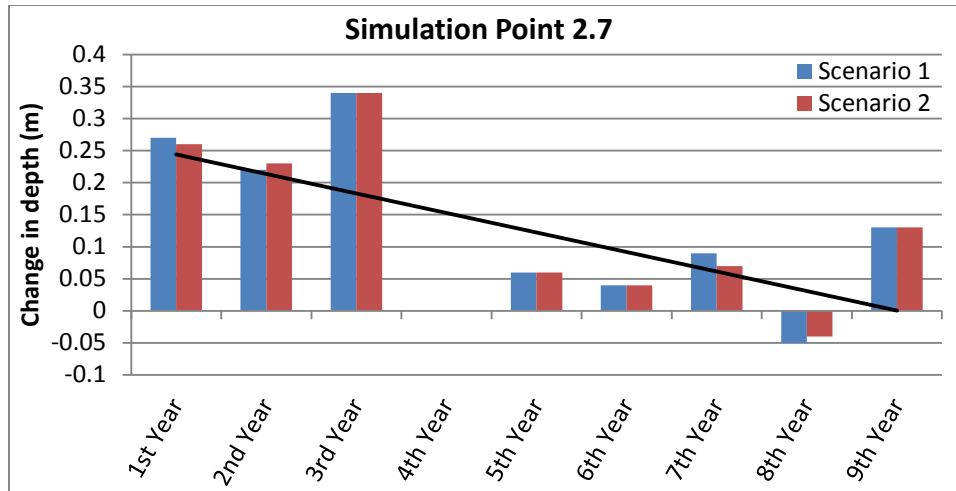


Figure 86: The effectiveness of the mature trees over the simulation period, for simulation point 2.7

The highest final change observed for points 2.6 and 2.7 were for scenarios 1 and 2, with the final change observed at point 2.6 being 2.18m and at point 2.7 the change was 1.11m. The degree of change at these points proved to be the lowest final changes for simulation line two. Scenarios 1 and 2 continued to perform equally by the end of the simulation period, as previously observed throughout simulation line two. The degree of difference observed between the scenarios, at points 2.6 and 2.7, were smaller than at points 2.1 to 2.5. For scenarios 5 and 6, the difference from scenarios 1 and 2 was 0.03m and 0.01m at points 2.6 and 2.7 respectively. For scenarios 3 and 4 the difference was 0.3m for both points 2.6 and 2.7, when compared with scenarios 1 and 2. This highlighted the importance of planting the *T. usneoides* along the Schoonspruit River.

Table 32: The highest final change that occurred at simulation points 2.4 and 2.5

SIMULATION POINT	FINAL CHANGE	
	Maximum final change experienced (m)	Scenario
Simulation Point 2.6	2.18	Scenario 1
		Scenario 2
Simulation Point 2.7	1.11	Scenario 1
		Scenario 2

In Figure 87, the percentage performance relative to the mean of scenarios 1 and 2 are shown. Scenarios 5 and 6 were observed to perform at 99.47% of scenarios 1 and 2. The corresponding figure for scenarios 3/4 is 86.38%. Figure 87 showed that not planting *T. usneoides* planting block led to a 13% decrease in groundwater level. These results were similar to those experienced for points 2.4 and 2.5.

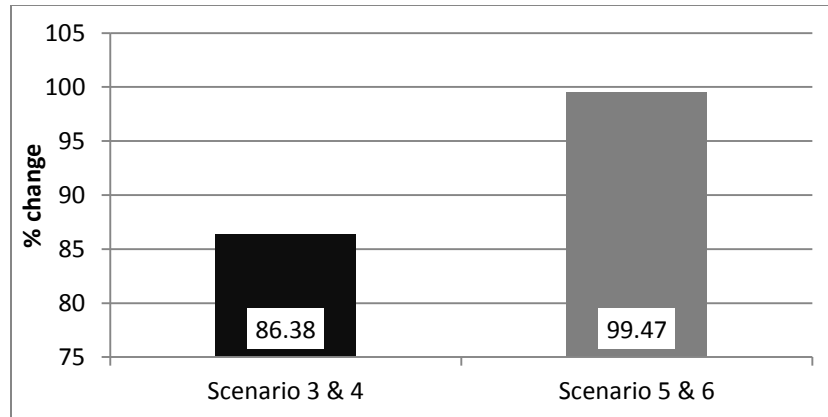


Figure 87: The performance (%) of scenarios, at simulation point 2.6 and 2.7, when compared with scenarios 1 & 2

5.6.3 Simulation Line Three

Simulation line three was located along the Schoonspruit River and comprised 5 points (Figure 45). The purpose of including a simulation line in this position was to show the effects of planting in the lower planting block, and to see what the overall effect of the woodlands was on groundwater levels before reaching the Schoonspruit River.

At simulation line three, the patterns observed in the previous lines were not duplicated at all the points. The water level patterns among the points did not follow a similar trend. One reason for this could be that these points are situated close to the Schoonspruit River, and therefore are under the influence of the water seeping from the river into the neighbouring ground. For simulation line three, points 3.1, 3.3 and 3.5 are discussed together, and then points 3.2 and 3.4. This grouping of the points was based on the patterns observed in the groundwater level graphs.

For simulation points 3.1, 3.3 and 3.5 there were two noticeable scenario groupings that occurred within the groundwater level change graphs (Figure 88, Figure 89 and Figure 90, respectively). Group one contained scenarios 3 and 4, whilst group two contained the remaining scenarios 1, 2, 5 and 6. The group one scenarios included *T. usneoides* along the Schoonspruit River, whereas group two scenarios did not include *T. usneoides* along the river. For group one, there was no significant change in groundwater level, whereas the change in group two scenarios was much greater. Simulation point 3.1 showed a strong seasonal difference, while points 3.3 and 3.5 showed less seasonal changes.

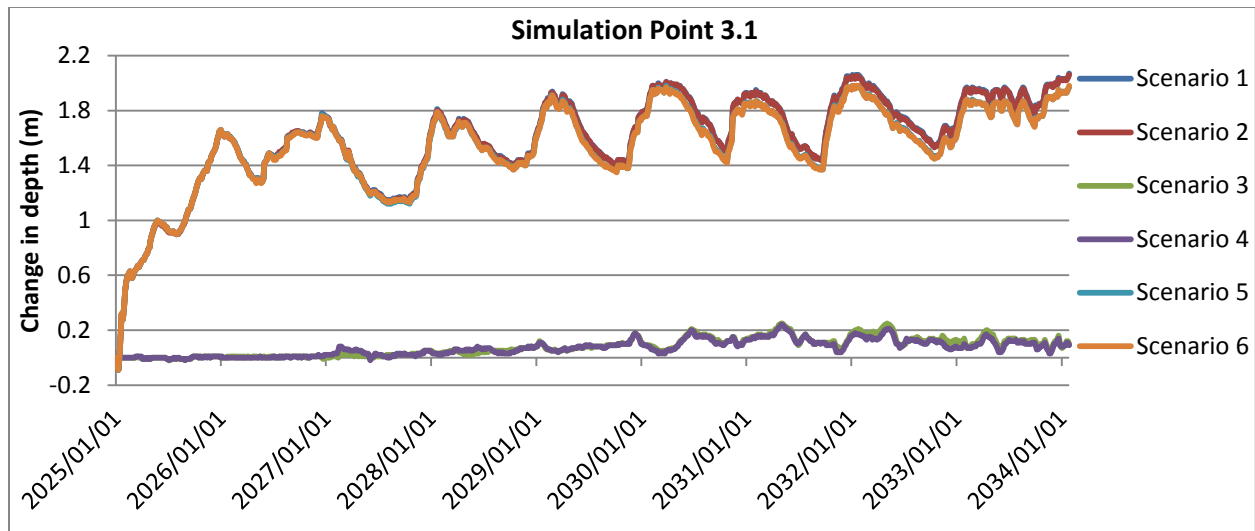


Figure 88: The change in depth (m) of the groundwater level at simulation point 3.1

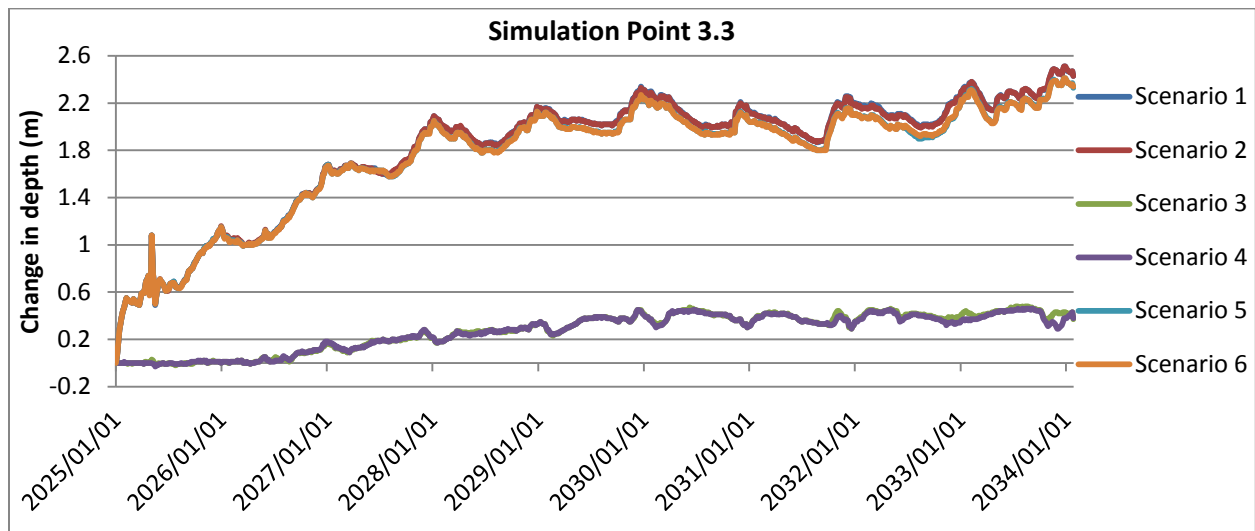


Figure 89: The change in depth (m) of the groundwater level at simulation point 3.3

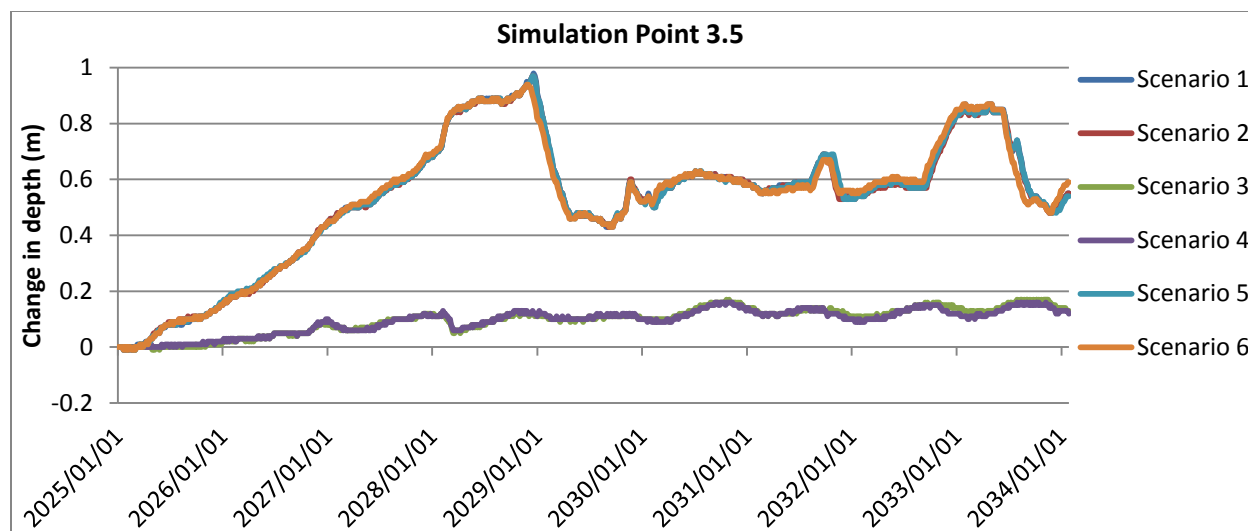


Figure 90: The change in depth (m) of the groundwater level at simulation point 3.5

As previously observed, the rate of the degree of change in the groundwater level decreased the longer the matured trees occupied the area (Figure 91, Figure 92 and Figure 93). As with previous points, points 3.1 and 3.3 followed a similar pattern, both showing a steeper first year change as the model adjusted to the new water balance inputs. Only point 3.1 showed an increase in the groundwater level at the eighth year. Point 3.3 showed an increase in the groundwater level in the sixth year. Point 3.5 proved to be an anomaly as there was no initial steep year, and the years of increase in the groundwater level were for the fifth, seventh and ninth years. This result could be due to the influx of water into point 3.1 and more into point 3.3 and even more in point 3.5, due to the plume depth and the topography of the area. The groundwater at such shallow depths flows southwards as well as westwards following the slope directions (AngloGold Ashanti, 2007). The decreasing trend observed for scenarios 1 and 2 were the same as for scenarios 3 through 6 (See Appendix C).

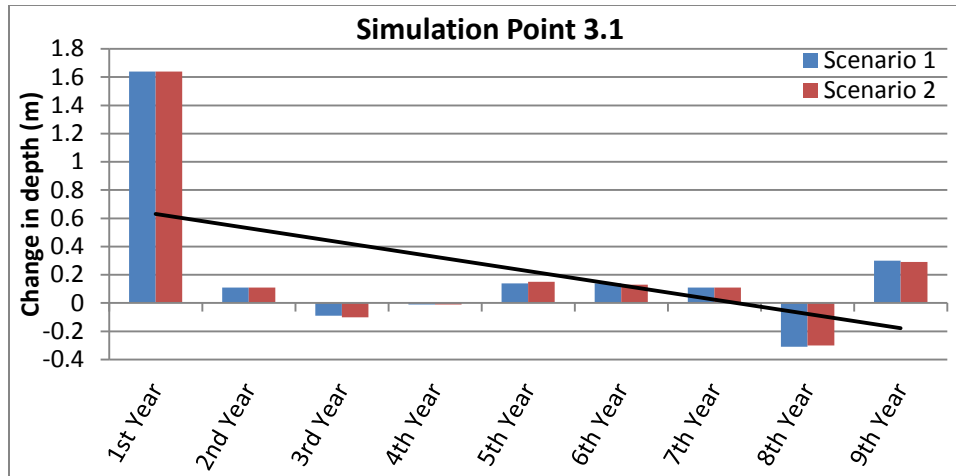


Figure 91: The effectiveness of the mature trees over the simulation period, for simulation point 3.1

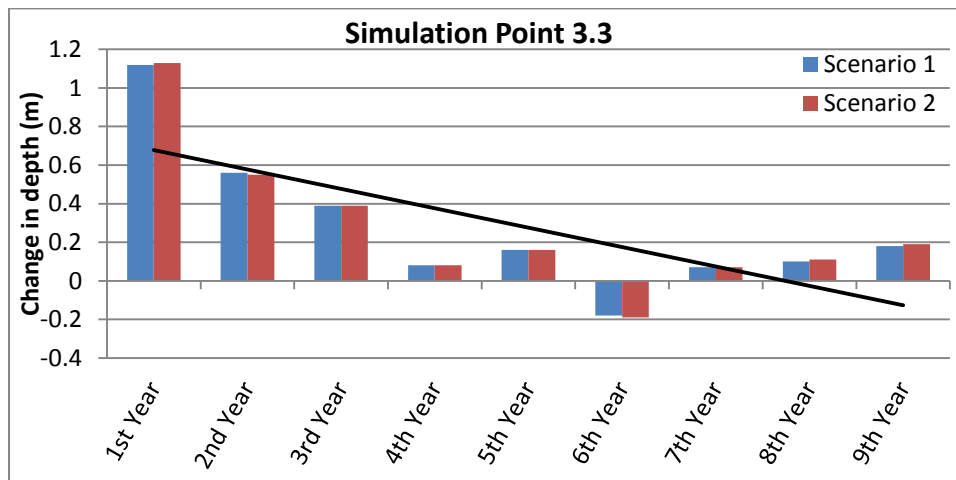


Figure 92: The effectiveness of the mature trees over the simulation period, for simulation point 3.3

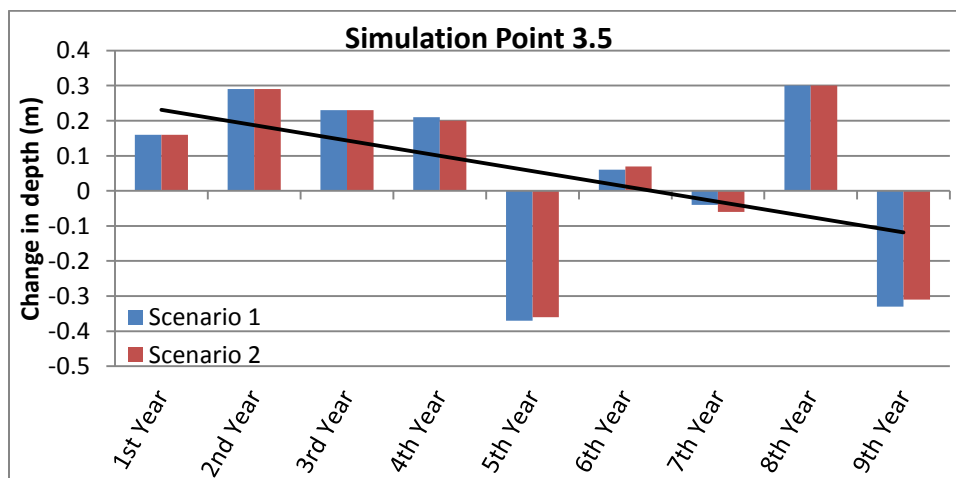


Figure 93: The effectiveness of the mature trees over the simulation period, for simulation point 3.5

Simulation points 3.1 and 3.3 showed similar degrees of change in the groundwater level, with both points showing a decrease in groundwater levels of 2m or more, while point 3.5 showed a final decrease of less than 1m. The reason for these variations in the groundwater level could be due to the influences of topography on the groundwater plume. As previously observed, for simulation lines one and two, the highest final change was observed under scenario 1 and 2, with a recorded change of 2.43m (Table 33). At point 3.5, for the first time in all the simulation lines, scenario 6 was observed as the best performer. However, this was less than 50% of the degree of change experienced at points 3.1 and 3.3. Scenario 2 showed a similar degree of change, of 0.01m, when compared to scenario 1. Scenarios 3 and 4 showed a marked decrease in performance, attaining 4.83% of scenario 1. Scenarios 1 and 2 performed equally for points 3.3 and 3.5 while once again, scenarios 3 and 4 performed the worst.

Table 33: The highest final change observed at simulation points 3.1, 3.3 and 3.5

SIMULATION POINT	FINAL CHANGE	
	Maximum final change experienced (m)	Scenario
Simulation Point 3.1	2.07	Scenario 1
Simulation Point 3.3	2.43	Scenario 1
		Scenario 2
Simulation Point 3.5	0.59	Scenario 6

On average, scenarios 1 and 2 showed the greatest decrease of groundwater, with scenarios 5 and 6 not dissimilar, performing at 98.17% of scenarios 1 and 2 (Figure 94). The small difference (1.83%) observed between scenarios 1 and 2 and scenarios 5 and 6 showed the effect of planting or not planting on the non-AGA owned planting blocks. The performance of scenarios 5 and 6 was expected, as these included the planting of *T. usneoides* along the Schoonspruit River. However, the difference was not expected to be as great, with scenarios 3 and 4 performing at only 12.01% of scenarios 1 and 2. This result could indicate that the *T. usneoides* have a major influence on the groundwater level.

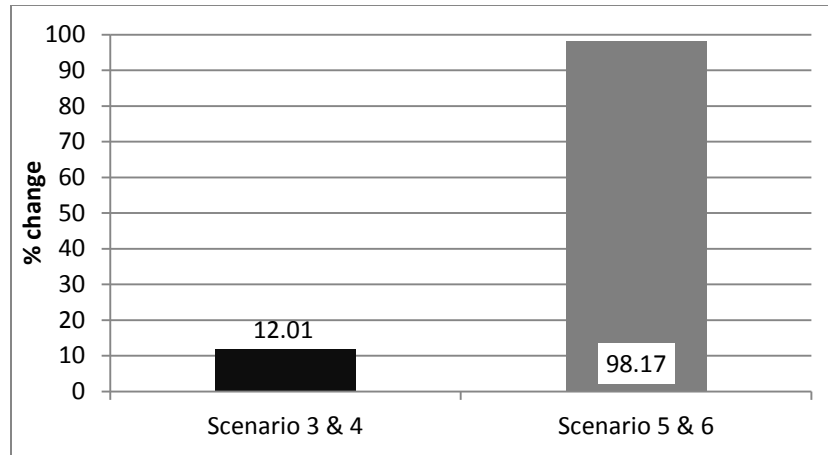


Figure 94: The performance of scenarios, at simulation point 3.1, 3.3 and 3.5, when compared with scenarios 1 & 2

Simulation points 3.2 and 3.4 are discussed together, as both these points showed less variation observed for scenarios 3 and 4. A possible explanation for the varying degree of change was that they were situated further from the Schoonspruit River and therefore were not under the influence of the river as much as points 3.1, 3.3 and 3.5. It is recommended for further research the relationship between the relative ET results and groundwater depths is analysed to support this result. Points 3.2 and 3.4 showed seasonal patterns similar to those observed in previous simulation points. These points showed the same grouping that was observed for points 3.1, 3.3 and 3.5, whereby group one was made up of scenarios 3 and 4 and group two included the remaining scenarios. This was again due to these points falling in the *T. usneoides* planting block, and scenarios 3 and 4 therefore simulating no *T. usneoides*.

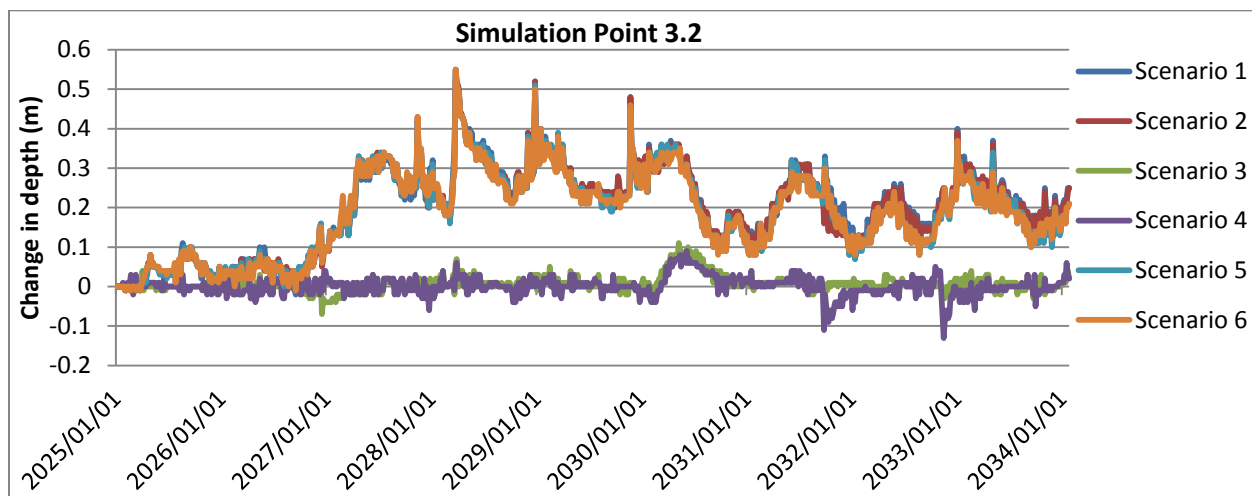


Figure 95: The change in depth (m) of the groundwater level at simulation point 3.2

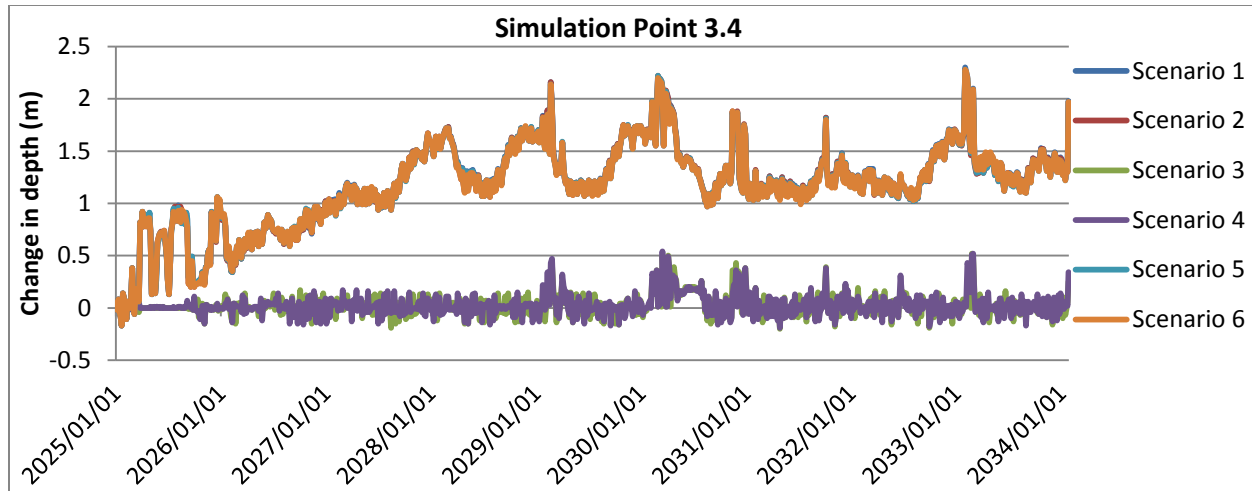


Figure 96: The change in depth (m) of the groundwater level at simulation point 3.4

Simulation point 3.2 showed the smallest decrease in the groundwater levels observed in simulation line three. The highest final change simulated at point 3.2 was 0.25m. Scenario 1 was observed to be the most effective at decreasing the groundwater level. For point 3.4, scenarios 2, 5 and 6 showed a 0.01m difference in their final change. This confirms how similarly scenarios 1 and 2 performed against 5 and 6. This was expected as scenarios 1, 2, 5, and 6 all modelled *T. usneoides* in this zone. They only differed in having (or not having) woodlands in the non-AGA owned blocks. Between points 3.2 and 3.4, scenarios 3 and 4 showed between 0.2m and 0.17m difference in the final change simulated in the groundwater levels.

Table 34: The highest final change observed at simulation points 3.2 and 3.4

SIMULATION POINT	FINAL CHANGE	
	Maximum final change experienced (m)	Scenario
Simulation Point 3.2	0.25	Scenario 1
		Scenario 2
Simulation Point 3.4	1.98	Scenario 1

Simulation point 3.2 showed a decrease in the degree of change observed in the second half of the simulation period. At point 3.2 the initial year did not see the steepest increase in depth to water table. Simulation point 3.4 showed a similar decreasing trend to what was simulated at simulation lines one and two. Simulation 3.3 did show an initial steep drop in level that was observed at previous points. At simulation point 3.2 there was the only increasing trend (although very slight) that was seen over all simulation points, and was for scenarios 3 and 4 (Figure 99).

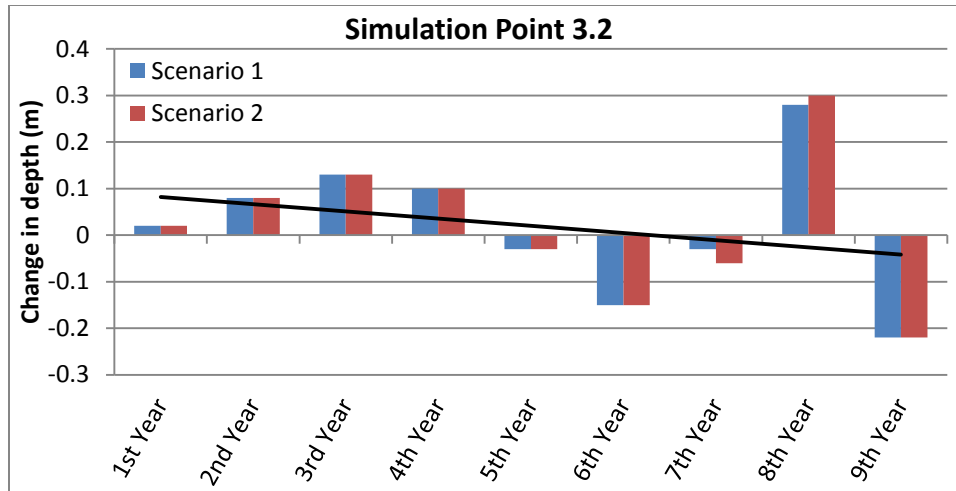


Figure 97: The effectiveness of the mature trees over the simulation period, for simulation point 3.2

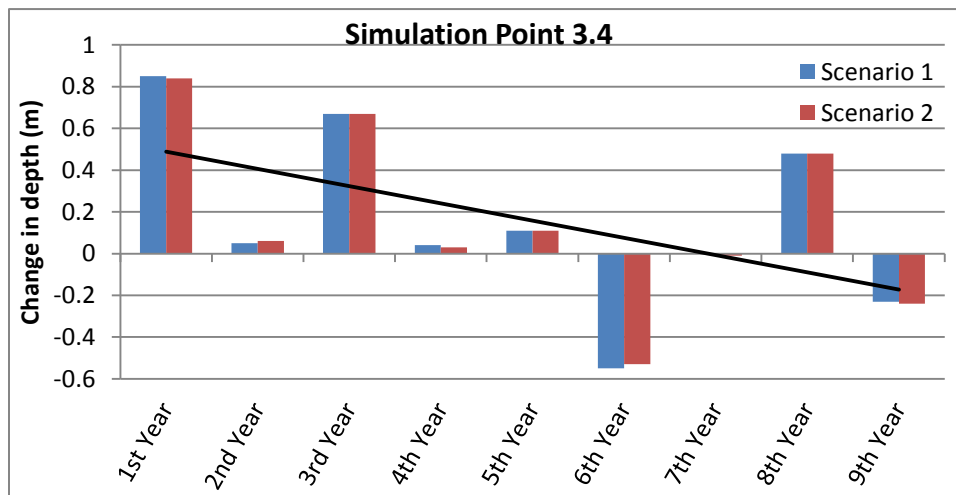


Figure 98: The effectiveness of the mature trees over the simulation period, for simulation point 3.4

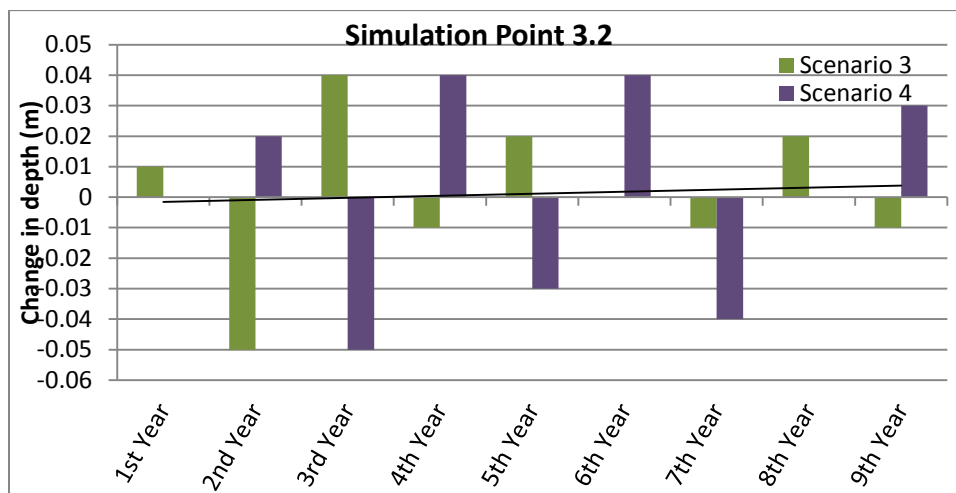


Figure 99: The effectiveness of the mature trees over the simulation period, for simulation point 3.4

As previously observed in Figure 95 and Figure 96, scenarios 1 and 2 showed the greatest decrease in the groundwater level, whilst scenarios 5 and 6 were the next best performer, 97.76% of scenarios 1 and 2 (Figure 100). As was expected from previous simulations, scenario 3 and 4 showed the lowest change in the groundwater level. It was observed that scenarios 3 and 4 performed at 2.09% of scenarios 1 and 2, confirming the importance of planting *T. usneoides* along the Schoonspruit River.

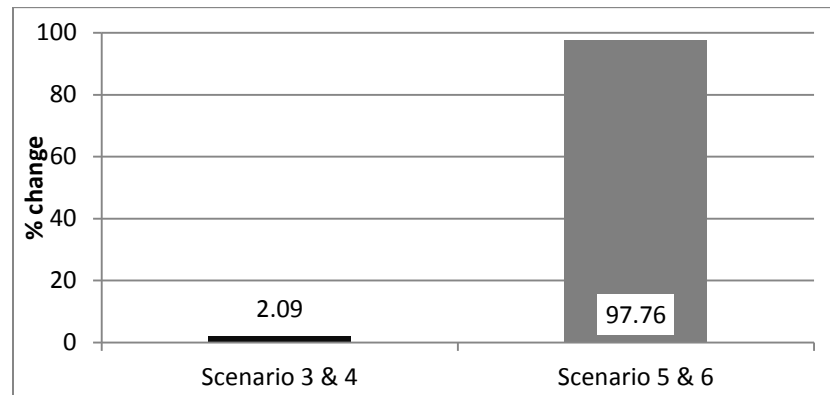


Figure 100: The performance of scenarios, at simulation point 3.2 and 3.4, compared with scenarios 1 & 2

5.6.4 Overview of Scenario Impacts

By calculating the overall performance, average of all the observation points, for each scenario across all simulation lines, scenarios 1 and 2 showed the greatest decrease in groundwater levels (Figure 101). Planting scenarios 3 and 4 showed the least decrease in the groundwater levels.

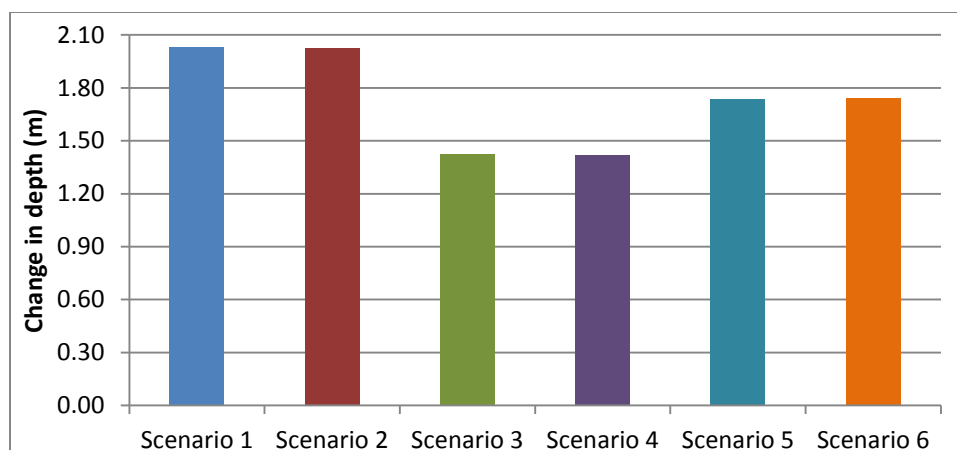


Figure 101: The overall average change in groundwater level observed for the planting scenarios across all simulation points

5.6.4.1 Scenario 1

For planting scenario 1, mature *S. lancea* were simulated across all the planting blocks, including non-AGA owned blocks, whilst *T. usneoides* were planted along the Schoonspruit River. The greatest degree of change observed was for the northern *S. lancea* planting blocks (Figure 102). These blocks were simulated to exhibit a decrease in the groundwater level of between 3.01 and 3.75m. The degree of change decreased in the southern blocks, with a simulated decrease in groundwater level of between 0 and 3m. This result could reflect a slower plume movement in the northern blocks due to their greater distance from the seepage source in the TSF. This hypothesis needs to be tested against field data.

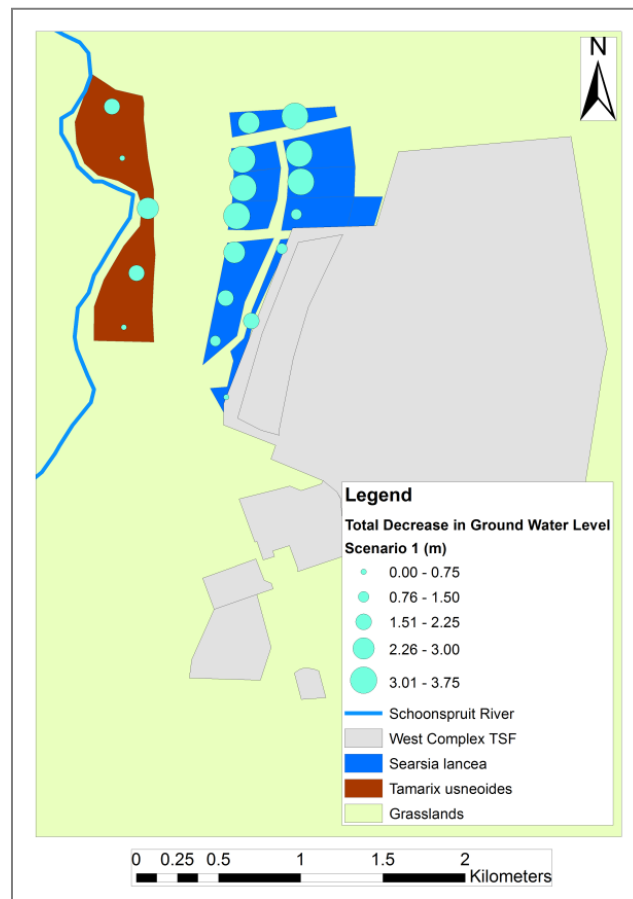


Figure 102: The impacts planting scenario 1 had on the groundwater level within the core focus area of the study site

The smallest degree of change observed in groundwater level, in the *S. lancea* planting blocks, was observed at the base of the West Complex TSF. Points in simulation line two showed a greater decrease in the groundwater level, than those of simulation line one. This result showed

the impact of the first line of planting blocks. The degree of change observed in the *T. usneoides* planting block, along the Schoonspruit River, was significantly less than that observed in the *S. lancea* planting blocks. This result indicates that planting *S. lancea* woodlands has a significant impact on groundwater levels.

5.6.4.2 Scenario 2

Planting scenario 2 was simulated with *E. dunnii* woodlands planted within all AGA and non-AGA owned planting blocks, as well as *T. usneoides* planted along the Schoonspruit River. The degree of change observed, for planting scenario 2, was similar to planting scenario 1 whereby the northern *E. dunnii* planting blocks were observed with the greatest degree of change (Figure 103). These blocks were observed to decrease the groundwater level by 3.01 to 3.75m. The southern *E. dunnii* planting blocks showed similar degrees of change in the groundwater as experienced in planting scenario 1, decreases ranged from a maximum of 3.01m to a minimum of 0.2m. The *T. usneoides* planting block was observed to perform similarly to scenario 1. This result could indicate that matured woodlands of *E. dunnii* were as effective as matured woodlands of *S. lancea*. It must be kept in mind, however, that the simulated *E. dunnii* ET was much less than expected from field measurements at other woodland sites (Dye *et al.*, 2014).

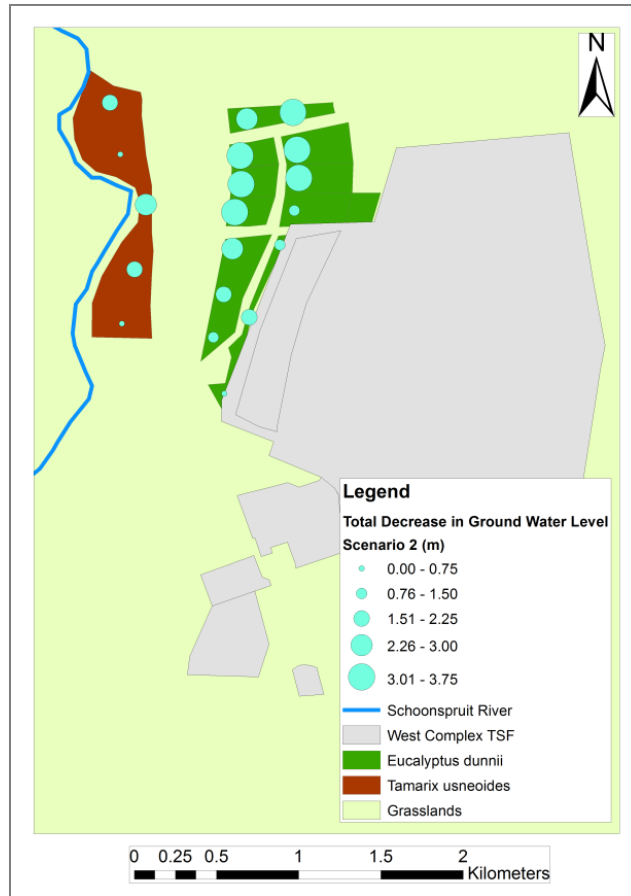


Figure 103: The impacts planting scenario 2 had on the groundwater level within the core focus area of the study site

5.6.4.3 Scenario 3

Planting scenario 3 differs from planting scenario 1 by having no *T. usneoides* planted along the Schoonspruit River (Figure 104). The effect of no *T. usneoides* resulted in a decrease in the degree of change experienced in the northern *S. lancea* planting blocks. Simulation points 2.1 and 2.2 indicate a lower change experienced, with a mean decrease in effectiveness of 0.75m recorded. The degree of change observed at the base of the West Complex TSF was similar to that experienced for planting scenario 1. In the planting block along the Schoonspruit River the impact of no *T. usneoides* was evident, with a decrease in change being observed.

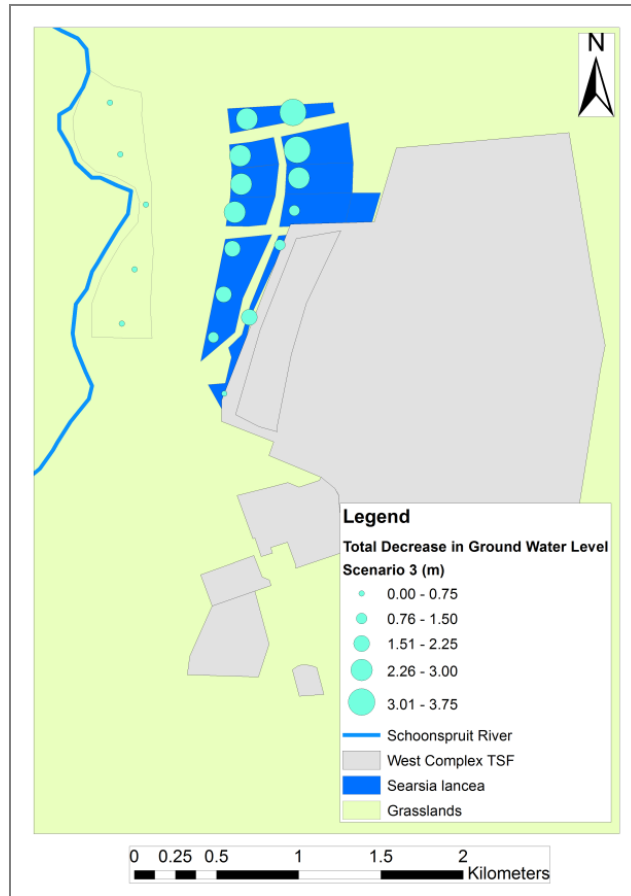


Figure 104: The impacts planting scenario 3 had on the groundwater level within the core focus area of the study site

5.6.4.4 Scenario 4

As seen in planting scenario 3, scenario 4 showed a similar decrease in change in groundwater level when compared with planting scenario 2, which included *T. usneoides*. As seen with planting scenario 3, there was a notable decrease in the degree of change experienced in groundwater level (Figure 105). These two scenarios both show that even though *T. usneoides* had a relatively small impact on the groundwater level, the overall impact of not having matured *T. usneoides* woodlands show the importance of *T. usneoides* as a tool for phytoextraction.

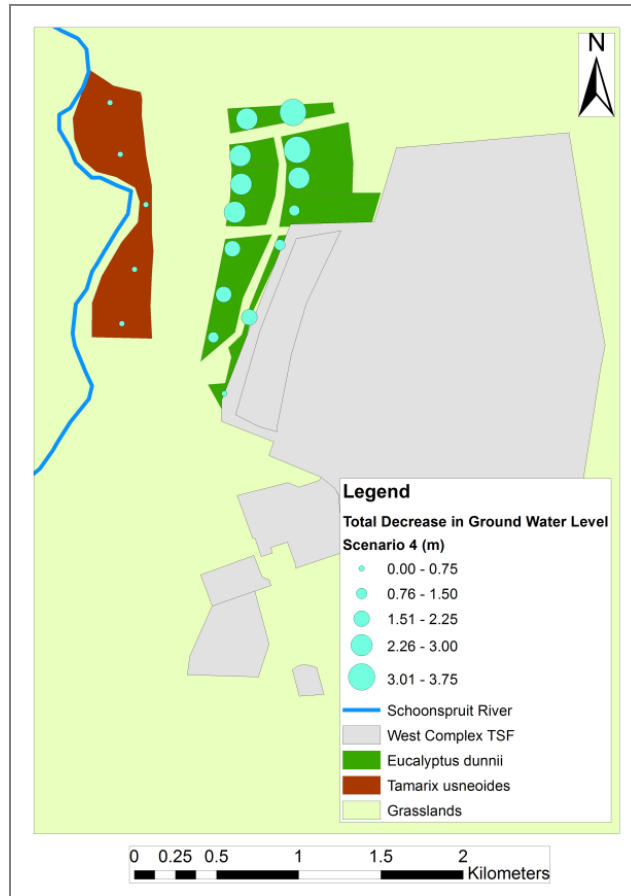


Figure 105: The impacts planting scenario 4 had on the groundwater level within the core focus area of the study site

5.6.4.5 Scenario 5

Planting scenario 5 had similar planting patterns to scenario 1. Scenario 5 did not include woodlands in non-AGA owned planting blocks. The effect of not planting in these blocks is quite evident when looking at Figure 106. There was a significant decrease, in the degree of change observed in the northern *S. lancea* planting blocks when compared to scenarios 1 and 2. This result showed the impact that planting within the non-AGA planting blocks had, not only on the non-AGA owned planting blocks but on the neighbouring planting blocks as well.

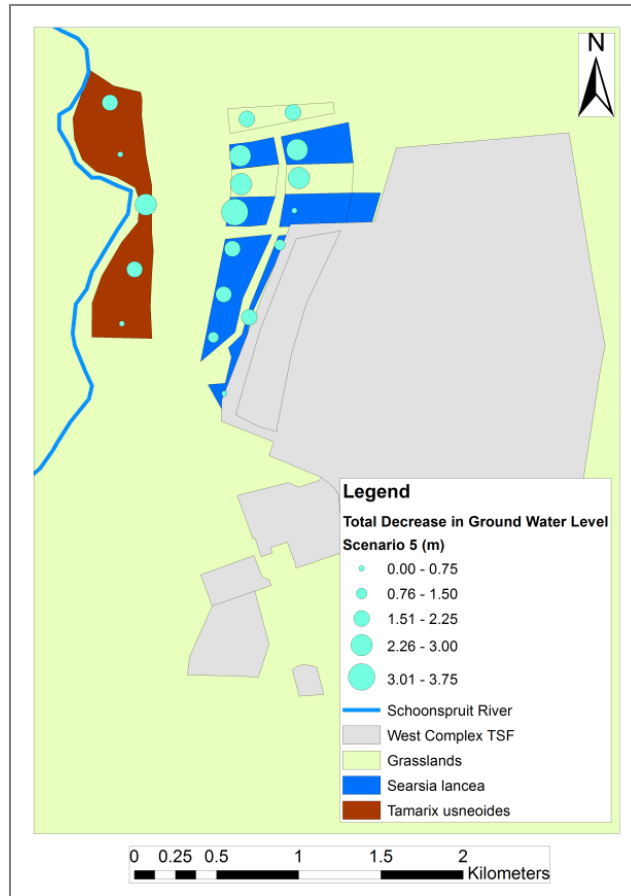


Figure 106: The impacts planting scenario 5 had on the groundwater level within the core focus area of the study site

5.6.4.6 Scenario 6

Planting scenario 6 was simulated to plant *E. dunnii* in only AGA owned planting blocks and *T. usneoides* along the Schoonspruit River. The results, similar to scenario 5, indicates that by not planting in the non-AGA owned planting blocks the degree of change observed in the northern *E. dunnii* planting blocks decreases significantly, compared to scenarios 1 and 2. This decrease was not only observed in the non-AGA owned planting blocks, but in the neighbouring AGA owned planting blocks (Figure 107). The *T. usneoides* planting block was observed having between 0 and 2.25m decrease in the groundwater level. The result reiterates the importance and impact of planting *T. usneoides* along the river.

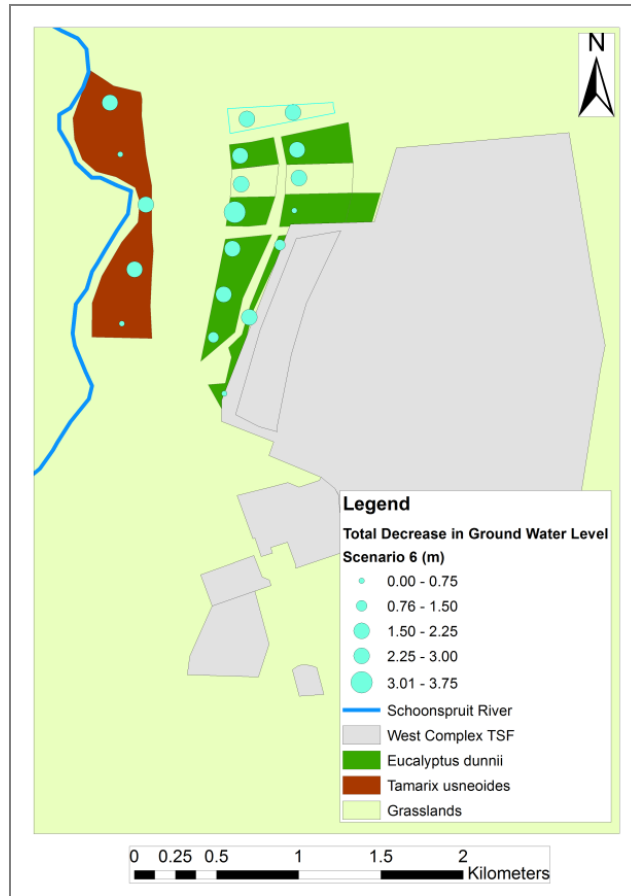


Figure 107: The impacts planting scenario 6 had on the groundwater level within the core focus area of the study site

5.7 Sulphate Concentrations

Within MIKE SHE the UZ is modelled with a fluctuating groundwater level, therefore to determine the changes in the SO_4 concentration in the groundwater the UZ's water quality outputs were analysed. These results are discussed only for two main transects (Figure 108) to highlight changes in SO_4 concentrations along the plume pathway from source to the Schoonspruit River. Transect one uses points 1.3, 2.3 and 3.3 from Figure 45, which for this section will be labelled 1.1, 1.2 and 1.3 (Figure 108). Transect two uses simulation points 1.6, 2.6 and 3.5 from Figure 45 which will be referred to 2.1, 2.2 and 2.3 in this section (Figure 108).

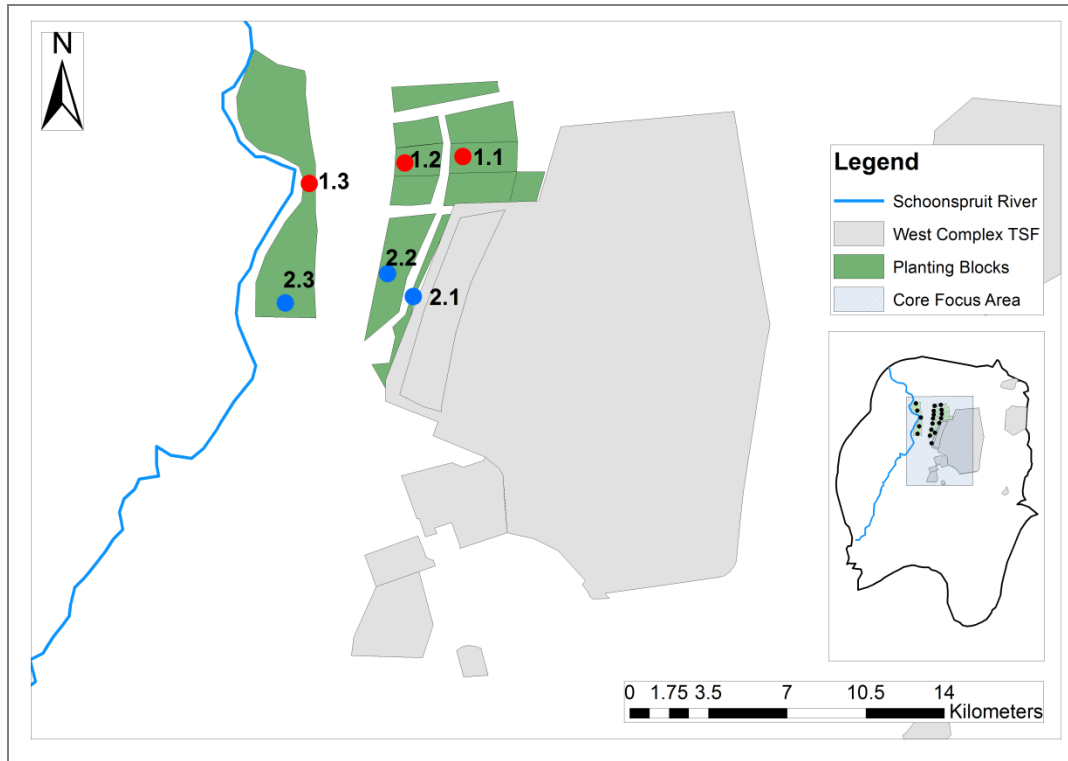


Figure 108: The location of the two transects used for the SO₄ concentration analysis

Each simulation point (simulation point 1.1 through to 3.5 see in Figure 45) was plotted using the built in *UZ plot* tool within MIKE SHE. This tool extracts simulated matrix phase SO₄ concentrations for the UZ at any given point. The option to change the unit used for this tool is not provided, and therefore all *UZ plots* are displayed in $\mu\text{g}/\text{m}^3$. Changes that occurred within the SZ were key to understanding how the woodlands impact on the spread of contaminants. The *UZ plot* tool in MIKE SHE takes into account the possibility of a fluctuating water table and can display the entire UZ as well as the upper part of the SZ. Therefore the *UZ plot* was used to generate the plots, with the groundwater level superimposed to indicate where the UZ ends and the SZ begins. These plots show the changes in the SO₄ concentrations (matrix phase) from the beginning to the end of the simulation period.

It must be noted that different colour scales have been used in the legends for different simulation points. The reason this was implemented over a universal colour scale was that the definition at some simulation points was lost when a fixed scale was used.

5.7.1 Transect One

Transect one contains points 1.1, 1.2 and 1.3, with points 1.1 and 1.2 lying within the non-AGA owned planting blocks whilst point 1.3 lies within the *T. usneoides* planting block.

5.7.1.1 Transect Point 1.1

For point 1.1, the current scenario cross section was observed to have low levels of SO_4 within the first 3mbgl (Figure 109). These levels increased as the depth below ground increased and the simulation period progressed. The highest SO_4 concentrations were observed from 2007 onwards which was located 5 metres below ground level (mbgl). The groundwater level was located above this peak of SO_4 and therefore depicts the SO_4 concentrations within the SZ.

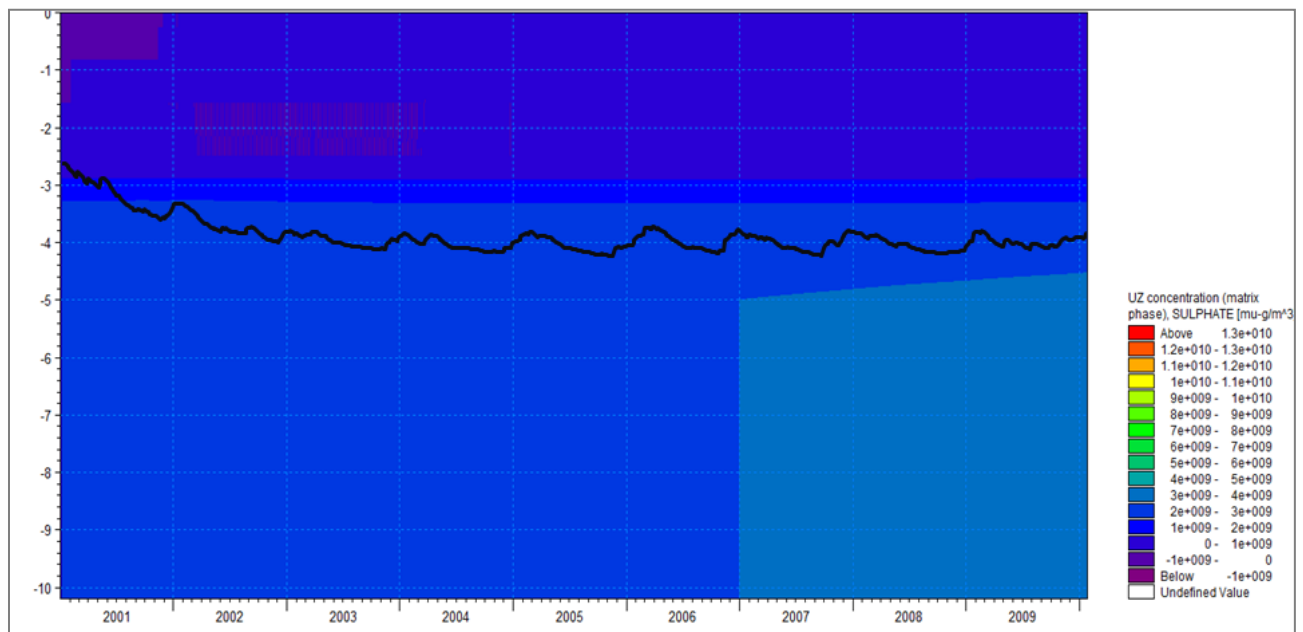


Figure 109: The SO_4 concentrations, below ground (mbgl), for the current scenario at point 1.1

With scenario 1 the first change that was observed was the decrease in the groundwater. The groundwater for scenario 1 dropped from 4mbgl, in the current scenario, to 7mbgl, at the end of the simulation period (Figure 110). This was the result of the *S. lancea* deep root system extracting the groundwater. This drying resulted in a higher concentration of SO_4 found within the UZ, as any SO_4 that was not extracted by the *S. lancea* was dissolved in less water. Therefore for UZ (0 to 7mbgl) an increase in SO_4 concentrations was observed. Whilst in the SZ there was also an increase in spread of high SO_4 concentrations observed midway through 2030. This was the result of the UZ drying.

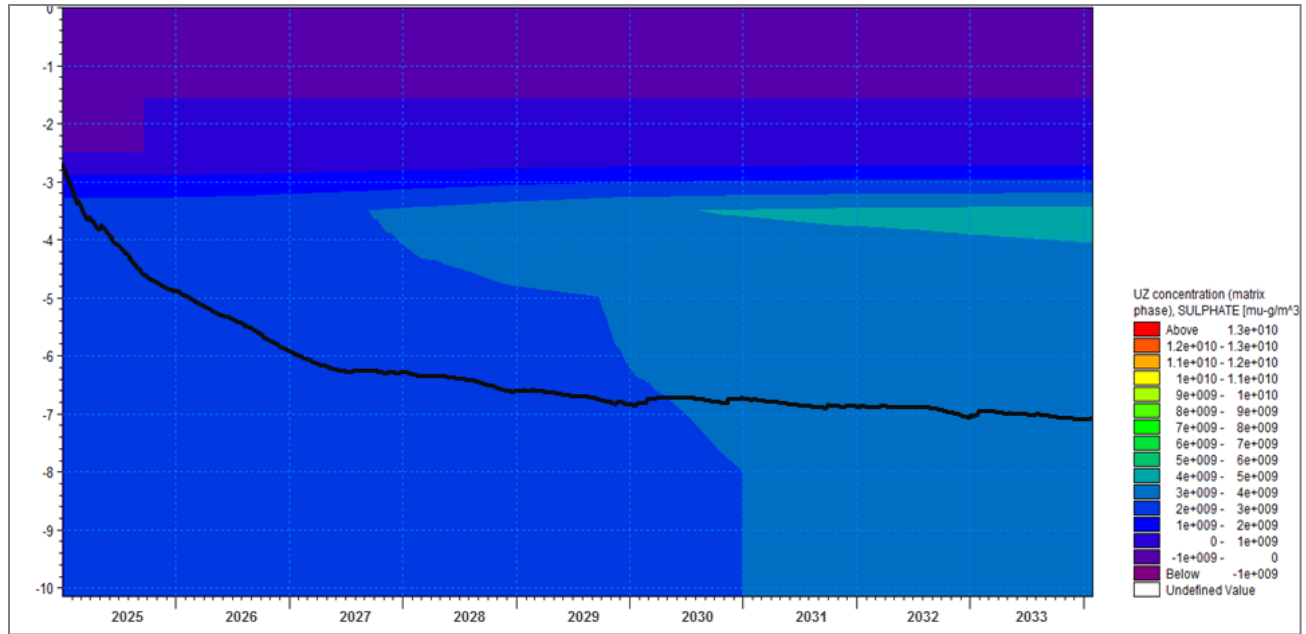


Figure 110: The SO₄ concentrations, below ground (mbgl), for the future scenario 1 at point 1.1

For planting scenario 2 a similar decrease in groundwater was observed (Figure 111). This drying of the UZ however resulted in higher SO₄ concentrations being observed specifically at around 3 to 4m depth. This was the result of planting scenario 2 using *E. dunnii* rather than *S. lancea*, which has a higher *ET uptake factor*. The lower *ET uptake factor* of the *E. dunnii* combined with similar water uptake ability of scenario 1 (*S. lancea*) resulted in less SO₄ being extracted, and therefore a higher SO₄ concentration in the UZ (3 to 5mbgl) (Figure 111). This resulted in a wider spread of high SO₄ concentrations within the SZ being observed, specifically in 2030.

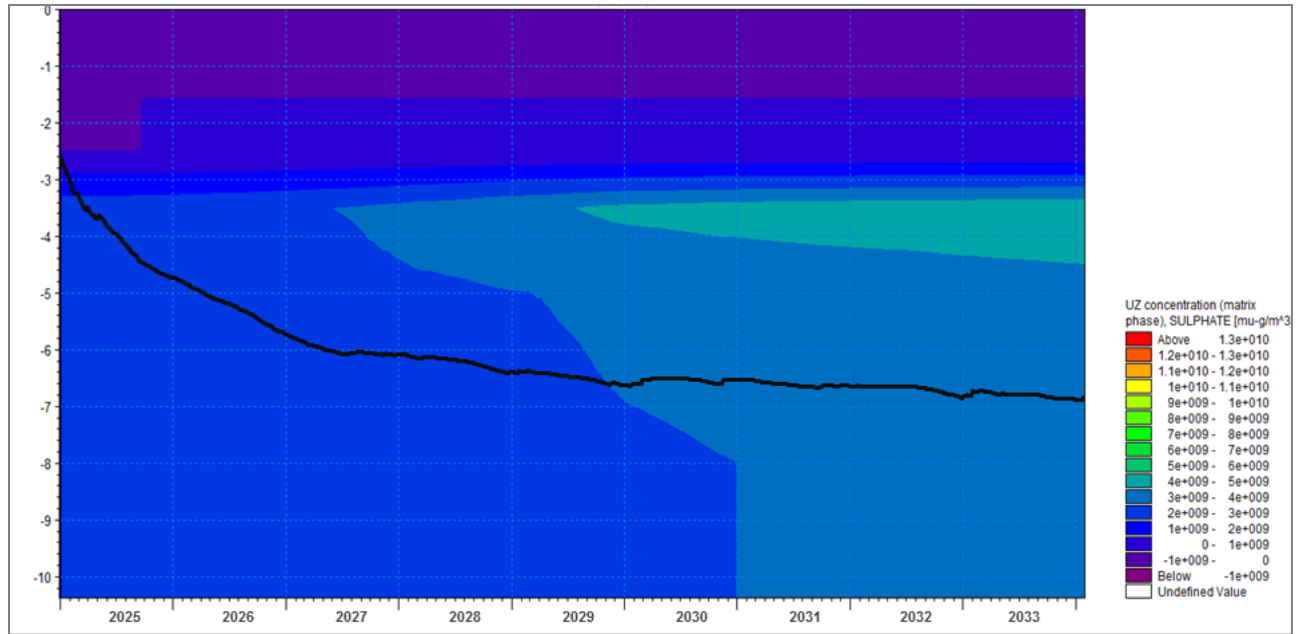


Figure 111: The SO₄ concentrations, below ground (mbgl), for the scenario 2 at point 1.1

The groundwater levels observed for scenario 3 were similar to those observed for scenarios 1 and 2. There was a significant increase in the SO₄ concentration observed for planting scenario 3 specifically at around 3 to 4m depth (Figure 112). Planting scenario 3 included the planting of *S. lancea* within all planting blocks, but did not include the planting of *T. usneoides* along the Schoonspruit River. However, point 1.1 does not lie within the *T. usneoides* planting block, and therefore this increase in SO₄ concentration should not be observed. This result was due to the limitations of the MIKE SHE model, with regards to the *ET uptake factor*. Due to the inability to define the *ET uptake factor* spatially, the *ET uptake factor* was taken as an average of all the plants used within this planting scenario. This averaging out has led to this SO₄ increase observed in Figure 112.

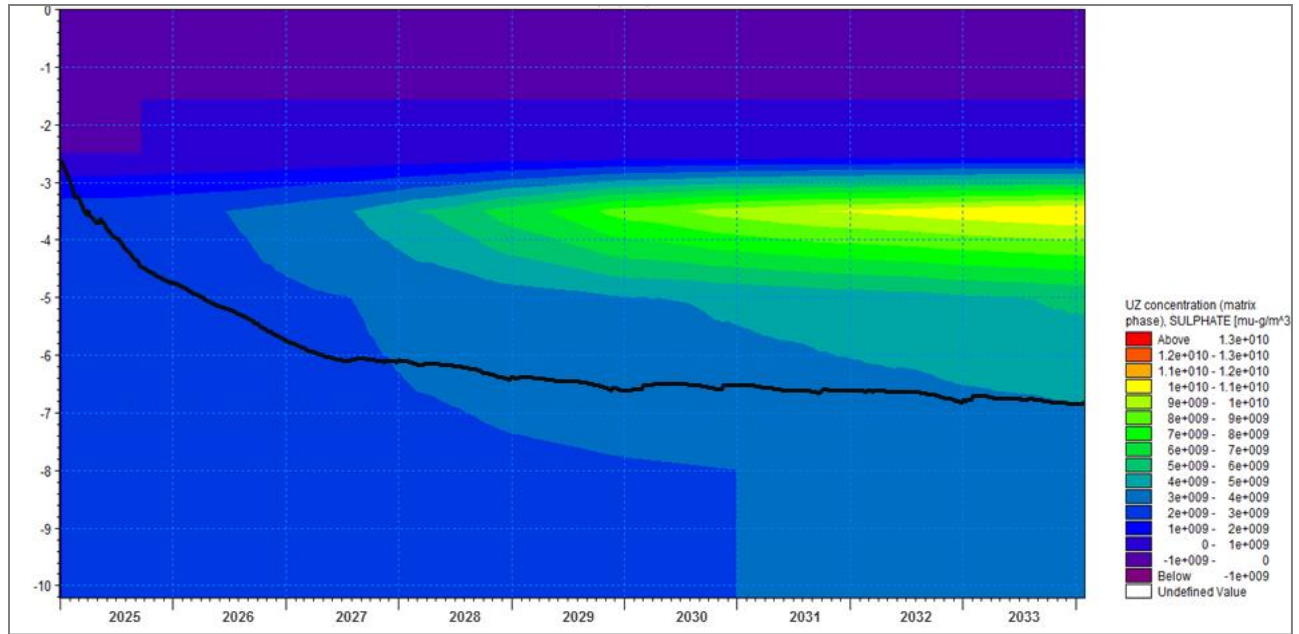


Figure 112: The SO₄ concentrations, below ground (mbgl), for the scenario 3 at point 1.1

The simulated results of planting scenario 4 were observed with a similar increase in SO₄ concentration levels. There was however an even increase in the spread of higher SO₄ concentrations observed within the 3mbgl band, specifically after 2030 (Figure 113). This increase when compared with scenario 3 was due to the *E. dunnii* being simulated in this scenario. The *E. dunnii* had a lower *ET uptake factor* with similar water extraction ability, and therefore resulted in lower levels of SO₄ being extracted by the trees and a higher SO₄ concentration remaining in the UZ. As with scenario 3, scenario 4 was observed to have an increase in SO₄ concentration within the SZ much earlier in the simulation period (2027 instead of 2029). This was the result of the *ET uptake factor*.

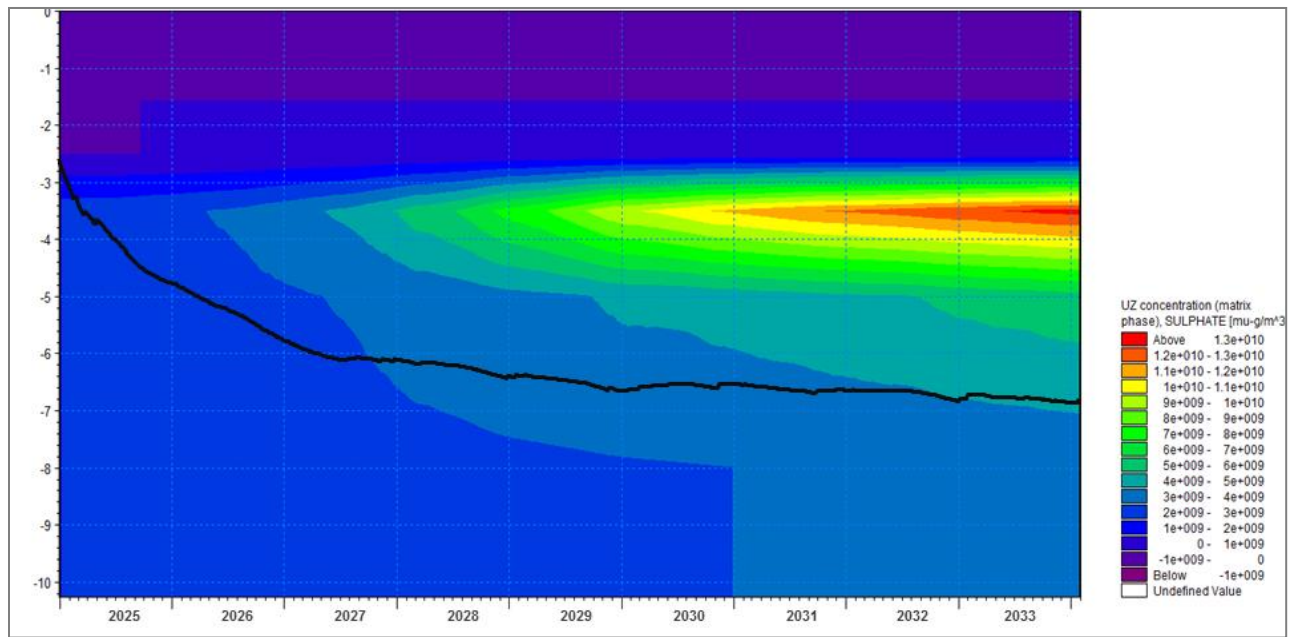


Figure 113: The SO₄ concentrations, below ground (mbgl), for the scenario 4 at point 1.1

Planting scenario 5 was similar to planting scenario 1, however no planting occurred within the non-AGA owned planting blocks. The impacts of not planting in the non-AGA owned planting blocks was observed in planting scenario 5's UZ/SZ cross section (Figure 114). In this cross-section the groundwater level does not decrease to the same level as witnessed in scenario 1, here it decreased to 6mbgl rather than 7mbgl. Another impact, of the non-AGA owned blocks not being planted, was the increase in the SO₄ concentration observed within the 3 to 4mbgl band. This increase was the result of less *S. lancea* being planted, and therefore the amount of SO₄ extracted from the groundwater was lower. This lower extraction resulted in a higher SO₄ concentration being observed within the UZ. As previously observed, there was also an increase spread of the higher SO₄ concentrations observed, within the SZ. This increase started towards the end of 2028 (in Figure 114), while in scenario 1 this increase was observed within the middle of 2029 (in Figure 110). This simulated result reiterates the impact of not planting within the non-AGA owned planting blocks.

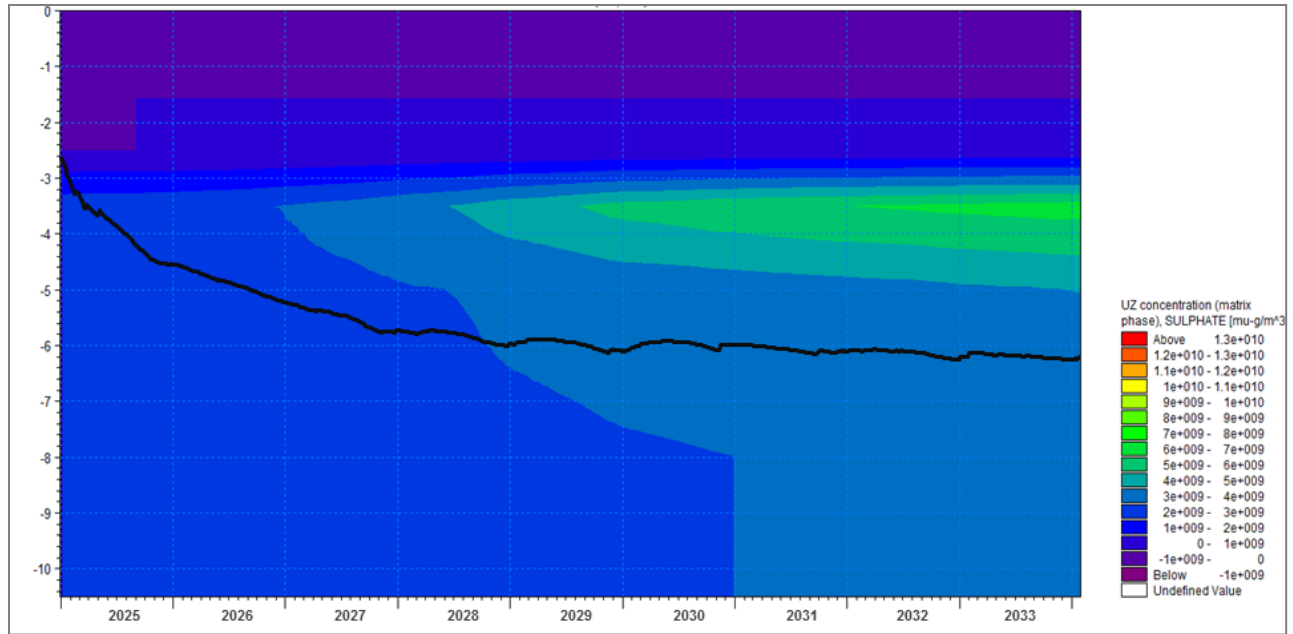


Figure 114: The SO_4 concentrations, below ground (mbgl), for the scenario 5 at point 1.1

For planting scenario 6 a decrease in groundwater was observed, this decrease was similar to that observed for planting scenarios 5 (Figure 115). The increase, when compared with scenario 5, in SO_4 concentration observed for the 3 to 4mbgl band was the result of the *E. dunnii* with a lower ability to absorb SO_4 . This result as well as the higher groundwater level indicates the impacts of choosing not to plant within the non-AGA owned planting blocks. Not planting in these blocks resulted in an increase in SO_4 concentration observed within the UZ and SZ, as well as an increase in the groundwater level, by as much as 1m.

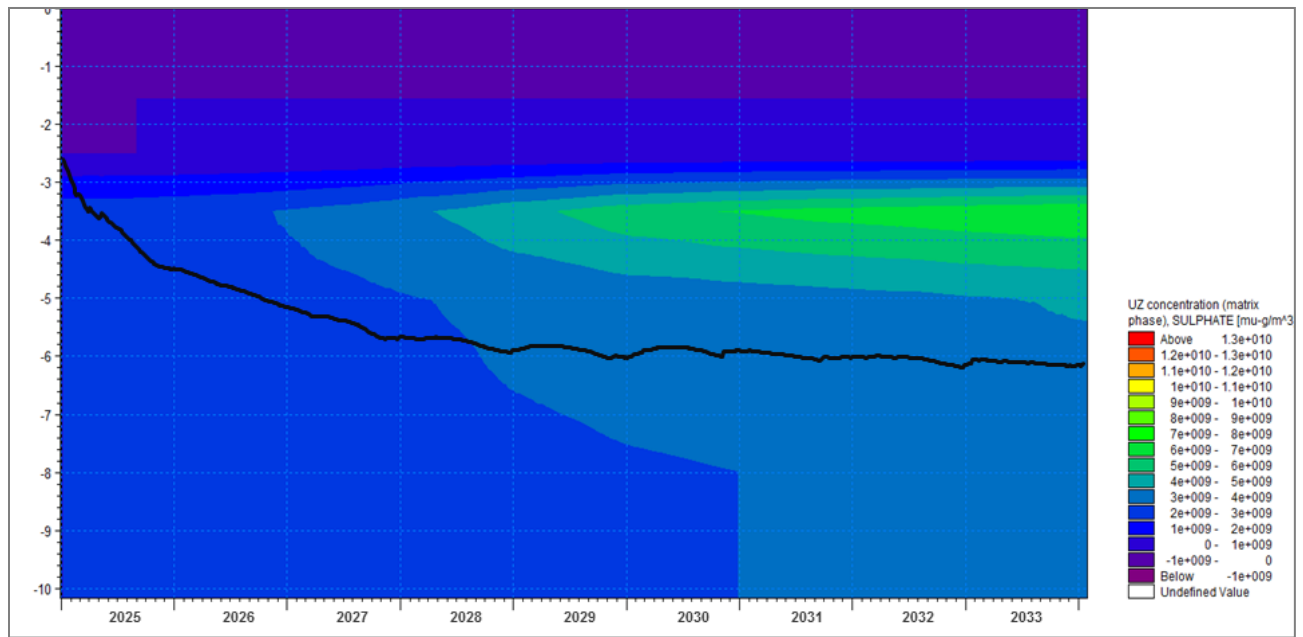


Figure 115: The SO₄ concentrations, below ground (mbgl), for the scenario 6 at point 1.1

To prove that the effects observed were in fact due to drying, the water content and SO₄ concentrations for point 1.3 was plotted on an XY scatter plot. Scenario 4's water content and SO₄ concentrations were used, as scenario 4 showed the greatest range in SO₄ concentrations for point 1.3. These values were taken for 4mbgl. This scatter plot (Figure 116) indicated there was a correlation between the simulated water content and the SO₄ concentration. This correlation suggests that the profile patterns mentioned above, and below, are driven by the soil drying rather than the SO₄ being transported around the profile by the plants root system. This plot indicates that as the soil dries up, the SO₄ concentration increases. The exponential pattern observed is hypothesized to be the result of the MIKE SHE model specifying that the amount of SO₄ extracted by the roots decreases over time as the plant's roots/foilage gets saturated with SO₄, and therefore cannot continually extract the same quantity across the simulation period.

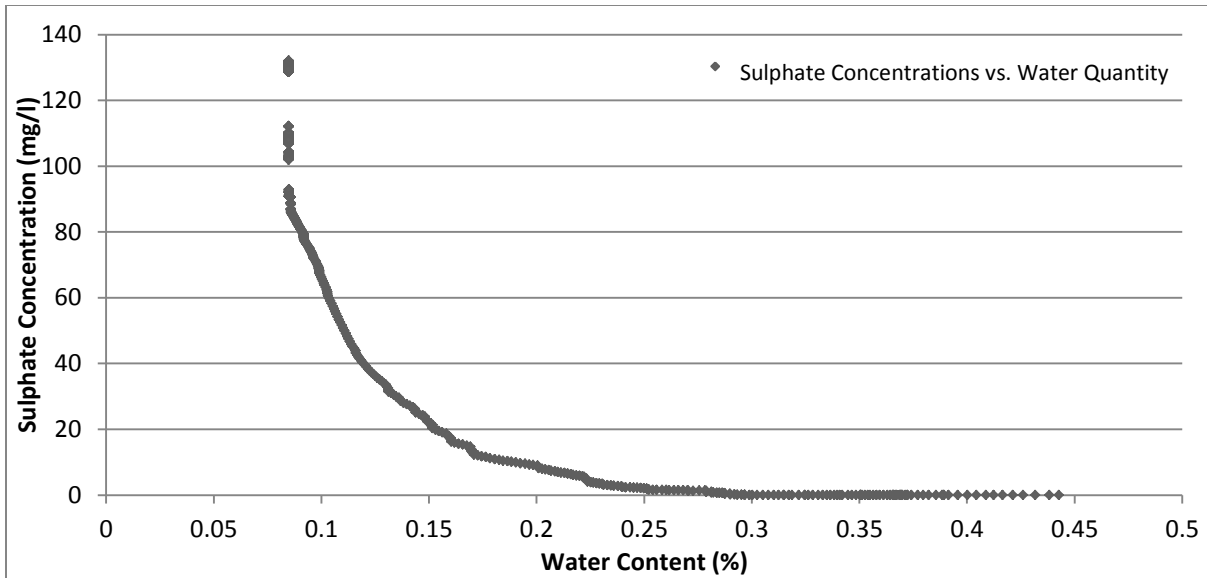


Figure 116: The correlation between the SO_4 concentrations and the water content for scenario 4 at point 1.3

5.7.1.2 Transect Point 1.2

Transect point 1.2 was similar to point 1.1 as these points both lie within the non-AGA owned planting blocks. It must be noted again that the colour scale used for point 1.2 was different to that used for point 1.1, and this difference must be taken into account when comparing the two points. That said the current scenario (Figure 117) for point 1.2 showed lower levels of SO_4 within the unsaturated and SZ. This result was due to point 1.2 lying geographically further from the West Complex TSF. Within point 1.1 the groundwater level was observed at the 4mbgl mark, whilst point 1.2 was observed with a groundwater level below the 4mbgl mark.

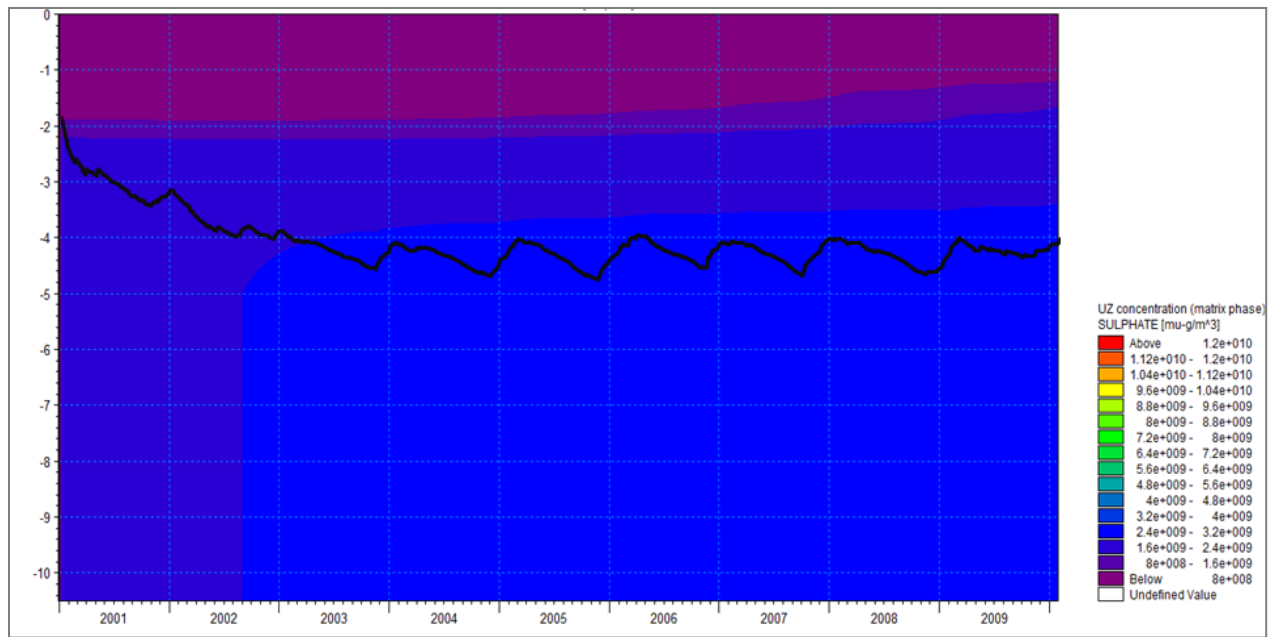


Figure 117: The SO₄ concentrations, below ground (mbgl), for the current scenario at point 1.2

There was a noticeable decrease in the groundwater level that was observed for planting scenario 1, when compared to the current scenario. The groundwater level decreased by 3m to a depth of 7mbgl (Figure 118), when the grasslands were replaced with *S. lancea*. This decrease in groundwater level resulted in the UZ becoming dryer than that found within the current scenario. This drying was the cause of the increase in SO₄ concentrations observed in the 2 to 5mbgl band. The drying of the UZ resulted in there being similar amounts of SO₄ in this zone, however dissolved in less water, which resulted in the higher concentrations.

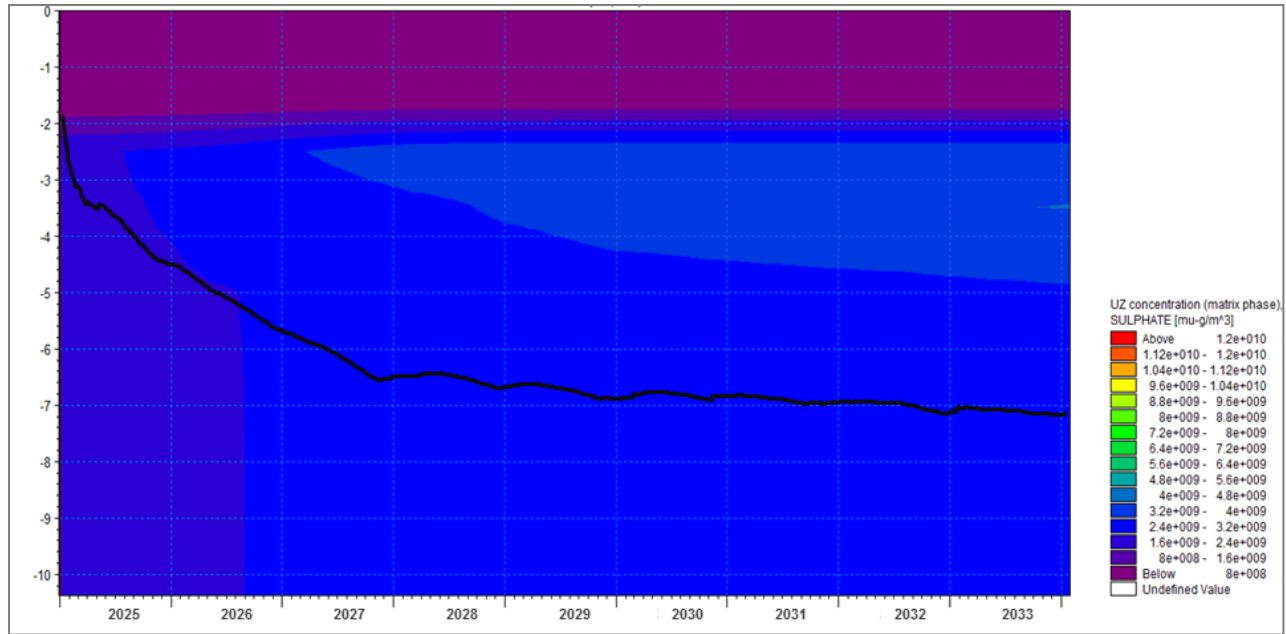


Figure 118: The SO₄ concentrations, below ground (mbgl), for the scenario 1 at point 1.2

As mentioned in the previous sections, the use of *S. lancea* and *E. dunnii* produced similar decreases in groundwater when compared to the current scenario (Figure 119). However, as the *S. lancea* has a greater ability to extract SO₄ when compared to *E. dunnii*, there was a noticeable increase in the SO₄ concentration being observed in the UZ. For planting scenario 2 the increase in SO₄ concentration was observed in the 2 to 5mbgl band. This was the impact of the drying of the UZ, as well as the lower *ET uptake factor* of the *E. dunnii*. The first 2mbgl were observed to have lower SO₄ concentrations, for both scenario 1 and 2 when compared with the current scenario.

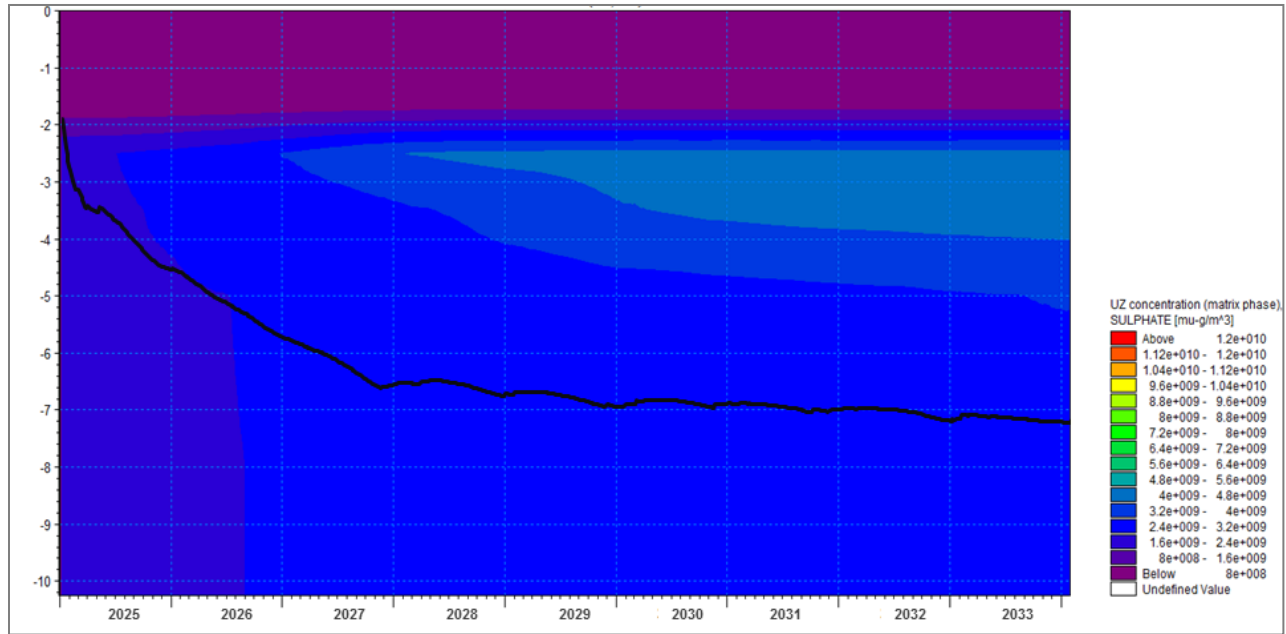


Figure 119: The SO_4 concentrations, below ground (mbgl), for the scenario 2 at point 1.2

Within planting scenario 3, rather than the groundwater decreasing to a depth of below 7mbgl, the groundwater level remained above 7mbgl (Figure 120). But the most noticeable change that was observed was the significant increase in the SO_4 concentration simulated between the 2 and 5mbgl mark. This result was again the impact of the non-spatially defined *ET uptake factor*, and this impact must be considered when determining the most appropriate planting scenario.

Similar groundwater level decreases were observed for planting scenario 4 when compared with planting scenario 3 (Figure 121). Again, there was an increase in the UZ SO_4 concentrations, which was a result of the non-spatially defined *ET uptake factor*. However, where scenario 3 was observed to have levels of $9.5 \times 10^9 \mu\text{g}/\text{m}^3$, scenario 4 was observed to have SO_4 concentrations of above $1.2 \times 10^{10} \mu\text{g}/\text{m}^3$. This increase was the result of the *E. dunnii* not having an equal ability to extract SO_4 . This result indicates that even though the MIKE SHE model is limited by the *ET uptake factors* spatial dispersion, the model had the ability to simulate the extraction of the SO_4 through the plant roots.

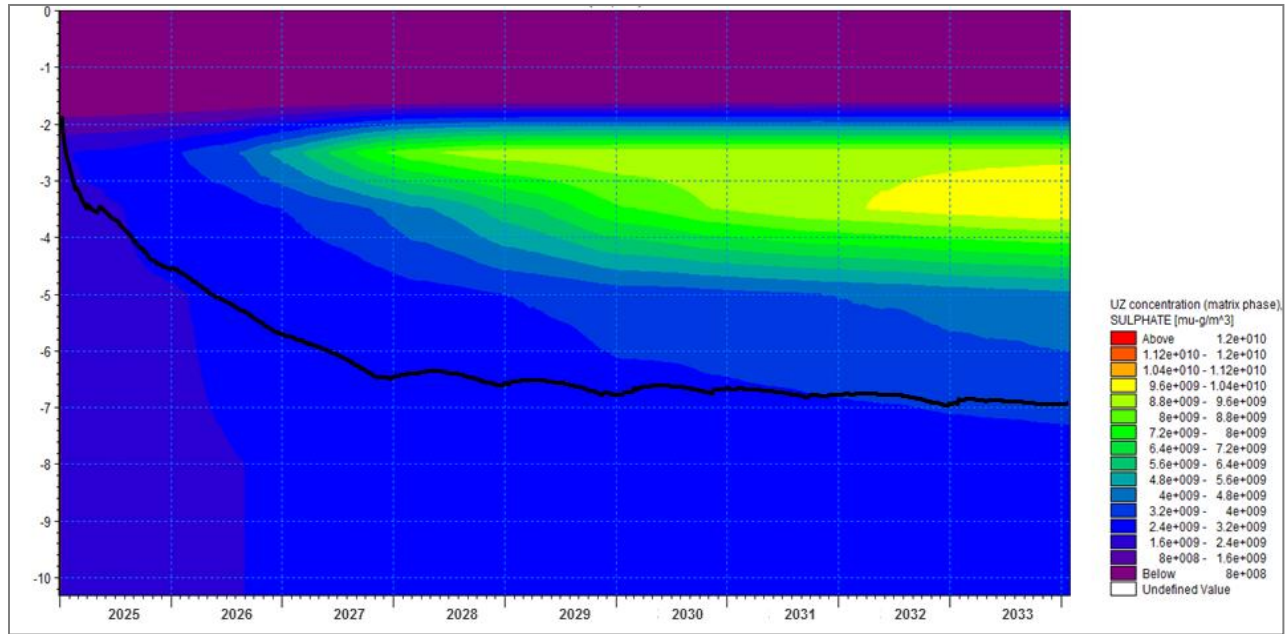


Figure 120: The SO₄ concentrations, below ground (mbgl), for the scenario 3 at point 1.2

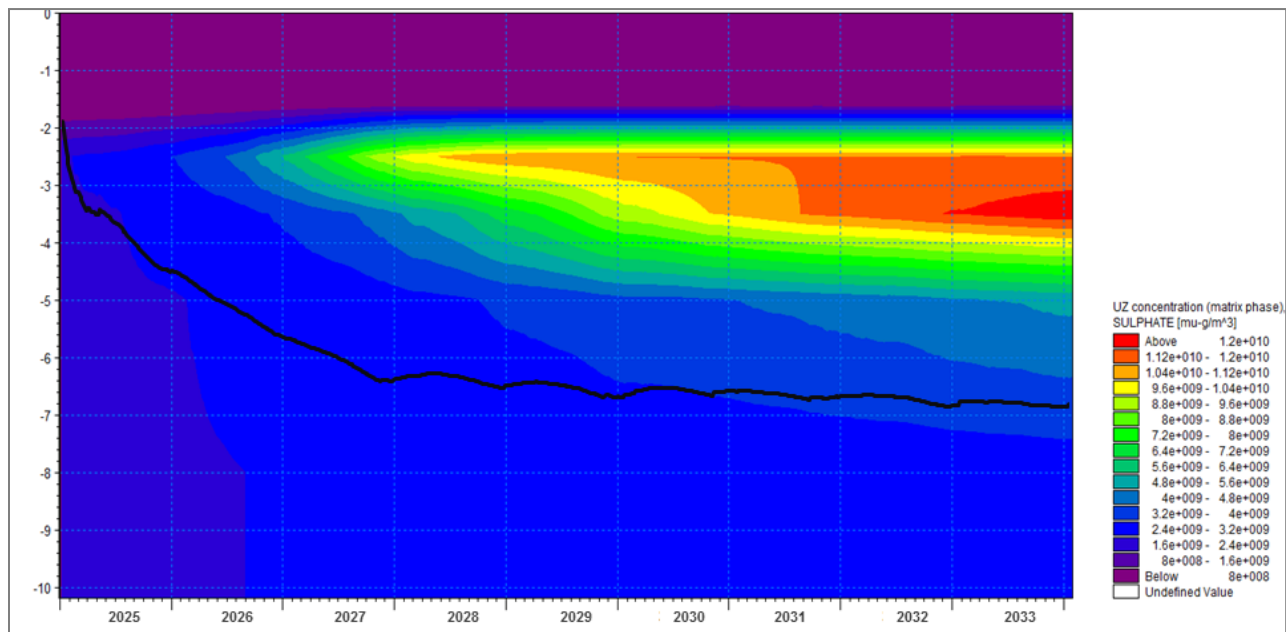


Figure 121: The SO₄ concentrations, below ground (mbgl), for the scenario 4 at point 1.2

Planting scenario 5 simulated the *S. lancea* not being planted within the non-Anglo owned planting blocks. When compared with planting scenario 1, there are two significant results observed. Firstly, the groundwater level has not decreased to the same levels as observed when the non-AGA owned planting blocks were planted (Figure 122). The groundwater level for planting scenario 5 was observed at 6.5mbgl while planting scenario 1's groundwater level was

at 7.2mbgl. Secondly, the SO₄ concentration levels were significantly higher than observed in planting scenario 1. The SO₄ concentrations in planting scenario 1 reached a peak of $5.6 \times 10^{-8} \mu\text{g}/\text{m}^3$, whilst planting scenario 5 was observed with a peak of $6.4 \times 10^{-8} \mu\text{g}/\text{m}^3$. These results highlight the impact of not planting in these blocks, not only does the groundwater increase but the concentrations of SO₄ found in the UZ also increase.

Planting scenario 6 (Figure 123) was observed with similar results to planting scenario 5, when compared with planting scenario 2. Planting scenario 6 was observed to have a shallower groundwater level, as well as an increase in the SO₄ concentrations simulated within the 2 to 5mbgl ban, when compared with planting scenario 2. However, when planting scenario 6's results were compared to planting scenario 5's results there was a significant increase in the SO₄ concentration spread. Both scenarios attained similar peaks in SO₄ concentration, however planting scenario 6 was observed to have a wider spread of this peak. In planting scenario 5 this peak was first observed towards the end of 2031, whilst in planting scenario 6 this peak was observed much earlier, in the middle of 2028. This result highlights the impacts of planting *E. dunnii* instead of *S. lancea*.

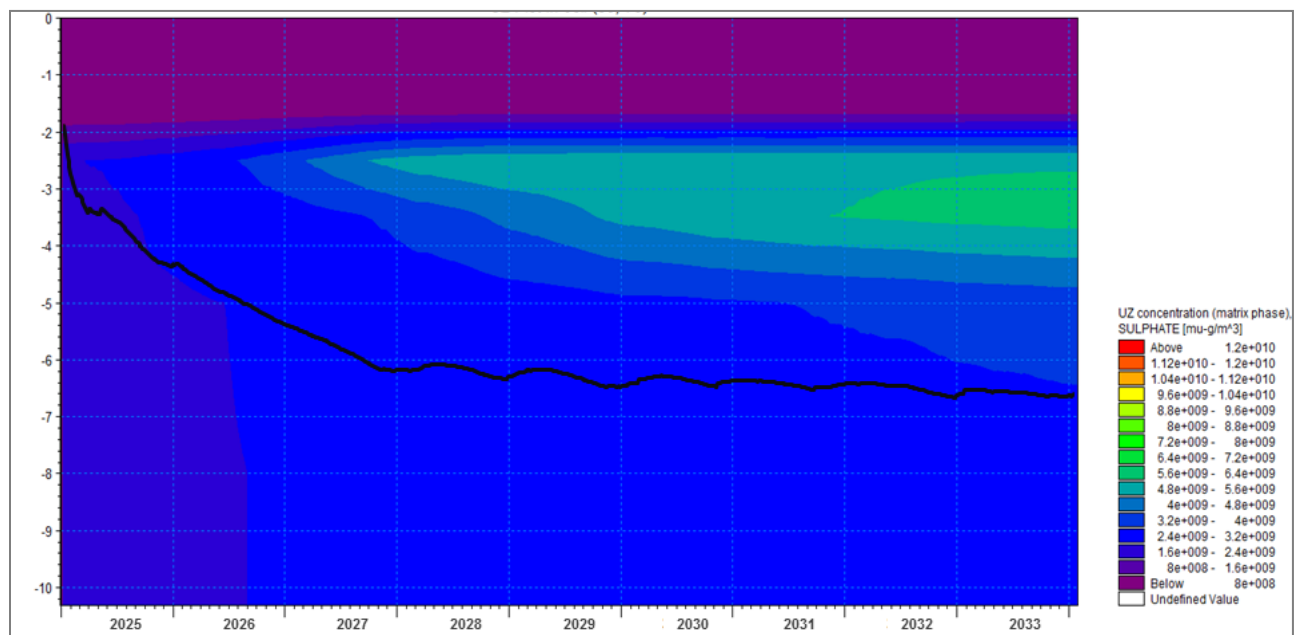


Figure 122: The SO₄ concentrations, below ground (mbgl), for the scenario 5 at point 1.2

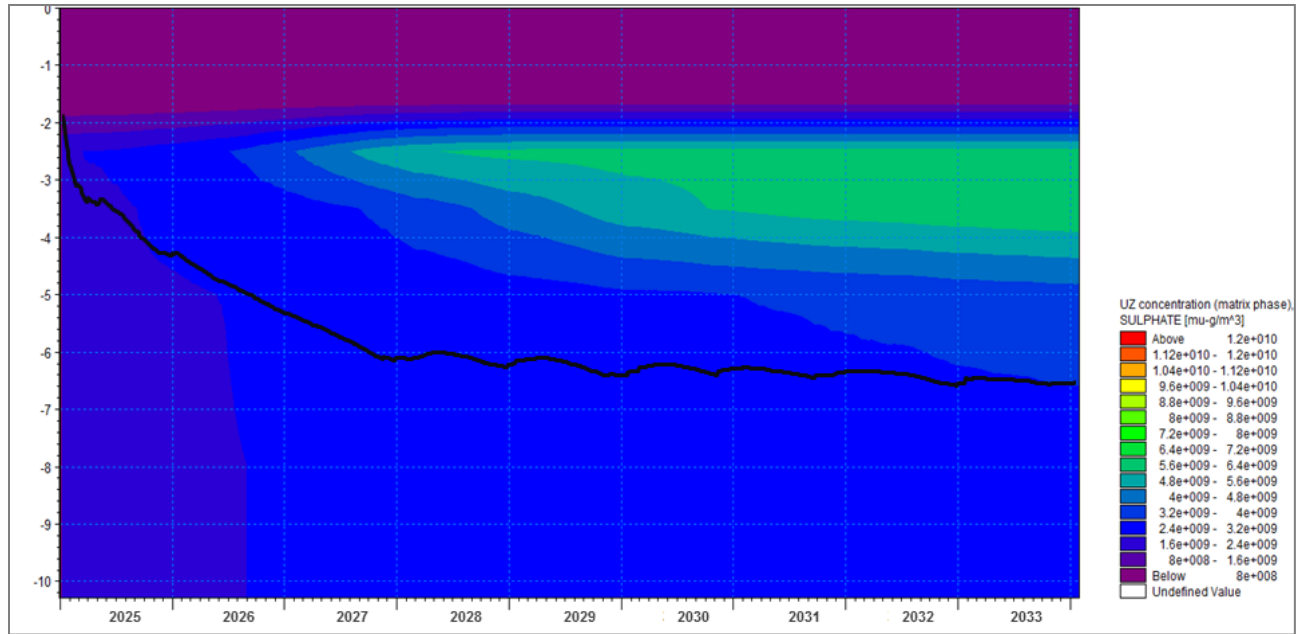


Figure 123: The SO₄ concentrations, below ground (mbgl), for the scenario 6 at point 1.2

5.7.1.3 Transect Point 1.3

Transect point 1.3 lies within the *T. usneoides* planting block alongside the Schoonspruit River. This point provided insight into the overall impacts of the planting scenarios on the contamination plume emerging from the West Complex TSF. For the current scenario, at point 1.3, the groundwater level was much shallower, with a final depth of 2mbgl (Figure 124). The highest SO₄ concentrations were found above the groundwater.

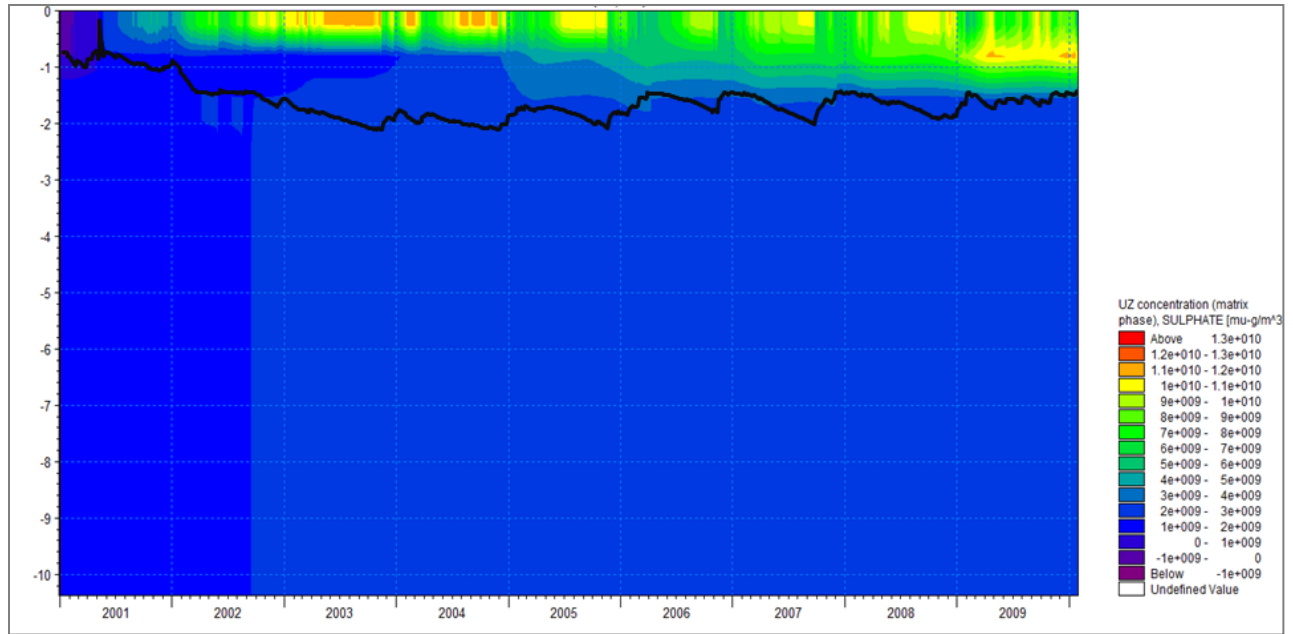


Figure 124: The SO_4 concentrations, below ground (mbgl), for the current scenario at point 1.3

The impacts of planting *T. usneoides* within this planting block were immediately evident from the cross-section for planting scenario 1 (Figure 125). For planting scenario 1 the first impact observed, when compared to the current scenario, was the decrease in the groundwater level. The groundwater level had decreased from 2mbgl, in the current scenario, to 4mbgl. This decrease in groundwater level resulted in a drying of the UZ. It would be expected that the SO_4 concentrations, observed in the UZ, would increase. However, due to the planting of *T. usneoides*, a hyperaccumulator, there is a significant decrease in the SO_4 concentrations of the UZ.

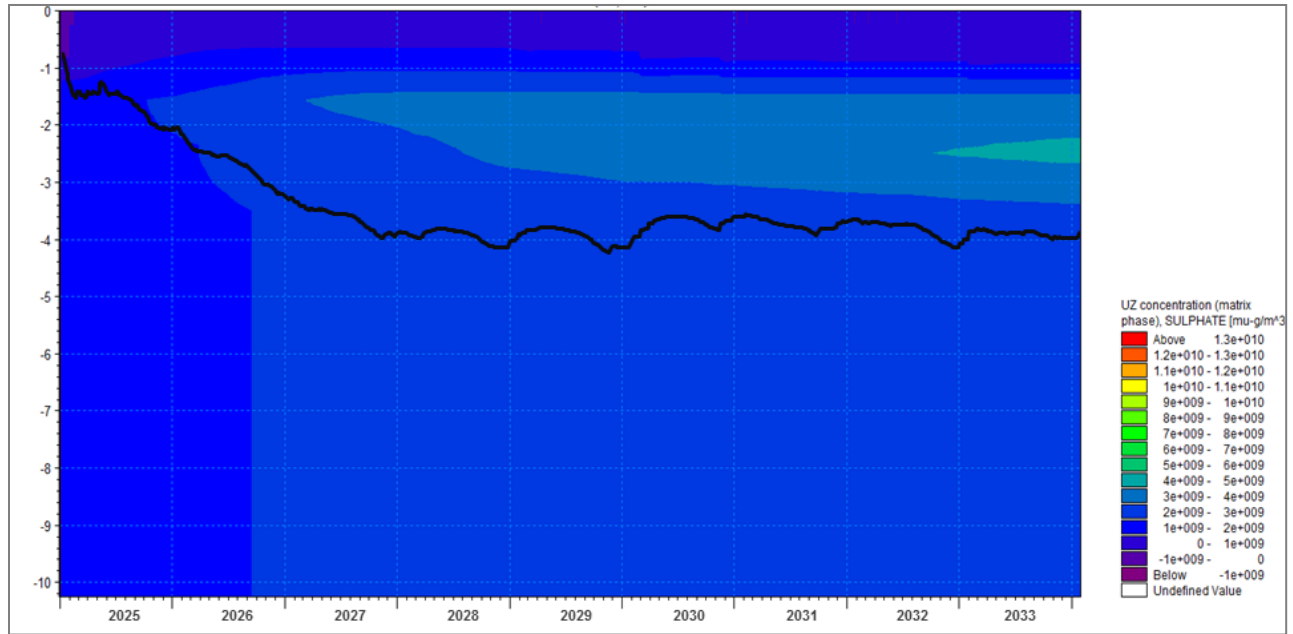


Figure 125: The SO₄ concentrations, below ground (mbgl), for the scenario 1 at point 1.3

With planting scenario 2, there was a similar decrease in groundwater level observed when compared to planting scenario 1 (Figure 126). The noticeable difference observed between planting scenario 1 and 2 was the earlier spread of the peak of the SO₄ concentrations. In scenario 1 this peak was observed towards the end of 2032, whilst in scenario 2 this peak was observed two years earlier. This result indicates that the *T. usneoides* extracts similar quantities of SO₄, but due to scenario 2 where the *E. dunnii* is extracting less and having a higher SO₄ concentration, the amount of SO₄ remaining in the UZ is higher.

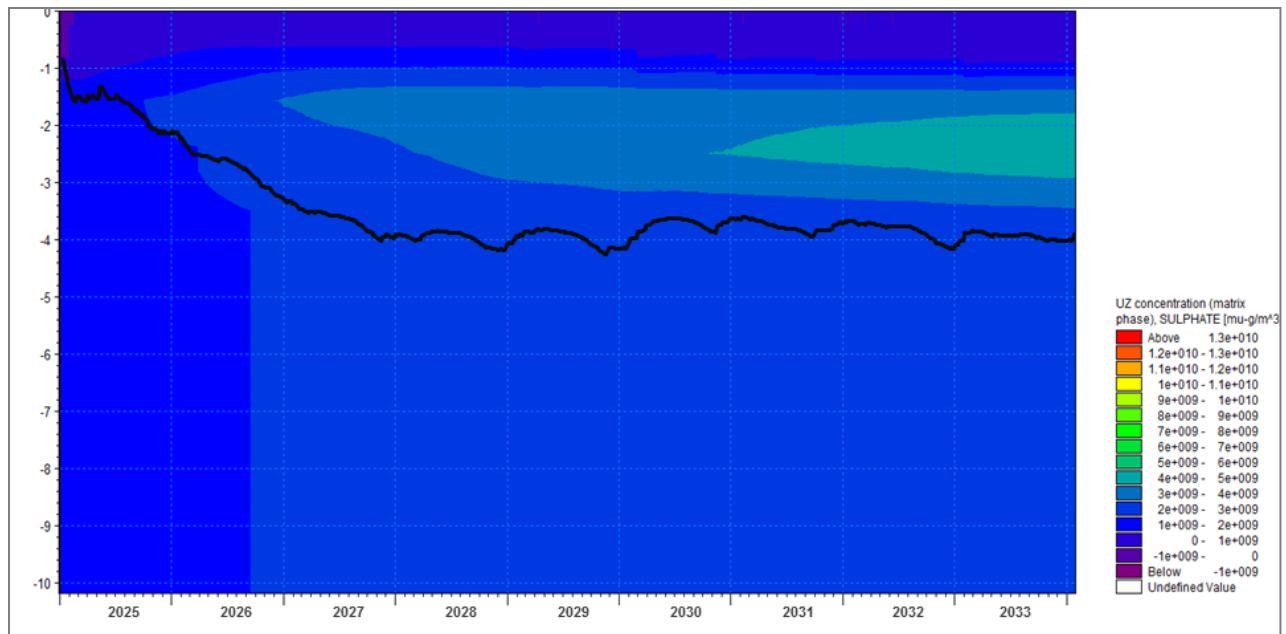


Figure 126: The SO_4 concentrations, below ground (mbgl), for the scenario 2 at point 1.3

With planting scenario 3, the impacts of not planting *T. usneoides* along the Schoonspruit River are immediately visible (Figure 127). The groundwater level was observed to decrease slightly, and the SO_4 concentration levels observed in the UZ were also decreased, but not as significantly as observed for planting scenario 1. The decrease in groundwater level observed was the result of the planting of *S. lancea* in the previous rows of planting blocks. The *S. lancea* were also responsible for the slight decrease in SO_4 observed. This scenario indicates the overall impact that the *S. lancea* planted in the planting blocks will have on the contamination plume before it reaches the Schoonspruit River. The result could indicate that there is a decrease in groundwater and SO_4 concentrations, however planting *T. usneoides* along the Schoonspruit River will increase the impact observed.

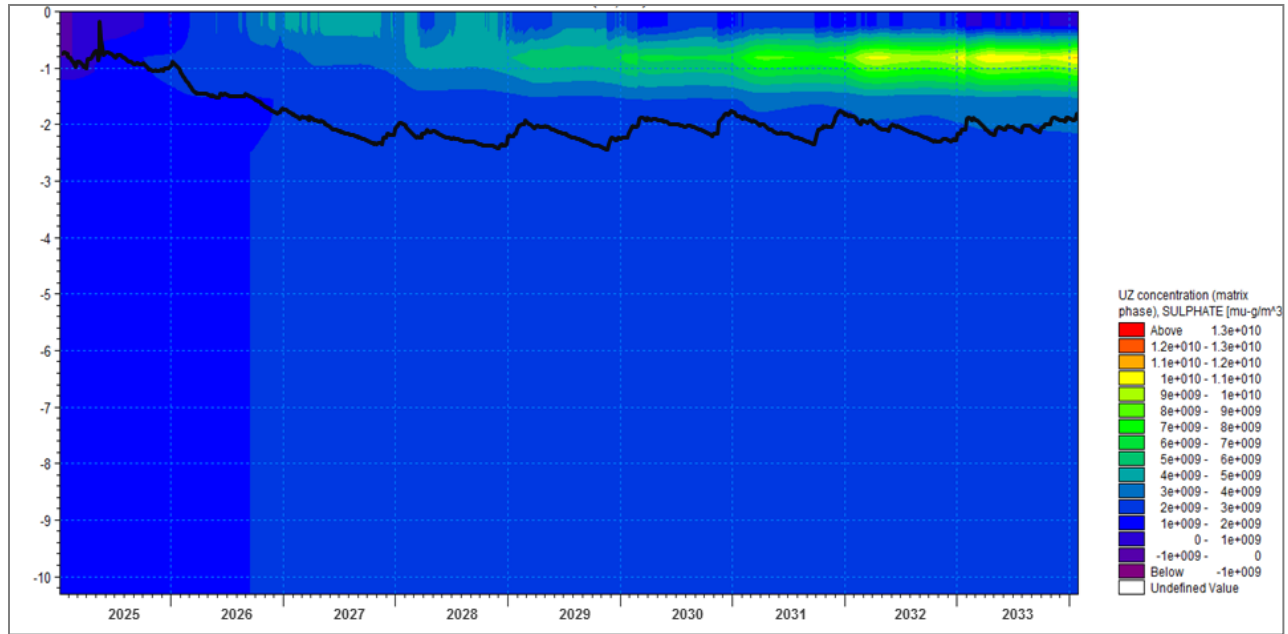


Figure 127: The SO_4 concentrations, below ground (mbgl), for the scenario 3 at point 1.3

Planting scenario 4 was observed to decrease the groundwater level to a similar degree as observed for planting scenario 3 (Figure 128). However, there was a noticeable increase in the SO_4 concentrations observed when compared to planting scenario 3. The SO_4 concentrations of scenario 4 were observed to decrease the SO_4 concentrations in the earlier years of the simulation for the current scenario. However, towards the end of the simulation period, in scenario 4 an increase in SO_4 concentration was observed. This increase was not evident in scenario 3. This result indicates that the overall impact of the *E. dunni* on the contamination plume is significantly less than observed for the *S. lancea*.

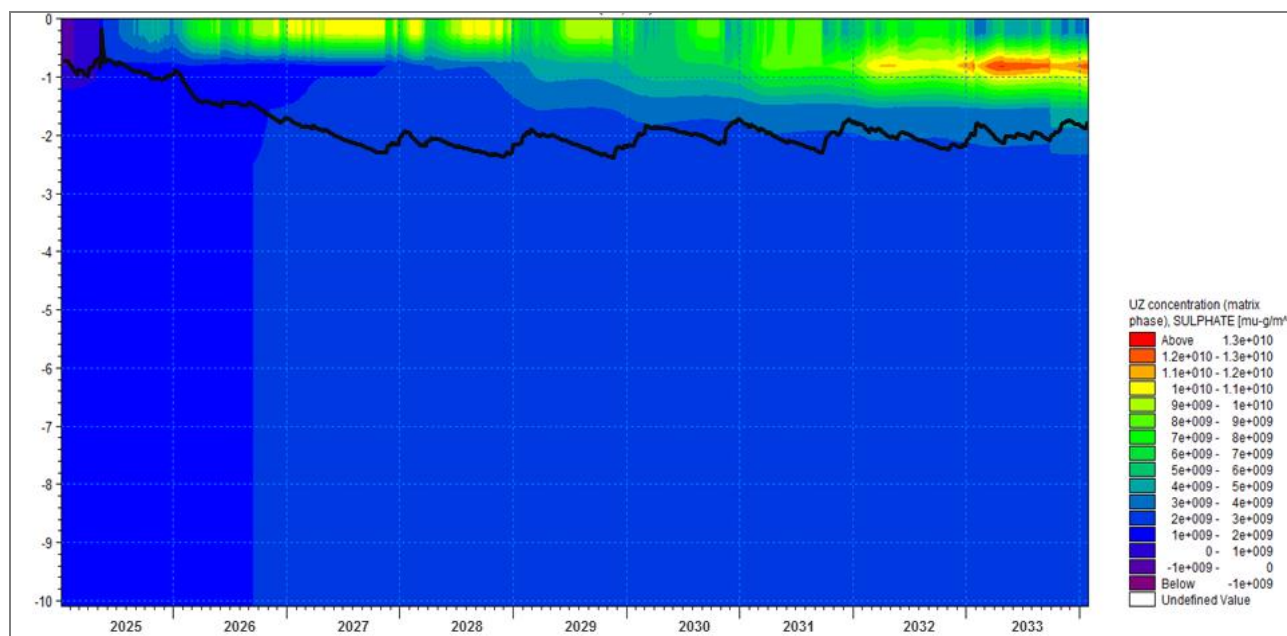


Figure 128: The SO₄ concentrations, below ground (mbgl), for the scenario 4 at point 1.3

Planting scenario 5 at point 1.3 provided insight into the overall impacts of not planting within the non-AGA owned planting blocks. When the cross-section for scenario 5 (Figure 129) was compared with scenario 1 (Figure 125) there was a significant increase in the SO₄ concentrations found in scenario 5. This increase can be directly linked to the non-planting of the non-AGA planting blocks as there were similar decreases in the groundwater level.

Planting scenario 6 (Figure 130) reiterated the previous result found in planting scenario 4, that the use of *E. dun nii* over *S. lancea* results in similar groundwater level decreases with an increase in the SO₄ concentration observed in the UZ.

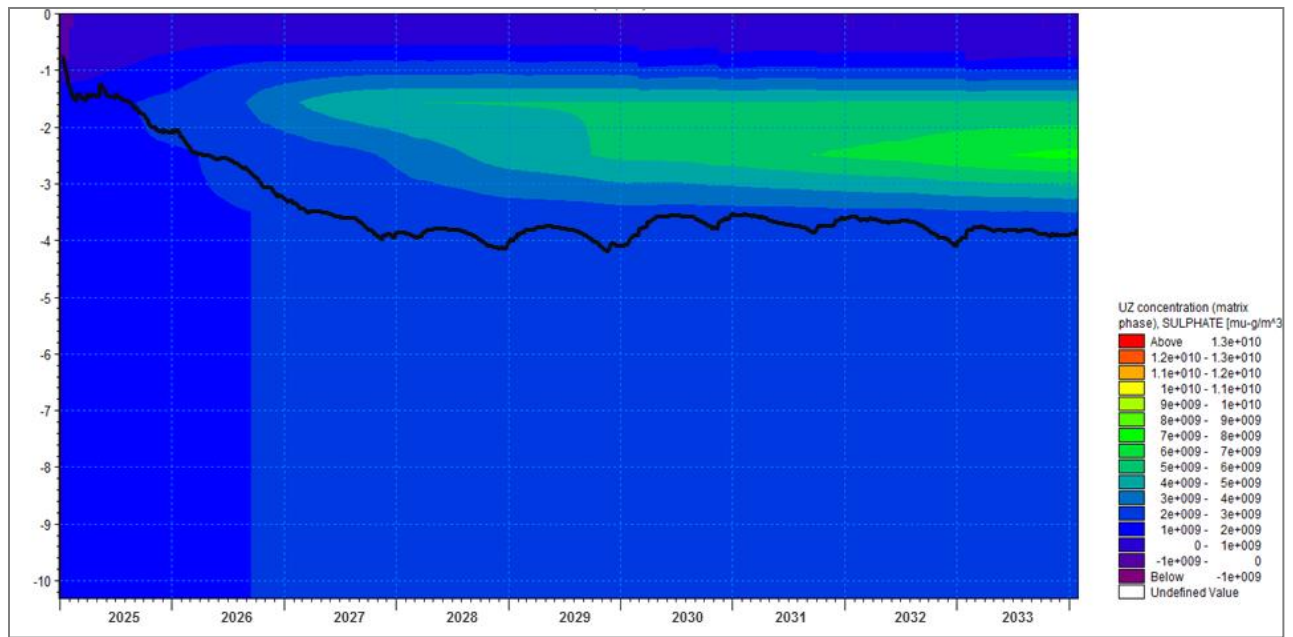


Figure 129: The SO₄ concentrations, below ground (mbgl), for the scenario 5 at point 1.3

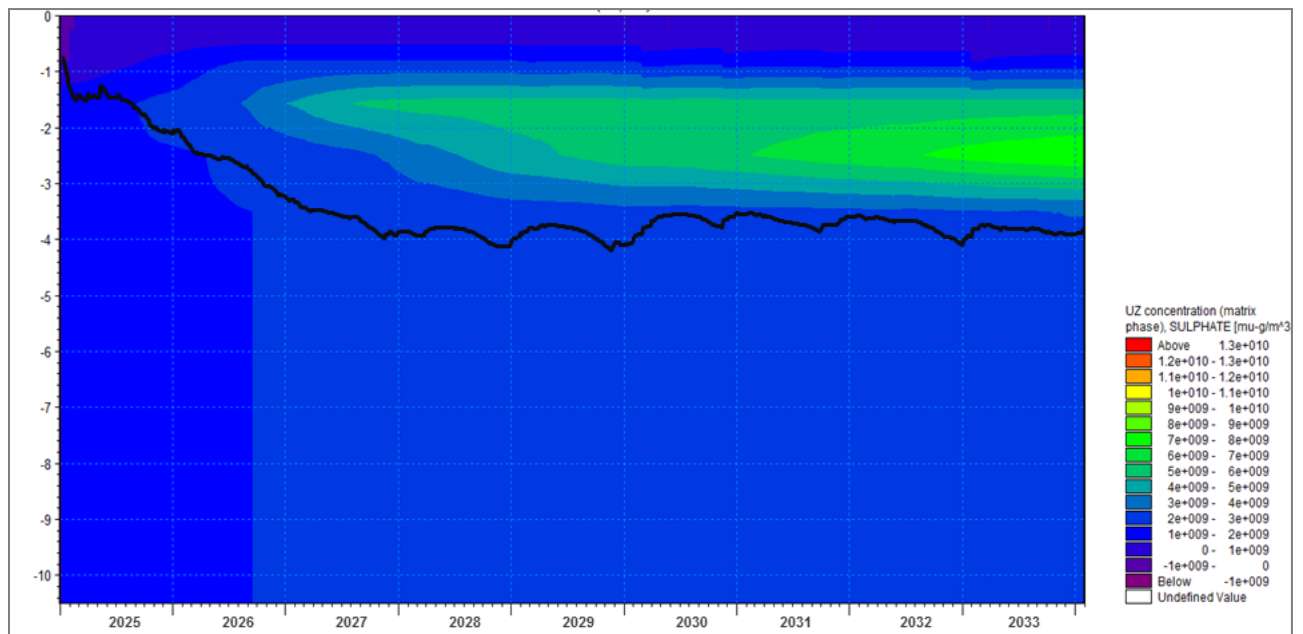


Figure 130: The SO₄ concentrations, below ground (mbgl), for the scenario 6 at point 1.3

5.7.2 Transect Two

Transect two contains three points, points 2.1, 2.2 and 2.3. Points 2.1 and 2.2 reside in AGA owned planting blocks, whilst point 2.3 lies within the planting block along the Schoonspruit River.

5.7.2.1 Transect Point 2.1

For point 2.1 the groundwater level was simulated at a depth of 7mbgl. The SO_4 concentrations within the UZ were observed to fall between 0 and $2.8 \times 10^{-9} \mu\text{g}/\text{m}^3$. These levels of SO_4 increased with depth below ground. These levels of SO_4 were similar to those observed at point 1.1 (Figure 109). This result indicates that these points were being impacted by the contamination plume to similar degrees.

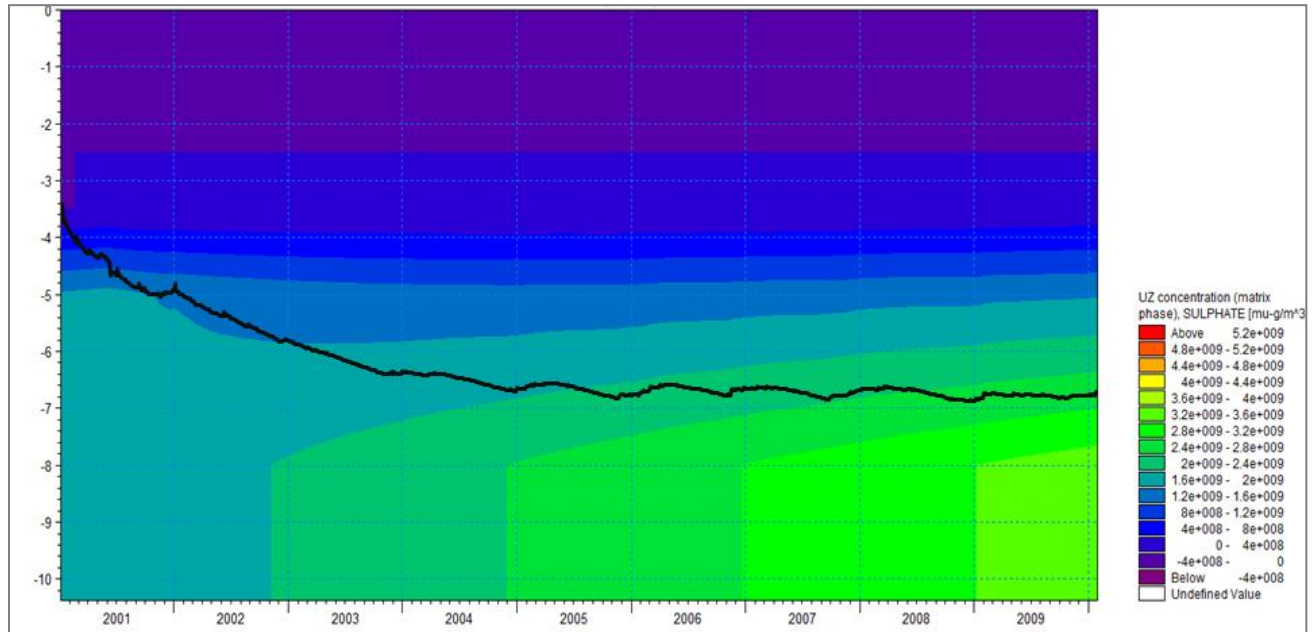


Figure 131: The SO_4 concentrations, below ground (mbgl), for the current scenario at point 2.1

Planting scenario 1 (Figure 132), which simulated the planting of *S. lancea* in all the planting blocks, was observed to decrease the groundwater level by 2m. This significant decrease in the groundwater resulted in the UZ becoming dryer than observed in the current scenario. This drying in turn, resulted in the increase in SO_4 observed for the UZ, specifically within the 3 to 9mbgl band. Another notable result was the decrease in the SO_4 concentration observed within the SZ.

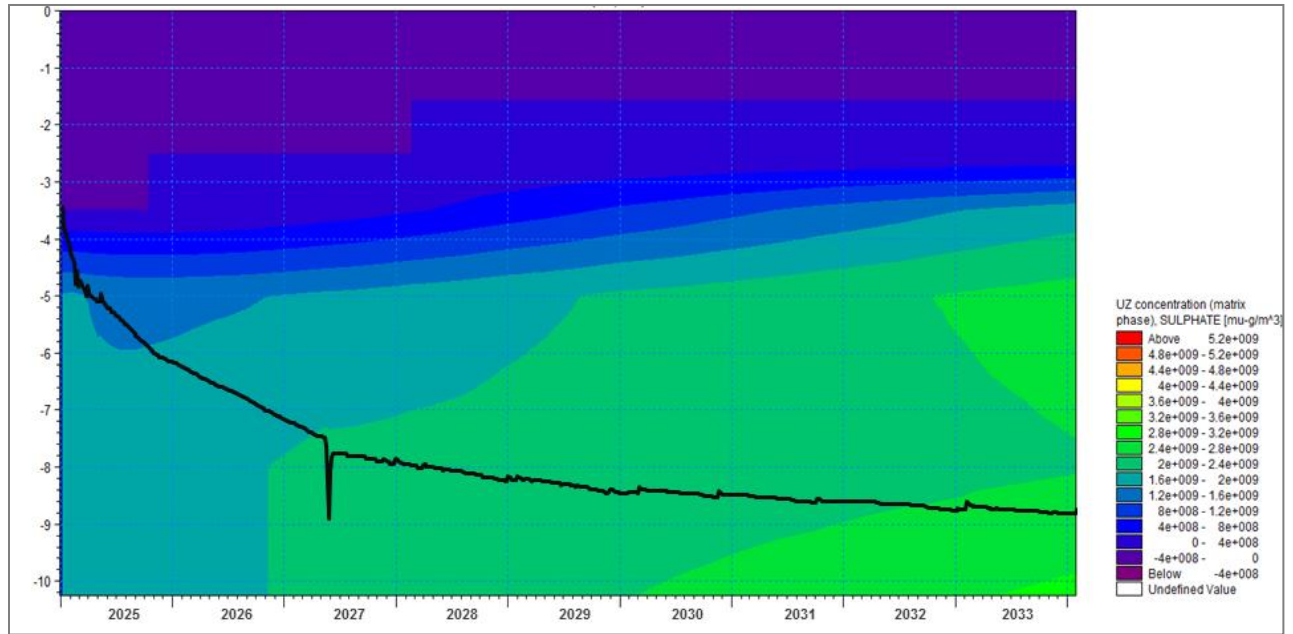


Figure 132: The SO₄ concentrations, below ground (mbgl), for the scenario 1 at point 2.1

Planting scenario 2 (Figure 133) was observed with a similar decrease in the groundwater level, whilst an increase in the SO₄ concentrations simulated in the UZ and the SZ. These results could indicate that *E. dunnii* was less effective than *S. lancea*.

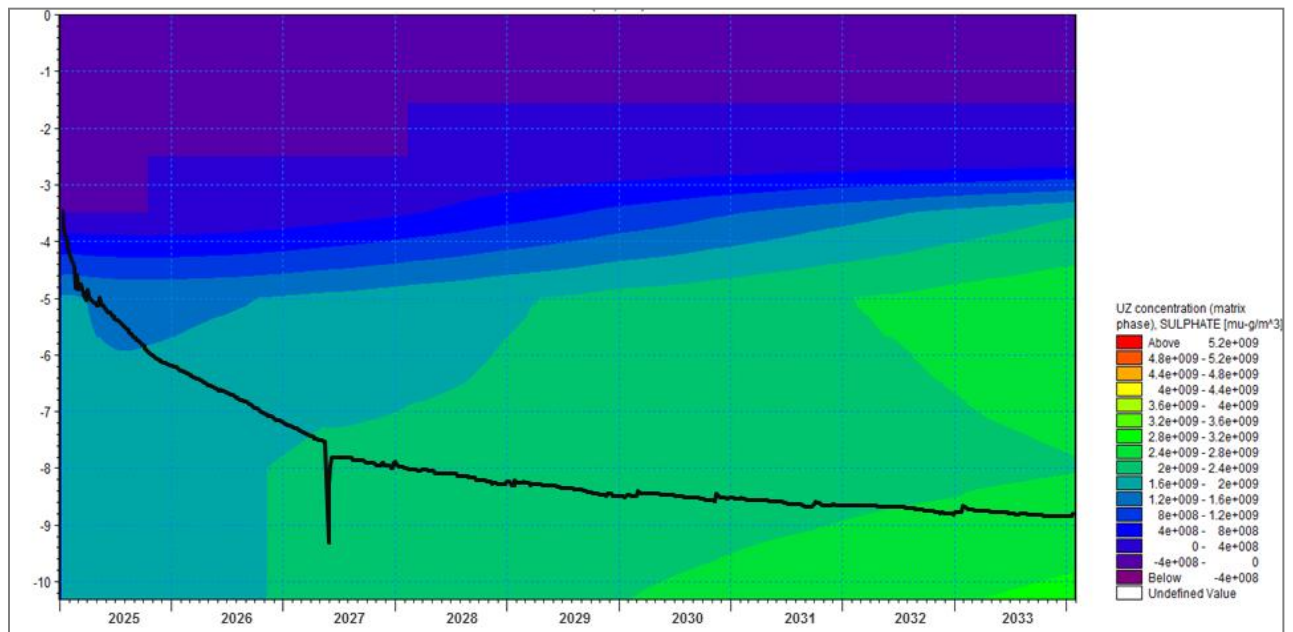


Figure 133: The SO₄ concentrations, below ground (mbgl), for the scenario 2 at point 2.1

As observed in transect one, the impacts of the non-spatial dispersion of the *ET uptake factor* are visible in scenario 3 (Figure 134) when they should not be. Scenario 3 was simulated with *S.*

lancea through the planting blocks and non *T. usneoides* alongside the Schoonspruit River. However, when the cross-section for scenario 3 was plotted the effect of no *T. usneoides* was evident, even though point 2.1 did not lie within the *T. usneoides* planting block.

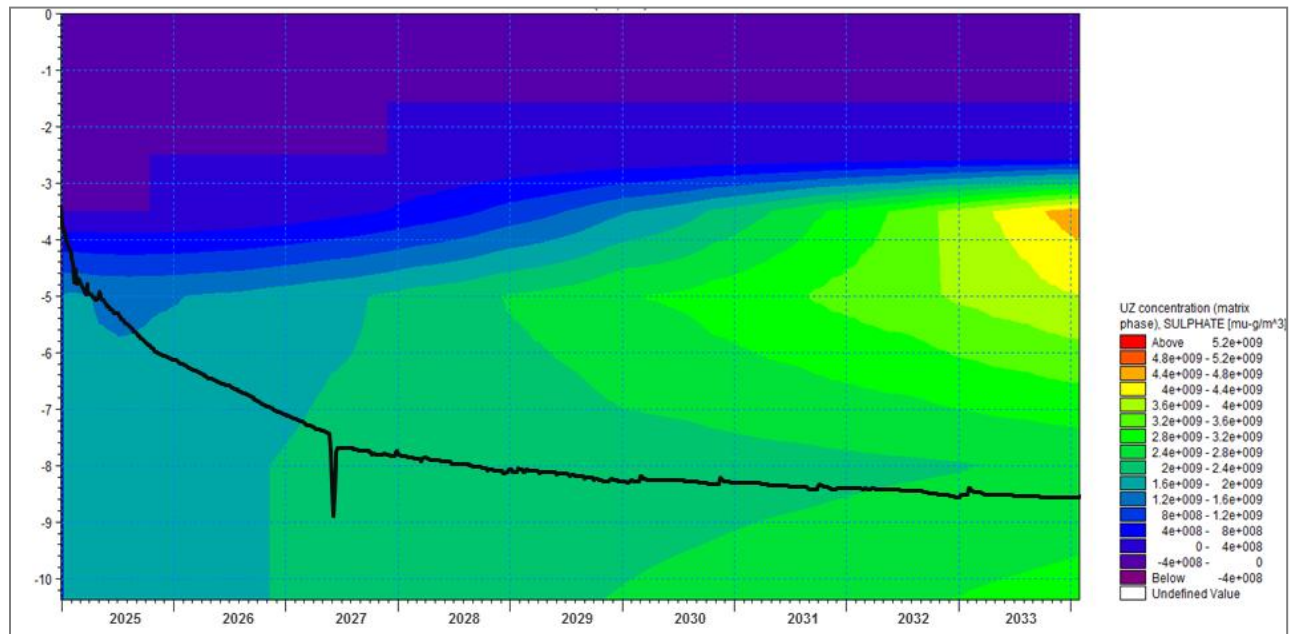


Figure 134: The SO_4 concentrations, below ground (mbgl), for the scenario 3 at point 2.1

Planting scenario 4, at point 2.1 reiterates what was previously observed for planting scenario 4 within transect one. Even though the *ET uptake factor* was resulting in the effect of no *T. usneoides* being observed in non- *T. usneoides* planting blocks (Figure 135). The impact of planting *E. dunnii* over *S. lancea* however was still evident in scenario 4's cross-section. Scenario 4 was observed to have a higher SO_4 concentration, for the UZ, than that observed for scenario 3.

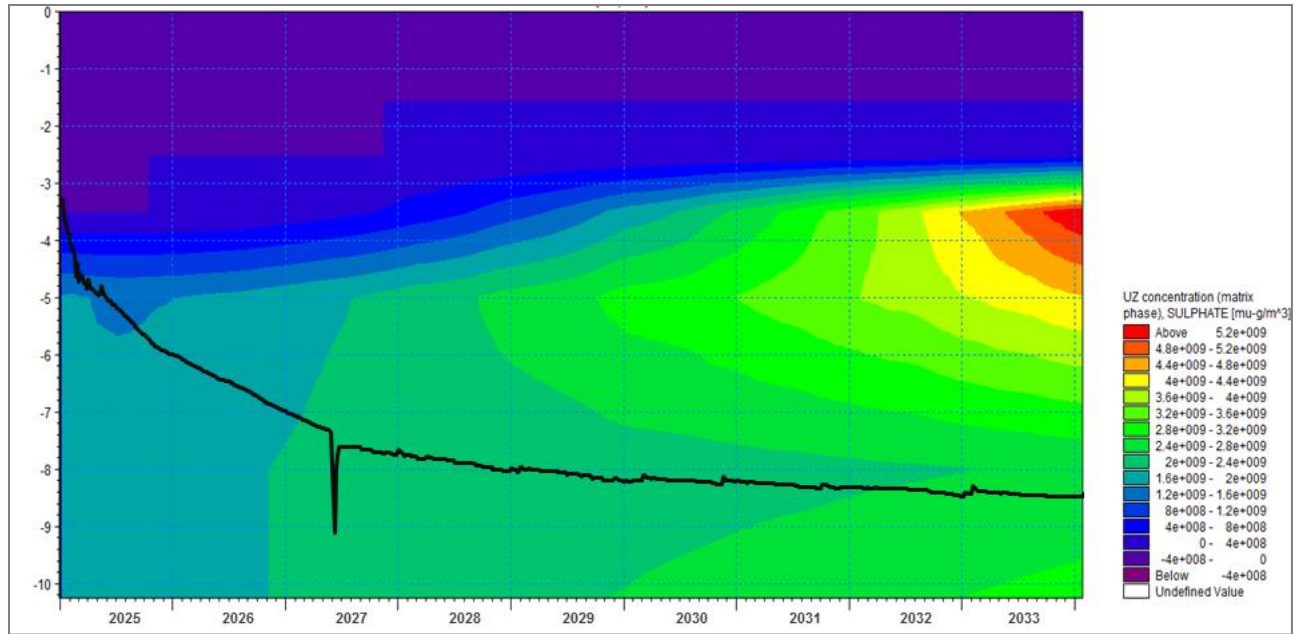


Figure 135: The SO₄ concentrations, below ground (mbgl), for the scenario 4 at point 2.1

Planting scenario 5's cross-section was observed with higher SO₄ concentration within the UZ (Figure 136). However, point 2.1 lies a distance away from the non-AGA owned planting blocks and therefore this result should not be evident. This result was again due to the impact of the *ET uptake factor*. Once again this result must be taken into account when determining which planting scenario was most effective. The same was observed for scenario 6 (Figure 137).

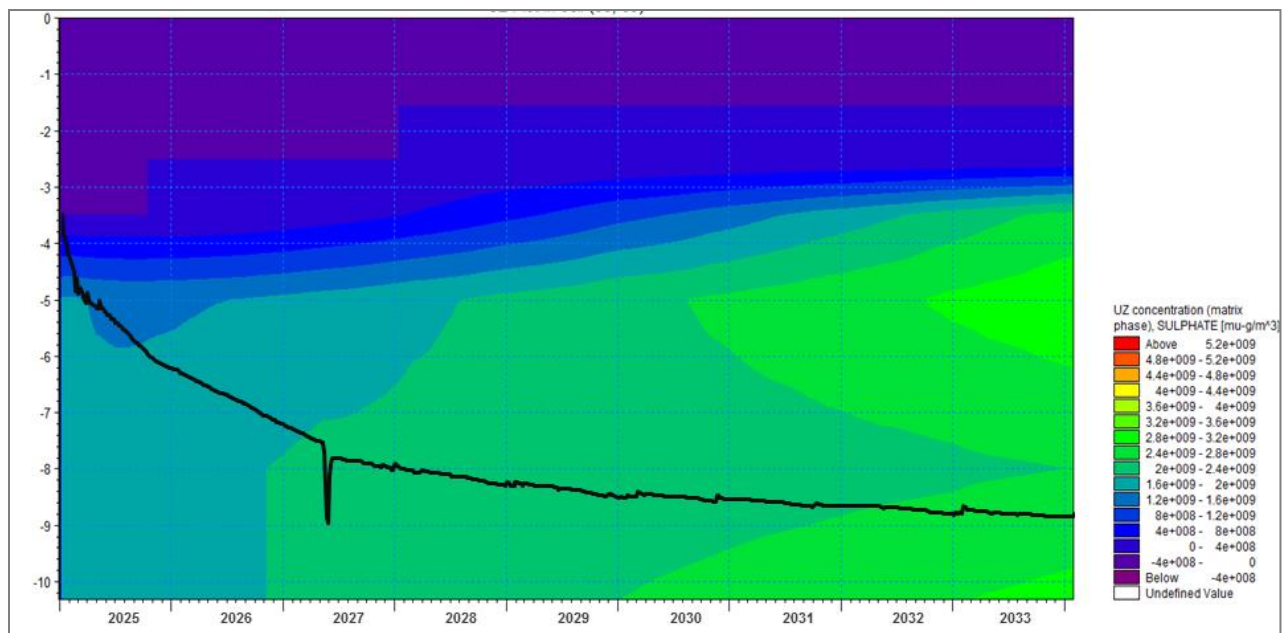


Figure 136: The SO₄ concentrations, below ground (mbgl), for the scenario 5 at point 2.1

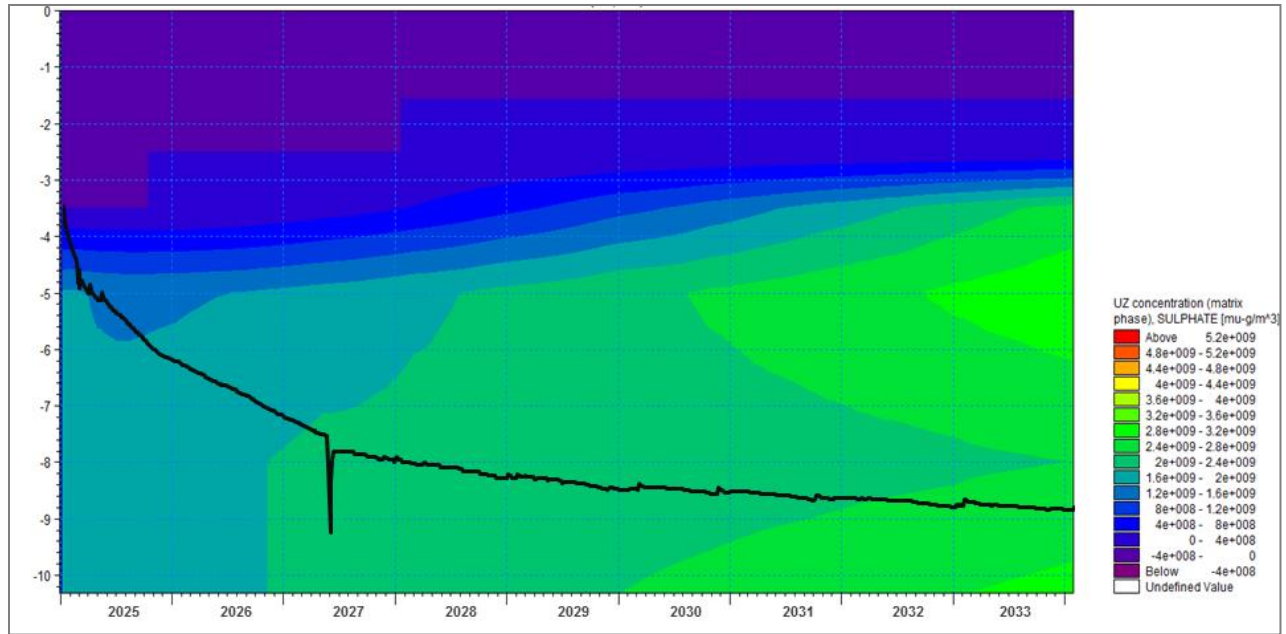


Figure 137: The SO_4 concentrations, below ground (mbgl), for the scenario 6 at point 2.1

5.7.2.2 Transect Point 2.2

The current scenario for point 2.2 was observed to have a shallower water table (3mbgl) than that of point 2.1 (above 7mbgl). The SO_4 concentrations for the current scenario for point 2.2 ranged from 0 to $4 \times 10^{-8} \mu\text{g}/\text{m}^3$ (Figure 138). These SO_4 concentrations increased with depth, however the peak SO_4 concentration level was observed at 1.5mbgl.

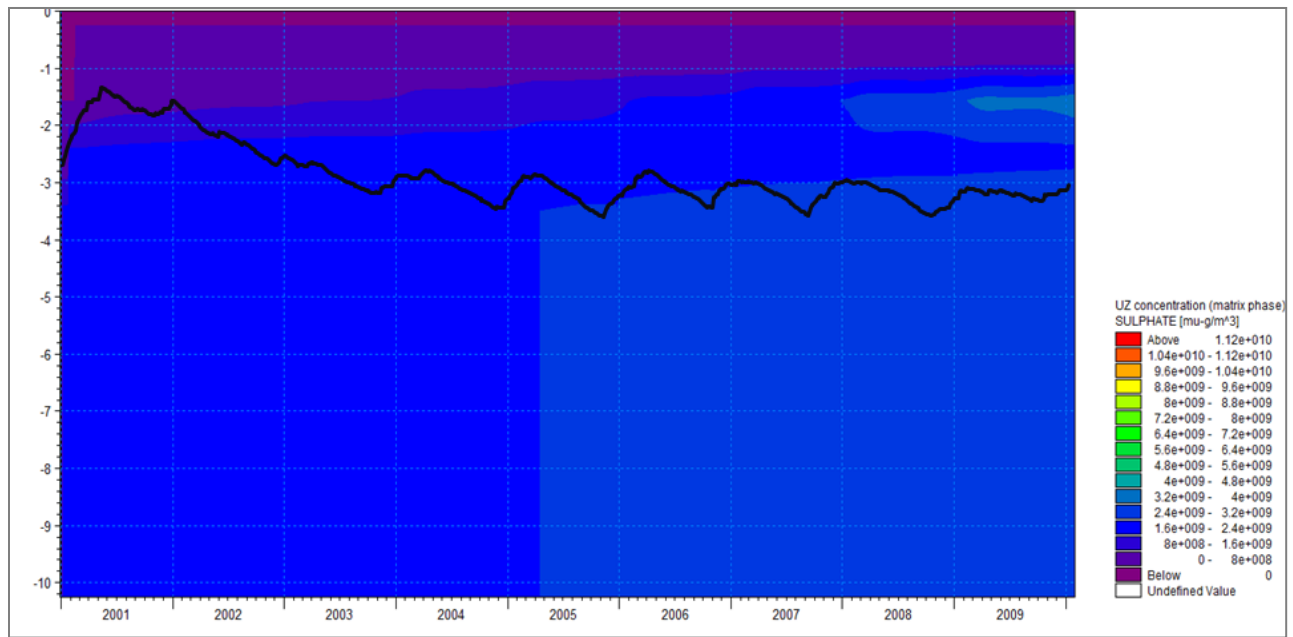


Figure 138: The SO₄ concentrations, below ground (mbgl), for the current scenario at point 2.2

Planting scenario 1 for point 2.2 was observed with a groundwater level that was over 2m deeper (Figure 139) than that observed for the current scenario. This deepening of the groundwater level resulted in the drying of the UZ, as seen for scenario 1 for transect one. This drying resulted in an observed increase in the SO₄ concentrations found within the 2 to 4mbgl band. There was also a measureable increase in the SO₄ concentration observed for the SZ.

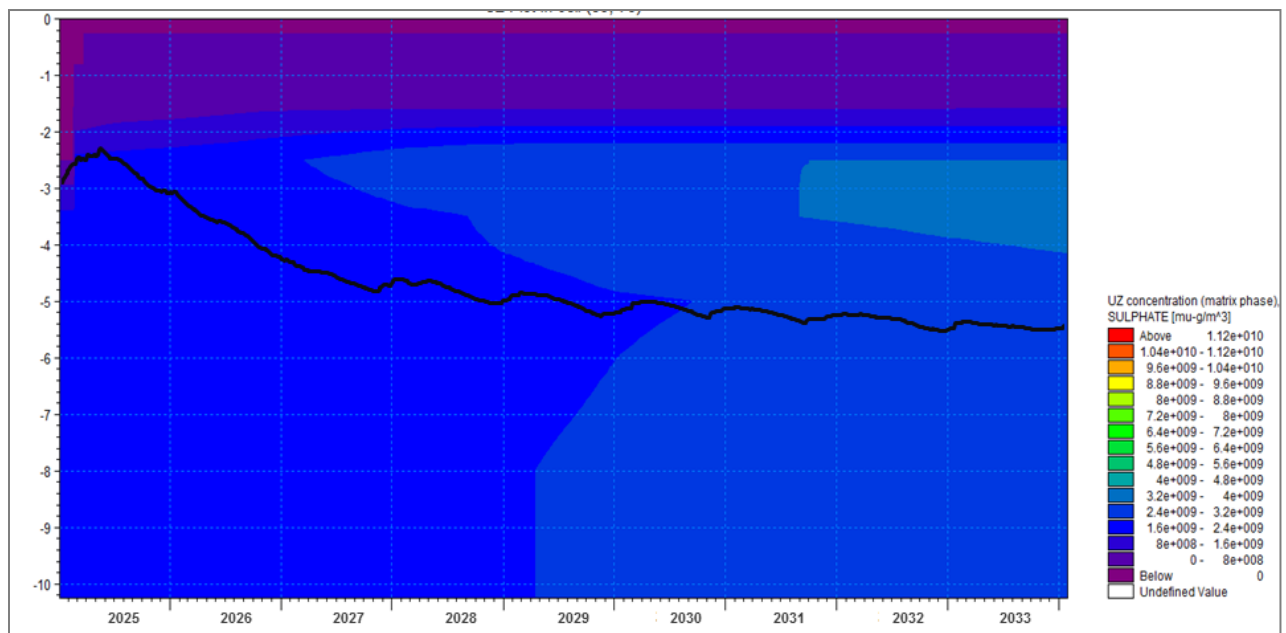


Figure 139: The SO₄ concentrations, below ground (mbgl), for the scenario 1 at point 2.2

As observed in transect one, when comparing the results for scenario 1 and 2, the peak SO_4 concentration levels were the in the same interval, however the peak was observed earlier in scenario 2 (Figure 140) than that of scenario 1 (Figure 139). For planting scenario 1 the peak concentration was observed to start midway through 2031, whilst for scenario 2 the peak concentrations' earliest date was observed midway through 2028, three years earlier. This result was the impact of planting *E. dunnii* versus the planting of *S. lancea*.

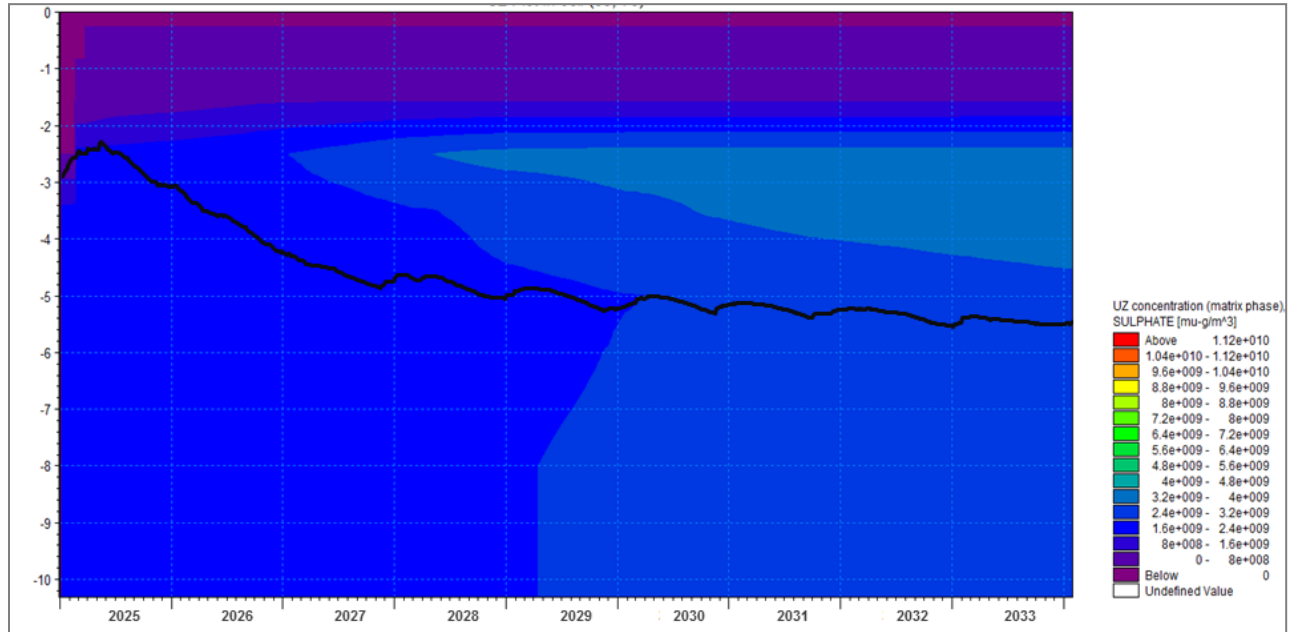


Figure 140: The SO_4 concentrations, below ground (mbgl), for the scenario 2 at point 2.2

As seen in transect 1, and at point 2.1, scenarios 3 (Figure 141) and 4 (Figure 142), for point 2.2, was observed to simulate the impact of not planting *T. usneoides* even though these points do not lie within the *T. usneoides* planting block. The impact of planting *S. lancea* versus *E. dunnii* was also evident, where by scenario 4 (*E. dunnii*) was observed with higher SO_4 concentrations than that observed for scenario 3 (*S. lancea*).

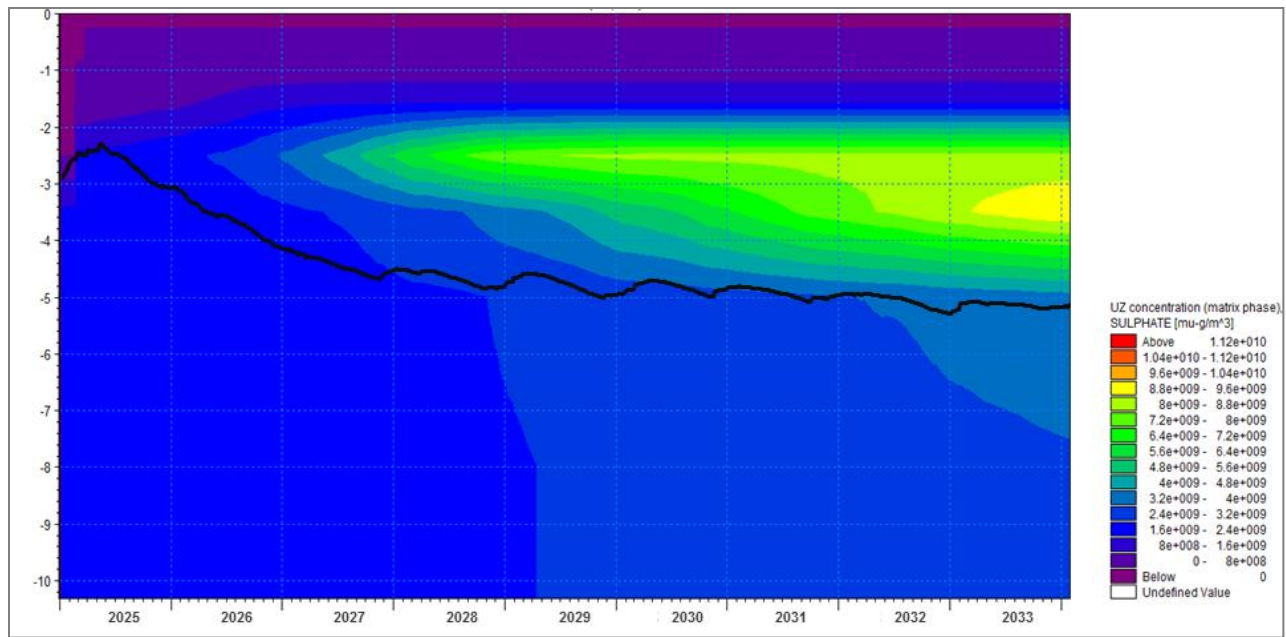


Figure 141: The SO₄ concentrations, below ground (mbgl), for the scenario 3 at point 2.2

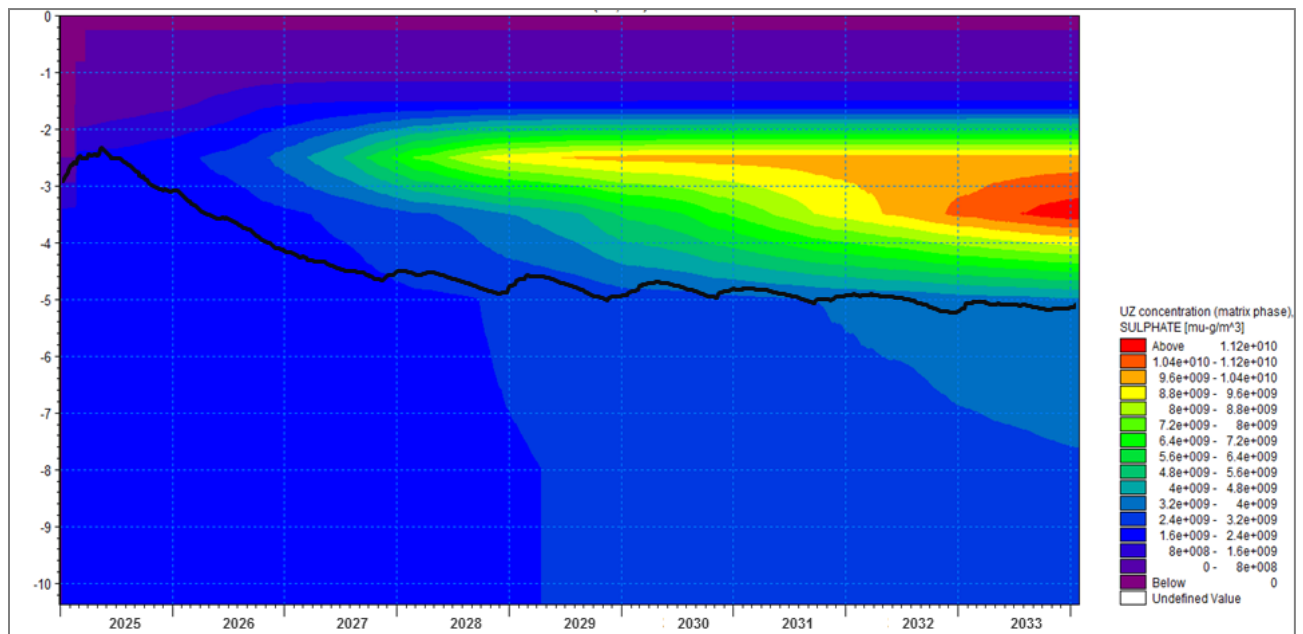


Figure 142: The SO₄ concentrations, below ground (mbgl), for the scenario 4 at point 2.2

A similar result was observed for scenarios 5 (Figure 143) and 6 (Figure 144) for point 2.2 when compared with that experienced at point 2.1. The effect of not planting within the non-AGA owned planting block was visible, when these points fall outside of the non-AGA owned planting blocks. As with scenarios 3 and 4, the impact of planting *S. lancea* versus *E. dunnii* was

also evident, where by scenario 6 (*E. dunnii*) was observed with higher SO_4 concentrations than that observed for scenario 5 (*S. lancea*).

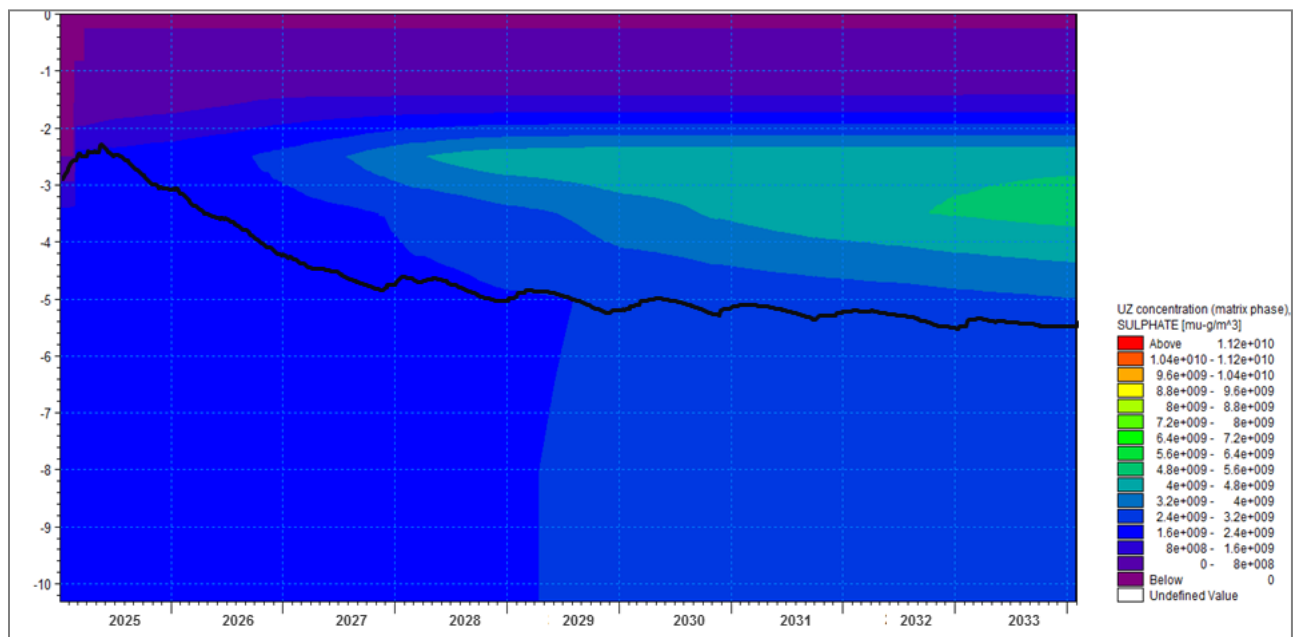


Figure 143: The SO_4 concentrations, below ground (mbgl), for the scenario 5 at point 2.2

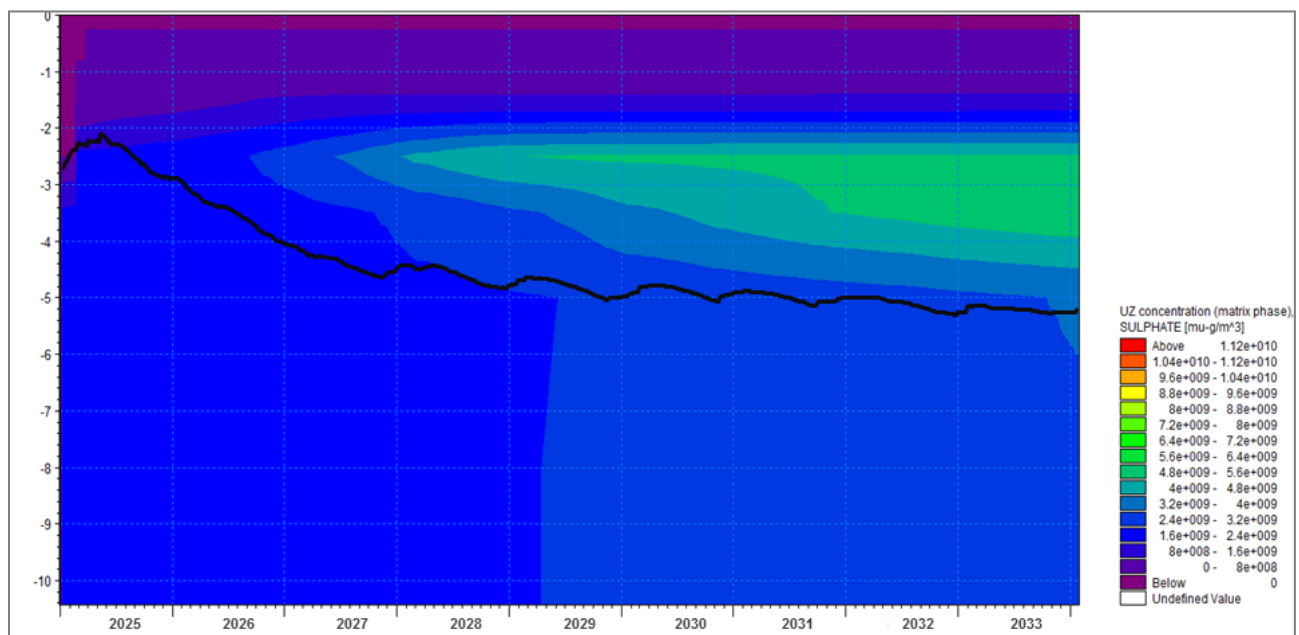


Figure 144: The SO_4 concentrations, below ground (mbgl), for the scenario 6 at point 2.2

5.7.2.3 Transect Point 2.3

Transect point 2.3 lay in the *T. usneoides* planting block, and therefore would not only provide the impacts of planting within this block but also the overall impacts the woodlands would have on the contamination plume emitting from the West Complex TSF.

As previously observed for point 1.3 (Figure 124), the current scenario for point 2.3 was observed to have a high SO₄ concentration band occurring between 1 and 3mbgl. However, for point 2.3 there was a significant decrease in the groundwater level when compared with that of point 1.3.

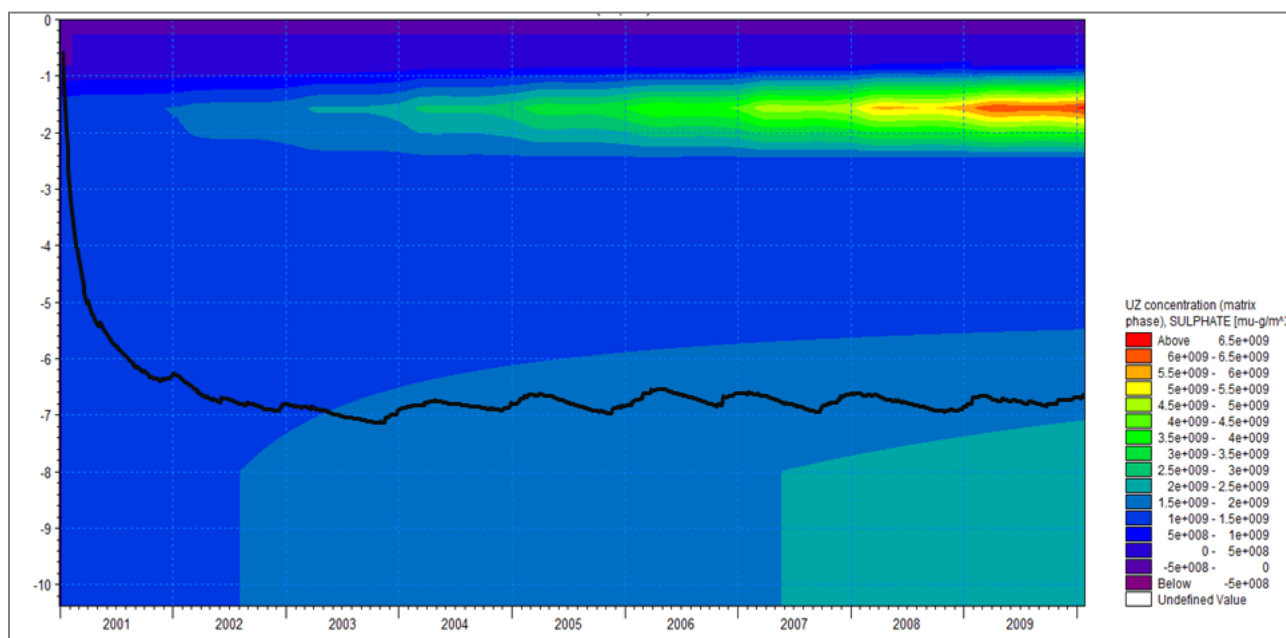


Figure 145: The SO₄ concentrations, below ground (mbgl), for the current scenario at point 2.3

Planting scenario 1 (Figure 146) provided insight into the impacts that planting *T. usneoides*, along the Schoonspruit River, as well as matured *S. lancea* woodlands throughout the remaining planting blocks. The first impact observed was the lowering of the groundwater level. This level decreased from 6.8 to 7.2mbgl. The second impact observed was the significant decrease in the SO₄ concentrations observed between 1 and 3mbgl. The peak SO₄ concentration levels decreased from above 6.5×10^{-8} to 2.5×10^{-8} µg/m³. The SZ for point 2.3 was observed having a slight increase in the SO₄ concentrations for 8mbgl.

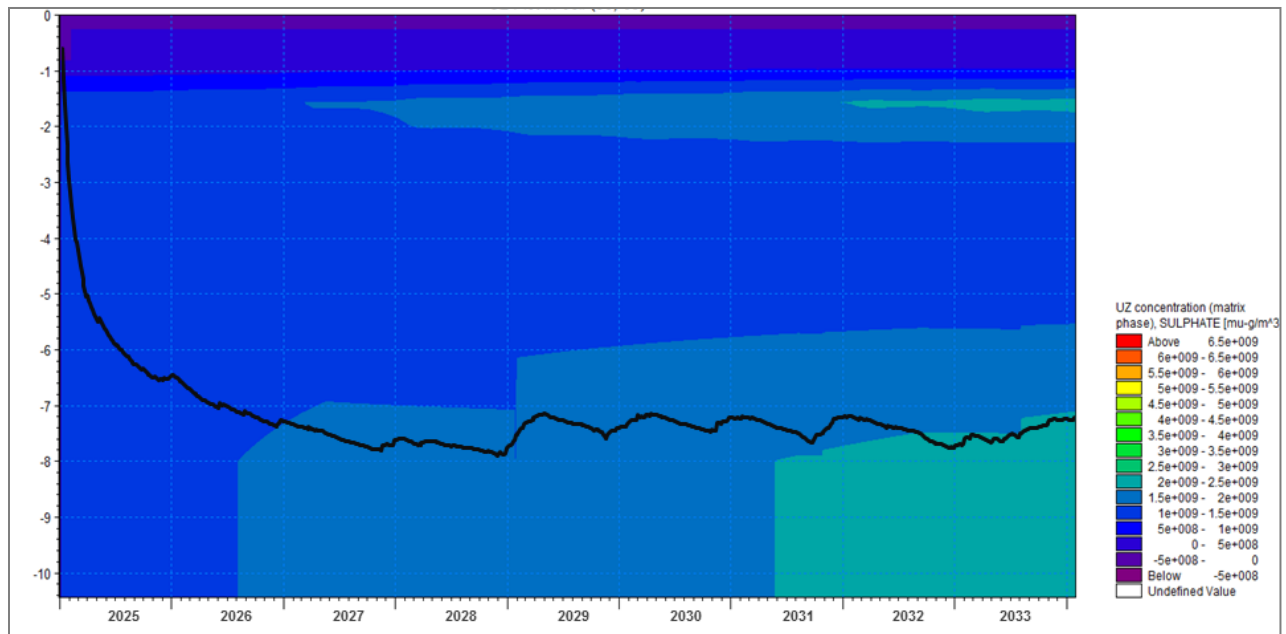


Figure 146: The SO₄ concentrations, below ground (mbgl), for the scenario 1 at point 2.3

Planting scenario 2 (Figure 147) was observed to decrease the peak SO₄ concentrations to similar levels that were observed for scenario 1. However, planting scenario 2 was observed to experience these peaks earlier (2031 instead of 2032) than scenario 1. This could indicate that the *S. lancea* combined with the *T. usneoides* was more effective at decreasing the SO₄ concentrations in the UZ, and delaying the peak of these concentrations.

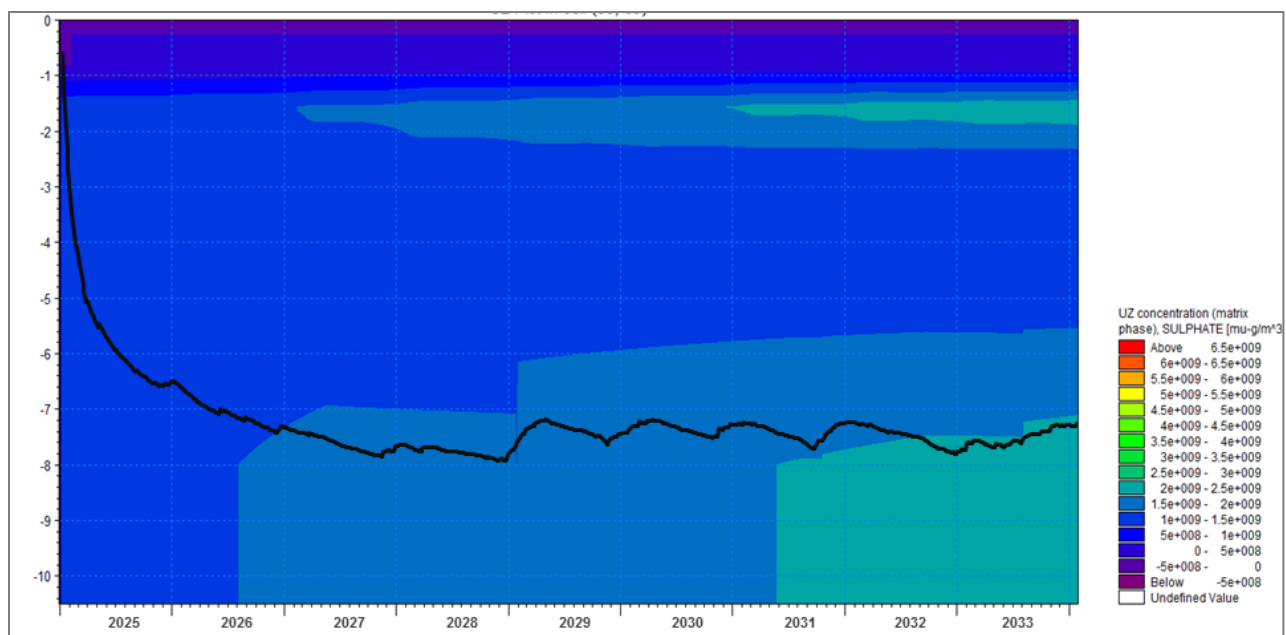


Figure 147: The SO₄ concentrations, below ground (mbgl), for the scenario 2 at point 2.3

An important result found was of how not planting *T. usneoides* would have impacts on the contamination plume, and that these impacts were visible in scenario 3 (Figure 148) and scenario 4 (Figure 149). Scenario 3 was simulated with matured *S. lancea* throughout the planting blocks, with no *T. usneoides* simulated along the Schoonspruit River. The effects of not planting *T. usneoides* resulted in not only a higher groundwater level, but also a significant increase in the SO_4 concentrations within the 1 to 3mbgl band. When *T. usneoides* combined with matured *S. lancea* woodlands were planted along the Schoonspruit River (scenario 1) the peak SO_4 concentration in this band was $2.5 \times 10^{-9} \mu\text{g}/\text{m}^3$. However, when matured *S. lancea* woodlands and no *T. usneoides* were simulated along the Schoonspruit River (scenario 3) the peak concentration in this band increased to $5.5 \times 10^{-9} \mu\text{g}/\text{m}^3$. A similar increase was observed between scenario 4, simulated no *T. usneoides* with matured *E. dunnii* woodlands, and scenario 2, simulated *T. usneoides* with matured *E. dunnii* woodlands. The difference between these two scenarios was $6.5 \times 10^{-9} \mu\text{g}/\text{m}^3$ for scenario 4 and $3 \times 10^{-9} \mu\text{g}/\text{m}^3$ for scenario 2.

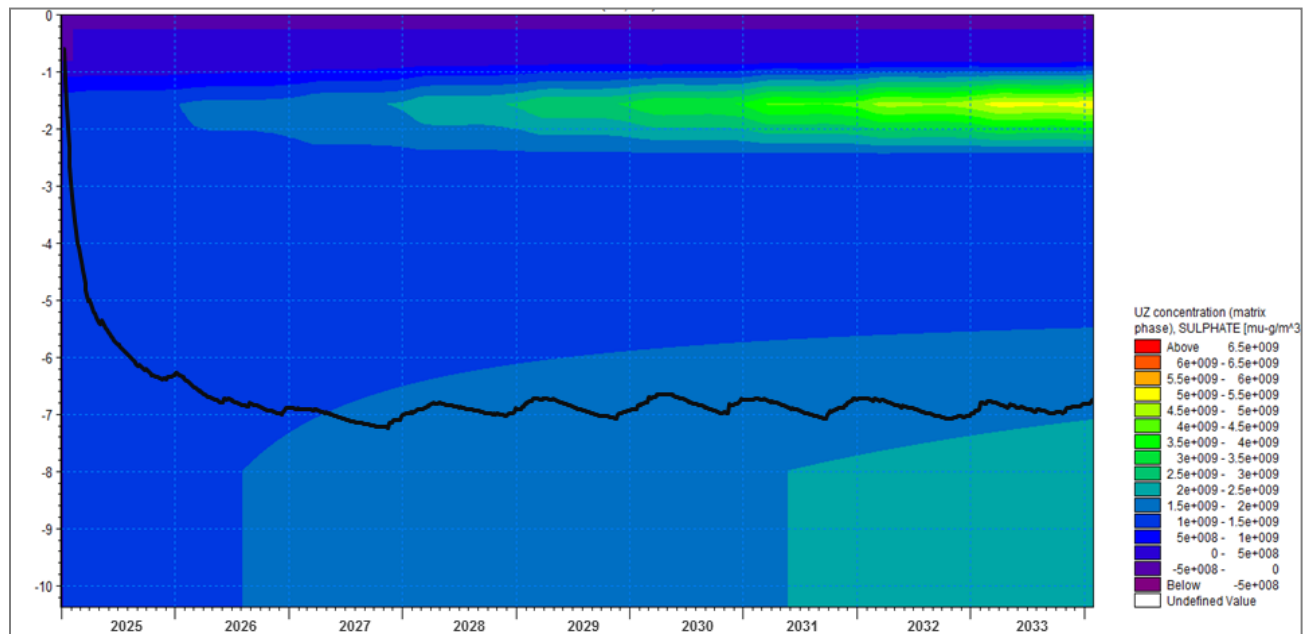


Figure 148: The SO_4 concentrations, below ground (mbgl), for the scenario 3 at point 2.3

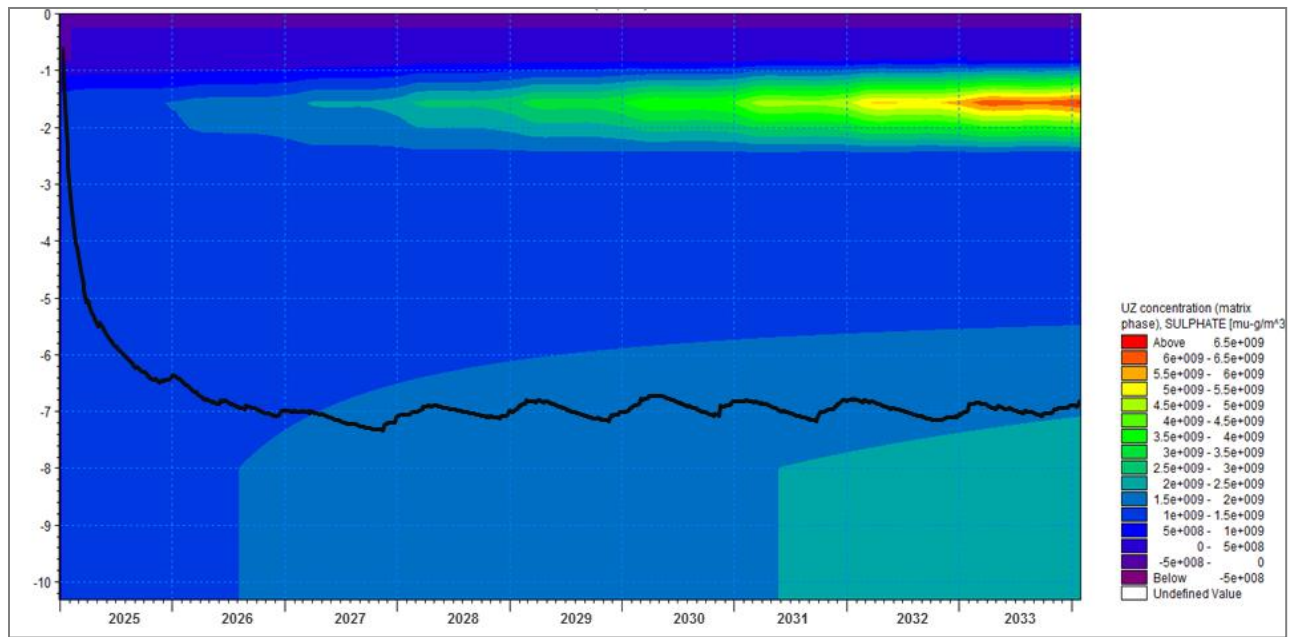


Figure 149: The SO_4 concentrations, below ground (mbgl), for the scenario 4 at point 2.3

The impacts of not planting within the non-AGA owned planting blocks was visible when comparing scenarios 5 (Figure 150) and 6 (Figure 151) when compared to scenarios 1 and 2. The first impact observed between scenarios 5 and 1 was the increase in the SO_4 concentration observed in 1 to 3mbgl band. For scenario 1 the peak SO_4 concentration was $2.5 \times 10^9 \mu\text{g}/\text{m}^3$. However, when the scenario was modelled where there was no matured *S. lancea* woodlands in the non-AGA owned planting blocks this value increased to $4.5 \times 10^9 \mu\text{g}/\text{m}^3$. A similar trend occurred when scenario 6 and scenario 2 were compared. Scenario 2 had a peak SO_4 concentration of $3 \times 10^9 \mu\text{g}/\text{m}^3$ whilst scenario 6 had $4.5 \times 10^9 \mu\text{g}/\text{m}^3$. Again, as observed for scenarios 3 and 4, there was a difference in concentration observed between scenarios 5 and 6, thus indicating the impact that planting *S. lancea* versus *E. dunnii* would have on the contamination plume emitting from the West Complex TSF.

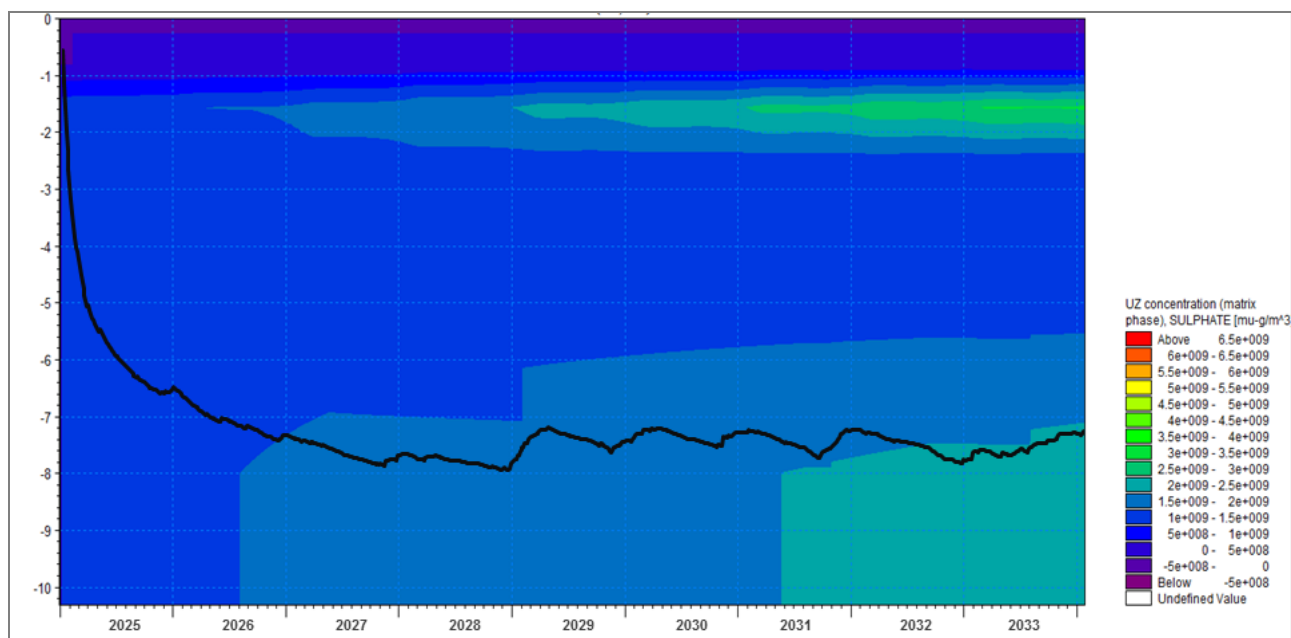


Figure 150: The SO₄ concentrations, below ground (mbgl), for the scenario 5 at point 2.3

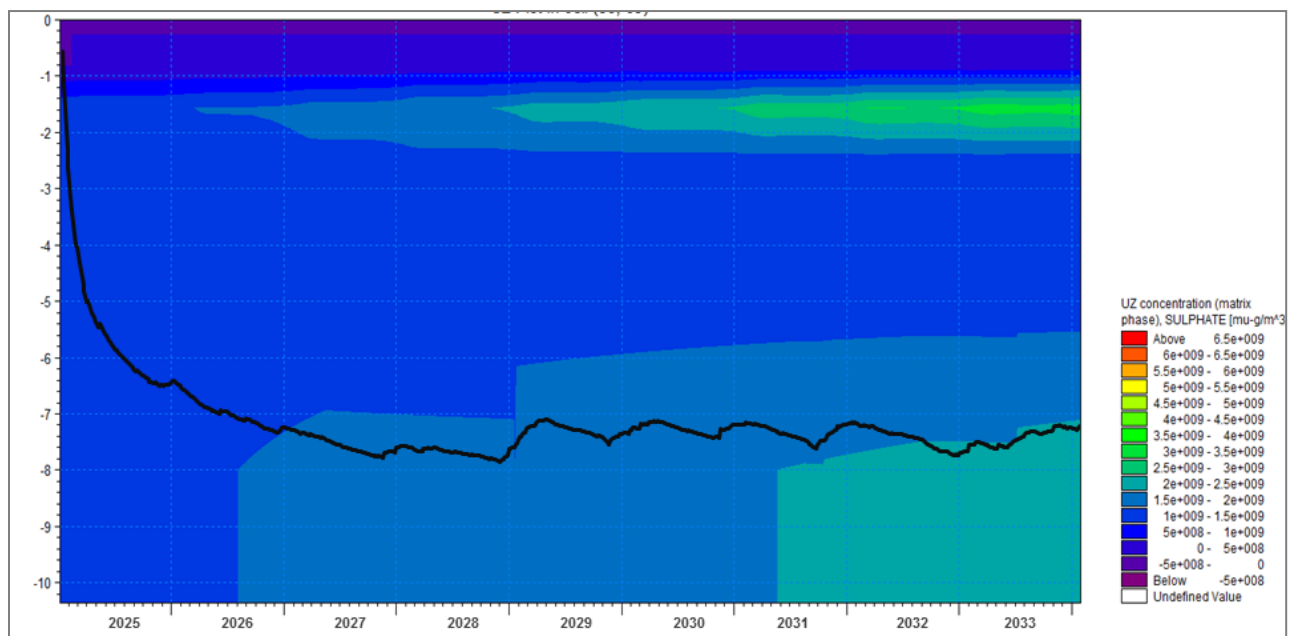


Figure 151: The SO₄ concentrations, below ground (mbgl), for the scenario 6 at point 2.3

5.8 Groundwater Flow Rates

An important aspect to consider in evaluating the effect of changing land use from grasslands to woodlands is the change in the groundwater flow rate. This was analysed for all scenarios at simulation points 3.1 and 3.5 (Figure 45). Simulation points 3.1 and 3.5 were chosen, as these points are close to the Schoonspruit and provide an estimate of groundwater discharge into the river. Positive groundwater flow rate values indicate groundwater flow (m^3/sec) moving from east to west, from the West Complex TSF towards the Schoonspruit River. Negative values indicate groundwater flow (m^3/sec) moving from west to east, from the Schoonspruit River towards the West Complex TSF. For both simulation points, the current scenario and the woodland scenarios were graphed onto the same set of axes to show the change in the groundwater flow rate throughout the simulation period.

5.8.1 Simulation Point 3.1

For simulation point 3.1, the groundwater flow rate increases significantly within the first six months of the simulation period as the water balance stabilizes. From July of the first year through the rest of the simulation period, the groundwater flow rate was simulated to fluctuate between 0.0002 and 0.0001 m^3/sec . A similar grouping of scenarios occurred to those observed for the groundwater level analysis (Figure 152). A first group contained scenarios 3 and 4, a second group contained scenarios 5 and 6 and a third and final group contained scenarios 1 and 2. Group 1 scenarios were those that did not include the planting of *T. usneoides* alongside the Schoonspruit River. This group indicated the lowest degree of change in the groundwater flow rate. The current scenario groundwater flow rate at the end of the simulation was 0.000157 m^3/sec , whilst the final groundwater flow rate for group one's scenarios was 0.000131 m^3/sec . Group one's scenarios followed similar seasonal patterns to those observed for the current scenario.

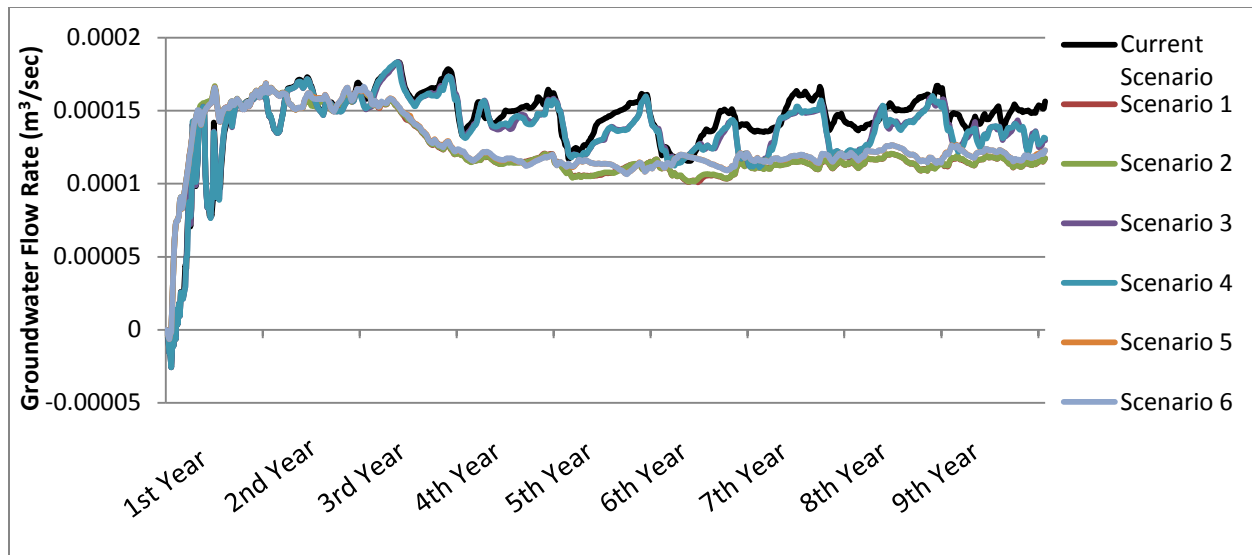


Figure 152: The change in groundwater flow rate (m^3/sec) observed for each scenario across the simulation period for simulation point 3.1

Group two scenarios, which contained the planting scenarios where woodlands were not simulated in the non-AGA owned planting blocks, were observed to decrease the groundwater flow rate even further than that observed for group one scenarios. Group two scenarios were observed to have a final groundwater flow rate of $0.000123\text{m}^3/\text{sec}$. This was a further decrease of $0.000008\text{ m}^3/\text{sec}$ compared with group one's scenarios. This result indicates the impact of planting *T. usneoides* along the river. Group two's scenarios did not exhibit seasonal patterns as observed for the current scenario.

Group three's scenarios, which included woodlands in all planting blocks (including *T. usneoides* along the river), were observed to decrease the groundwater flow rate the most. The final groundwater flow rate observed for group three's scenarios was $0.000117\text{m}^3/\text{sec}$. This was a further decrease of $0.000006\text{m}^3/\text{sec}$ when compared with group two's scenarios. Similarly to group two's scenarios, group three's scenarios did not follow similar seasonal patterns as observed for the current scenario and group one's scenarios. Group two and three's scenarios were observed to decrease the groundwater flow rate the most.

5.8.2 Simulation Point 3.5

As seen at point 3.1, the groundwater flow rate (Figure 153) at point 3.5 showed an initial steep increase as a stable water balance developed. From July in the first year throughout the rest of the simulation period, groundwater flow rate was observed to range between 0.0003 and

0.0002m³/sec. Two scenario groups are seen. The first group contained planting scenarios 1, 2, 5 and 6, whilst the second group contained scenarios 3 and 4.

Planting scenarios 3 and 4 were observed to decrease the groundwater flow rate the least. A final groundwater flow rate of 0.000252m³/sec is seen, whilst the final rate for the current scenario was 0.000274m³/sec. This was a decrease of 0.000022m³/sec. Scenarios 1, 2, 5 and 6 all had a final groundwater flow rate of 0.00024m³/sec, a further 0.000002 m³/sec decrease compared with the scenarios 3 and 4. Thus, flow rates are highest for lowest ET, and lowest for scenarios with highest ET, suggesting that groundwater flow rate decreases as upslope ET increases and groundwater levels decline.

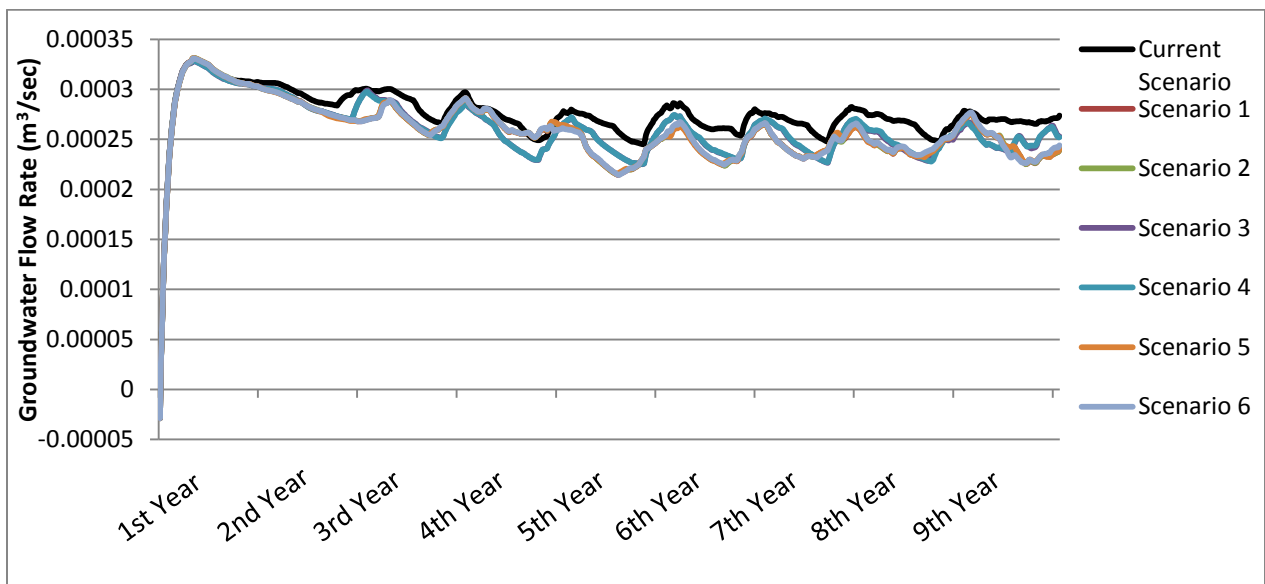


Figure 153: The change in groundwater flow rate (m³/sec) observed for each scenario across the simulation period for simulation point 3.5

Within simulation point 3.5 there was little to no differentiation between scenarios that included the planting of the non-AGA owned planting blocks (scenarios 1 and 2) and those that did not (scenarios 5 and 6). However, at simulation point 3.1 there was a differentiation between the two sets of scenarios. This result could be directly linked to the direction the contamination plume takes after it emerges from the West Complex TSF. The plume moves west and south from the West Complex TSF towards the Schoonspruit River (Figure 154), and therefore, simulation point 3.1 could be less under the influence of the plume than simulation point 3.5.

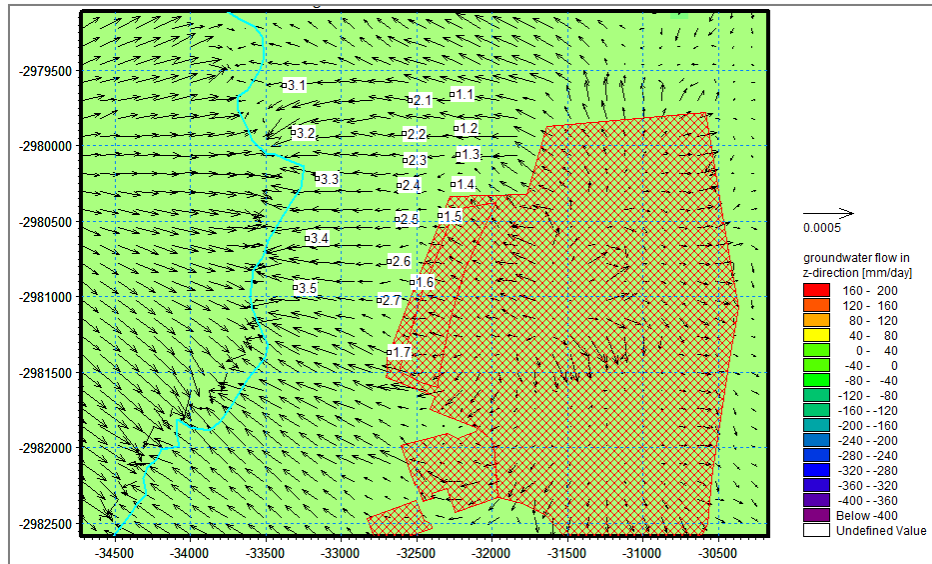


Figure 154: Direction of groundwater flow within the core study site

5.9 Sulphate Mass Flux

The aim of this thesis was to determine the impacts of planting woodlands on the contamination plume moving from the West Complex TSF towards the Schoonspruit River. A good indicator of the impacts of woodlands would be the analysis of the change in mass flux of SO_4 entering the Schoonspruit River. For this section, the mass flux of SO_4 was analysed at 2mbgl for simulation points 3.2 and 3.4, which lies within the groundwater zone (Figure 45). These simulation points were selected for analysis as they were both observed to show decreases in mass flux at the same depth (2mbgl).

5.9.1 Simulation Point 3.2

In the current scenario (black line in Figure 155) there was a significant deviation from the normal range of mass flux of SO_4 within the 5th year of the simulation period. This deviation occurs in a particularly low rainfall period (Figure 9). Within the first year of the simulation, the current scenario and scenario 1 (Figure 155) showed similar patterns and values for the mass flux of SO_4 . This period is considered the model's "stabilizing" period, and therefore little to no difference would be observed in this year. There was a significant decrease in flux of SO_4 simulated for woodland scenarios for the remaining simulation period. Whilst the current scenario showed peaks of $0.001 \text{ g/m}^2/\text{s}$ towards the Schoonspruit River and troughs of $-0.0018 \text{ g/m}^2/\text{s}$ away from the river, scenario 1 had a mass flux range from 1.83×10^{-4} to $-1.0 \times 10^{-4} \text{ g/m}^2/\text{s}$.

A similar decrease in flux was observed for scenario 2 (Figure 156), with rates falling within the range of 1.71×10^{-4} and -7.4×10^{-5} g/m²/s. These decreases for scenarios 1 and 2 were the result of the grasslands of the current scenario being replaced by woodlands in all planting blocks and *T. usneoides* along the Schoonspruit River. By replacing shallow rooted grasslands with deep rooted woody species, the groundwater level decreases, as observed in previous sections. This in turn results in a lowered groundwater flow rate, which subsequently decreases the mass flux of SO₄ entering the Schoonspruit River. This result highlights the impact of woodlands species as a phytostabilization tool.

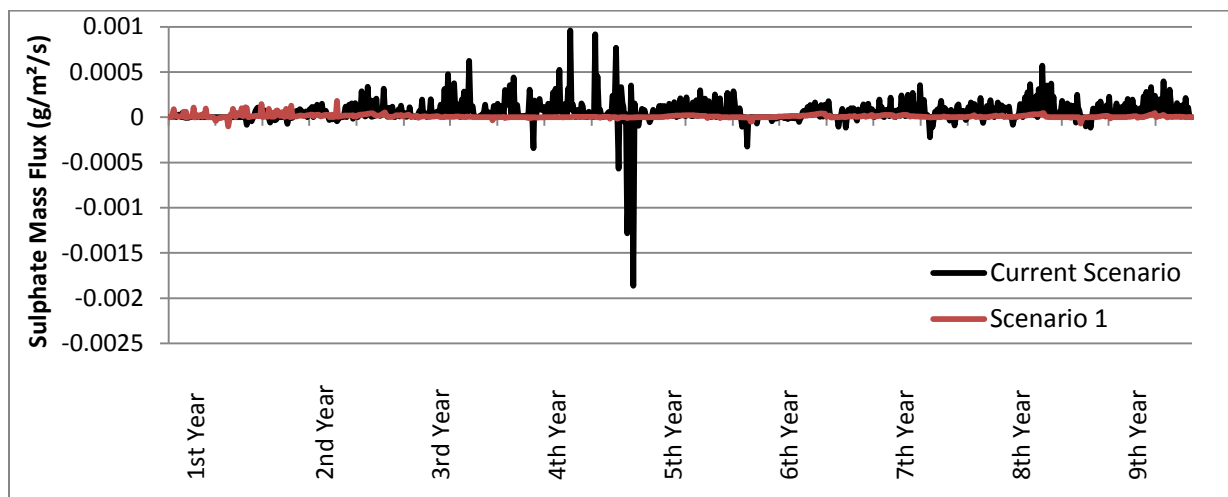


Figure 155: Sulphate mass flux (g/m²/s), for simulation point 3.2, for the current scenario and scenario 1

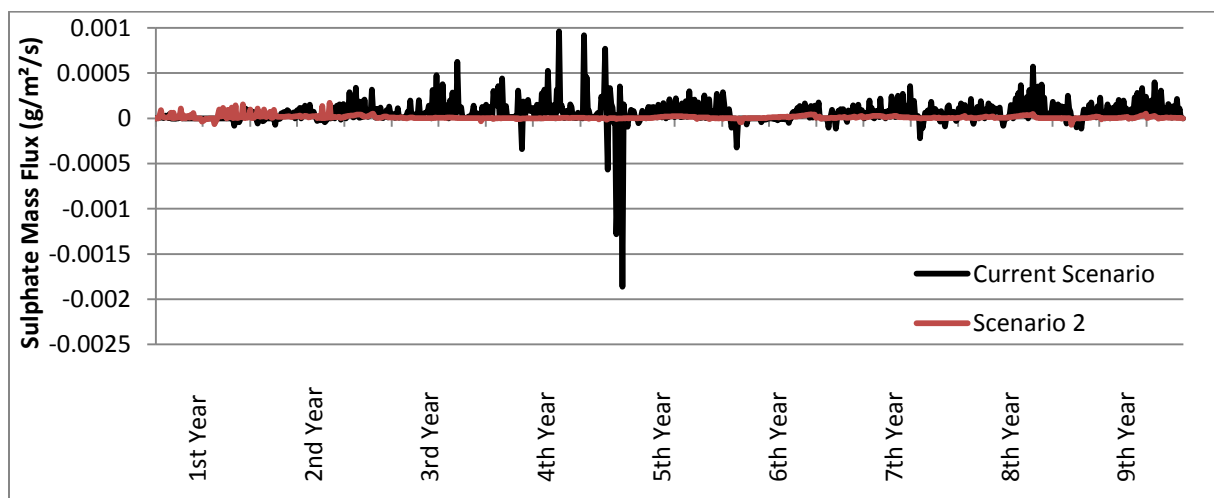


Figure 156: Sulphate mass flux (g/m²/s), for simulation point 3.2, for the current scenario and scenario 2

Planting scenarios 3 (Figure 157) and 4 (Figure 158) showed some decrease in the mass flux of SO₄ entering the Schoonspruit River. However this decrease was not as large as observed for

scenarios 1 and 2. Scenario 3 and 4 showed an average decrease in mass flux of 30.27 and 18.48%, respectively, when compared to the current scenario, whilst scenarios 1 and 2 showed an average decrease of 80.67 and 80.93% respectively. This difference between scenarios 1 and 2 and between scenarios 3 and 4 was the result of scenarios 3 and 4 not including the planting of *T. usneoides* along the Schoonspruit River. This highlights the impacts that planting hyperaccumulators, *T. usneoides*, along the river will have on the contamination plume.

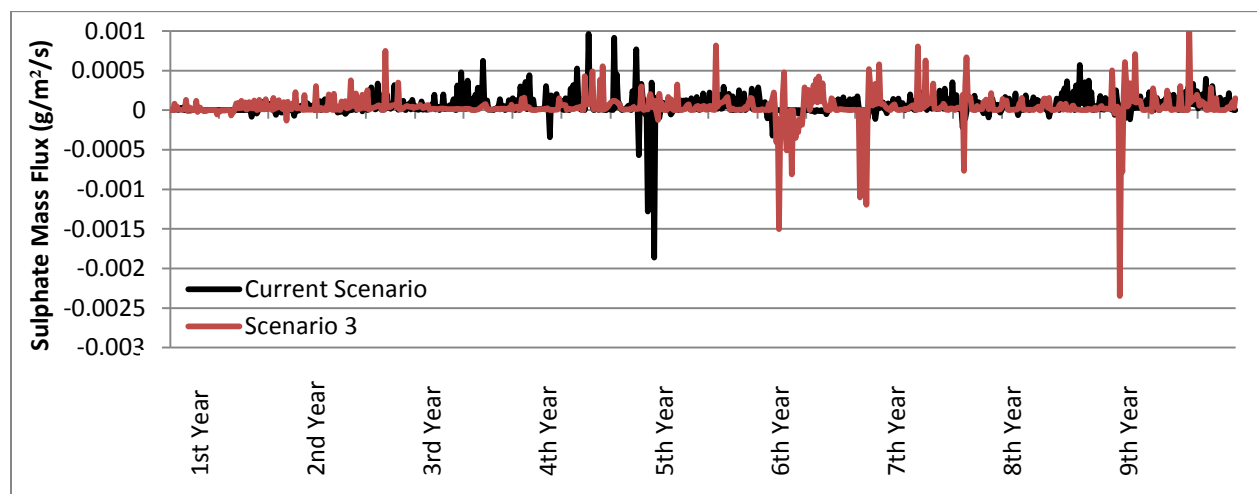


Figure 157: Sulphate mass flux ($\text{g/m}^2/\text{s}$), for simulation point 3.2, for the current scenario and scenario 3

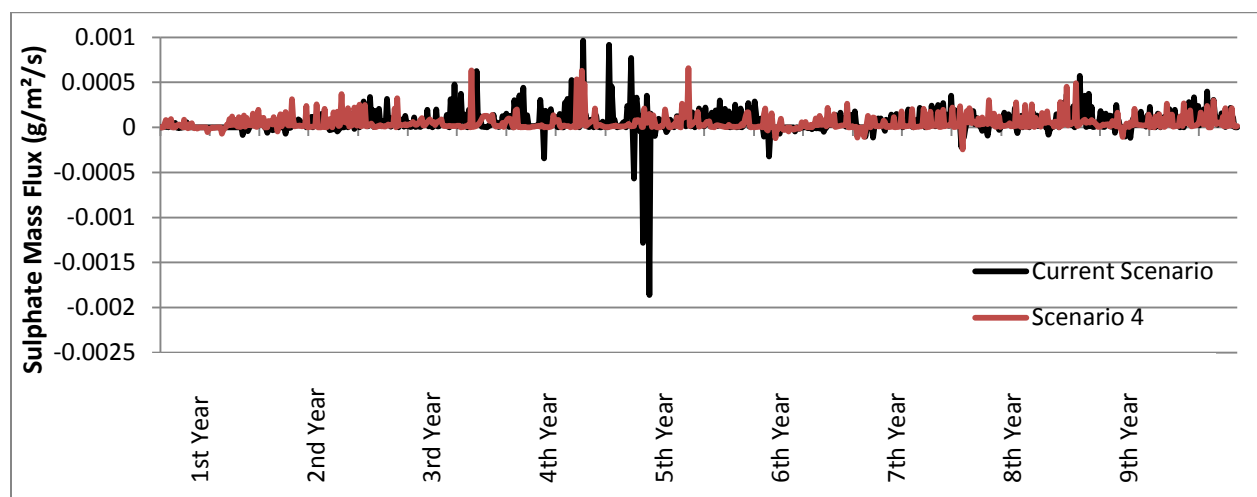


Figure 158: Sulphate mass flux ($\text{g/m}^2/\text{s}$), for simulation point 3.2, for the current scenario and scenario 4

Scenarios 5 (Figure 159) and 6 (Figure 160) showed similar decreases in the mass flux of SO_4 to scenarios 1 and 2. These scenarios both included *T. usneoides* along the Schoonspruit River. The differences in the mass flux of SO_4 between scenarios 1 and 5 (with *S. lancea*), and between 2 and 6 (with *E. dunnii*) reflect the effects of planting or not planting the non-AGA owned blocks.

Planting scenario 5 was observed to be 2.44% less effective than scenario 1, while scenario 6 was 1.41% less effective than scenario 2.

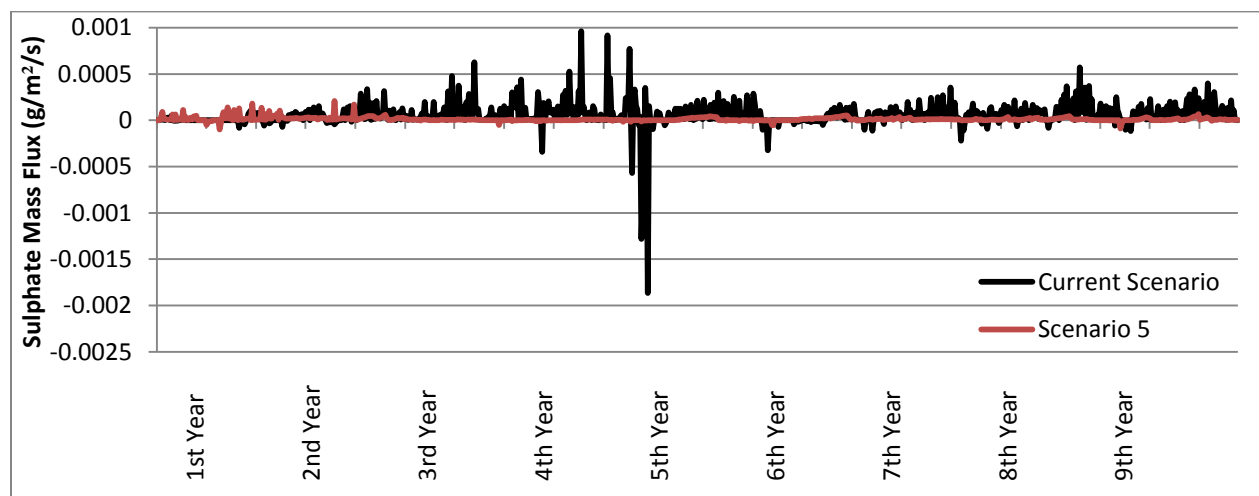


Figure 159: Sulphate mass flux (g/m²/s), for simulation point 3.2, for the current scenario and scenario 5

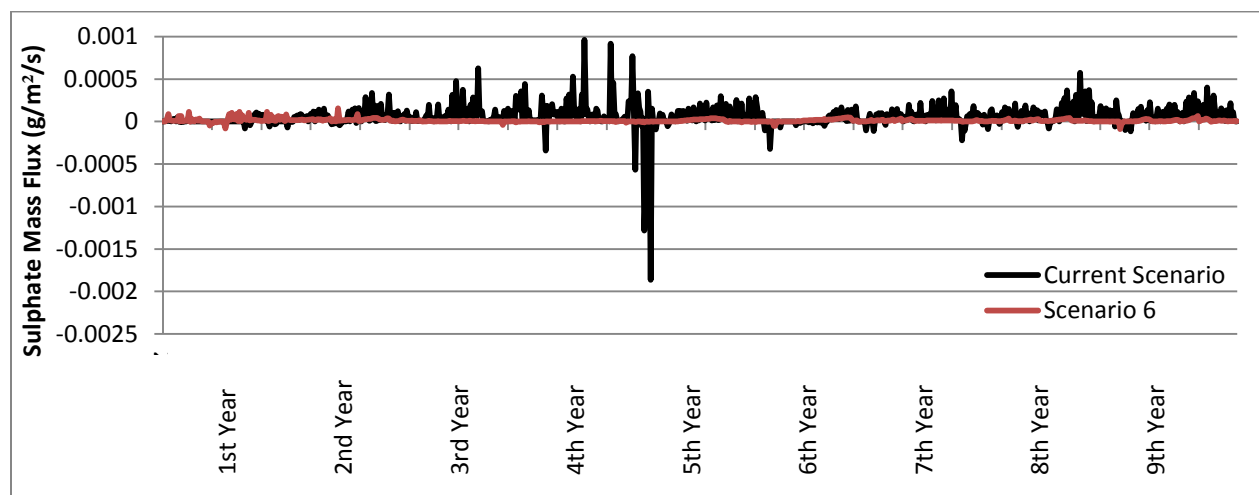


Figure 160: Sulphate mass flux (g/m²/s), for simulation point 3.2, for the current scenario and scenario 6

5.9.2 Simulation Point 3.4

For the current scenario, at simulation point 3.4, a similar deviation in the mass flux of SO₄ observed within the 5th year. This deviation is again linked to the dry spell observed in Figure 9 for the 5th year. Planting scenarios 1 and 2 were simulated with a significant decrease in the mass flux of SO₄ entering the Schoonspruit River. This result highlights the impacts of replacing grasslands with woodlands.

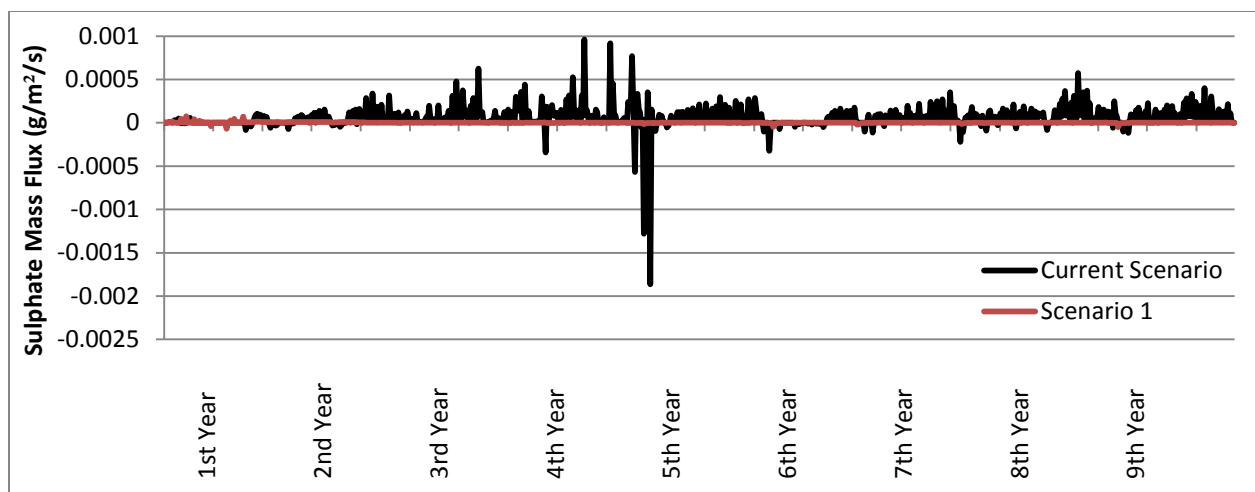


Figure 161: Sulphate mass flux ($\text{g/m}^2/\text{s}$), for simulation point 3.4, for the current scenario and scenario 1

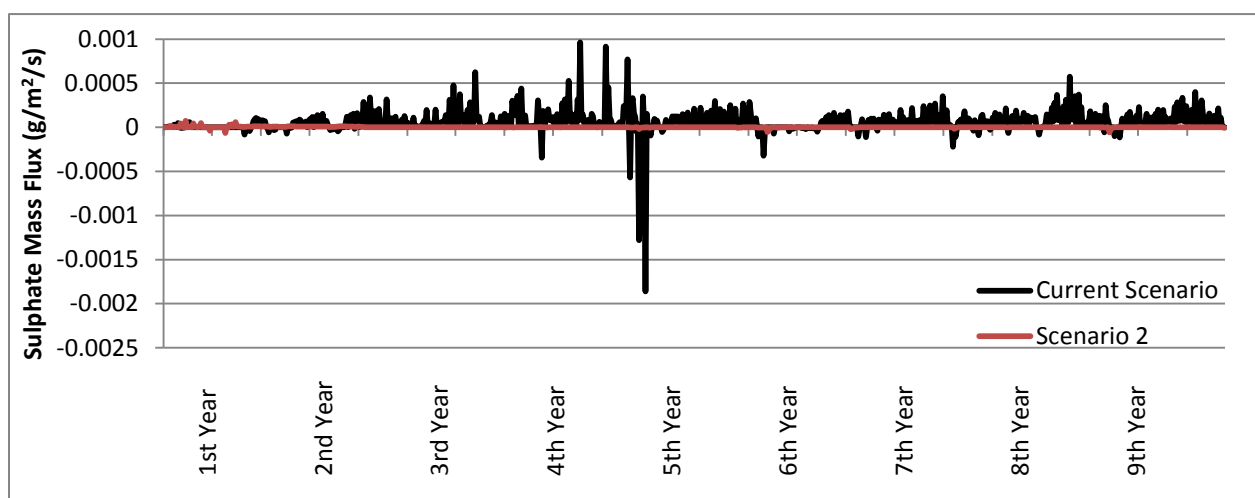


Figure 162: Sulphate mass flux ($\text{g/m}^2/\text{s}$), for simulation point 3.4, for the current scenario and scenario 2

Planting scenarios 3 (Figure 163) and 4 (Figure 164) were poor performers in decreasing the mass flux of SO_4 entering the Schoonspruit River. This result was largely linked to these scenarios not including the planting of hyperaccumulators, *T. usneoides*, along the Schoonspruit River. For these scenarios, decreases in the mass flux of SO_4 were observed, however there were increases in flux observed as well. Scenarios 3 and 4 resulted in an average increase in flux observed for this point. Scenario 3 was observed with a 14.63% increase, on average, while scenario 4 was observed with a 20.65% increase. This result highlights the impacts of the *T. usneoides* on controlling the SO_4 entering the Schoonspruit River and of *T. usneoides* as a phytostabilization and phytoextraction tool.

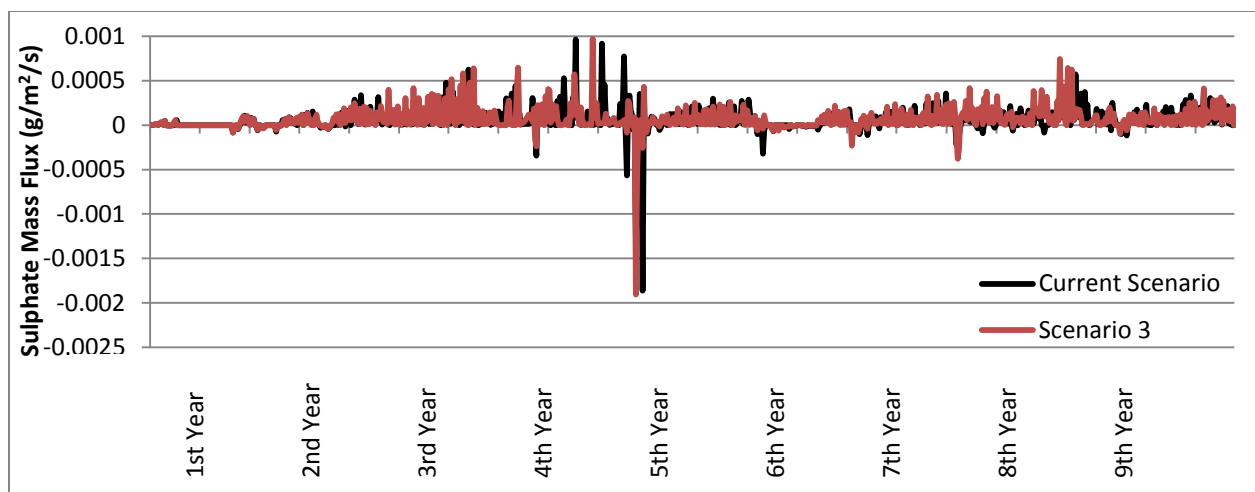


Figure 163: Sulphate mass flux ($\text{g/m}^2/\text{s}$), for simulation point 3.4, for the current scenario and scenario 3

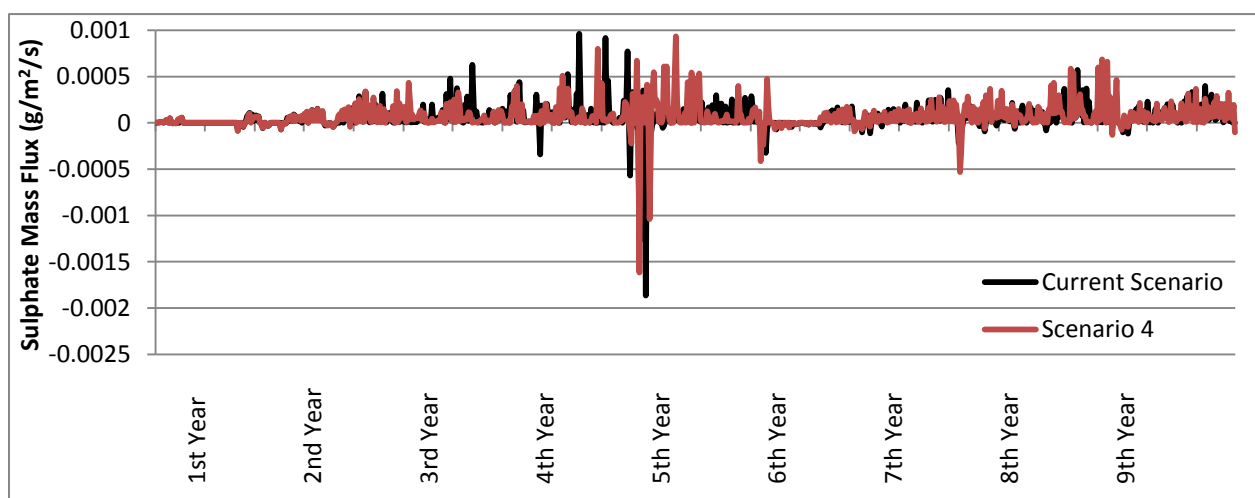


Figure 164: Sulphate mass flux ($\text{g/m}^2/\text{s}$), for simulation point 3.4, for the current scenario and scenario 4

Planting scenarios 5 and 6 were similar in performance to scenarios 1 and 2, where they significantly decreased the flux of SO_4 entering the Schoonspruit River. Scenarios 5 and 6 were 2.44 and 1.41% more effective at decreasing the flux of SO_4 entering the Schoonspruit River than scenarios 1 and 2. This result was not expected, as this point is located further away from the non-AGA owned planting blocks (Figure 154), and therefore should not be affected by whether these blocks are planted or not. This result could be linked to the *ET uptake factor* that was not able to be defined spatially. The impact of riparian woodlands on mass flux of SO_4 is clearly significant and is likely to be more so if *T. usneoides* uptake can be adequately simulated. Currently there is only one uptake rate for all species.

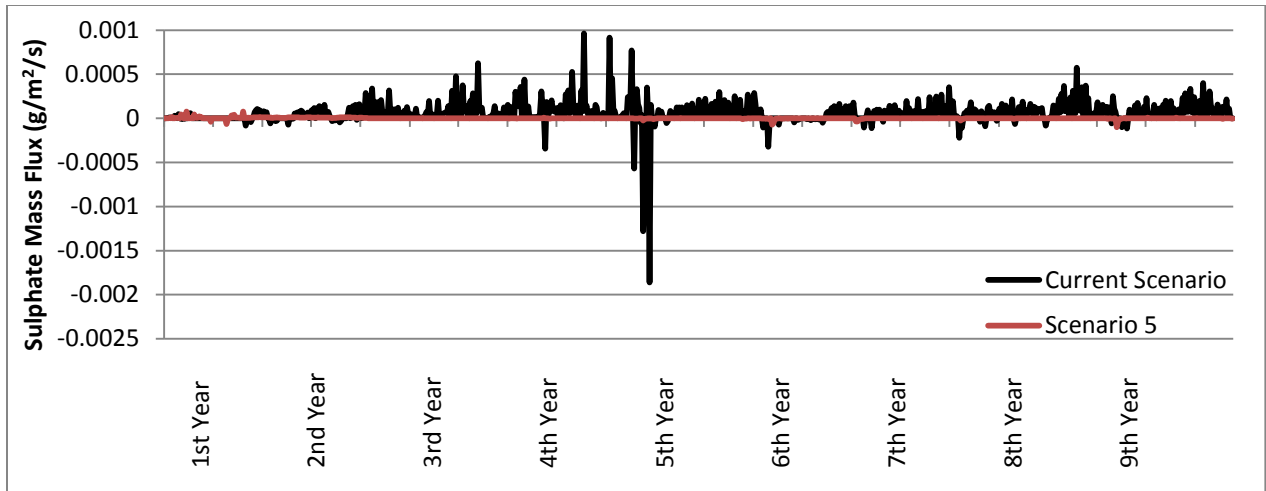


Figure 165: Sulphate mass flux (g/m²/s), for simulation point 3.4, for the current scenario and scenario 5

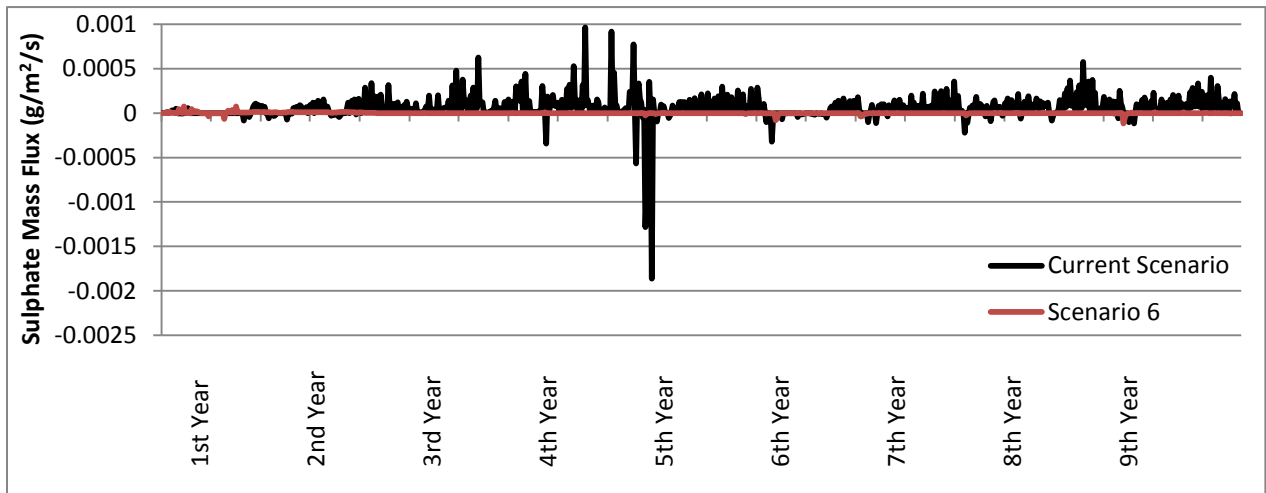


Figure 166: Sulphate mass flux (g/m²/s), for simulation point 3.4, for the current scenario and scenario 6

6 Discussions and Conclusions

This dissertation aimed to assess the likely future impacts of phytoremediation woodlands on the storage, transport and discharge of mine water and contaminants over a typical contamination plume originating on the western side of the West Complex TSF within the Vaal River mine lease area. Previous modelling studies in the area have focused on groundwater, and only incorporated surface and unsaturated zone processes in a superficial way. This dissertation aimed to provide a more holistic assessment based on all hydrological processes, to assess the impacts the trees will have on the groundwater flow and contaminant movement to the Schoonspruit River. More detailed information is now available, on the characteristics of tree species found to have potential for phytoremediation, allowing various planting scenarios to be more fully investigated. The hydrological model MIKE SHE was chosen to undertake the integration of a wide range of information from the study site. In addition to simulating all significant hydrological processes in a computationally efficient way, MIKE SHE has a proven record for simulating at large catchment scale, allowing for future woodland impacts to be quantified at district and regional scales. This was not within the scope of this study but can be undertaken in future studies. Some important findings have emerged from this dissertation and these are described below.

6.1 Tree Root Access to Groundwater

A great deal of effort was put into a search for an affordable means of drilling boreholes for tracer release into the groundwater. Two hydraulically powered auger drills were used in the field with limited success. Problems encountered included rocks in the profile that could not be penetrated, and a high level of resistance to the turning bit which eventually stopped rotating. Only one borehole was successful in reaching the water table. The conclusion drawn was that hydraulic auguring cannot reliably penetrate to the water table, even in relatively rock-free subsoil derived from Ventersdorp lavas. The tracer Rhodamine B was added to the ground water at the one successful borehole. Subsequent analysis of leaves collected before and after tracer release showed that the tracer was taken up by the nearby *S. lancea* tree, demonstrating that the roots were absorbing groundwater, and that this tracer technique can be used to determine if trees

are in contact with the groundwater. However, the difficulty and high cost of drilling boreholes at the site severely restricts the practical use of this technique.

An alternative approach to this problem was to measure pre-dawn xylem pressure potentials in a sample of mature trees growing on the study site. Despite over six months of no rain and extremely dry soil conditions, none of the trees showed high balancing pressure potentials, strongly suggesting that they were accessing groundwater to maintain their physiological functioning during this driest time of year. This technique was found to be effective in time, costs and ease of use, while it does still need to be used on a wider scale to provide more information on tree access to groundwater plumes.

6.2 Overland Flow and Soil Infiltration

An important process to describe accurately is the partition of rainfall between overland flow and soil infiltration. Double-ring infiltration measurements were performed on two soil types for which no previous measurements could be found. These values were inputted into MIKE SHE prior to the simulation runs. Runoff outputs suggest that these can be too high during certain rainfall events, and that further work is needed to match simulated overland flow to field measurements.

6.3 Hydraulic Conductivity Calibration

The hydraulic conductivity input is an important input variable within MIKE SHE as this value determines the amount of water that infiltrates versus the amount that will form surface run off. The majority of these values were taken from reports of previous modelling research conducted for the study site, and values for any missing data were calculated from the double ring infiltrometer tests. The data taken from the previous research was calibrated values for the FEFLOW model, not the MIKE SHE model. The use of this data combined with field work results introduced a level of error within the model, specifically affecting the groundwater levels simulated. In attempting to overcome this error, the model was calibrated by tweaking the hydraulic conductivity values and comparing the simulated outputs. This was a long a tedious process, as a large portion of the simulation needed to be run to determine the effects, taking roughly 30 minutes, for every tweak that was made. The major change in hydraulic conductivity was regarding the alluvial soils. Here the value was increased by $7.95 \times 10^{-6} \text{m/s}$. This difference in

value between measured and calibrated could be a direct result of the size of the inner ring of the double ring infiltrometer test. Lai and Ren (2007) found that the variability in measured hydraulic conductivity was larger for inner rings with a diameter of less than 40cm than tests that were conducted with inner rings of greater than 80cm diameter. Research conducted by Cook (2012) suggests that MIKE SHE is sensitive to hydraulic conductivity and therefore it is recommended that further work needs to be conducted in completing the double ring infiltrometer tests, with 40 and 80cm, for all soil types and soil depths to determine the impact ring size has on the accuracy of the simulated groundwater level.

6.4 Evapotranspiration and Groundwater Uptake by Trees

Evapotranspiration from woodland species showed a declining trend over the future scenario simulations that appeared to track declining groundwater levels. Later ET rates showed relatively low and unrealistic rates. This problem is attributed in part to the way MIKE SHE distributes root mass in the soil. It assumes an exponentially declining root mass in which most of the soil water abstraction takes place in the upper soil horizons. This is typical for many crops and grasslands, but many exceptions are documented in the literature for trees in arid zones where they have adapted to obtain water from deeper levels where reliability of supply is greater. Furthermore, it has been shown in several cases that tree roots proliferate where there is water, to increase supply to the tree. An example of this was shown by Kimber (1974) for *Eucalyptus marginata* in Western Australia (Figure 167). Certain tree models like WAVES build in this ability of trees to grow out roots into moist layers in deep profiles (Dawes and Short, 1993). The design of MIKE SHE therefore severely limits water uptake in deep soils/subsoils, and this needs to be addressed in order to simulate tree water use under these conditions.

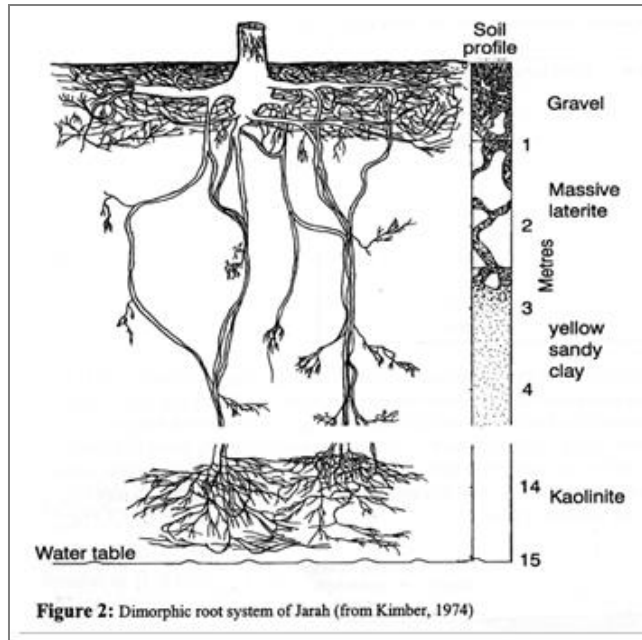


Figure 167: Diagram of the true nature of deep rooted trees (*E. marginata*) rooting system

6.5 Changes in Water Table Levels

Much attention has been given to highlighting differences in water table levels across the study site for the various planting scenarios. This was to emphasize the variability caused by microtopography, slope position, proximity to the plume source, geometry of the tailings dam, spatial variability in the woodland establishment and species planted. These influences will affect the performance of the different species, and so it is important to understand the likely future changes in order to match species to sites. One example can be given to illustrate this. At certain simulation points situated close to the TSF, water levels are relatively high and their decline under trees was simulated to be relatively small. Such sites may be suited to *T. usneoides*, which is normally associated with riparian footslope sites. Sulphate uptake by this hyperaccumulator species may be influential in reducing the contaminant load reaching the Schoonspruit River. It is recommended that further research is undertaken for the analysis of the relative mass balance between the water uptake, retention and load to the river.

6.6 Changes in Sulphate Concentrations in the UZ and SZ

There was much uncertainty in deciding initial values to the SO_4 content of the deeper UZ, since data was scarce. Therefore the SO_4 from the upper UZ was used for the whole UZ horizon within MIKE SHE, allowing the software to calculate the SZ concentrations with the built-in equations.

This was a reasonable assumption for the UZ just above the water table, but higher up-slope, episodes of high water table will be scarce, allowing SO_4 to move in response to water fluxes. Simulated changes in SO_4 content appear mainly to reflect declining water contents brought about by the trees.

6.7 Sulphate Uptake by Trees

A critical weakness of MIKE SHE for this kind of study is that one cannot simulate different contaminant uptake rates by different tree species. Only one fixed rate can be used for all the vegetation. This is a major limitation in this study since there are very large differences in contaminant uptake among the tree species. *T. usneoides* in particular is a hyperaccumulator of salts which is able to take up very large quantities of sulphates. A species-specific uptake rate needs to be coded into MIKE SHE to simulate this kind of situation, as this could have made a difference in the final sulphate reaching the stream.

6.8 Groundwater Flow Rate and Sulphate Mass Flux

The simulated change in the groundwater flow rate and sulphate mass flux was further evidence of the impacts of woodlands on the contamination plume. The decrease in groundwater flow rates was the result of greater ET and subsequently a lower groundwater level. The results observed from the planting scenarios were similar to those observed for modelling of Poplar trees by Quinn *et al.* (2001). The decrease in groundwater flow rate observed by Quinn *et al.* (2001) was linked to an increase in ET and resulted in a large containment of groundwater from upslope sources. However, the decline in trend observed for the groundwater flow rate was not observed. This highlights the limitations of the MIKE SHE rooting depth algorithms.

The mass flux of SO_4 results highlighted the importance of planting *T. usneoides* along the Schoonspruit River to decrease the contaminants entering the river. However, these results should be considered with caution due to the serious limitations of MIKE SHE's ET uptake factor.

6.9 Run Times and Grid Cell Sizes

Very long run times exceeding 400 hours were encountered earlier on, due to the need for multi-year simulations to take the variable rainfall regime into account, and the choice of a relatively small 30 by 30m cell size. Such long run times were impractical considering the need to

sequentially run the model many times to explore the effects of varying parameter values. Shorter run times were achieved by selecting fewer, larger cells (120 by 120 m) to reduce the number of calculations. When a faster more powerful computer becomes available, it would be better to revert to smaller cell sizes for greater spatial resolution and enhanced realism (Vazquez *et al.*, 2002) and explore other means of shortening run times. Another strategy would be to use the option in MIKE SHE of grouping cells that function similarly, and copying changes calculated in one representative cell to the others, thus reducing calculation times. It is recommended for further research that the model is run at a 30x30m resolution on a more powerful computer to determine the loss of accuracy that was incurred due to the change in the grid cell resolution, from 30x30m to 120x120m resolution.

6.10 Future Simulation Improvements

The following steps are recommended to improve the model accuracy:

1. Explore how the problem of root proliferation in capillary zones can be simulated.
2. Approach DHI about the possibility of modifying MIKE SHE code to allow users to specify contaminant uptake rates for different tree species.
3. After ensuring that tree water use and contaminant uptake is realistically simulated, conduct a more detailed calibration exercise using a parameter estimation programme such as PEST. This should be undertaken in conjunction with geohydrologists and other appropriate specialists to obtain consensus on the realism of the simulation.
4. Measurements of flow rates using Passive flux meters (PFMs) installed in existing boreholes in the area would add some valuable field data to incorporate into the validation exercise.

6.11 Recommendation for further research

A potentially useful device for measuring slow lateral groundwater flows was discovered in the literature. Passive flux meters are described at www.enviroflux.com/pfm.htm and are suitable for single-borehole deployment. They can be manufactured to fit any size of borehole. The flow of water past a packed collar of activated carbon saturated with five different alcohol tracers is highly correlated to the amount of tracer removed from the column. Analysis of the tracer concentrations before and after deployment can therefore be used to estimate the total flow of

groundwater past the sampler. Such groundwater flow measurements will be invaluable in calibrating the model.

Another recommendation for further research would be to run the model at a 30x30m resolution on a more powerful computer to determine the loss of accuracy that was incurred due to the change in the grid cell resolution, from 30x30m to 120x120m resolution.

The final recommendation for future work would be to determine the chemical effects of woodlands on subsurface SO_4 and how the redox is changed, as well as determining the effects of decaying organic matter and soil nutrient build-up on the SO_4 .

6.12 Conclusion

This dissertation was successful in determining that mature *S. lancea* woodland plantings are effective in reducing water table levels and slowing lateral groundwater movement. This dissertation was also successful in determining that the use of *T. usneoides* alongside the river was effective in reducing the quantity of contaminants reaching the Schoonspruit River.

There are, however, two major deficiencies in MIKE SHE relating to the uptake of water and contaminants by trees, which must be overcome before reliable quantitative estimates of woodland impacts can be obtained. A thorough calibration and parameter estimation then needs to take place, together with AGA and consultant groundwater experts, to arrive at an assessment that is judged by all to be realistic.

The first objective of this dissertation was the gathering of relevant datasets from various sources to set up MIKE SHE for the study area. A large number of reports, papers and maps were found to contain useful information, which was used to set up the current and planting scenario simulations. Where data was not available, the relevant individuals, companies and departments were approached, or fieldwork was undertaken. An example of this was the Schoonspruit River flow rate data that was obtained from DWAF, for both upstream and downstream points.

The second objective was to estimate the groundwater flow across the study area. This proved impossible given the difficulties of drilling boreholes at affordable cost. Rock-boring machinery is required to drill through rocky profiles, and quotations from various drilling companies showed this to be prohibitively costly. Motorized auguring proved to be much less costly but was found to be impractical where rocks are present in the profile.

Estimating the depth at which tree roots can take up groundwater was the third objective for this dissertation and was determined at one site where a successful new borehole was used to introduce a Rhodamine B tracer into the groundwater. Supplementary data was gathered at other sites where pre-dawn xylem pressure potential readings indicated favourable water potentials after six months of no rain. This dissertation provides a realistic view of the problems of drilling boreholes on Highveld mining sites and also an alternative plant-based technique for determining whether trees can access groundwater.

The fourth and fifth objectives were to simulate water and contaminant movement in the current pre-woodland scenario and future mature woodland scenario. These objectives were accomplished, illustrating the likely changes in water balance and contaminant transport after establishing woodlands. Both the current pre-woodland scenario and the future mature woodland scenarios (1-6) showed, to varying degrees, an increase in contaminant uptake by the trees of the mine woodlands project and a decrease in ground water levels, further emphasizing the effectiveness of phytoremediation on Acid Mine Drainage in old goldmine Tailing Storage Facilities.

7

References

- Akcil, A. and Koldas, S., 2006, Acid Mine Drainage (AMD): causes, treatment and case studies, *Journal of Cleaner Production*, 14, 1139 – 1145.
- Alder, R.A., Claasen, M., Godfrey, L. and Turton, A.R., 2007, Water, mining, and waste: an historical and economic perspective on conflict management in South Africa, *The Economics of Peace and Security Journal*, 2 (2), 33 – 42.
- Ali, H., Khan, E., Sajad, M.A., 2013, Phytoremediation of heavy metals – Concepts and applications, *Chemosphere*, 91, 869 – 881.
- Alyamani, M.S. and Sen, Z., 1993, Determination of hydraulic conductivity from complete grain-size distribution curves, *Groundwater*, Vol. 31(4), 551 – 555.
- Allen R, Pereira L., Raes D., Smith M., 1998, Crop evapotranspiration: guidelines for computing crop water requirements, FAO Irrigation and Drainage Paper No. 56. Rome, Italy: FAO.
- AngloGold Ashanti, 2003, *AngloGold Vaal River and West Wits Operations – Development of monitoring boreholes for the Wits AngloGold Woodlands Project*, AGES – Africa Geo-Environmental Services, Pretoria, Technical Report: AS/R/04/09/14.
- AngloGold Ashanti, 2004, Environment; 04 Report to Society, www.anglogold.co.za/subwebs/informationforinvestors/reporttosociety04/values_business_principles/environment/e_cs_sa_7_11.htm (5 December 2013)
- AngloGold Ashanti, 2005, *AngloGold Ashanti Vaal River and West wits operations – Geotechnical assessment for the Woodlands Project*, AGES – Africa Geo-Environmental Services, Pretoria, Technical Report: AS/R/05/04/21.
- AngloGold Ashanti, 2009, *Meteorological Information to be used in the Vaal River and West Wits mining area Stormwater Masterplan*, Aurecon, Pretoria.

- AngloGold Ashanti, 2011a, *Update of the Sulphate Groundwater Plume Delineation for the AngloGold Ashanti Vaal River and West Wits Operations*, GCS, Derby Downs Office Park, Westville, GCS Project number: 09-539.
- AngloGold Ashanti, 2011b, *Strategic Plan for the lining of Trenches at the Vaal River and West Wits Operations*, Environmental Management Department; Water and Air Quality Management Section, Project Reference: SAD0130/EMD/WAT/PPrev/2010.
- Baker, A.J.M., McGarth, S.P., Sidoli, C.M.D. and Reeves, R.D., 1994, The possibility of in situ heavy metal decontamination of polluted soils using crops of metal-accumulating plants, *Resources Conservation Recycling*, 11, 41 – 49.
- Barcelo, J. and Poschenrieder, C., 2003, Phytoremediation: principles and perspectives, *Contributions to Science*, 2(3), 333 – 344.
- Batista, M.J., Abreu, M.M. and Tavares, M.T., 2007, Potential use of *Erica andevalensis* and *Erica australis* in phytoremediation of sulphide mine environments: Sao Domingos, Portugal, *Journal of Geochemical Exploration*, 96, 210 – 222.
- Blaylock, M.J., Salt, D.E., Dushenkov, S., Zakharova, O., Gussman, C., Kapulnik, Y., Ensley, B.D. and Raskin, I., 1997, Enhanced accumulation of Pb in Indian Mustard by Soil Applied Chelating Agents, *Environmental Science and Technology*, 31, 860 – 865.
- Boyer, J.S., 1995, *Measuring the Water Status of Plants and Soils*. Academic Press, San Diego.
- Brooks, R.R., Robinson, B.H., Howes, A.W. and Chiarucci, A., 2001, An evaluation of *Berkheya coddii* Roessler and *Alyssum bertolonii* Desv. for phytoremediation and phytomining of nickel, *South African Journal of Science*, 67, 558 – 560.
- Burken, J.G., and Schnoor, J.L., 1997, Uptake and Fate of organic Contaminants by Hybrid Poplar trees, *Proceedings, 213th ACS National Meeting, American Chemical Society Environmental Division Symposia*, San Francisco, Paper 106, 302 – 304.
- Canadell, J., Jackson, R.B., Ehleringer, J.R., Mooney, H.A., Sala, O.E. and Schulze, E.D., 1996, Maximum rooting depth of vegetation types at the global scale, *Oecologia*, 180, 583 – 595.

- Chen, J.M., Rich, P.M., Gower, S.T., Norman, J.M., Plummer, S., 1997, Leaf Area Index of boreal forests; Theory, techniques, and measurements, *Journal of Geophysical Research*, 102, 29429 – 29443.
- Chorley, R.J., 1971, *Introduction to Fluvial Processes*, University Paperback, London.
- Cipollini, M.L., and Pickering, J.L., 1986, Determination of the Phytotoxicity of Barium in Leach-field Disposal of Gas Well Brines, *Plant and Soil*, 92, 159 – 169.
- Cleary, B. and Zaerr, J., 1984, Guidelines for measuring plant moisture stress with a pressure chamber, Corvallis, OR: PMS Instrument Co, 17p.
- Cook, A., 2012, Development of an Integrated surface and subsurface Model of the Everglades National Park, FIU Electronic Thesis and Dissertations, Paper 634.
- Cui, Y.J. and Zornberg, J.G., 2008, Water Balance and Evapotranspiration Monitoring, *Geotechnical and Geoenvironmental Engineering*, 26, 783 – 798.
- Cunningham, S.D. and Ow, D.W., 1996, Promises and Prospects of Phytoremediation, *Plant Physiology*, 110, 715 – 719.
- Dawes, W.R. and Short, D.L. 1993, The efficient numerical solution of differential equations for coupled water and solute dynamics: the WAVES model, CSIRO Division of Water Resources Technical Memorandum 93/18, Canberra, ACT, Australia.
- Demetriou, C. and Punthakey, J.F., 1999, Evaluating sustainable groundwater management options using the MIKE SHE integrated hydrogeological modelling package, *Environmental Modelling & Software*, 14, 129 - 140.
- Dennis, I., Pretorius, J., van Deventer, P. and Steyl, G., 2008, Methods to assess the impacts of tailings dams on the groundwater system in South Africa, *Journal of Mining and Metallurgy*, 44, 59 – 66.
- Department of Water Affairs and Forestry, 2007, Best practice guideline A2: Water management for mine residual deposits, 18, Figure 6.4.
- De Sousa, E., Marais, A. and Prinsloo, M., 2006, AngloGold Ashanti Emergency Dam Construction Project: Hydrogeological Study, Not Published, GCS (Pty) Ltd, South Africa.

- De Villiers, D.P.D., 2014, Mapping Acid Mine Drainage, Current MSc in the School of Geosciences, University of the Witwatersrand.
- DHI Software, 2007, *MIKE SHE User Manual: Volume 1: User Guide*, DHI Water and Environment, Edition 2007.
- Donaldson, D.E. and Robinson, T.W., 1971, Fluorescent Dyes, their uptakes and translocation in plants, *Water Resources Research*, 7(3), 692 – 696.
- Dressel, M., 2005, AngloGold Ashanti Vaal River Operations Proposed Stormwater Dam Seepage Analysis, unpublished paper, GCS, South Africa.
- Dye, P.J., Jarman, C., Le Maitre, D., Everson, C.S., Gush, M., and Clulow, A., 2006, Modelling vegetation water use for general application in difference categories of vegetation, Final report to the Water Research Commission, WRC Report No. July 2006.
- Dye, P.J., Jarman, C., and Oageng, B., Xaba, J. and Weiersbye, I.M., 2008, The Potential of Woodlands and Reed-beds for Control of Acid Mine Drainage in the Witwatersrand Gold Fields, South Africa, In: Mine Closure 2008: Proceedings of the Third International Seminar on Mine Closure, Johannesburg, South Africa, 487 – 497.
- Dye, P.J. and Weiersbye, I.M., 2010, The Mine Woodlands Project in the Witwatersrand Basin gold fields of South Africa: strategy and progress, Mine Water and Innovative Thinking, Sydney, Nova Scotia.
- Dye, P.J., Clulow, A., Prinsloo, E., Onang, B., Naiken, V. and Weiersbye, I., 2014, The annual pattern of sap flow in two Eucalyptus species established in the vicinity of gold tailings dams in Central South Africa, Submitted.
- Eijkelkamp, 2012, Double Ring Infiltrometer: Operating Instructions”, Netherlands, www.eijkelkamp.com.
- Flathman, P.E. and Lanza, G.R., 1998, Phytoremediation: Current Views on an Emerging Green Technology, *Journal of Soil Contamination*, 7(4), 415 – 432.
- Garbisu, C. and Alkorta, I., 2000, Phytoextraction: a cost-effective plant-based technology for the removal of metals from the environment, *Bioresource Technology*, 77, 229 – 236.

- Graham, D.N. and Butts, M.B., 2005, Flexible, integrated watershed modelling with MIKE SHE. In *Watershed Models*, Eds. V.P. Singh & D.K. Frevert, 245 – 272.
- Herbert, M., 2008, Mine woodlands research project annual report: 2007-08. Ecological Engineering and Phytoremediation Programme, School of Animal, Plant and Environmental Sciences, University of the Witwatersrand, Johannesburg.
- Hinchman, R.R., Negri, M.C. and Gatliff, E.G., 1997, Phytoremediation: Using green plants to clean up contaminated soil, groundwater, and Wastewater, Submitted to the U.S Department of Energy, Assistant Secretary for Energy Efficient and Renewable Energy under Contract W-31-109-Eng-38.
- Hooda, V., 2007, Phytoremediation of toxic metals from soil and waste water, *Journal of Environmental Biology*, Vol. 28(2), 367 – 376.
- Im, S., Kim, H., Kim, C. and Jang, C., 2009, Assessing the impacts of land use changes on watershed hydrology using MIKE SHE, *Environmental Geology*, 57, 231 - -239.
- ITRC (Interstate Technology & Regulator Council), 2009, *Phytotechnology Technical and Regulatory Guidance and Decision Trees*, revised, PHYTO-3, Washington, D.C.: Interstate Technology & Regulatory Council, Phytotechnologies team, Tech Reg update, www.itrcweb.org
- Jackson, R.B., Canadell, J., Ehleringer, J.R., Mooney, H.A., Sala, O.E. and Schulze, E.D., 1996, A global analysis of root distributions for terrestrial biomes, *Oecologia*, 108, 389 – 411.
- Jarmain, C., Govender, M. and Everson, C.S., 1996, Improving the basis for predicting total evaporation from natural veld types in South Africa: a focus of moist upland grassland, valley thicket and coastal bushveld/grassland, WRC Report No. 1219/1/04, ISBN No. 1-77005-171-6.
- Johnson, A.I., 1963, A Field Method for measurement of infiltration, Geological Survey Water-Supply Paper, 1554-F.
- Kadlec, R.H. and Knight, R.L., 1996, *Treatment Wetlands*, CRC Press, Lewis Publishers.

- Keiffer, C.H., 1996, Comparison of Salt Tolerance and Ion Accumulation of Halophytes and their potential use for remediating Brine Contaminated Soil, Ph.D. dissertation, College of Arts and Sciences of Ohio University, Athens.
- Keiffer, C.H. and Ungar, I.A., 1996, *Bioremediation of Brine Contaminated Soil*, Final Report, PERF Project, 91-98.
- Khaleel, R. and Freeman, E.J., 1995, *Variability and scaling of hydraulic properties for 200 area soils, Hanford site*, Report number: WHC-EP-0883.
- Kimber, P.C., 1974, The root system of Jarrah (*Eucalyptus marginata*), Research Paper NO. 10 Forests Department of Western Australia, Perth, Australia, 5.
- Kohne, J.M., Junior, J.A., Kohne, S., Tiemeter, B., Lennartz, B. and Kruse, J., 2011, Double-Ring and Tension Infiltrometer measurements of hydraulic conductivity and mobile soil regions, *Agricultural Research in the Tropics*, 41, 336 – 347.
- Kruger, T., 2008, *Decline in SA gold production accelerated in 2007*, www.midweb.com/mineweb/content/en/mineweb-gold-news?oid=49132&sn=Detail, 27 November 2013.
- Kumar, P.B.A.N., Dushenkov, V., Motto, H., and Raskin, I., 1995, Phytoextraction: the use of plants to remove heavy metals from soils, *Environmental Science and Technology*, 29, 1232 – 1238.
- Leij, F. J., Alves, W. J., van Genuchten, M. T. and Williams, J. R., 1996, The UNSODA unsaturated soil hydraulic database, version 1.0. *EPA Report, EPA/600*, 96, 095.
- McGrath, S.P., Sidoli, C.M.D., Baker, A.J.M., and Reeves, R.D., 1993, The potential for the use of metal-accumulating plants for the in situ decontamination of metal-polluted soils, *Integrated Soil and Sediment Research: A Basis for Proper Protection*, eds H.J.P. Eijsackers and T. Hamers, 673 – 676.
- McKenzie, N., Coughlan, K. and Cresswell, H., 2002, *Soil Physical Measurement and Interpretation for Land Evaluation*, CSIRO Publishing, Melbourne.
- McLaughlin, M.J., 1982, A Review of the Use of Dyes as Soil Water Tracers, *Water SA*, Vol. 8(4), 196 – 201.

- Mendex, M.O. and Maier, R.M., 2008, Phytoremediation of mine tailing in temperate and arid environments, *Reviews in Environmental Science and Biotechnology*, 7, 47 – 59.
- Mntungwa, N., Weiersbye, I.M., Dye, P.J. and Chimuka, L., 2014, Risk assessment of above ground biomass for wood fuel use in Eucalyptus species cultivated on acid mine drainage in the Witwatersrand Basin gold fields, Current MSc project in the School of Chemistry and School of Animal, Plant and Environmental Sciences, University of the Witwatersrand, Johannesburg.
- Morgan, R.P.C., 1995, *Soil Erosion & Conservation*, 2nd Ed, Longman, Silsoe College, Cranfield University.
- Mucina, L. and Rutherford, M.C., 2006, The vegetation of South Africa, Lesotho and Swaziland, SANBI, Pretoria.
- Naicker, K., Cukrowska, E. and McCarthy, T.S., 2003, Acid mine drainage arising from gold mining activity in Johannesburg, South Africa and environs, *Environmental Pollution*, Vol. 122 (1), 29 – 40.
- Newman, L.A, Gordon, M.P., Heilman, p., Cannon, D.L., Lory, E., Miller, K., Osgood, J. and Strand, S.E., 1999, Phytoremediation of MTBE at a California Naval Site, Soil and Groundwater Cleanup, Feb/Mar, 42 – 45.
- Oelofse, S.H.H., Hobbs, P.J., Rascher, J. and Cobbing, J.E., 2007, The pollution and destruction threat of gold mining waste on the Witwatersrand – A West Rand case study, *Journal of Environmental Issues*, 617 – 628.
- Parr, J.R. and Bertrand, A.R., 1960, Water infiltration into soils, *Advances in Agronomy*, 12, 311 – 363.
- Paterson, K.G. and Schnoor, J.L., 1992, Fate of Alachlor and Atrazine in Riparian Zone Field Site, *Water Environment Research*, 64, 274 – 283.
- Phytotech, Inc, 1997, *Phytoremediation Technical Summary*, Phytotech, Inc. New Jersey, USA.
- Pilon-Smits, E., 2005, Phytoremediation, *Annual Review of Plant Biology*, 56, 15-39.

- Potgieter, A.S. and Calitz, F., 2005, AngloGold Ashanti Vaal River and West Wits Operations – Geotechnical assessment for the Woodlands Project, Not Published, University of Witwatersrand, South Africa.
- Quinn, J.J., Negri, M.C., Hinchman, R.R., Moos, L.P., Wozniak, J.B. and Gatliff, E.G., 2001, Predicting the effect of Deep-rooted hybrid Poplars on the Groundwater Flow System at a large-scale phytoremediation site, *International Journal of Phytoremediation*, 3(1), 41 – 60.
- Refsgaard, J.C., Thorsen, M., Jensen, J.B., Kleeschulte, S. and Hansen, S., 1999, Large scale modelling of groundwater contamination from nitrate leaching, *Journal of Hydrology*, 221, 117 – 140.
- Ritchie, G.A. and Hinckley, T.M., 1975, The Pressure Chamber as an instrument for Ecological Research, *Advanced Ecological Research*, 9, 165 – 253.
- Robb, L.J. and Meyer, F.M., 1995, The Witwatersrand Basin, South Africa: Geological Framework and mineralization processes, *Ore Geology Review*, 10, 67 – 94.
- Rosner, T. and van Schalkwyk, A., 2000, The Environmental impact of gold mine tailings footprint in the Johannesburg region, South Africa, *Bulletin of Engineering Geology and the Environment*, 59, 137 – 148.
- Rosselli, W., Keller, C. and Boschi, K., 2003, Phytoextraction capacity of trees growing on a metal contaminated soil, *Plant and Soil*, Vol. 256, 265 – 272.
- Salt, C.A., Blaylock, M., Kumar, P.B.A.N., Dushenkov, V., Ensley, B.D., Chet, I. and Riskin, I., 1992, Effects of Season, Grazing Intensity, and Diet Composition on the Radiocaesium Intake by Sheep on Reseeded Hill Pasture, *Journal Of Applied Ecology*, 29, 378 – 387.
- Schnoor, J.L., Aitchison, E.W., Kelley, S.L., Alvarez, P.J.J., Wakefield, S., Burken, J.G. and Just, C.L., 1997, Phytoremediation of 1,4 Dioxane by Hybrid Poplars, *Proceedings, 213th ACS National Meeting, American Chemical Society Environmental Division Symposia*, San Francisco, Paper 195, 197 – 199.

- Scholander, P.F., Hammel, H.T., Bradstreet, E.D. and Hemmingsen, E.A., 1965, Sap Pressure in Vascular Plants: Negative Hydrostatic Pressure can be measured in Plants, *Science*, 148, 339 – 346.
- Sheoran, A.S., 2005, Performance of a Natural Wetland Treating Acid Mine Drainage in Arid Conditions, *Mine Water and the Environment*, 24, 150 – 154.
- Sheoran, A.S. and Sheoran, V., 2006, Heavy Metal removal mechanism of acid mine drainage in wetlands: A critical review, *Minerals Engineering*, 19, 105 – 116.
- Sherrard, J.L., Dunningan, L.P., and Talbot, J.R., 1984, Basic properties of Sand and Gravel Filters, *Journal of Geotechnical Engineering*, Vol. 110, 684 – 700.
- Singh, R., Subramanian, K. and Refsgaard, J.C., 1999, Hydrological modelling of a small watershed using MIKE SHE for irrigation planning, *Agricultural Water Management*, 41, 149 – 166.
- Spier, T.W., August, J.A. and Feltham, C.W., 1992, Assessment of the Feasibility of using CCa9 Copper, Chromium and Arsenic) treated and Boric Acid Treated Sawdust as Soil Amendments, I. Plant Growth and Element Uptake, *Plant and Soil*, 142, 235 – 248.
- Swart, E., 2003, The South African Legislative framework for mine closure, *The Journal of The South African Institute of Mining and Metallurgy*, 489 – 492.
- Tegelhoffova, M., 2010, Analysis of the development of a hydrological balance for future decades in the Senianska depression in the Eastern Slovak lowland, *Slovak Journal of Civil Engineering*, Vol. 18(4), 30 – 40.
- Truong, P., 2000, Application of The Vetiver System for Phytoremediation of Mercury Pollution in The Lake and Yolo Counties, Northern California, In: Invited paper presented at the pollution solutions seminar, Clear Lake, 550 – 562.
- Tutu, H., McCarthy, T.S., and Cukrowska, E., 2008, The Chemical characteristics of acid mine drainage with particular reference to sources, distribution and remediation: The Witwatersrand Basin, South Africa as a case study, *Applied Geochemistry*, 23, 3666 – 3684.

- Vazquez, R.F., Feyen, L., Feyen, J. and Refsgaard, C.J., 2002, Effect of grid size on effective parameters and model performance of the MIKE SHE code, *Hydrological Processes*, 16 (2), 355 – 372.
- Weiersbye, I.M. and Witkowski, E.T.F, 2007, *Impacts of Acid Mine Drainage of the Regeneration potential of Highveld Phreatophytes*, In: Bester, J.J., Seydack, A.H.W., Vorster, T., Van der Merwe, I.J., Dzivhani, S. (Eds.), *Multiple Use Management of Natural Forests and Woodlands: Policy Refinements and Scientific Progress IV*. Department of Water Affairs and Forestry of South Africa, 224 – 237.
- Winde, F. and Sandham, L.A., 2004, Uranium pollution of South Africa streams – An overview of the situation in gold mining areas of the Witwatersrand, *GeoJournal*, Vol. 61, 131 – 149.
- Youngs, E.G., 1987, Estimating hydraulic conductivity values from ring infiltrometer measurements, *Journal of Soil Science*, 38, 623 – 632.
- Zhang, Q.L., Davis, L.C. and Erickson, L.E., 1998, Using vegetation to treat Methyl-Tert-Burtyl-Ether contaminated groundwater, *Proceedings, Conference on Hazardous Waste Research*, USA, 76.

8 Appendices

8.1 Appendix A (Mike She Input Values)

Table 35: The MIKE SHE input data for the Simulation Specification Module

SIMULATION SPECIFICATIONS								
INPUT FIELD		CURRENT SCENARIO	SCENARIO 1	SCENARIO 2	SCENARIO 3	SCENARIO 4	SCENARIO 5	SCENARIO 6
Simulation Period		1 st January 2001 until 29 th January 2010	1 st January 2030 until 29 th January 2010	1 st January 2030 until 29 th January 2010	1 st January 2030 until 29 th January 2010	1 st January 2030 until 29 th January 2010	1 st January 2030 until 29 th January 2010	1 st January 2030 until 29 th January 2010
Time Step Control	Time Steps							
	Initial time step	0.5 (hrs)	0.5 (hrs)	0.5 (hrs)	0.5 (hrs)	0.5 (hrs)	0.5 (hrs)	0.5 (hrs)
	Max allowed OL time step	2 (hrs)	2 (hrs)	2 (hrs)	2 (hrs)	2 (hrs)	2 (hrs)	2 (hrs)
	Max allowed UZ time step	12 (hrs)	12 (hrs)	12 (hrs)	12 (hrs)	12 (hrs)	12 (hrs)	12 (hrs)
	Max allowed SZ time step	24 (hrs)	24 (hrs)	24 (hrs)	24 (hrs)	24 (hrs)	24 (hrs)	24 (hrs)
	Increment of reduced time step length							
	Increment Rate	0.05	0.05	0.05	0.05	0.05	0.05	0.05
	Parameters for Precipitation-dependent time step control							
	Max precipitation per time step	10 (mm)	10 (mm)	10 (mm)	10 (mm)	10 (mm)	10 (mm)	10 (mm)
	Max infiltration amount per time step	10 (mm)	10 (mm)	10 (mm)	10 (mm)	10 (mm)	10 (mm)	10 (mm)
	Input precipitation rate requiring its own time step	0.1 (mm/hr)	0.1 (mm/hr)	0.1 (mm/hr)	0.1 (mm/hr)	0.1 (mm/hr)	0.1 (mm/hr)	0.1 (mm/hr)
OL Computational Control Parameters	Solver Type and Solver-specific Parameters (Successive Overrelaxation (SOR))							
	Maximum number of iterations	200	200	200	200	200	200	200
	Maximum	0.0001 (m)	0.0001 (m)	0.0001 (m)	0.0001 (m)	0.0001 (m)	0.0001 (m)	0.0001 (m)

Appendix A (MIKE SHE Input Values)

	head change per iteration							
	Maximum residual error	0.0001 (m/d)	0.0001 (m/d)	0.0001 (m/d)	0.0001 (m/d)	0.0001 (m/d)	0.0001 (m/d)	0.0001 (m/d)
	Under-relaxation factor (0.01 – 1.0)	0.9	0.9	0.9	0.9	0.9	0.9	0.9
	Common stability parameters							
	Threshold water depth for overland flow	0.0001 (m)	0.0001 (m)	0.0001 (m)	0.0001 (m)	0.0001 (m)	0.0001 (m)	0.0001 (m)
	Threshold gradient for applying low-gradient flow reduction	0.0001	0.0001	0.0001	0.0001	0.0001	0.0001	0.0001
	Overland-River exchange calculation	Manning equation (using OL flow manning numbers)	Manning equation (using OL flow manning numbers)	Manning equation (using OL flow manning numbers)	Manning equation (using OL flow manning numbers)	Manning equation (using OL flow manning numbers)	Manning equation (using OL flow manning numbers)	Manning equation (using OL flow manning numbers)
UZ Computational Control Parameters	UZ-SZ Coupling Control							
	Maximum profile water balance error	0.001 (m)	0.001 (m)	0.001 (m)	0.001 (m)	0.001 (m)	0.001 (m)	0.001 (m)
	Richards equation parameters							
	Maximum number of iterations	50	50	50	50	50	50	50
	Iteration stop criteria (Fraction of Psi)	0.002	0.002	0.002	0.002	0.002	0.002	0.002
	Time step Reduction Control (UZ Restart)							
	Maximum water balance	0.03	0.03	0.03	0.03	0.03	0.03	0.03

Appendix A (MIKE SHE Input Values)

	error in one node (fraction)							
SZ Computational Control Parameters	Solver Type	Preconditioned Conjugate Gradient, Transient	Preconditioned Conjugate Gradient, Transient	Preconditioned Conjugate Gradient, Transient	Preconditioned Conjugate Gradient, Transient	Preconditioned Conjugate Gradient, Transient	Preconditioned Conjugate Gradient, Transient	Preconditioned Conjugate Gradient, Transient
	Iteration Control							
	Maximum number of iterations	50	50	50	50	50	50	50
	Maximum head change per iteration	0.005 (m)	0.005 (m)	0.005 (m)	0.005 (m)	0.005 (m)	0.005 (m)	0.005 (m)
	Maximum residual error	0.0005 (m/d)	0.0005 (m/d)	0.0005 (m/d)	0.0005 (m/d)	0.0005 (m/d)	0.0005 (m/d)	0.0005 (m/d)
	Sink de-activation in drying cells							
	Saturated thickness threshold	0.05 (m)	0.05 (m)	0.05 (m)	0.05 (m)	0.05 (m)	0.05 (m)	0.05 (m)
	Advanced Settings							
	Under Relaxation	No under-relaxation	No under-relaxation	No under-relaxation	No under-relaxation	No under-relaxation	No under-relaxation	No under-relaxation
	Maximum exchange from river during one time step							
	Maximum fraction of H-point volume	0.9	0.9	0.9	0.9	0.9	0.9	0.9

Table 36: The MIKE SHE input data for the *Water Quality Simulation Specification Module*

WATER QUALITY SIMULATION SPECIFICATIONS								
INPUT FIELD		CURRENT SCENARIO	SCENARIO 1	SCENARIO 2	SCENARIO 3	SCENARIO 4	SCENARIO 5	SCENARIO 6
Simulation Period		1 st January 2001 until 29 th January 2010	1 st January 2030 until 29 th January 2010	1 st January 2030 until 29 th January 2010	1 st January 2030 until 29 th January 2010	1 st January 2030 until 29 th January 2010	1 st January 2030 until 29 th January 2010	1 st January 2030 until 29 th January 2010
Time step Control	Maximum simulation time step							
	Saturated Zone	1000000000 (hrs)	1000000000 (hrs)	1000000000 (hrs)	1000000000 (hrs)	1000000000 (hrs)	1000000000 (hrs)	1000000000 (hrs)
	Unsaturated Zone	1000000000 (hrs)	1000000000 (hrs)	1000000000 (hrs)	1000000000 (hrs)	1000000000 (hrs)	1000000000 (hrs)	1000000000 (hrs)
	Overland flow	1000000000 (hrs)	1000000000 (hrs)	1000000000 (hrs)	1000000000 (hrs)	1000000000 (hrs)	1000000000 (hrs)	1000000000 (hrs)
	Maximum Advective Courant Number							
	Saturated Zone	0.8	0.8	0.8	0.8	0.8	0.8	0.8
	Unsaturated Zone	0.8	0.8	0.8	0.8	0.8	0.8	0.8
	Overland flow	0.8	0.8	0.8	0.8	0.8	0.8	0.8
	Maximum Dispersion Courant Number							
	Saturated Zone	0.5	0.5	0.5	0.5	0.5	0.5	0.5
	Unsaturated Zone	0.5	0.5	0.5	0.5	0.5	0.5	0.5
	Overland flow	0.5	0.5	0.5	0.5	0.5	0.5	0.5
	Maximum Transport Limit							
	Saturated Zone	0.95	0.95	0.95	0.95	0.95	0.95	0.95
	Unsaturated	0.95	0.95	0.95	0.95	0.95	0.95	0.95

Appendix A (MIKE SHE Input Values)

	Zone							
	Overland flow	0.95	0.95	0.95	0.95	0.95	0.95	0.95
	Maximum Macropore Courant Number							
	All	0.8	0.8	0.8	0.8	0.8	0.8	0.8

Table 37: The MIKE SHE input data for the *Species Module*

SPECIES MODULE								
INPUT FIELD		CURRENT SCENARIO	SCENARIO 1	SCENARIO 2	SCENARIO 3	SCENARIO 4	SCENARIO 5	SCENARIO 6
	Name	SO ₄	SO ₄	SO ₄	SO ₄	SO ₄	SO ₄	SO ₄
	Type	Dissolved	Dissolved	Dissolved	Dissolved	Dissolved	Dissolved	Dissolved
	ET Uptake Factor	0	0.674	0.628	0.12	0.029	0.449	0.419
	Solubility in Surface	1×10^{-8}	1×10^{-8}	1×10^{-8}	1×10^{-8}	1×10^{-8}	1×10^{-8}	1×10^{-8}

Table 38: The MIKE SHE input data for the *Model Domain and Grid Module*

MODEL DOMAIN AND GRID								
INPUT FIELD		CURRENT SCENARIO	SCENARIO 1	SCENARIO 2	SCENARIO 3	SCENARIO 4	SCENARIO 5	SCENARIO 6
Catchment size and orientation	NX	75	75	75	75	75	75	75
	NY	100	100	100	100	100	100	100
	Cell size	120	120	120	120	120	120	120
	Rotation	0	0	0	0	0	0	0
	Catchment origin and map projection							
	X0 (m)	- 36936.941481	- 36936.941481	- 36936.941481	- 36936.941481	- 36936.941481	- 36936.941481	- 36936.941481
	Y0 (m)	- 2989240.7231	- 2989240.7231	- 2989240.7231	- 2989240.7231	- 2989240.7231	- 2989240.7231	- 2989240.7231
	Map Projection type	LO 27 (UTM)	LO 27 (UTM)	LO 27 (UTM)	LO 27 (UTM)	LO 27 (UTM)	LO 27 (UTM)	LO 27 (UTM)

Table 39: The MIKE SHE input data for the *Topography Module*

TOPOGRAPHY							
INPUT FIELD	CURRENT SCENARIO	SCENARIO 1	SCENARIO 2	SCENARIO 3	SCENARIO 4	SCENARIO 5	SCENARIO 6
File input	5m DEM re-sampled to 30m	5m DEM re-sampled to 30m	5m DEM re-sampled to 30m	5m DEM re-sampled to 30m	5m DEM re-sampled to 30m	5m DEM re-sampled to 30m	5m DEM re-sampled to 30m

Table 40: The MIKE SHE input data for the *Climate Module*

CLIMATE								
INPUT FIELD		CURRENT SCENARIO	SCENARIO 1	SCENARIO 2	SCENARIO 3	SCENARIO 4	SCENARIO 5	SCENARIO 6
Precipitation Rate		Daily rainfall from January 2001 until January 2010	Daily rainfall from January 2001 until January 2010	Daily rainfall from January 2001 until January 2010	Daily rainfall from January 2001 until January 2010	Daily rainfall from January 2001 until January 2010	Daily rainfall from January 2001 until January 2010	Daily rainfall from January 2001 until January 2010
Reference Evapotranspiration		Daily reference evapo-transpiration from January 2001 until January 2010	Daily reference evapo-transpiration from January 2001 until January 2010	Daily reference evapo-transpiration from January 2001 until January 2010	Daily reference evapo-transpiration from January 2001 until January 2010	Daily reference evapo-transpiration from January 2001 until January 2010	Daily reference evapo-transpiration from January 2001 until January 2010	Daily reference evapo-transpiration from January 2001 until January 2010

Table 41: The MIKE SHE input data for the *Land Use Module*

LAND USE								
INPUT FIELD		CURRENT SCENARIO	SCENARIO 1	SCENARIO 2	SCENARIO 3	SCENARIO 4	SCENARIO 5	SCENARIO 6
Vegetation type		See Appendix B	See Appendix B	See Appendix B	See Appendix B	See Appendix B	See Appendix B	See Appendix B
Evapo-transpiration Parameters	General ET Parameters							
	Canopy interception	4 (mm)	4 (mm)	4 (mm)	4 (mm)	4 (mm)	4 (mm)	4 (mm)
	2-Layer Water Balance ET Parameters							
	Reduce ET from roots when UZ deficit fraction is below	1	1	1	1	1	1	1
	Gravity Flow and Richards ET parameters (Kristensen and Jensen)							
	C1 (mm/d)	0.3	0.3	0.3	0.3	0.3	0.3	0.3
	C2 (mm/d)	0.2	0.2	0.2	0.2	0.2	0.2	0.2
	C3 (mm/d)	20	20	20	20	20	20	20
	Aroot (1/m)	0.25	0.25	0.25	0.25	0.25	0.25	0.25

Table 42: The MIKE SHE input data for the *River and Lakes Module*

RIVERS AND LAKES								
INPUT FIELD		CURRENT SCENARIO	SCENARIO 1	SCENARIO 2	SCENARIO 3	SCENARIO 4	SCENARIO 5	SCENARIO 6
NETWORK EDITOR								
Branches	Flow Direction	Positive	Positive	Positive	Positive	Positive	Positive	Positive
	Maximum dx (m)	1000	1000	1000	1000	1000	1000	1000
	Branch Type	Regular	Regular	Regular	Regular	Regular	Regular	Regular
MIKE SHE Links	Conductance	Aquifer and Bed	Aquifer and Bed	Aquifer and Bed	Aquifer and Bed	Aquifer and Bed	Aquifer and Bed	Aquifer and Bed
	Leakage Coefficient	0.00001	0.00001	0.00001	0.00001	0.00001	0.00001	0.00001
	Flood Area	No flooding	No flooding	No flooding	No flooding	No flooding	No flooding	No flooding

Appendix A (MIKE SHE Input Values)

CROSS SECTION EDITOR								
	Section Type	Open	Open	Open	Open	Open	Open	Open
	Radius Type	Resistance Radius	Resistance Radius	Resistance Radius	Resistance Radius	Resistance Radius	Resistance Radius	Resistance Radius
	Transversal Distribution	High/Low flow zones	High/Low flow zones	High/Low flow zones	High/Low flow zones	High/Low flow zones	High/Low flow zones	High/Low flow zones
Resistance Type		Relative Resistance	Relative Resistance	Relative Resistance	Relative Resistance	Relative Resistance	Relative Resistance	Relative Resistance
	Left high flow	1	1	1	1	1	1	1
	Right High flow	1	1	1	1	1	1	1
	Low flow	1	1	1	1	1	1	1
BOUNDARY EDITOR								
Upstream Boundary	Boundary Description	Open	Open	Open	Open	Open	Open	Open
	Boundary Type	Inflow	Inflow	Inflow	Inflow	Inflow	Inflow	Inflow
	Data Type	Discharge	Discharge	Discharge	Discharge	Discharge	Discharge	Discharge
	AD Boundary	Included	Included	Included	Included	Included	Included	Included
Downstream Boundary	Boundary Description	Open	Open	Open	Open	Open	Open	Open
	Boundary Type	Q-h	Q-h	Q-h	Q-h	Q-h	Q-h	Q-h
	Data Type	Discharge and Water Level	Discharge and Water Level	Discharge and Water Level	Discharge and Water Level	Discharge and Water Level	Discharge and Water Level	Discharge and Water Level
	AD Boundary	Included	Included	Included	Included	Included	Included	Included
HYDRODYNAMIC PARAMETERS								
Initial	Water Depth	0.242	0.242	0.242	0.242	0.242	0.242	0.242
	Discharge	0.752	0.752	0.752	0.752	0.752	0.752	0.752
Bed Resistance	Resistance Number	30	10	10	10	10	10	10
	Approach	Uniform Section	Uniform Section	Uniform Section	Uniform Section	Uniform Section	Uniform Section	Uniform Section
	Resistance Formula	Manning (M)	Manning (M)	Manning (M)	Manning (M)	Manning (M)	Manning (M)	Manning (M)

Appendix A (MIKE SHE Input Values)

Wave approximation	High order fully dynamic	High order fully dynamic	High order fully dynamic	High order fully dynamic	High order fully dynamic	High order fully dynamic	High order fully dynamic	High order fully dynamic
Default Values	Delta	0.5	0.5	0.5	0.5	0.5	0.5	0.5
	Delhs	0.01	0.01	0.01	0.01	0.01	0.01	0.01
	Delh	0.1	0.1	0.1	0.1	0.1	0.1	0.1
	Alpha	1	1	1	1	1	1	1
	Theta	1	1	1	1	1	1	1
	Eps	0.0001	0.0001	0.0001	0.0001	0.0001	0.0001	0.0001
	Dh nodes	0.01	0.01	0.01	0.01	0.01	0.01	0.01
	Zeta min	0.1	0.1	0.1	0.1	0.1	0.1	0.1
	Struct Fac	0	0	0	0	0	0	0
	InterlMax	10	10	10	10	10	10	10
	Nolter	1	1	1	1	1	1	1
	MaxIterSteady	100	100	100	100	100	100	100
	FroudeMax	-1	-1	-1	-1	-1	-1	-1
	FroudeExp	-1	-1	-1	-1	-1	-1	-1
ADVECTION DISPERSION PARAMETERS								
Components	Component	SO ₄	SO ₄	SO ₄	SO ₄	SO ₄	SO ₄	SO ₄
	Units	Mg/l	Mg/l	Mg/l	Mg/l	Mg/l	Mg/l	Mg/l
	Type	Normal	Normal	Normal	Normal	Normal	Normal	Normal
Dispersion	Dispersion Factor	0.000	0.000	0.000	0.000	0.000	0.000	0.000
	Exponent	0.000	0.000	0.000	0.000	0.000	0.000	0.000
	Minimum Dispersion Coefficient	0.000	0.000	0.000	0.000	0.000	0.000	0.000
	Maximum Dispersion Coefficient	100.00	100.00	100.00	100.00	100.00	100.00	100.00
Initial conditions	Component	SO ₄	SO ₄	SO ₄	SO ₄	SO ₄	SO ₄	SO ₄
	Concentration	80 (mg/l)	80 (mg/l)	80 (mg/l)	80 (mg/l)	80 (mg/l)	80 (mg/l)	80 (mg/l)

Appendix A (MIKE SHE Input Values)

Table 43: The MIKE SHE input data for the *Overland Flow Module*

OVERLAND FLOW								
INPUT FIELD		CURRENT SCENARIO	SCENARIO 1	SCENARIO 2	SCENARIO 3	SCENARIO 4	SCENARIO 5	SCENARIO 6
Manning number	$(m^{\frac{1}{3}}/s)$	30	10	10	10	10	10	10
Detention Storage	(mm)	2	2	2	2	2	2	2
Initial Water Depth	(m)	0	0	0	0	0	0	0
Initial Mass	SO ₄	0	0	0	0	0	0	0
Dispersion along the Columns	(m ² /s)	0	0	0	0	0	0	0
Dispersion along the Rows	(m ² /s)	0	0	0	0	0	0	0

Table 44: The MIKE SHE input data for the *Unsaturated Flow Module*

UNSATURATED FLOW								
INPUT FIELD		CURRENT SCENARIO	SCENARIO 1	SCENARIO 2	SCENARIO 3	SCENARIO 4	SCENARIO 5	SCENARIO 6
Calculation Column Classification Type		Calculated in all grid points	Calculated in all grid points	Calculated in all grid points	Calculated in all grid points	Calculated in all grid points	Calculated in all grid points	Calculated in all grid points
Initial Conditions		Equilibrium pressure profile	Equilibrium pressure profile	Equilibrium pressure profile	Equilibrium pressure profile	Equilibrium pressure profile	Equilibrium pressure profile	Equilibrium pressure profile
Macropore Flow		Simple by-pass flow	Simple by-pass flow	Simple by-pass flow	Simple by-pass flow	Simple by-pass flow	Simple by-pass flow	Simple by-pass flow
Soil Profile Definition		See Table 45	Remains unchanged	Remains unchanged	Remains unchanged	Remains unchanged	Remains unchanged	Remains unchanged
Bypass Constants	Maximum bypass constant	0.25	0.25	0.25	0.25	0.25	0.25	0.25
	Water content for reduced bypass flow	0.15	0.15	0.15	0.15	0.15	0.15	0.15
	Minimum water content for bypass flow	0.05	0.05	0.05	0.05	0.05	0.05	0.05

Appendix A (MIKE SHE Input Values)

Initial Concentration	Lower level	-10 (m)	-10 (m)	-10 (m)	-10 (m)	-10 (m)	-10 (m)	-10 (m)
	Concentration	0	0	0	0	0	0	0

Table 45: The MIKE SHE input data for the soil profiles definitions

SOIL PROFILES					
VENTERSDORP LAVAS					
Soil Profile	From Depth (m)	To Depth (m)	Soil Names		
	0	0.5	SandyClay		
	0.5	1.5	SandyFINES		
	1.5	5	Silt		
	5	70	Silt		
Vertical Discretization	From Depth	To Depth	Cell Height	Number of Cells	Dispersivity
	0	70	14	5	0
DOLOMITE					
Soil Profile	From Depth (m)	To Depth (m)	Soil Names		
	0	0.5	SiltyClay		
	0.5	1	SandyGRAVEL1		
	1	70	SandyGRAVEL1		
Vertical Discretization	From Depth	To Depth	Cell Height	Number of Cells	Dispersivity
	0	70	14	5	0
BLACK REEF QUARTZITE					
Soil Profile	From Depth (m)	To Depth (m)	Soil Names		
	0	0.25	SandyClayLoam		
	0.25	0.55	SandyClayLoam		
	0.55	1	SandyClayLoam		
	1	70	SandyClayLoam		
Vertical Discretization	From Depth	To Depth	Cell Height	Number of Cells	Dispersivity
	0	70	14	5	0
ALLUVIUM					
Soil Profile	From Depth (m)	To Depth (m)	Soil Names		
	0	0.3	ClayLoam		
	0.3	0.65	ClayLoam		
	0.65	70	SandyGRAVEL2		

Appendix A (MIKE SHE Input Values)

Vertical Discretization	From Depth	To Depth	Cell Height	Number of Cells	Dispersivity
	0	70	14	5	0
WEST COMPLEX TSF					
Soil Profile	From Depth (m)	To Depth (m)	Soil Names		
	0	5	Silt		
	5	70	Silt		
Vertical Discretization	From Depth	To Depth	Cell Height	Number of Cells	Dispersivity
	0	70	14	5	0

Table 46: The MIKE SHE input data for the Saturated Zone Module

SATURATED ZONE								
INPUT FIELD		CURRENT SCENARIO	SCENARIO 1	SCENARIO 2	SCENARIO 3	SCENARIO 4	SCENARIO 5	SCENARIO 6
Geological Units		See Table 48	Remains unchanged	Remains unchanged	Remains unchanged	Remains unchanged	Remains unchanged	Remains unchanged
Lower Levels	Tailings and Geology	-30 (m)	-30 (m)	-30 (m)	-30 (m)	-30 (m)	-30 (m)	-30 (m)
	Geology	-70 (m)	-70 (m)	-70 (m)	-70 (m)	-70 (m)	-70 (m)	-70 (m)
Geological Distribution	Tailings and Geology	Figure 19	Remains unchanged	Remains unchanged	Remains unchanged	Remains unchanged	Remains unchanged	Remains unchanged
Water Quality Layers	Lower level	-100 (m)	-100 (m)	-100 (m)	-100 (m)	-100 (m)	-100 (m)	-100 (m)
Computational Layers								
Tailings and Geology	Initial Potential Head	See Appendix A	See Appendix A	See Appendix A	See Appendix A	See Appendix A	See Appendix A	See Appendix A
	Outer Boundary Conditions	Vaal = -0.00793 (m/s)	Vaal = -0.00793 (m/s)	Vaal = -0.00793 (m/s)	Vaal = -0.00793 (m/s)	Vaal = -0.00793 (m/s)	Vaal = -0.00793 (m/s)	Vaal = -0.00793 (m/s)
		All = Zero Flux	All = Zero Flux	All = Zero Flux	All = Zero Flux	All = Zero Flux	All = Zero Flux	All = Zero Flux
	Internal Boundary Conditions	None	None	None	None	None	None	None
	Initial Concentration	See Appendix A	See Appendix A	See Appendix A	See Appendix A	See Appendix A	See Appendix A	See Appendix A

Table 47: The MIKE SHE input data for the original geological units

GEOLOGICAL UNITS								
SOIL NAME	SOIL CODE	HORIZONTAL CONDUCTIVITY (m/s)	VERTICAL CONDUCTIVITY (m/s)	SPECIFIC YIELD	SPECIFIC STORAGE (1/m)	POROSITY	LHH	THH
Ventersdorp	1	4.93e-007	0.00273	0.2	0.0001	0.02	0.2	0.01
Dolomite	2	6.72 e-007	2.53 e-005	0.2	0.0001	0.02	0.2	0.01
Black Reef	3	4.12e-008	2 e-005	0.2	0.0001	0.02	0.2	0.01
Alluvium	4	4.93 e-007	0.00273	0.2	0.0001	0.02	0.2	0.01
TSF	5	5.68 e-007	8e-008	0.2	0.0001	0.02	0.2	0.01

Table 48: The MIKE SHE input data for the calibrated geological units

GEOLOGICAL UNITS								
SOIL NAME	SOIL CODE	HORIZONTAL CONDUCTIVITY (m/s)	VERTICAL CONDUCTIVITY (m/s)	SPECIFIC YIELD	SPECIFIC STORAGE (1/m)	POROSITY	LHH	THH
Ventersdorp	1	4.05e-006	0.00273	0.2	0.0001	0.02	0.2	0.01
Dolomite	2	5.75e-006	0.00253	0.2	0.0001	0.02	0.2	0.01
Black Reef	3	8.45e-006	0.000245	0.2	0.0001	0.02	0.2	0.01
Alluvium	4	6.5e-007	0.00273	0.2	0.0001	0.02	0.2	0.01
TSF	5	5.68e-007	0.00008	0.2	0.0001	0.02	0.2	0.01

Table 49: The MIKE SHE input data for the Water Quality Sources Module

WATER QUALITY SOURCES								
INPUT FIELD		CURRENT SCENARIO	SCENARIO 1	SCENARIO 2	SCENARIO 3	SCENARIO 4	SCENARIO 5	SCENARIO 6
	Source Name	SO ₄	SO ₄	SO ₄	SO ₄	SO ₄	SO ₄	SO ₄
	Species	SO ₄	SO ₄	SO ₄	SO ₄	SO ₄	SO ₄	SO ₄
	Location	Subsurface	Subsurface	Subsurface	Subsurface	Subsurface	Subsurface	Subsurface
	Source Type	Saturated Zone fixed concentration	Saturated Zone fixed concentration	Saturated Zone fixed concentration	Saturated Zone fixed concentration	Saturated Zone fixed concentration	Saturated Zone fixed concentration	Saturated Zone fixed concentration
	Extent Type	Full Domain	Full Domain	Full Domain	Full Domain	Full Domain	Full Domain	Full Domain
	Upper Level	-5	-5	-5	-5	-5	-5	-5

Appendix A (MIKE SHE Input Values)

	(m)							
	Lower Level (m)	-35	-35	-35	-35	-35	-35	-35
	Strength	See Figure 24	See Figure 24	See Figure 24	See Figure 24	See Figure 24	See Figure 24	See Figure 24

Table 50: The MIKE SHE input data for the *Storing of Results Module*

STORING OF RESULTS								
INPUT FIELD		CURRENT SCENARIO	SCENARIO 1	SCENARIO 2	SCENARIO 3	SCENARIO 4	SCENARIO 5	SCENARIO 6
Water Movement Outputs	Storing Interval for grid series output							
	Overland	96 (hrs)	96 (hrs)	96 (hrs)	96 (hrs)	96 (hrs)	96 (hrs)	96 (hrs)
	Precipitation Evapo- transpiration	96 (hrs)	96 (hrs)	96 (hrs)	96 (hrs)	96 (hrs)	96 (hrs)	96 (hrs)
	Saturated Zone Heads	96 (hrs)	96 (hrs)	96 (hrs)	96 (hrs)	96 (hrs)	96 (hrs)	96 (hrs)
	Saturated Zone Fluxes	96 (hrs)	96 (hrs)	96 (hrs)	96 (hrs)	96 (hrs)	96 (hrs)	96 (hrs)
Water Quality Outputs	Storing interval for grid series output							
	Overland	48	48	48	48	48	48	48
	Unsaturated Flow	96	96	96	96	96	96	96
	Saturated Zone	96	96	96	96	96	96	96
	Storing interval for mass balance output							
	Time Series (.dfs0)	96	96	96	96	96	96	96
	Summary (ASCII)	96	96	96	96	96	96	96

8.2 Appendix B (Maps showing the Future Planting Scenarios)

Appendix B (Maps showing the Future Planting Scenarios)

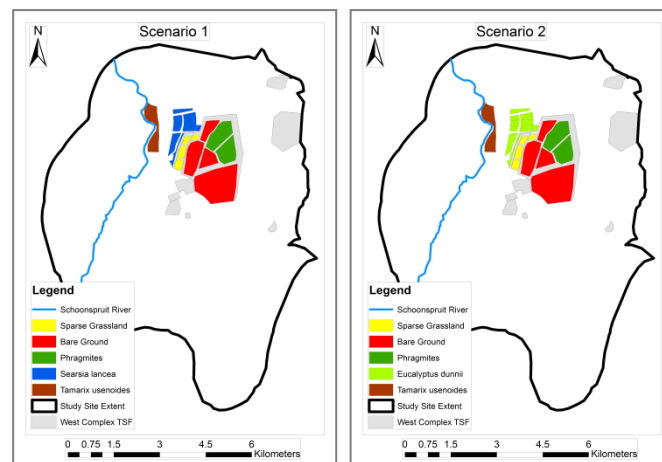


Figure 168: The future planting scenario one (left) and scenario two (right)

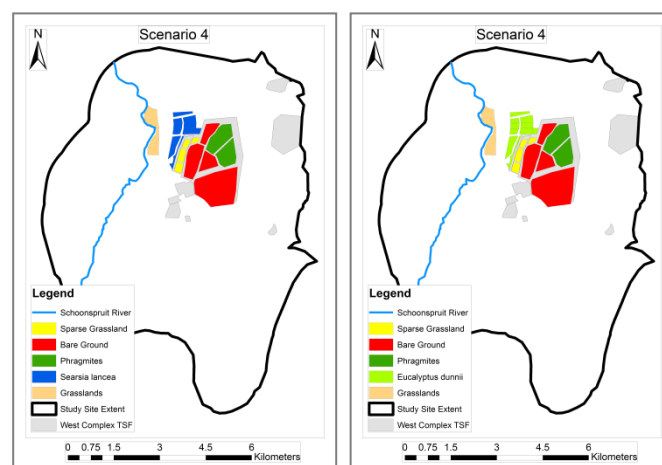


Figure 169: The future planting scenario three (left) and scenario four (right)

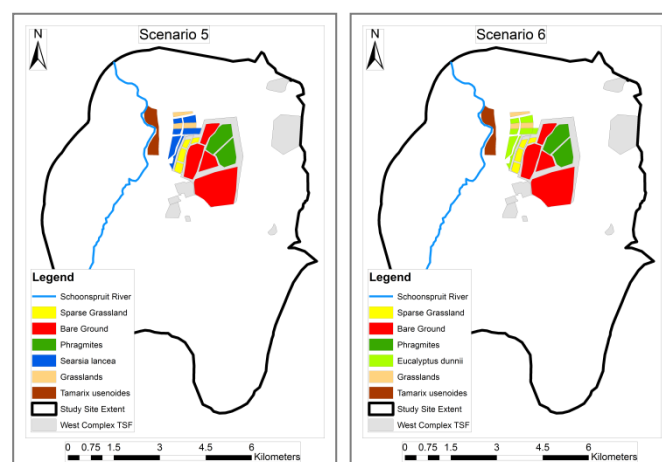


Figure 170: The future planting scenario five (left) and scenario six (right)

8.3 Appendix C (Graphs showing the change per year observed for Scenarios 3 to 6)

Appendix C (Graphs showing the change per year observed for Scenarios 3 to 6)

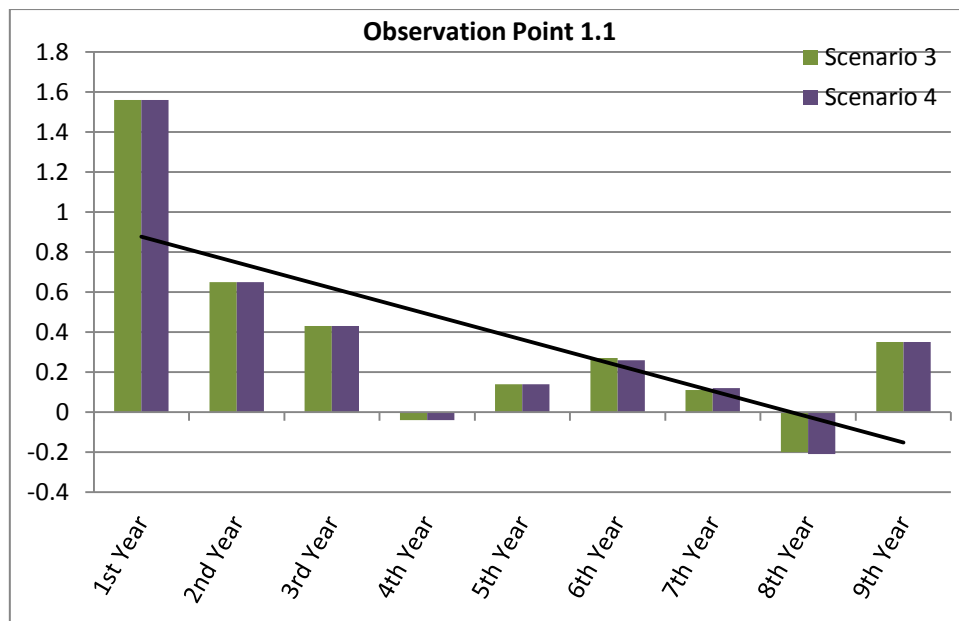


Figure 171: The decreasing trend of Scenarios 3 and 4 for simulation point 1.1

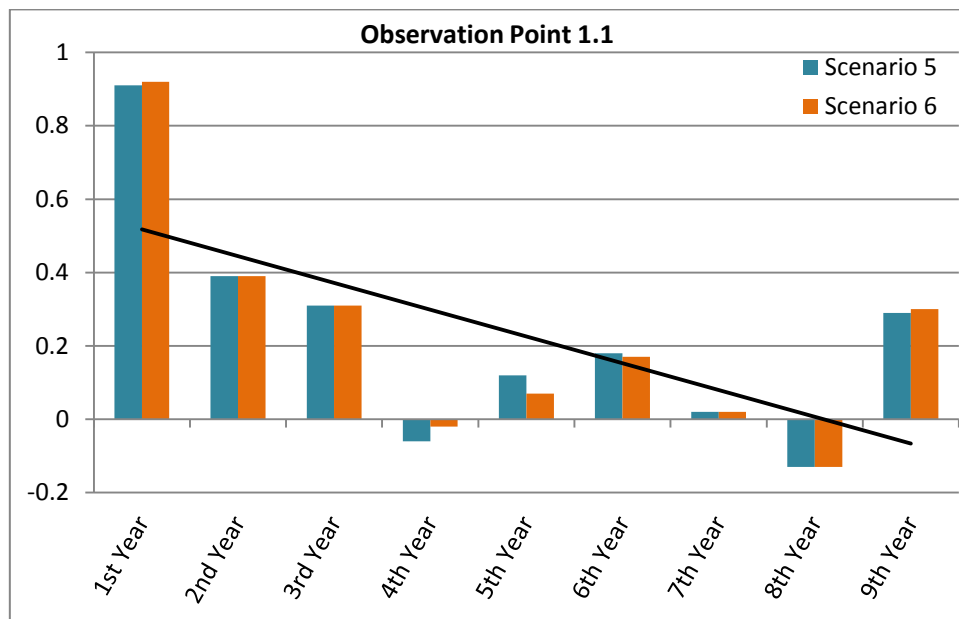


Figure 172: The decreasing trend of Scenarios 5 and 6 for simulation point 1.1

Appendix C (Graphs showing the change per year observed for Scenarios 3 to 6)

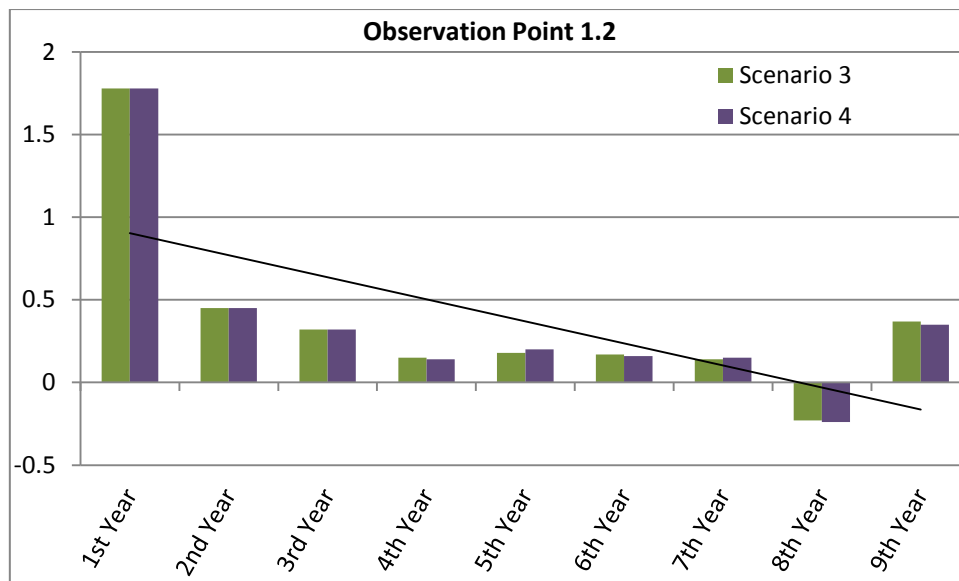


Figure 173: The decreasing trend of Scenarios 3 and 4 for simulation point 1.2

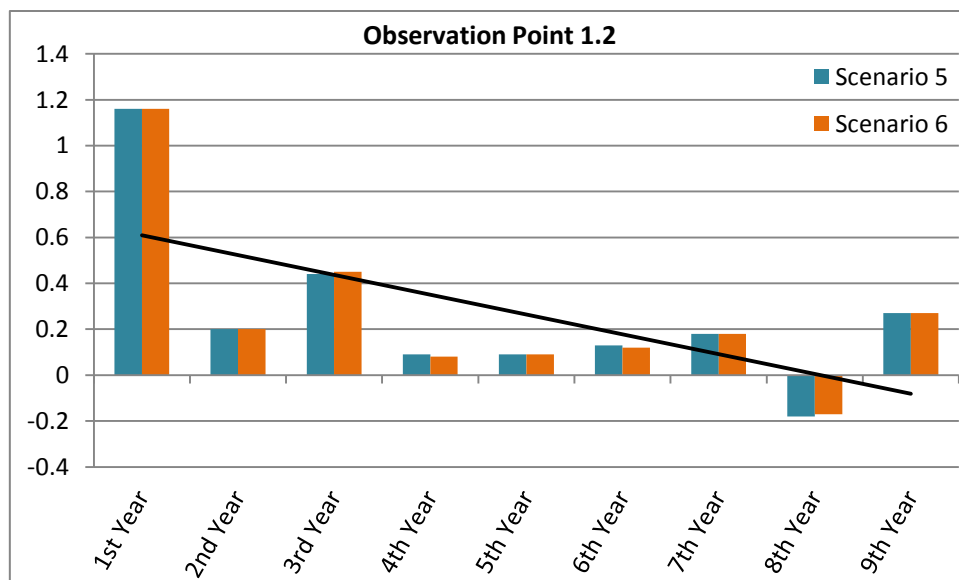


Figure 174: The decreasing trend of Scenarios 5 and 6 for simulation point 1.2

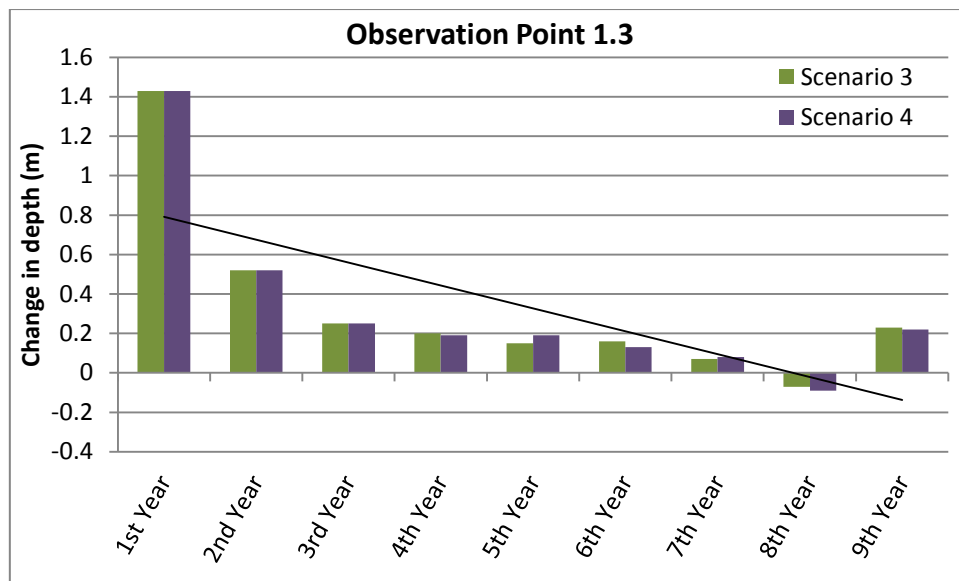


Figure 175: The decreasing trend of Scenarios 3 and 4 for simulation point 1.3

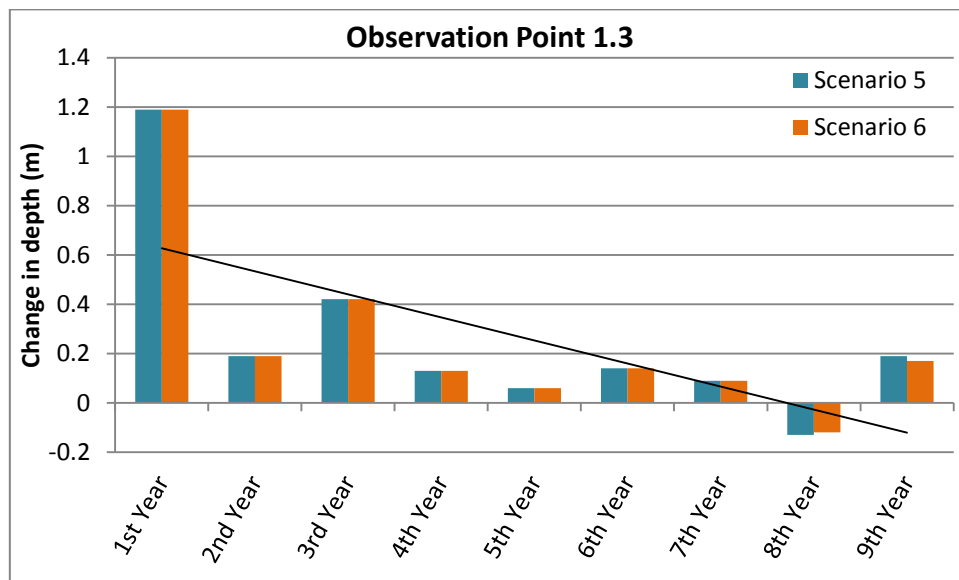


Figure 176: The decreasing trend of Scenarios 5 and 6 for simulation point 1.3

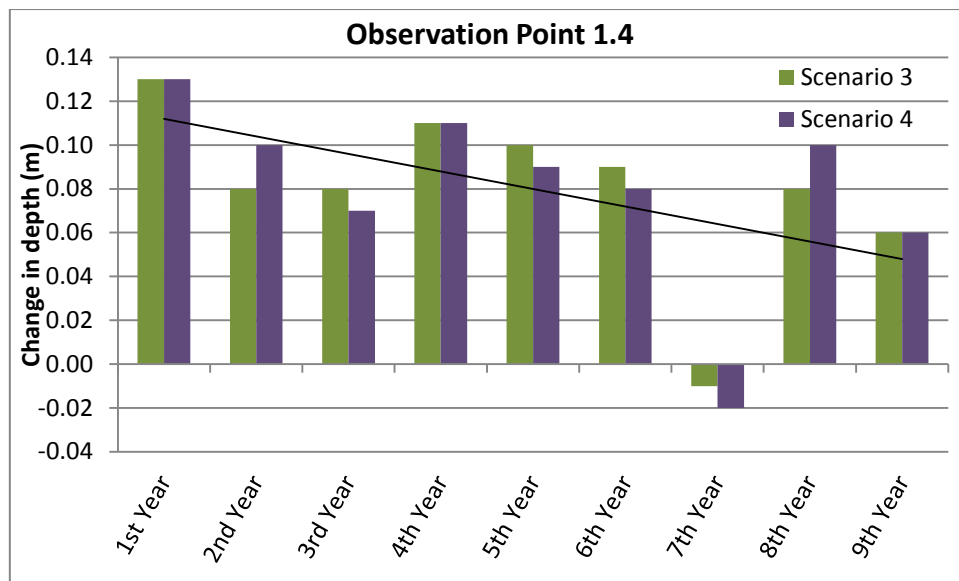


Figure 177: The decreasing trend of Scenarios 3 and 4 for simulation point 1.4

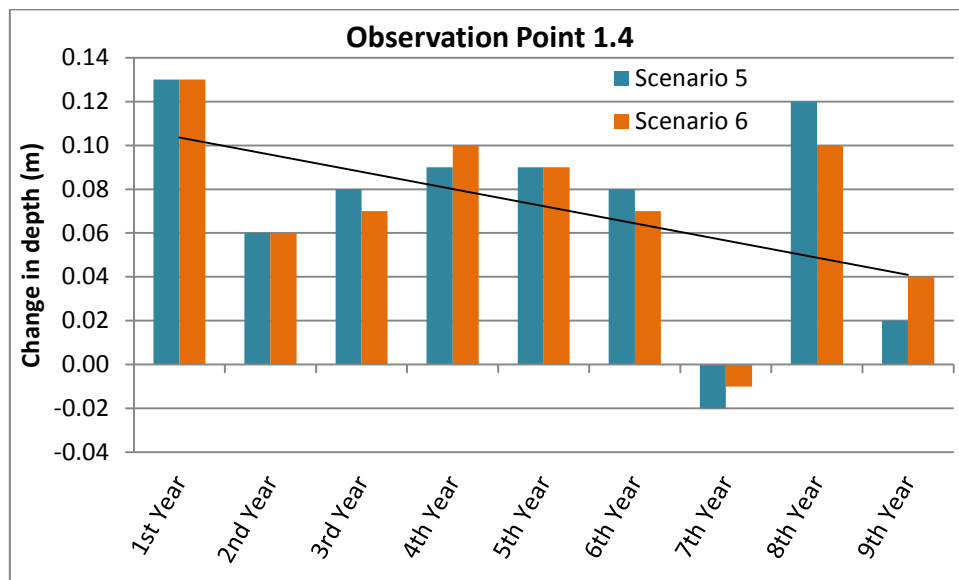


Figure 178: The decreasing trend of Scenarios 5 and 6 for simulation point 1.4

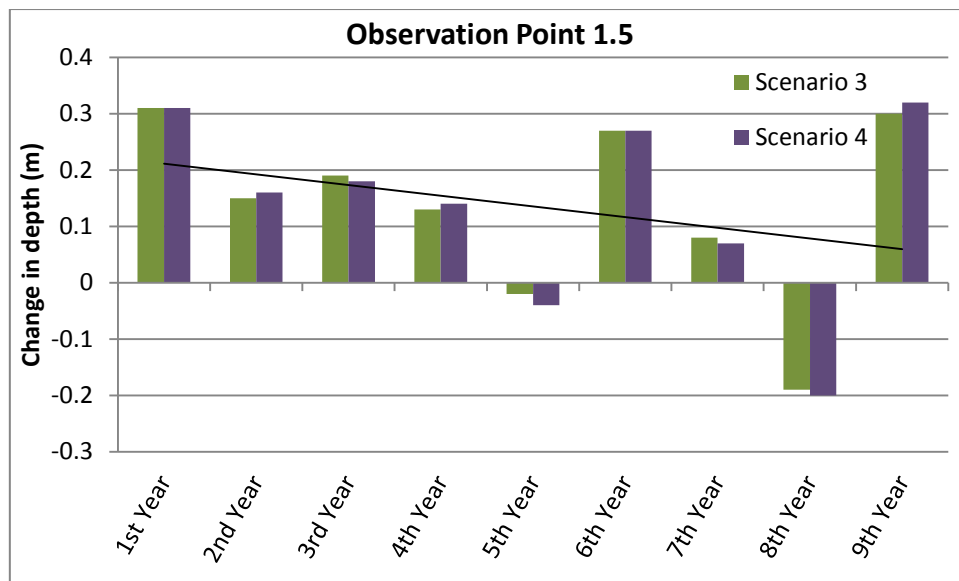


Figure 179: The decreasing trend of Scenarios 3 and 4 for simulation point 1.5

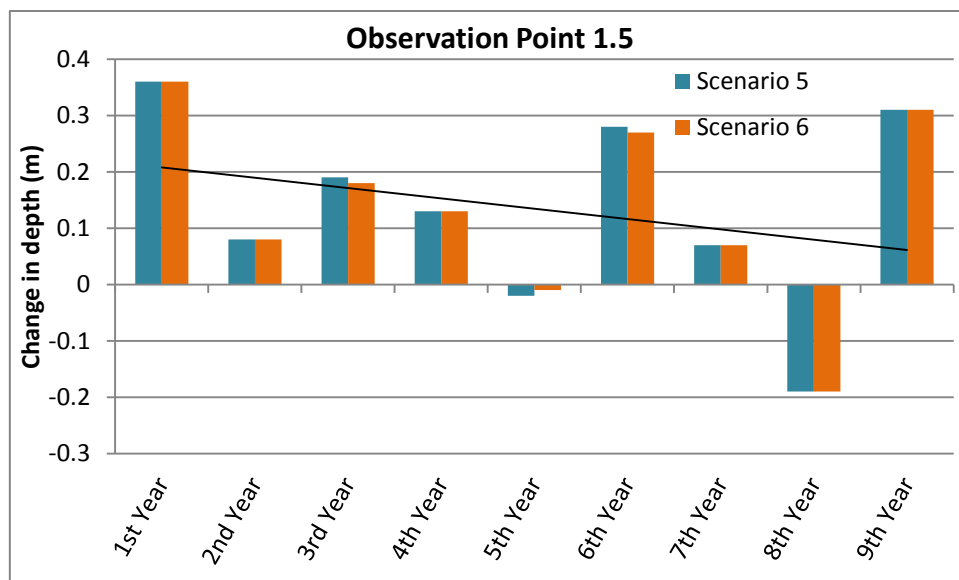


Figure 180: The decreasing trend of Scenarios 5 and 6 for simulation point 1.5

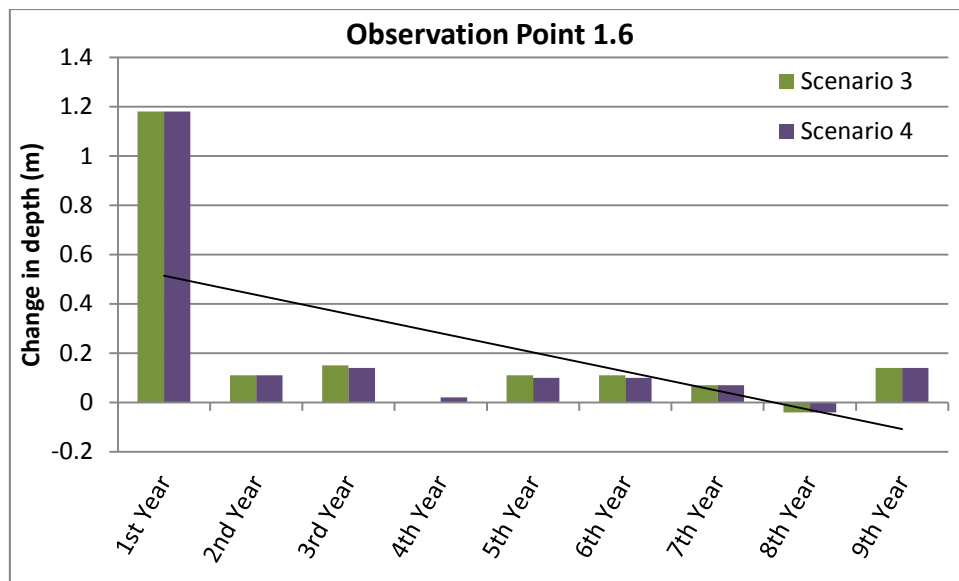


Figure 181: The decreasing trend of Scenarios 3 and 4 for simulation point 1.6

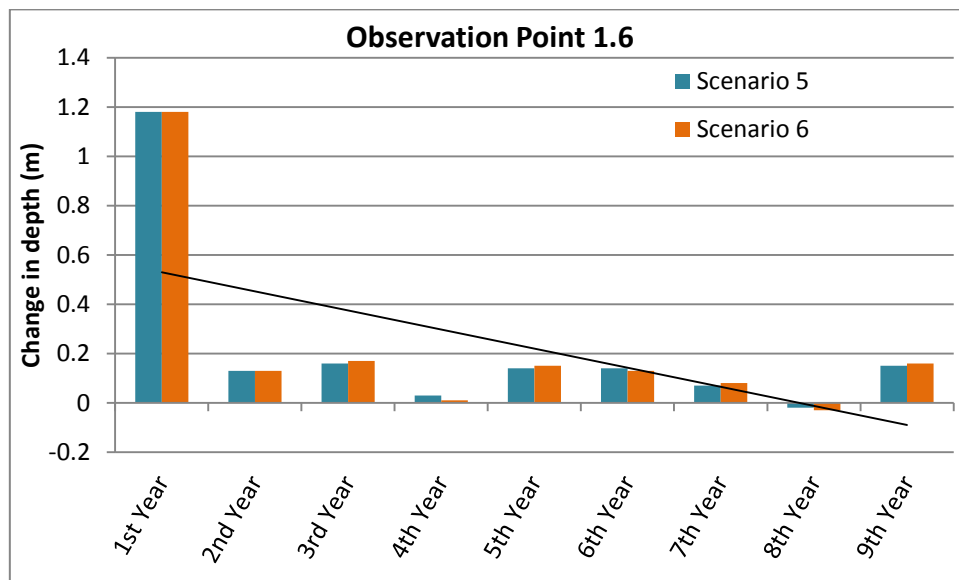


Figure 182: The decreasing trend of Scenarios 5 and 6 for simulation point 1.6

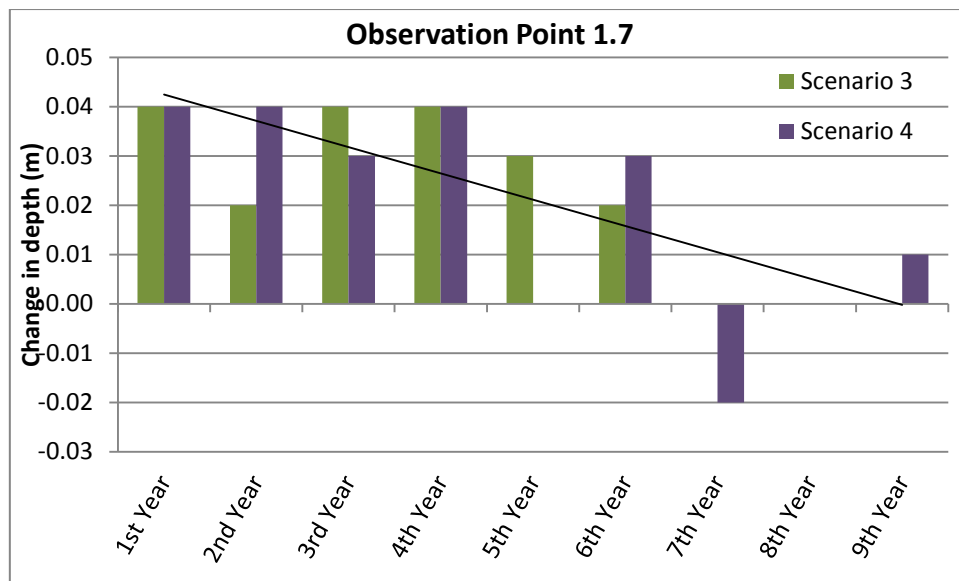


Figure 183: The decreasing trend of Scenarios 3 and 4 for simulation point 1.7

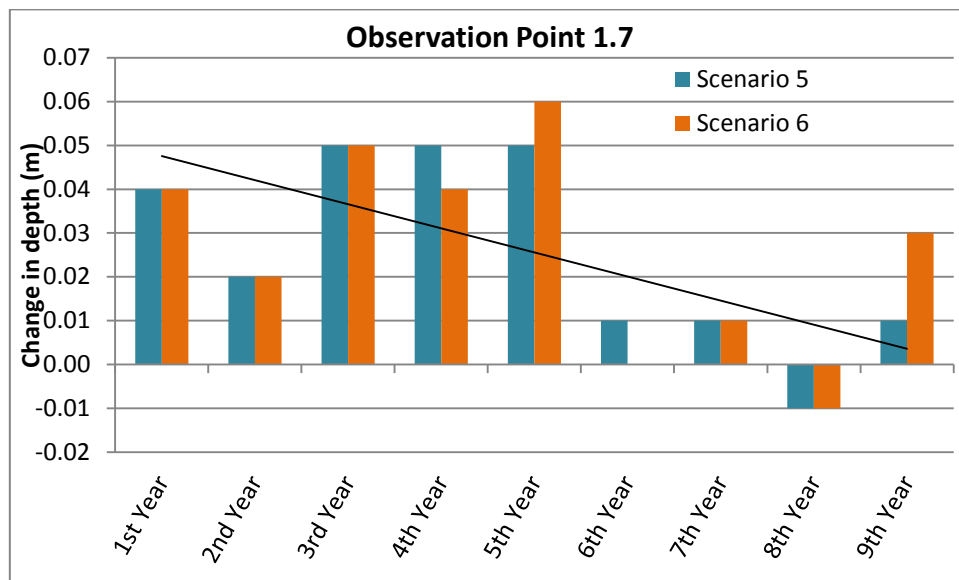


Figure 184: The decreasing trend of Scenarios 5 and 6 for simulation point 1.7

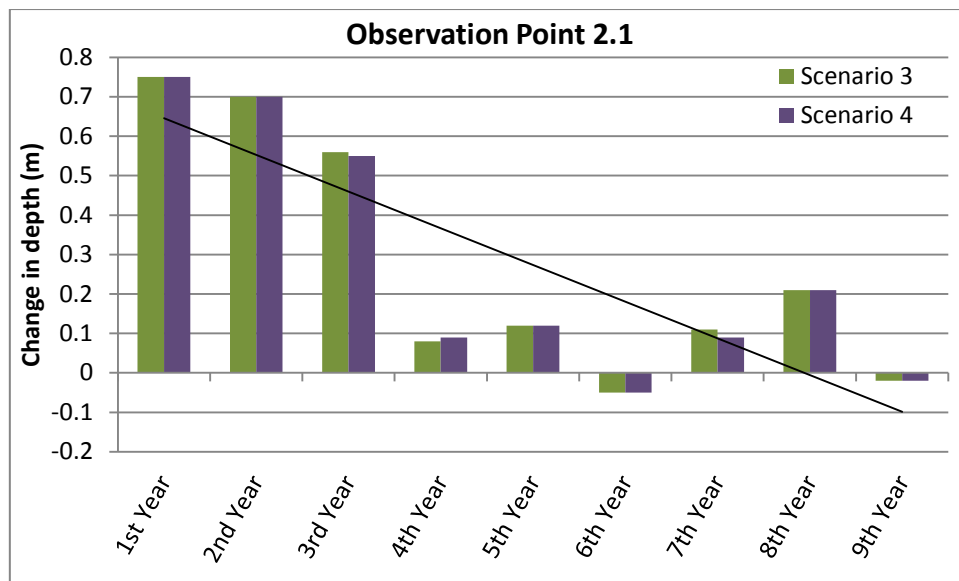


Figure 185: The decreasing trend of Scenarios 3 and 4 for simulation point 2.1

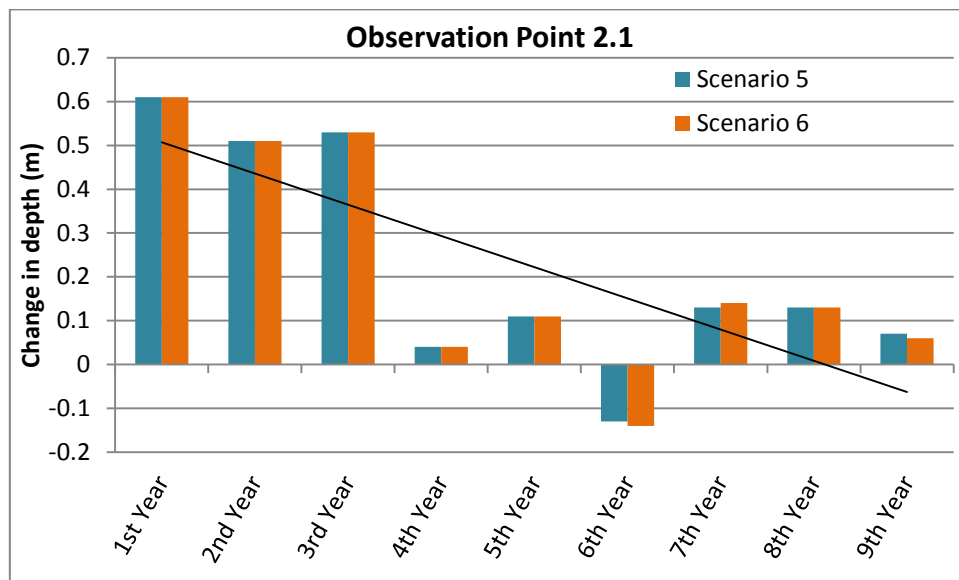


Figure 186: The decreasing trend of Scenarios 5 and 6 for simulation point 2.1

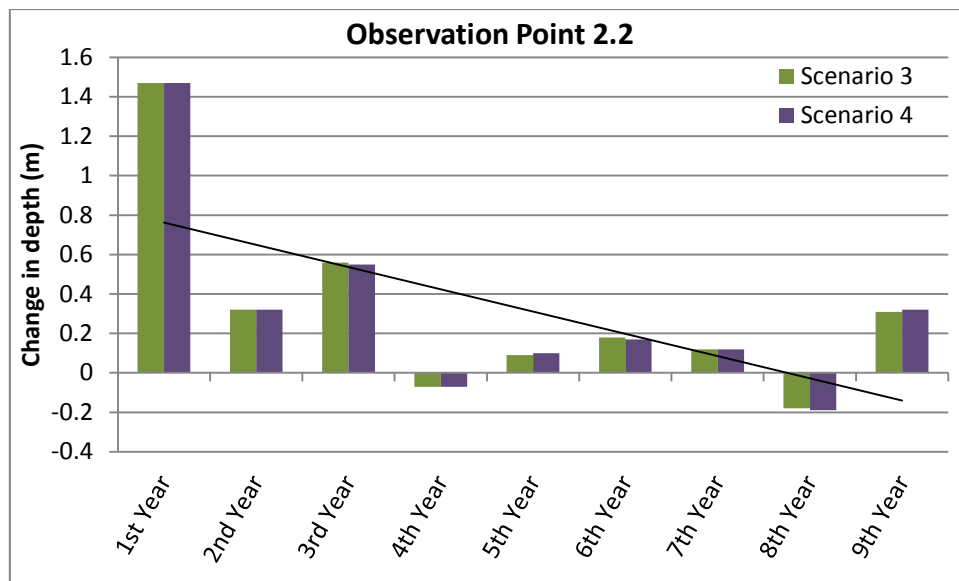


Figure 187: The decreasing trend of Scenarios 3 and 4 for simulation point 2.2

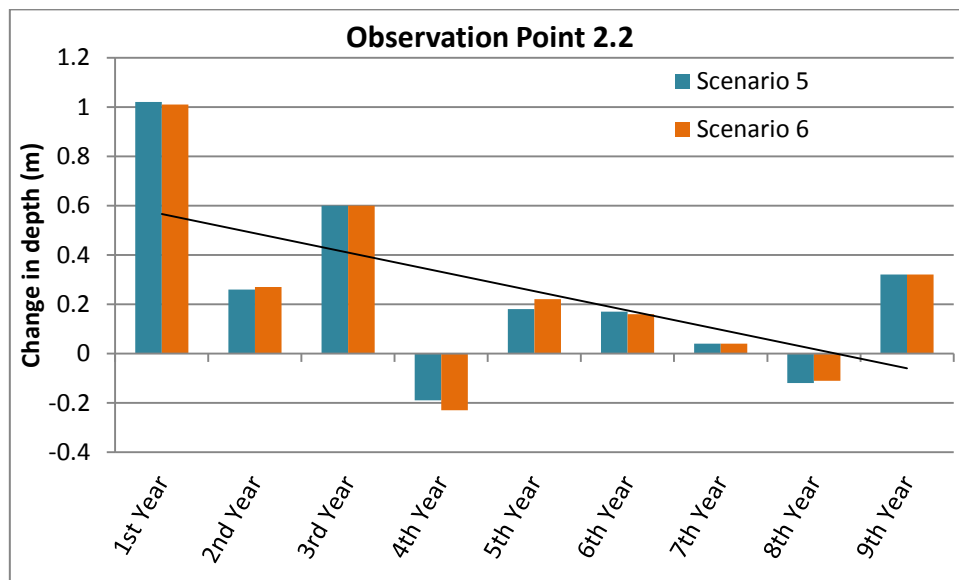


Figure 188: The decreasing trend of Scenarios 5 and 6 for simulation point 2.2

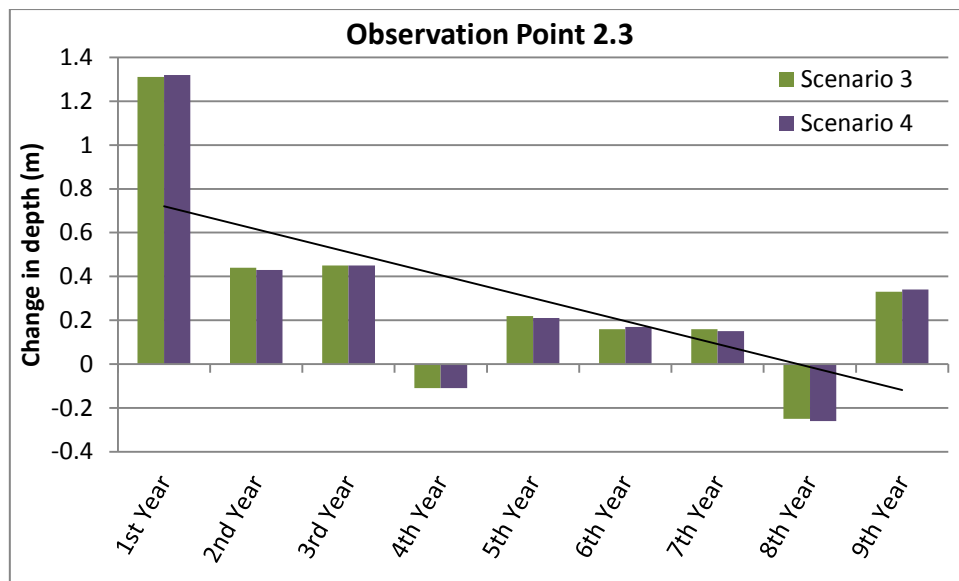


Figure 189: The decreasing trend of Scenarios 3 and 4 for simulation point 2.3

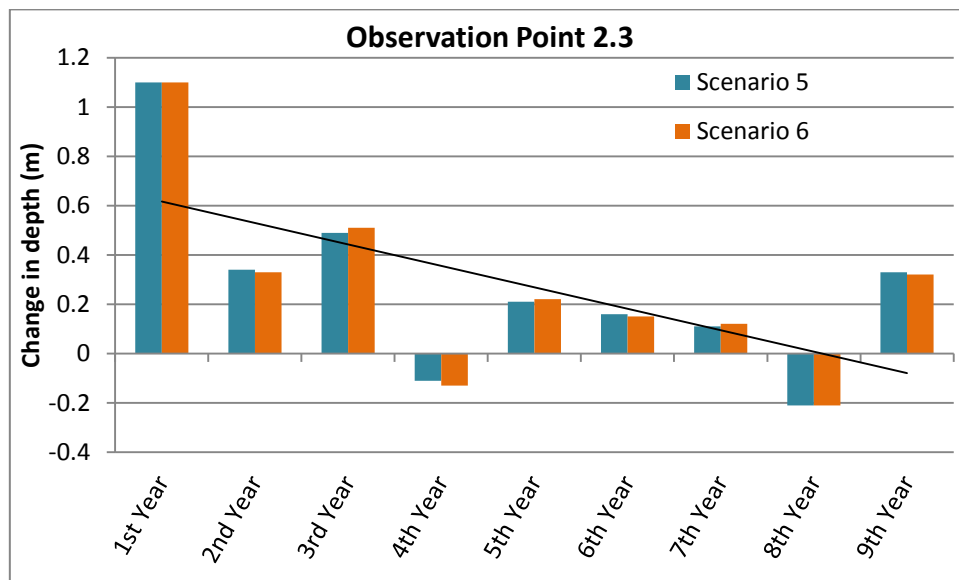


Figure 190: The decreasing trend of Scenarios 5 and 6 for simulation point 2.3

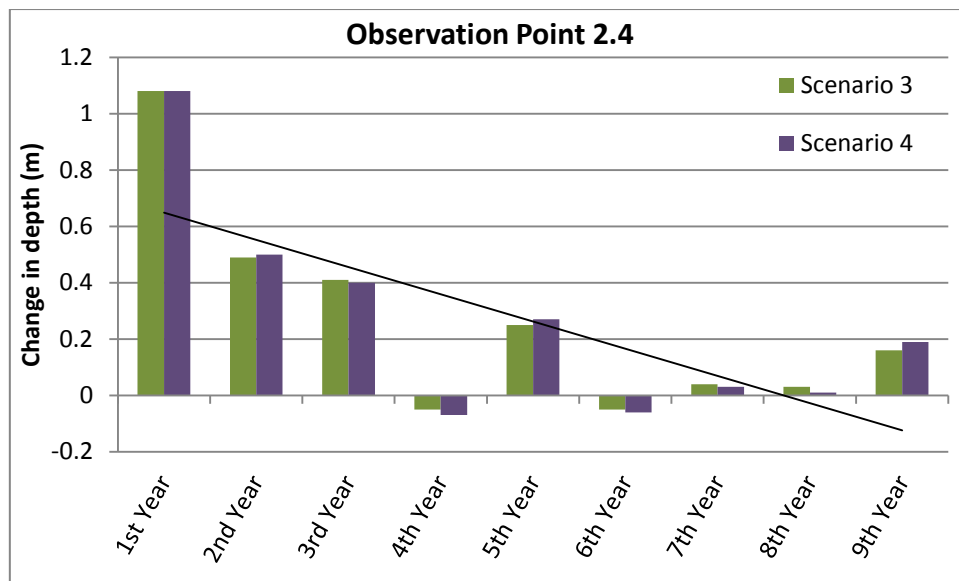


Figure 191: The decreasing trend of Scenarios 3 and 4 for simulation point 2.4

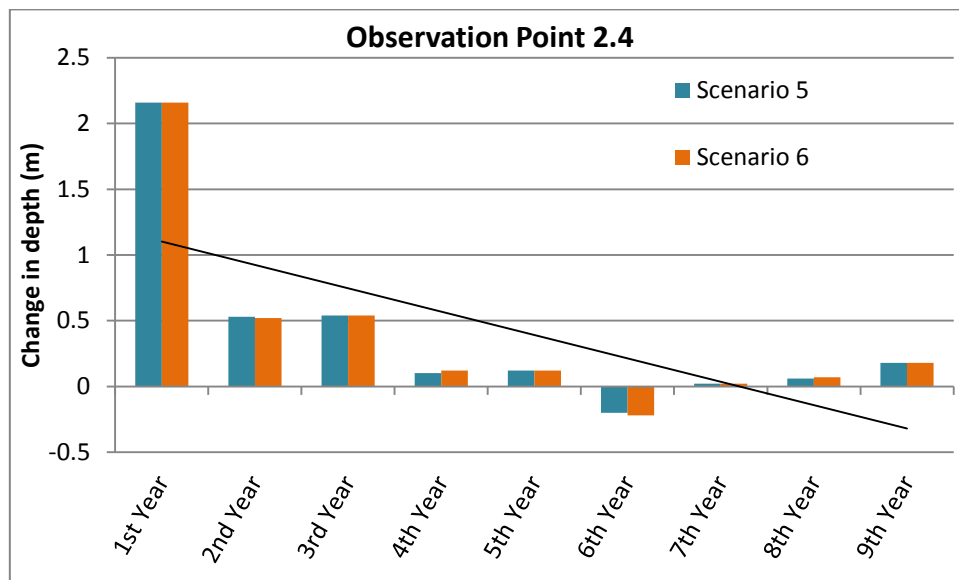


Figure 192: The decreasing trend of Scenarios 5 and 6 for simulation point 2.4

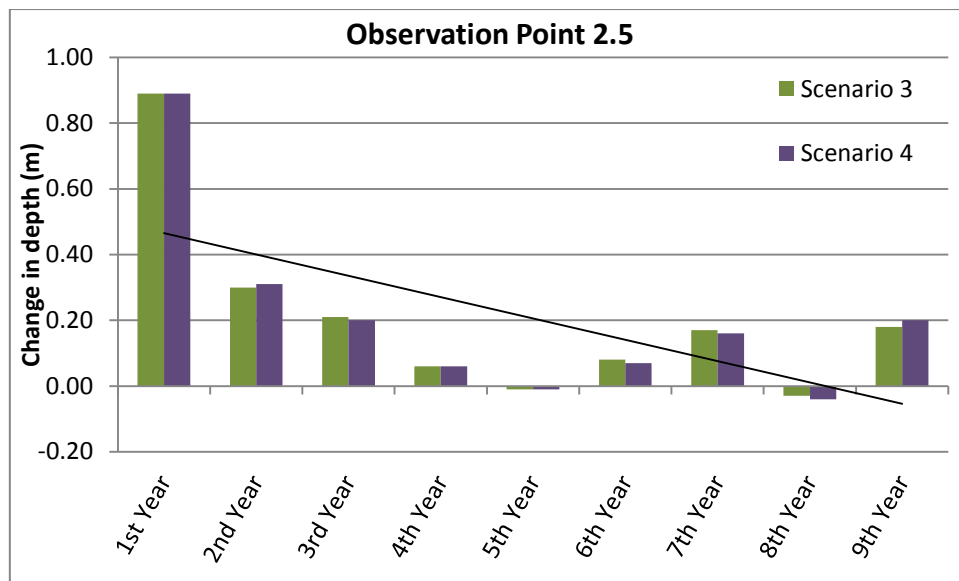


Figure 193: The decreasing trend of Scenarios 3 and 4 for simulation point 2.5

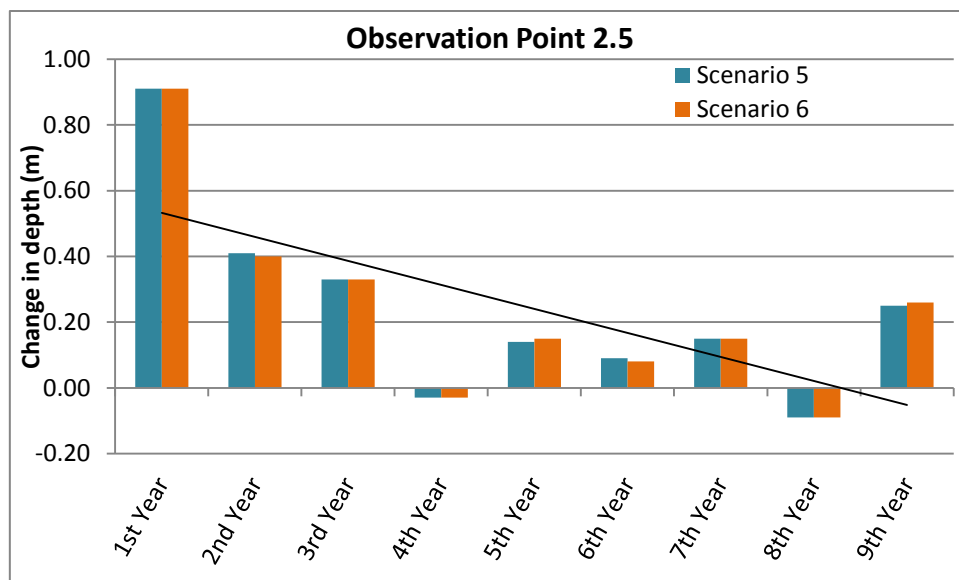


Figure 194: The decreasing trend of Scenarios 5 and 6 for simulation point 2.5

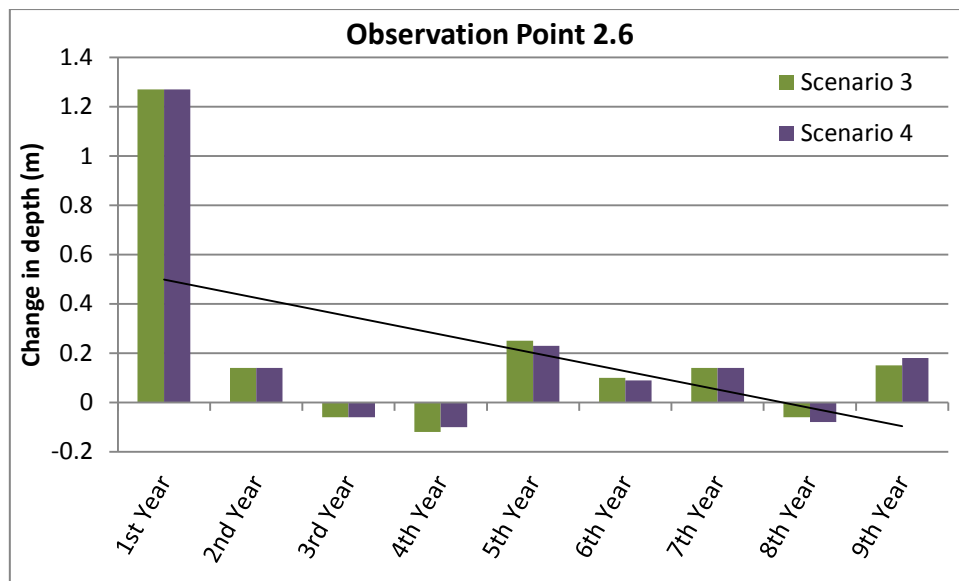


Figure 195: The decreasing trend of Scenarios 3 and 4 for simulation point 2.6

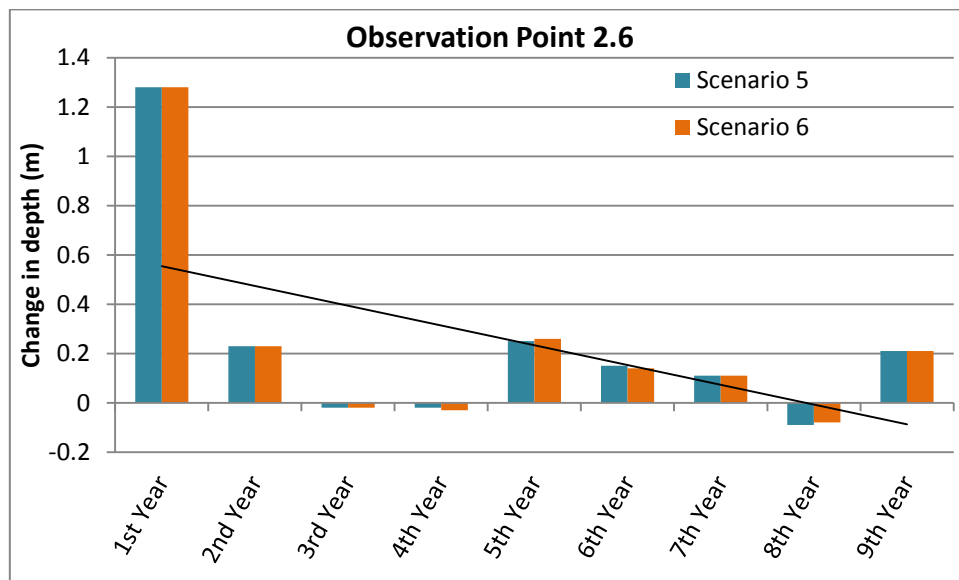


Figure 196: The decreasing trend of Scenarios 5 and 6 for simulation point 2.6

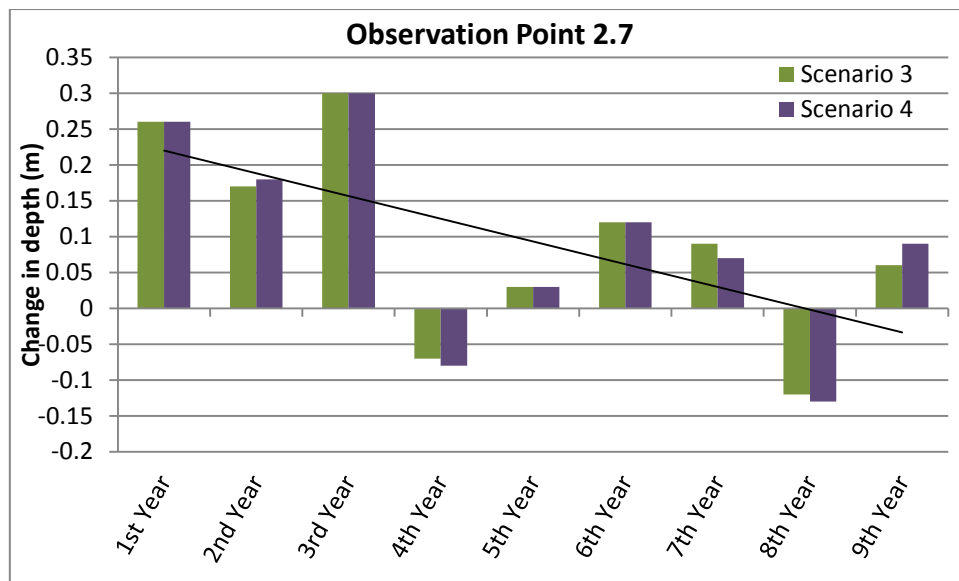


Figure 197: The decreasing trend of Scenarios 3 and 4 for simulation point 2.7

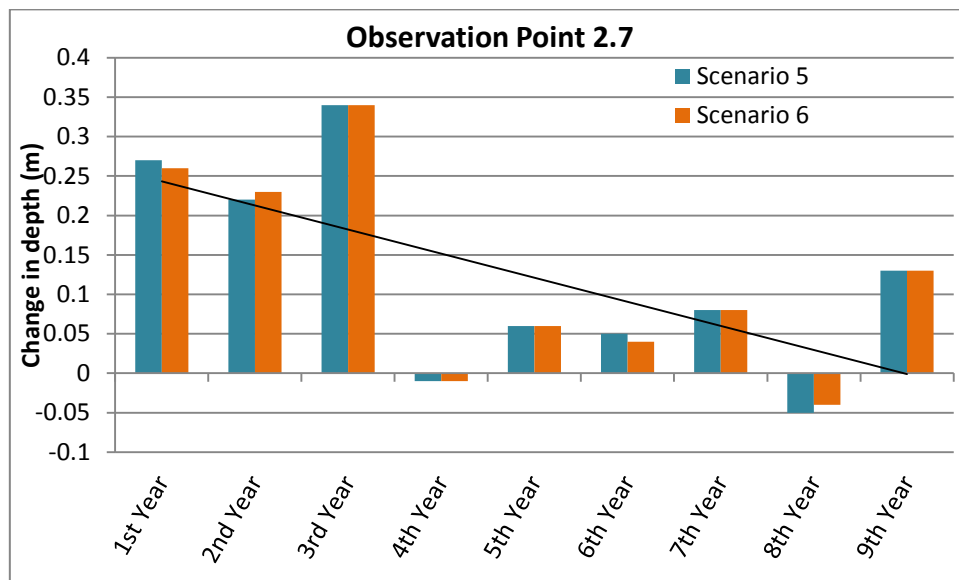


Figure 198: The decreasing trend of Scenarios 5 and 6 for simulation point 2.7

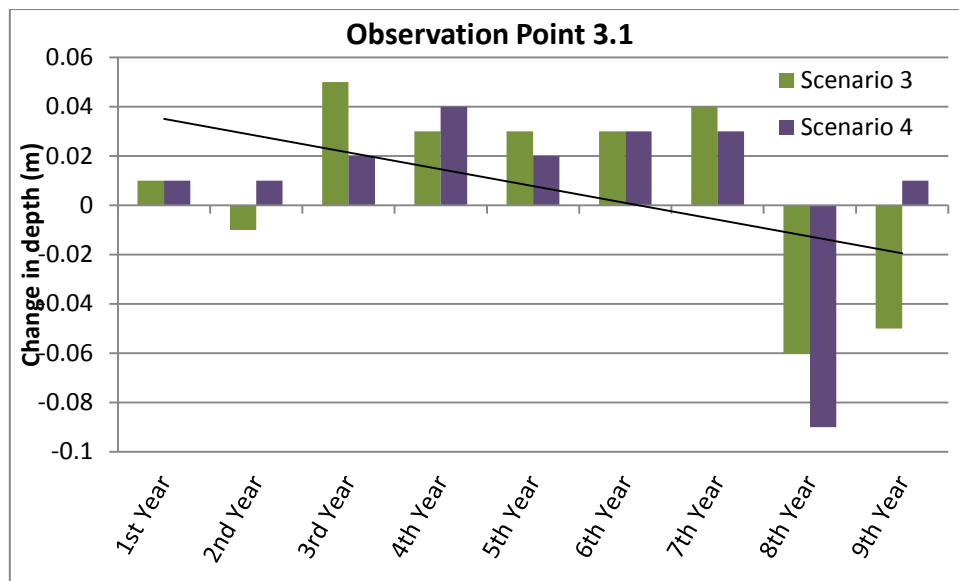


Figure 199: The decreasing trend of Scenarios 3 and 4 for simulation point 3.1

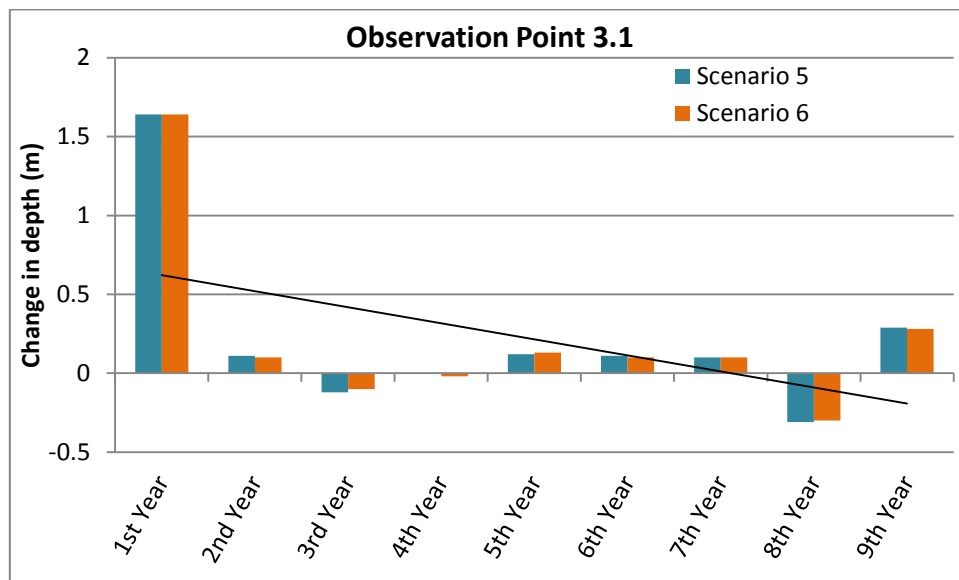


Figure 200: The decreasing trend of Scenarios 5 and 6 for simulation point 3.1

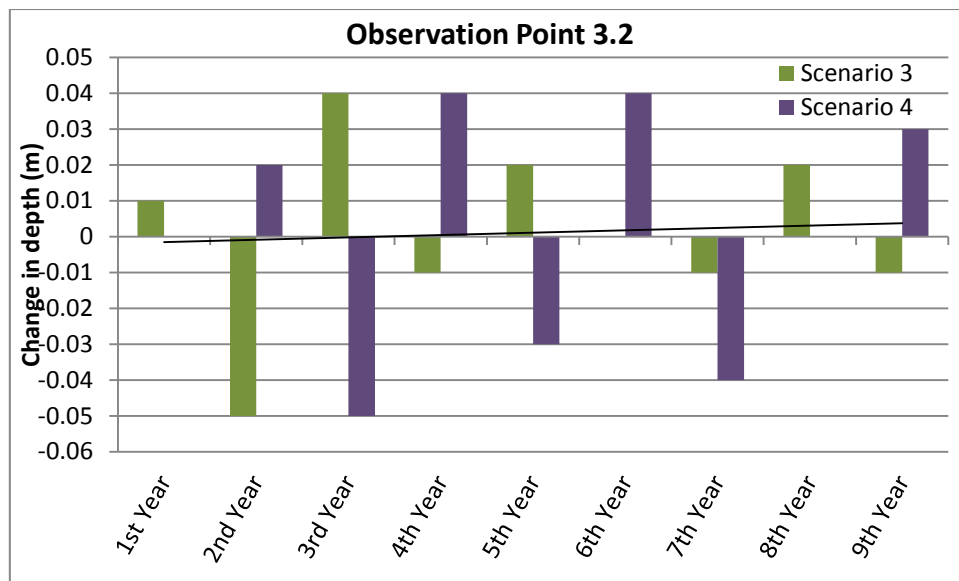


Figure 201: The decreasing trend of Scenarios 3 and 4 for simulation point 3.2

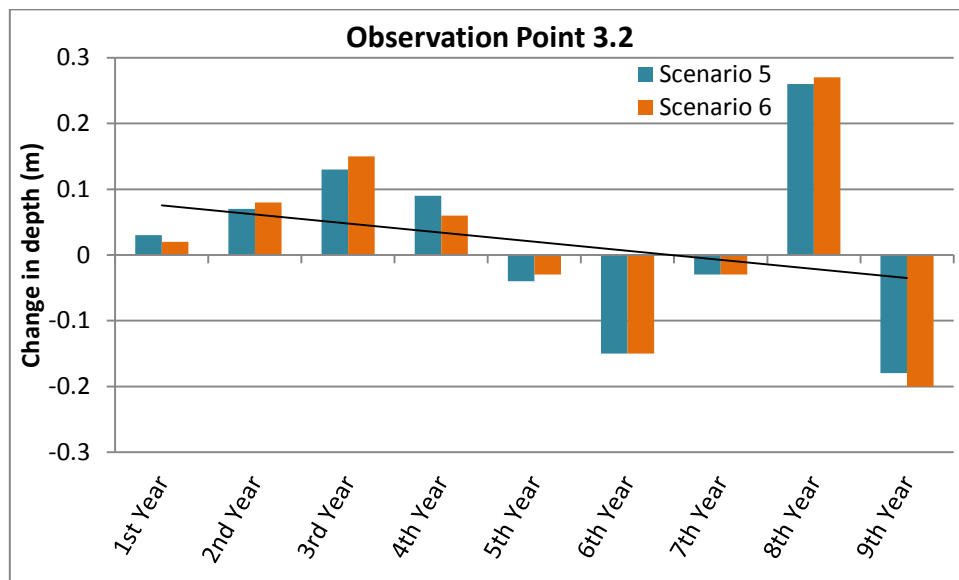


Figure 202: The decreasing trend of Scenarios 5 and 6 for simulation point 3.2

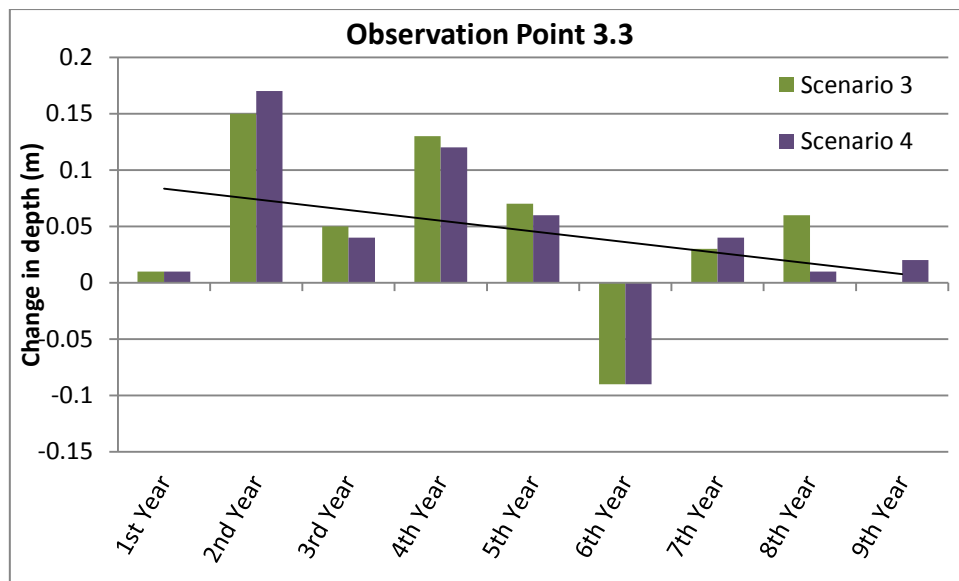


Figure 203: The decreasing trend of Scenarios 3 and 4 for simulation point 3.3

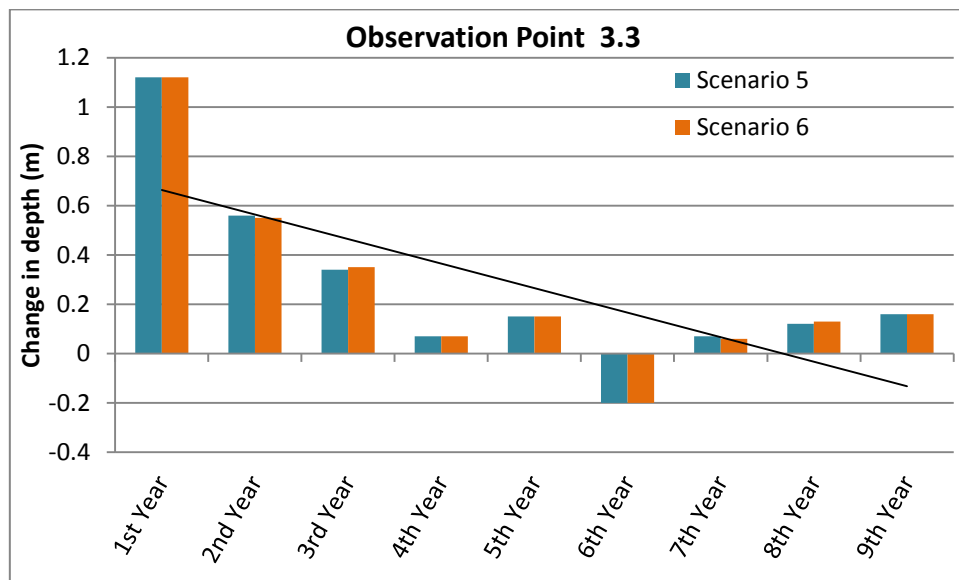


Figure 204: The decreasing trend of Scenarios 5 and 6 for simulation point 3.3

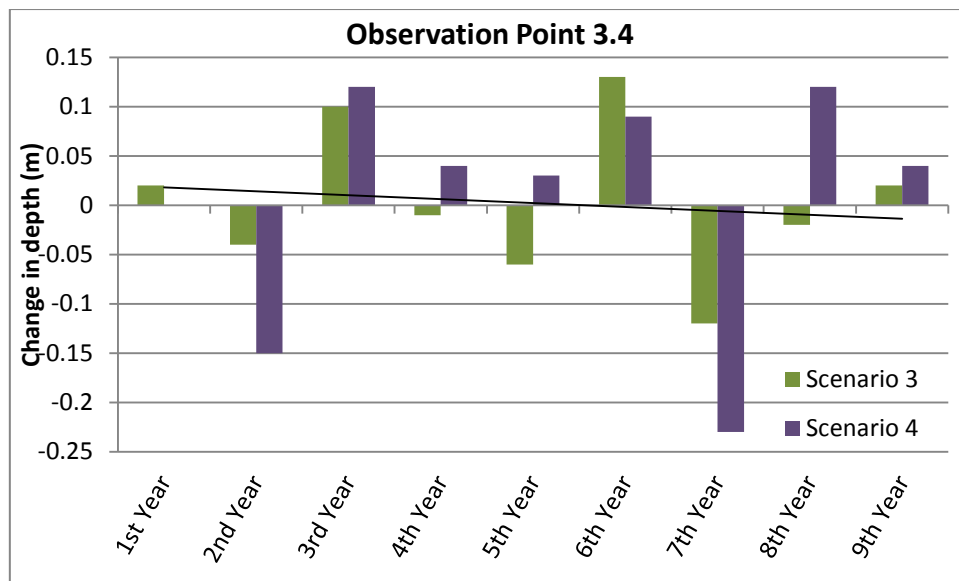


Figure 205: The decreasing trend of Scenarios 3 and 4 for simulation point 3.4

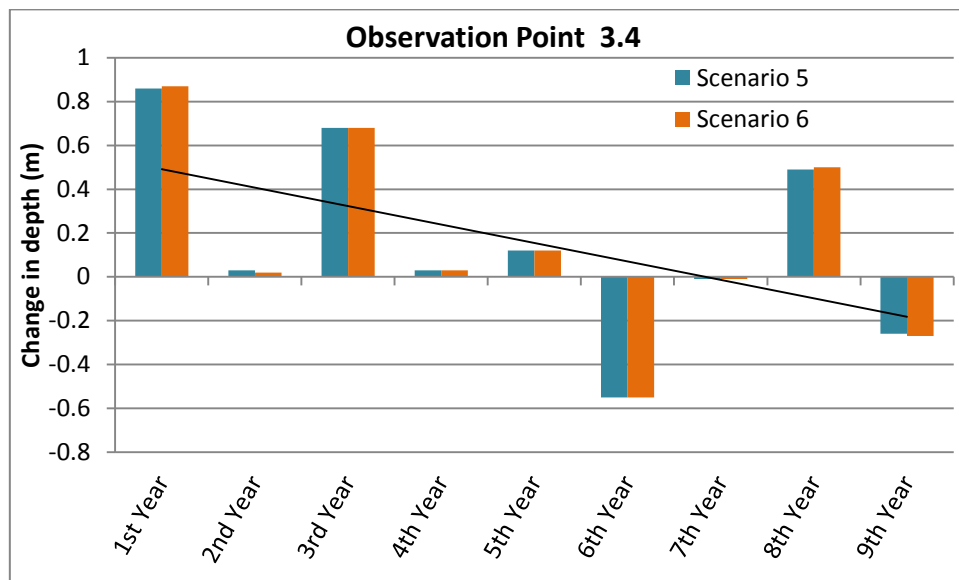


Figure 206: The decreasing trend of Scenarios 5 and 6 for simulation point 3.4

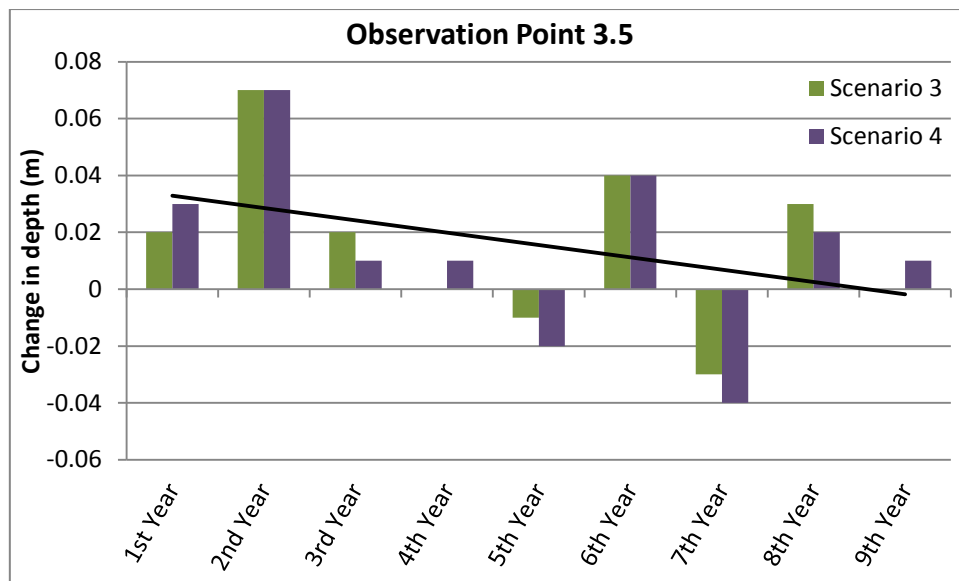


Figure 207: The decreasing trend of Scenarios 3 and 4 for simulation point 3.5

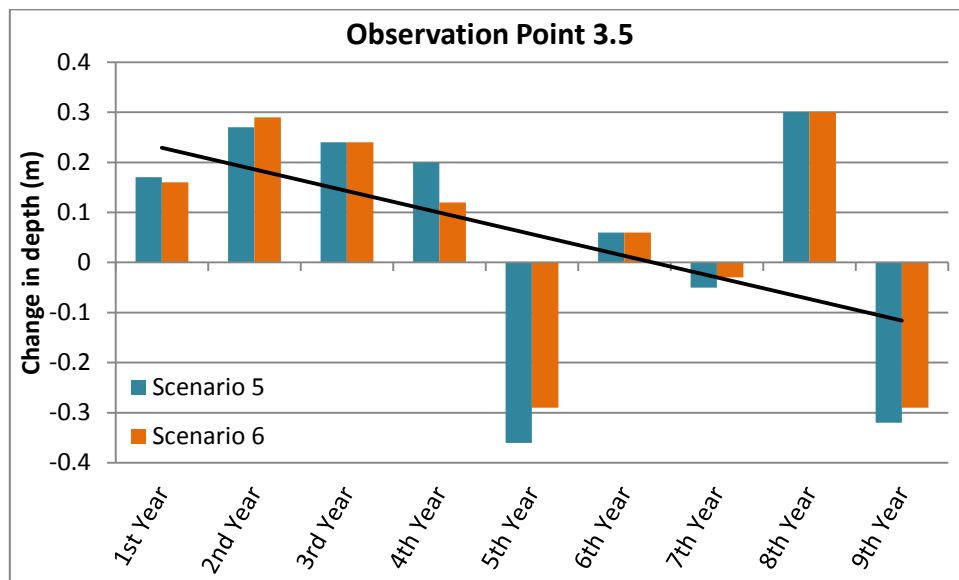


Figure 208: The decreasing trend of Scenarios 5 and 6 for simulation point 3.5